HYDRODENITROGENATION OF QUINOLINE, ACRIDINE AND THEIR MIXTURE

By

RIBHI FAYEZ EL-BISHTAWI

Bachelor In Chemical Engineering
Cairo University
Cairo, Egypt
1961

Master of Science
Cairo University
Cairo, Egypt
1974

Submitted to the faculty of the
Graduate College of the
Oklahoma State University
in partial fulfilment of
the requirements for
the Degree of
DOCTOR OF PHILOSOPHY
May, 1986

HYDPODENITROGENATION OF QUNOLINE,

ACRIDINE, AND THEIR MIXTURE

Thesis approved

Mayis Seapan
Thesis Adviser

Billy L Cypes

Robert S Robinson Jr.

Arland H. Johannes

E. J. Eisenbraun

Norman N Durham
Dean of the Graduate College

AKNOWLEDGEMENT

I wish to express my sincere gratitude to Dr Mayis Seapan, my major advisor for his invaluable help and guidance I would also like to express my appreciation to the members of the advisory committee, Dr Billy L. Crynes, Dr Robert L Robinson, Jr , Dr Edmund J. Eisenbraun and Dr A.H Johannes for their valuable contributions and kind help. I wish to thank Dr. Khalid Gasem, Dr Abdullatif M Bhairi, Rich Tebo, and Charles Baker for their technical help, and also, Marwan Kobbe and his wife Mary for typing this manuscript.

Finally, I would like to express my gratitude to the school of Chemical Engineering and the University Center for Energy Research, for providing the facilities and funds for this project, and the University of Jordan for financial support

TABLE OF CONTENTS

Chapter			Page
I	INTRODUCTION.		1
II	CHEMISTRY OF COAL LIQUIDS UPGRADING . . .		6
	A	Hydrodenitrogenation of Model Nitrogen Compounds . . .	8
		1 Pyridine	9
		2 Quinoline	19
		3 Isoquinoline .	34
		4. Acridine .	34
		5 Indole	39
		6 Carbazole	43
	B	Hydrodenitrogenation of Coal Derived Liquids	46
		1. First-Order Model	46
		2. Second-Order Model . . .	53
	C	Summary of Kinetics Review . .	63
III	EXPERIMENTAL APPARATUS AND TECHNIQUE .		66
	A	Experimental Apparatus .	66
		1 Reactor System. . .	66
		The Reactor . . .	66
		Gas Feeding. . . .	69
		Liquid Feeding . . .	69
		Sampling .	69
		Venting.	70
		2 Catalyst Preparation System .	70
		Calcination. . .	72
		Sulfidation. . . .	72
		3 Analytical Instruments . .	73
		Liquid Analysis . .	73
		Catalyst Analysis .	74
	B.	Experimental Technique	74
IV	EXPERIMENTAL RESULTS		77
	A	Quinoline Hydrodenitrogenation .	78
		1 Temperature Effect . . .	96
		2 Reaction Network	106
	B.	Acridine Hydrogenitrogenation	108
		1 Temperature Effect. .	123

Chapter Page

2 Initial Concentration Effect 124
3 Reaction Network . . . 131
C Quinoline-Acridine Mixture Hydrodenitrogenation . . . 131
D Catalyst Analysis 168

V KINETICS MODELING 172

Model #1 172
Model #2 174
Model #3 178
Model #4 183
Model #5 186
Model #6 188
Model #7 189
Effect of The Amount of Catalyst 189

VI. DISCUSSION OF RESULTS 190

Model #1 190
Model #2 203
Model #3 211
Model #4 217
Model #5 217
Model #6 243
Model #7 243
Interactions in Quinoline-Acridine Mixture HDN 273

VII CONCLUSIONS AND RECOMMENDATIONS 287

REFERENCES 291

APPENDIX A. SPECIFICATIONS OF MAIN VALVES AND ACCESSORIES 298

APPENDIX B. ANALYTICAL PROCEDURES 301

APPENDIX C REACTOR OPERATING PROCEDURE 321

APPENDIX D EFFECTIVENESS FACTOR. 324

LIST OF TABLES

Table		Page
I	Nitrogen Content of Some Fossil Fuels .	2
II.	Kinetic Data for Coal Tar Hydrotreatment .	49
III	Kinetic Data for Hydrotreatment of SRC-II. .	51
IV.	Kinetic Constants for Hydrotreatment of Coal Liquids	55
V.	Effect of Blend Composition on Heteroatom Removal Kinetics	56
VI.	Estimated Parameters for Catalyst Deactivation Model	64
VII	List of Experiments	78
VIII.	Reaction Products of NQ5 (357°C).	80
IX.	Reaction Products of NQ6 (370°C).	81
X.	Reaction Products of NQ9 (390°C).	82
XI	Quinoline HDN Reaction Paths	108
XII	Reduced Acridines	111
XIII.	Reaction Products of NA1 (370°C).	114
XIV.	Reaction Products of NA2 (390°C)	115
XV.	Reaction Products of NA3 (357°C).	116
XVI.	Reaction Products of NQA1	134
XVII	Reaction Products of NQA3	135
XVIII.	Reaction Products of NQA6	136
XIX.	Reaction Products of NQA8	137
XX.	Properties of American Cyanamide HDS-9A Catalyst	169

Table		Page
XXI.	Catalyst Analysis	170
XXII.	Model # 1 - Quinoline HDN	191
XXIII.	Model # 1 - Acridine HDN	196
XXIV.	Model # 1 - Quinoline-Acridine Mixture HDN. .	199
XXV	Model # 2 - Quinoline HDN	204
XXVI.	Parameters of Model #2 for Quinoline HDN	205
XXVII	Model #2 - Acridine HDN	208
XXVIII.	Parameters of Model #2 for Acridine HDN . . .	209
XXIX.	Model #2 - Quinoline-Acridine Mixture HDN . .	212
XXX.	Parameters of Model #2 for Quinoline -Acridine Mixture HDN	213
XXXI.	Model #3 - Quinoline HDN.	215
XXXII.	Parameters of Model #3 for Quinoline HDN. . .	216
XXXIII	Parameters of Model #4 for Quinoline HDN. .	230
XXXIV	Parameters of Model #5 for Quinoline HDN.	244
XXXV	Parameters of Model #6 for Acridine HDN . . .	245
XXXVI.	Parameters of Model #7 for Quinoline HDN. . .	253
XXXVII	Parameters of Model #7 for Acridine HDN .	254
XXXVIII.	Relative Quinoline Concentrations	274
XXXIX.	Relative Total Nitrogen Concentrations. . . .	278
XL.	Relative Acridine Concentrations.	282
XLI.	Main Valves	298
XLII.	Accessories	299
XLIII.	HDN Products of Quinoline/n-hexadecane. . . .	302
XLIV.	Precision and Accuracy of Analysis.	304
XLV.	Retention Times for Quinoline HDN Products. .	307

Table		Page
XLVI.	Composition of Standard Solutions Used in Quinoline HDN Products Analysis	309
XLVII.	Retention Times for Other Expected Compounds	310
XLVIII	Retention Times for Acridine HDN Products	313
XLIX.	Composition of Standard Solutions Used in Acridine HDN Products	314
L.	Retention Times for Quinoline-Acridine Mixture HDN Products.	318
LI	Composition of Standard Solutions Used in Mixture HDN Products Analysis	319
LII	Parameters Used in Effectiveness Factor Calculations	326

LIST OF FIGURES

Figure		Page
1.	Nitrogen-Containing Compounds in Liquid Fossil Fuels..	7
2.	Reaction Network of Piperidine HDN at 6.1 MPa, Co-Mo/Alumina Catalyst	16
3.	Reaction Network of Quinoline HDN at 342°C, 13.7 MPa, Ni-Mo/Alumina Catalyst	23
4.	Reaction Network of Quinoline HDN at 230-420°C, 3.6-7.0 MPa, Ni-Mo/Alumina Catalyst	25
5.	Reaction Network of Quinoline HDN at 330-420°C, 3.6-7.0 MPa, Ni-Mo/Alumina Catalyst	27
6.	Reaction Network of Quinoline HDN at 350-390°C, 6.9 MPa, HDS-3A Catalyst	32
7.	Reaction Network for Isoquinoline HDN	35
8.	Reaction Network for Acridine HDN at 342°C, 13.7 MPa, Ni-Mo/Alumina Catalyst	36
9.	Reaction Network for Acridine HDN at 200-350°C, 2.5-14.6 MPa, Prereduced Mo/Alumina Catalyst	38
10.	Reaction Network for Indole HDN	40
11.	Reaction Network for Indole HDN at 350-400°C, 20.2 MPa, Co-Mo/Alumina	40
12.	Reaction Network for Indole HDN at 350°C, 6.9 MPa	42
13.	Reaction Network for Carbazole HDN	44
14.	Reaction Network for Carbazole HDN at 270-310°C, 10.1 MPa, Prereduced Mo/Alumina Catalyst	47
15.	Shematic Diagram of the Reactor System	67
16.	Catalyst Ampoule	71

Figure Page

17. Quinoline HDN Products at 357°C 83

18 Quinoline HDN Products at 357°C. 84

19. Quinoline HDN Products at 357°C. 85

20. Quinoline HDN Products at 357°C. 86

21. Quinoline HDN Products at 370°C. 87

22. Quinoline HDN Products at 370°C. 88

23. Quinoline HDN Products at 370°C. 89

24. Quinoline HDN Products at 370°C. 90

25. Quinoline HDN Products at 390°C. 91

26. Quinoline HDN Products at 390°C. 92

27. Quinoline HDN Products at 390°C. 93

28 Quinoline HDN Products at 390°C. 94

29. Effects of Temperature on Concentration of Quinoline. 97

30. Effects of Temperature on Concentration of 1,2,3,4,-tetrahydroquinoline 98

31. Effects of Temperature on Concentration of 5,6,7,8-tetrahydroquinoline. 99

32. Effects of Temperature on Concentration of decahydroquinoline 100

33. Effects of Temperature on Concentration of Propylcyclohexane. 101

34 Effects of Temperature on Concentration of O-Propylaniline. 102

35 Effects of Temperature on Concentration of Propylbenzene. 103

36. Effects of Temperature on Concentration of O-ethylaniline 104

37. Effects of Temperature on Concentration of O-methylaniline. 105

Figure Page

38. Reaction Network for Quinoline HDN at 357-390°C, 8.2 MPa, HDS-9A Catalyst. 107

39. Acridine HDN Products at 357°C 117

40. Acridine HDN Products at 357°C 118

41. Acridine HDN Products at 370°C 119

42. Acridine HDN Products at 370°C 120

43. Acridine HDN Products at 390°C 121

44. Acridine HDN Products at 390°C 122

45. Effects of Temperature on Concentration of Acridine 125

46. Effects of Temperature on Concentration of Tetrahydroacridine 126

47. Effects of Temperature on Concentration of Sym-Octahydroacridine. 127

48. Effects of Temperature on Concentration of Asym-Octahydroacridine 128

49. Effects of Temperature on Concentration of Perhydroacridine 129

50. Effects of Temperature on Concentration of Dicyclohexylmethane. 130

51. Reaction Network for Acridine HDN at 357-390°C, 8.2 MPa, HDS-9A Catalyst. 132

52. Quinoline-Acridine Mixture HDN Products at 390°C 139

53. Quinoline-Acridine Mixture HDN Products at 390°C 140

54. Quinoline-Acridine Mixture HDN Products at 390°C 141

55. Quinoline-Acridine Mixture HDN Products at 390°C 142

56. Quinoline-Acridine Mixture HDN Products at 390°C 143

Figure Page

57. Quinoline-Acridine Mixture HDN Products at 390°C 144

58. Quinoline-Acridine Mixture HDN Products at 357°C 145

59. Quinoline-Acridine Mixture HDN Products at 357°C 146

60. Quinoline-Acridine Mixture HDN Products at 357°C 147

61 Quinoline-Acridine Mixture HDN Products at 357°C 148

62. Quinoline-Acridine Mixture HDN Products at 357°C 149

63. Quinoline-Acridine Mixture HDN Products at 357°C 150

64. Quinoline-Acridine Mixture HDN Products at 370°C 151

65. Quinoline-Acridine Mixture HDN Products at 370°C 152

66. Quinoline-Acridine Mixture HDN Products at 370°C 153

67. Quinoline-Acridine Mixture HDN Products at 370°C 154

68. Quinoline-Acridine Mixture HDN Products at 370°C 155

69. Quinoline-Acridine Mixture HDN Products at 370°C 156

70. Quinoline-Acridine Mixture Long-Run HDN Products at 370°C 160

71. Quinoline-Acridine Mixture Long-Run HDN Products at 370°C 161

72. Quinoline-Acridine Mixture Long-Run HDN Products at 370°C 162

73. Quinoline-Acridine Mixture Long-Run HDN Products at 370°C 163

Figure Page

74. Quinoline-Acridine Mixture Long-Run HDN Products at 370°C 164

75. Quinoline-Acridine Mixture Long-Run HDN Products at 370°C 165

76. Reactions of some Acridine HDN Products . . 167

77. Quinoline Hydrodenitrogenation - Model #1 . . . 193

78. Temperature Dependency of Quinoline HDN Reaction Rate 194

79. Acridine Hydrodenitrogenation - Model #1 197

80 Temperature Dependency of Quinoline HDN Reaction Rate 198

81. Quinoline-Acridine Mixture Hydrodenitrogenation - Model #1 201

82. Temperature Dependency of Quinoline-Acridine Mixture HDN Reaction Rate 202

83. Quinoline Hydrodenitrogenation - Model #2 206

84. Temperature Dependency of Quinoline HDN Reaction Rate 207

85 Acridine Hydrodenitrogenation - Model #2 210

86. Quinoline-Acridine Mixture Hydrodenitrogenation - Model #2 214

87 Quinoline HDN Products at 357°C - Model #4. . . . 218

88. Quinoline HDN Products at 357°C - Model #4. . . 219

89. Quinoline HDN Products at 357°C - Model #4. . . . 220

90. Quinoline HDN Products at 357°C - Model #4. . . 221

91 Quinoline HDN Products at 370°C - Model #4. . 222

92. Quinoline HDN Products at 370°C - Model #4. . . 223

93. Quinoline HDN Products at 370°C - Model #4. . . . 224

94. Quinoline HDN Products at 370°C - Model #4. . . . 225

Figure Page

95. Quinoline HDN Products at 390°C - Model #4. . . 226

96. Quinoline HDN Products at 390°C - Model #4 . . . 227

97 Quinoline HDN Products at 390°C - Model #4. . . . 228

98. Quinoline HDN Products at 390°C - Model #4 . . . 229

99. Quinoline HDN Products at 357°C - Model #5. . . . 231

100. Quinoline HDN Products at 357°C - Model #5. . . . 232

101. Quinoline HDN Products at 357°C - Model #5. . . . 233

102. Quinoline HDN Products at 357°C - Model #5 . . 234

103. Quinoline HDN Products at 370°C - Model #5. . . . 235

104. Quinoline HDN Products at 370°C - Model #5. . . . 236

105. Quinoline HDN Products at 370°C - Model #5. . . . 237

106. Quinoline HDN Products at 370°C - Model #5. . . . 238

107. Quinoline HDN Products at 390°C - Model #5. . . . 239

108 Quinoline HDN Products at 390°C - Model #5. . . 240

109. Quinoline HDN Products at 390°C - Model #5. . . . 241

110. Quinoline HDN Products at 390°C - Model #5. . . . 242

111. Acridine HDN Products at 357°C - Model #6 . . . 246

112. Acridine HDN Products at 357°C - Model #6 247

113. Acridine HDN Products at 370°C - Model #6 . . . 248

114. Acridine HDN Products at 370°C - Model #6 . . . 249

115. Acridine HDN Products at 390°C - Model #6 . . . 250

116. Acridine HDN Products at 390°C - Model #6 251

117. Quinoline-Acridine Mixture HDN Products at 357°C - Model #7 255

118. Quinoline-Acridine Mixture HDN Products at 357°C - Model #7 256

Figure Page

119. Quinoline-Acridine Mixture HDN Products at 357°C - Model #7 257

120. Quinoline-Acridine Mixture HDN Products at 357°C - Model #7 258

121. Quinoline-Acridine Mixture HDN Products at 357°C - Model #7 259

122. Quinoline-Acridine Mixture HDN Products at 357°C - Model #7 260

123. Quinoline-Acridine Mixture HDN Products at 370°C - Model #7 261

124 Quinoline-Acridine Mixture HDN Products at 370°C - Model #7 262

125 Quinoline-Acridine Mixture HDN Products at 370°C - Model #7 263

126. Quinoline-Acridine Mixture HDN Products at 370°C - Model #7 264

127. Quinoline-Acridine Mixture HDN Products at 370°C - Model #7 265

128. Quinoline-Acridine Mixture HDN Products at 370°C - Model #7 266

129. Quinoline-Acridine Mixture HDN Products at 390°C - Model #7 267

130. Quinoline-Acridine Mixture HDN Products at 390°C - Model #7 268

131. Quinoline-Acridine Mixture HDN Products at 390°C - Model #7 269

132. Quinoline-Acridine Mixture HDN Products at 390°C - Model #7 270

133. Quinoline-Acridine Mixture HDN Products at 390°C - Model #7 271

134. Quinoline-Acridine Mixture HDN Products at 390°C - Model #7 272

135 Effect of Acridine on Quinoline Conversion at 357°C 275

Figure Page

136. Effect of Acridine on Quinoline Conversion at 370°C 276

137 Effect of Acridine on Quinoline Conversion at 390°C 277

138 Effect of Acridine on Quinoline -Nitrogen Removal at 357°C 279

139 Effect of Acridine on Quinoline -Nitrogen Removal at 370°C 280

140. Effect of Acridine on Quinoline -Nitrogen Removal at 390°C 281

141. Effect of Quinoline on Acridine Conversion at 357°C 284

142. Effect of Quinoline on Acridine Conversion at 370°C 285

143. Effect of Quinoline on Acridine Conversion at 390°C 286

144. A Typical Chromatogram for Quinoline-Acridine Mixture HDN Products. 320

TABLE OF ABBREVIATIONS

ASOHA	1,2,3,4,9,10,4a,9a, - octahydroacridine or asymmetric-octahydroacridine
ASTHA (THA)	1,2,3,4-tetrahydroacridine
Bz-THQ	5,6,7,8-tetrahydroquinoline
DCHM	dicyclohexylmethane
DDHA	dodecahydroacridine
DHA	dihydroacridine
DHQ	decahydroquinoline
HHA	hexahydroacridine
MPA	monopentylamine
MPCP	methylpropylcyclopentane
OEA	o-ethylaniline
OMA	o-methylaniline
OPA	o-propylaniline
PB	propylbenzene
PCH	propylcyclohexane
PCHA	propylcyclohexylamine
PCHE	propylcyclohexene
PHA	perhydroacridine
Py-THQ	1,2,3,4-tetrahydroquinoline
SOHA	1,2,3,4,5,6,7,8-octahydroacridine or symmetric-octahydroacridine
STHA	1,2,7,8-tetrahydroacridine or symmetric-tetrahydroacridine

CHAPTER I

INTRODUCTION

In the seventies, great interest arose in the production of synthetic liquid fuels derived from coal, oil shale, and tar sands Despite the oil glut of the eighties, these alternate fuels are expected to become of great value in the future. Petroleum feedstocks are becoming harder to process as crude quality decreases, and as it becomes more important to process the bottom of the barrel. The alternate feedstocks and heavier petroleum fractions contain higher concentrations of nitrogen compounds than the lighter petroleum crudes. Table I gives the nitrogen content of some representative fossil fuels (1,2,3) Nitrogen compounds lower the grade of the fuels due to the following reasons

1. Fuel bound nitrogen contributes directly to the formation of NOx in combustion processes

2. The activity of catalysts used in cracking (4-6) and other processes (4, 6-8) such as reforming, isomerization, and polymerization is reduced because these catalysts are acidic whereas nitrogen compounds are basic.

3 High nitrogen concentrations are detrimental to both product quality and product stability.

TABLE I

NITROGEN CONTENT OF SOME FOSSIL FUELS

Coals	Wt%	Synthetic Liquids Petroleum Crudes	Wt%
Oil Shale	2.39	SRCI	1.71
Lignite (Glenhowold Mines)	1.01	H-Coal	0.77
		Synthoil	0.97
Sub-bituminous (Big Horn)	1.23	Colorado Shale Oil	2.14
Bituminous (Kentucky #9 and #11)	1.42	El Palito #6 Fuel	0.41
Bituminous (Pittsburgh Steam)	1.61	1000 °F+ West Texas Residuum	0.40
High volatility bituminous (Illinois #6)	1.01		
Anthracite (Black Mountain Pennsylvania)	0.66		

In fact, gums, precipitates and lacquers formed during the storage or use of oils and fuels are directly related to the presence of nitrogen compounds (9-10). In addition, the presence of these compounds, even in trace amounts, leads to poor color and color stability of oils (11-12).

4. Most aromatic nitrogen compounds are biologically harmful and often carcinogenic.

It is necessary to remove the nitrogen from these oils before they can be utilized or processd further. Hydrodenitrogenation is a common process to up-grade these fuels. The oils are reacted with hydrogen which results in the removal of nitrogen as ammonia.

A major portion of the nitrogen present in these fuels is found as heterocyclic compounds, which are usually resistant to hydrodenitrogenation. Nonheterocyclic compounds are present in small concentrations. They include aliphatic amines and nitriles. The latter compounds are relatively more reactive than the previous ones. The low concentrations and relatively high reactivity of these compounds make them of little engineering significance.

Studies on the nature of the nitrogen-containing compounds in petroleum have shown that nitrogen concentration increases with increasing boiling point of the petroleum fractions (13). One or two-ring heterocyclic nitrogen compounds (pyridines, quinolines, pyroles and indoles) are concentrated in the lighter fractions, whereas multiring nitrogen-containing compounds predominate the heavier fractions. Pyridines and quinolines are found in both cracked gasoline and catalytically cracked jet fuel (14) Furthermore, quinolines, benzoquinolines and hydroxybenzoquinolines have been identified in a straight-run heavy-gas oil (15).

Nitrogen concentrations in synthetic liquids are typically two to five times higher than those in petroleum.

Several laboratories have carried out research on the characterization of coal derived liquids. It has been reported that similar types of nitrogen-containing compounds are present in petroleum, coal derived liquids, and shale oils (16-18). Hence, the principles of hydrodenitrogenation (HDN) of petroleum liquids will also apply to the HDN of both coal derived liquids and shale oils. However, the synthetic liquids are difficult to hydroprocess because of high nitrogen content, high aromaticity, and larger molecules.

Design of any hydroprocessing operation for a nitrogen containing feedstock requires an adequate knowledge of HDN kinetics of that feedstock. The feedstock hydroprocessing kinetics are usually obtained from laboratory or pilot plant studies. No predictive technique exists to permit an estimation of HDN kinetics of a crude feedstock from its chemical analysis. Developement of such a prediction technique requires a thorough study of the kinetics of the individual compounds and their mixtures.

Most of the previous HDN kinetic studies have considered either single model nitrogen compounds or a whole coal derived liquid, whereas, little work has been performed to relate the model compound kinetics to the kinetics of the crude oil. These pure compound studies remain of little practical value without the knowledge to predict the kinetics of the whole liquids. Hence, this work is undertaken to study the kinetics of two pure compounds and

their binary mixture. More specifically the objectives of this work are to.

1. Establish reaction networks for the HDN of single compounds, quinoline and acridine.

2. Develop kinetic models for each reaction.

3. Study the interactions between these two compounds in their binary system and the effects of mixing on mechanisms and kinetics of HDN.

CHAPTER II

CHEMISTRY OF COAL LIQUIDS UPGRADING

In general, coal derived liquids are very complex mixtures of hydrocarbons with sulfur, nitrogen and oxygen containing heterocompounds. In addition, they contain traces of organometallic and other inorganic impurities (19). However, coal derived liquids are quite different in composition than petroleum fractions. They contain higher concentrations of polynuclear aromatics and oxygen- and nitrogen-containing compounds. In general, the relative amounts of these compounds depend upon the initial coal and the liquefaction technique (20). The prominent aromatic nitrogen-containing compounds as well as their structures are presented in Figure 1 (21-23).

These heterocompounds can be removed from liquid fossil fuels by hydrotreatment. Hydrotreatment is a mild hydrogenation process where the primary objective is the removal of heteroatoms (19). This process includes hydrodesulfurization (HDS), hydrodenitrogenation (HDN), hydrodeoxygenation (HDO), and hydrodemetalation (HDM). In addition, hydrotreatment causes some hydrogenation of unsaturated bonds with minimal cracking of large molecules. Hydrotreatment is usually achieved in the presence of

PYRIDINE

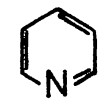

INDOLE

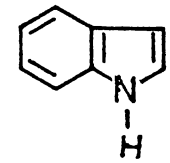

CARBAZOLE

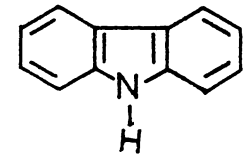

QUINOLINE

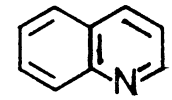

ACRIDINE

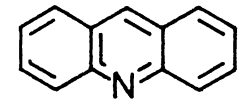

BENZ(C) ACRIDINE

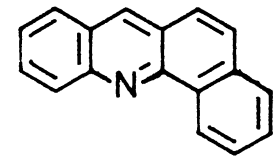

BENZ(A) ACRIDINE

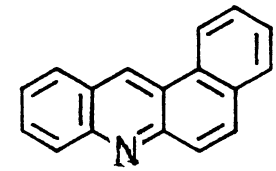

DIBENZACRIDINE

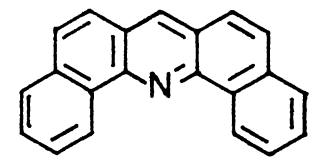

Figure 1. Nitrogen-Containing Compounds in Liquid Fossil Fuels

hydrogen at pressures of 7-14 MPa, temperatures of 300-450°C, and a catalyst. In general, the oxides and the sulfides of Mo and of W are effective catalysts in hydrotreatment. They are usually supported on γ-alumina (Al_2O_3) or silica-alumina (20) and are promoted with Co or Ni oxides. The main reactions which occur can be represented as follows.

Nitrogen containing compound + H_2 --> Hydrocarbon + NH_3

Sulfur containing compound + H_2 --> Hydrocarbon + H_2S

Oxygen containing compound + H_2 --> Hydrocarbon + H_2O

Some degree of aromatic saturation also takes place

From the above discussion, it is clear that the hydrotreatment of liquid fossil fuels includes complex reactions which are achieved on a mixture of a wide variety of organic compounds. Thus, it is difficult to achieve a detailed study of the kinetics and mechanisms of the above reactions. An understanding of hydrotreatment can be gained through studies made on individual compounds which are prominent.

A. Hydrodenitrogenation of Model Nitrogen Compounds

Hydrodenitrogenation (HDN) is the reaction of nitrogen containing compounds with hydrogen leading to a reduction in the nitrogen content of the oil. As a result, nitrogen is removed as ammonia (19).

HDN has received less attention in the literature than HDS. Nevertheless, it has been considered in the last few years as an important part of the heavy fuel hydroprocessing. HDN is a more difficult process than HDS, hence, it requires more severe conditions and consumes more hydrogen (24,25). This large hydrogen consumption is attributed to the obligatory complete saturation of carbon atoms either bound directly to nitrogen or at meta position with respect to the nitrogen atom. This saturation is necessary for HDN both in the presence of sulfur (24,26-28) and in its absence (26,29-34)

The nitrogen containing compounds, present in liquid fossil fuels can be classified into basic compounds, like pyridine, quinoline, and acridine, and non-basic compounds like pyrrole, indole, and carbazole. In general, the HDN mechanism is looked upon as heterocyclic ring hydrogenation, which has been observed to be reversible under most circumstances, followed by hydrogenolysis and subsequent nitrogen removal as NH_3 (20). A literature review of the HDN kinetics is presented here.

A.1. Pyridine

Cox (35) studied the hydrogenation of pyridine and some of its derivatives. He reported that the reaction is first order with respect to pyridine. Furthermore, the reaction order increases with nitrogen concentration in the feed.

McIlvried (36) studied the HDN of pyridine and found that the reaction involves successive steps in the following manner

pyridine --> piperidine --> n-pentylamine -->
n-pentane + ammonia

Since the reaction is complex, he concluded that it would be much helpful to study not only the denitrification of pyridine, but also the denitrification of piperidine and n-pentylamine, hoping that the kinetics of one step could be better understood if the kinetics of the following steps were known. Therefore, he ran his experiments on pyridine, piperidine, and n-hexylamine. The last amine was used since it was immediately available and was expected to have kinetics close to those of n-pentylamine. All runs were made in a bench scale, fixed-bed, flow reactor, using a presulfided Co-Mo/alumina catalyst at 316°C, and a hydrogen pressure in the range of 5.2-10.3 MPa. He found that both the first step in the reaction, the hydrogenation of pyridine to piperidine and the last step, the denitrification of n-pentylamine, are rapid On the other hand, the second step, the ring rupture of piperidine to n-pentylamine is slow. Ammonia appears to be strongly adsorbed on hydrogenation sites, whereas other nitrogen compounds appear to be almost equally strongly adsorbed on denitrification sites or are present in concentrations so small that have no significant effect on kinetics. The data obtained

from piperidine denitrification, fit a Langmuir-Hinshelwood type kinetic model. This model is expressed in the following manner

$$\frac{dP_N}{d(1/LHSV)} = \frac{-0.71\pi P_H P_N}{(1+R)(1+1.57P_{P_o})} \times 10^{-4}$$

This rate expression was then used to develope the following kinetic model for pyridine denitrification,

$$\frac{dP_p}{d(1/LHSV)} = \frac{-4.55\pi P_H P_p}{(1+R)(1+10.5P_A)} \times 10^{-4}$$

where P's are the partial pressures of the components in psia,

R is the gas rate, mole H_2/mole liquid feed,

LHSV is the volumetric liquid hourly space velocity in hr^{-1},

and π is the total pressure in psia.

The subscripts:

H refers to hydrogen,

A refers to ammonia,

N refers to piperidine,

p refers to pyridine,

and o refers to conditions at reactor inlet

Sonnemans et al.(31), studied the pyridine hydrogenation at high hydrogen pressures on Mo/alumina and Co-Mo/alumina catalysts and found the following rate equation.

$$r = kP_p P_{H_2}^n / P_{p_o}$$

Also, they reported that n equals 1.0 at 250°C and 1.5 at 300-375°C. This is a derived rate function assuming strong adsorption of pyridine and its products; all compounds having identical adsorption constants. In addition, the hydrocracking of piperidine has a low order in H_2, which is probably lower than 0.5. Furthermore, the adsorption of nitrogen bases and H_2 appeared to be very strong on alumina and molybdenum-containing catalysts. Adsorption increases in the order of pipridine > pyridine > ammonia. However, H_2 and nitrogen bases adsorb on different sites.

Goudriaan et al. (27), in their experiments to study the effect of H_2S on the HDN of pyridine, hydrogenated pyridine over a Co-Mo/alumina catalyst at about 8.1 MPa pressure and at temperatures of 250-400°C. They found that at high conversions, the temperature required to attain a certain HDN level is about 25°C lower with a presulfided catalyst than with the catalyst in its oxidic state. In addition, the presence of H_2S reduces this temperature by some 60°C. It was also reported that pyridine ring hydrogenation is 25-45% higher on the presulfided catalyst than on the oxidic catalyst. Furthermore, piperidine ring

opening at 250-350°C, on presulfided catalyst is higher than on the oxidic catalyst by 5-15% of the original amount of pyridine. However, the presence of H_2S increases this reaction by another 20-50%. Thus, it can be concluded that the presence of H_2S has two beneficial effects on the HDN of pyridine. First, sulfidic catalyst pyridine-ring-hydrogenation-activity is greater than that of oxidic catalyst. Second, the hydrocracking catalyst activity is increased.

Sonnemans et al. (26) studied the conversion of pentylamine on Mo/alumina catalysts between 250 and 350°C at various hydrogen pressures. Considering the fact that pentylamine is an intermediate compound formed during the HDN of pyridine, they ran their experiments to distinguish whether deamination of pentylamine is rate determining step in this process. Several reactions were observed cracking to pentene and ammonia, hydrocracking to pentane and ammonia, dehydrogenation to pentanimine and butylcarbonitrile, and disproportionation to ammonia and dipentylamine. However, it was reported that, under most of the experimental conditions, the disproportionation reaction with zero order in hydrogen, and -1 order in the inital pentyalamine pressure, attains equilibrium. At 250°C the equilibrium constant is about 9, whereas it is about 5 at 320°C. In addition, dehydrogenation reaction was observed at low hydrogen pressures, and especially at high temperatures and was found to be first order in pentylamine. Both cracking and hydrocracking take place, mainly above

300°C. Furthermore, the rate of cracking is almost independent of the hydrogen pressure while hydrocracking is half order in hydrogen. On the other hand, hydrocarbon formation is of zero order in pentylamine or dipentylamine. Sonnemans et al.(26) reconsidered their previously reported results that the deamination of primary amines is fast compared with the denitrogenation of heterocyclic nitrogen bases (36-38) and that the rate determining step in the denitrogenation of these bases is the hydrogenation of the aromatic ring (39) or the rupture of this ring (36). These considerations, combined with the results of their experiments, led to the conclusion that deamination of primary amines is not rate determining step, may be incorrect.

In a later study on the mechanism of pyridine HDN, Sonnemans et al. (33) ran experiments to investigate the conversion of piperidine on Co-Mo/alumina catalysts as a function of the temperature, reaction time, initial piperidine partial pressure and hydrogen pressure. The following conclusions were drawn from the results.

1. Piperidine is converted into ammonia, pentane and pyridine.

2. N-pentylpiperidine is an intermediate in the ammonia formation.

3. N-pentylpiperidine is converted into ammonia and pentane with the production of piperidine, dipentylamine and pentylamine as intermediate products.

This reaction scheme is presented in Figure 2. It was reported that below 50% piperidine conversion, at 6.1 MPa of hydrogen, piperidine is selectively converted to ammonia and n-pentylpiperidine by a two-step reaction. ring opening to n-pentylamine followed by a fast alkyl transfer from n-pentylamine to piperidine. However, the piperidine conversion is first order in piperidine as well as in hydrogen, whereas it is of minus one order in the total pressure of the nitrogen bases. On the other hand, at higher conversions the rate of formation of pentane and ammonia is affected by the equilibrium constants of the alkyl transfer equilibria and by the rate of the hydrocracking steps. Furthermore, when a ring is present in the nitrogen base, the rate of a hydrocracking reaction is lower. The activation energies of these reactions are 160 kJ/mol, whereas the alkyl transfer reactions have smaller activation energies, about 100 kJ/mol. On the other hand, at one atmosphere hydrogen pressure a completely different product composition was observed.

Satterfield et al. (32) reported that the equilibrium between pyridine and piperidine can be a rate-limiting factor under some conditions. Thus, a maximum in the pyridine HDN rate occurs at about 400°C over Ni-Mo/alumina catalyst at 1100 kPa pressure. This maximum is caused by a thermodynamic limitation on the allowable concentration of piperidine. In addition, Ni-Mo/alumina catalyst appears to have greater hydrogenation-dehydrogenation activity than

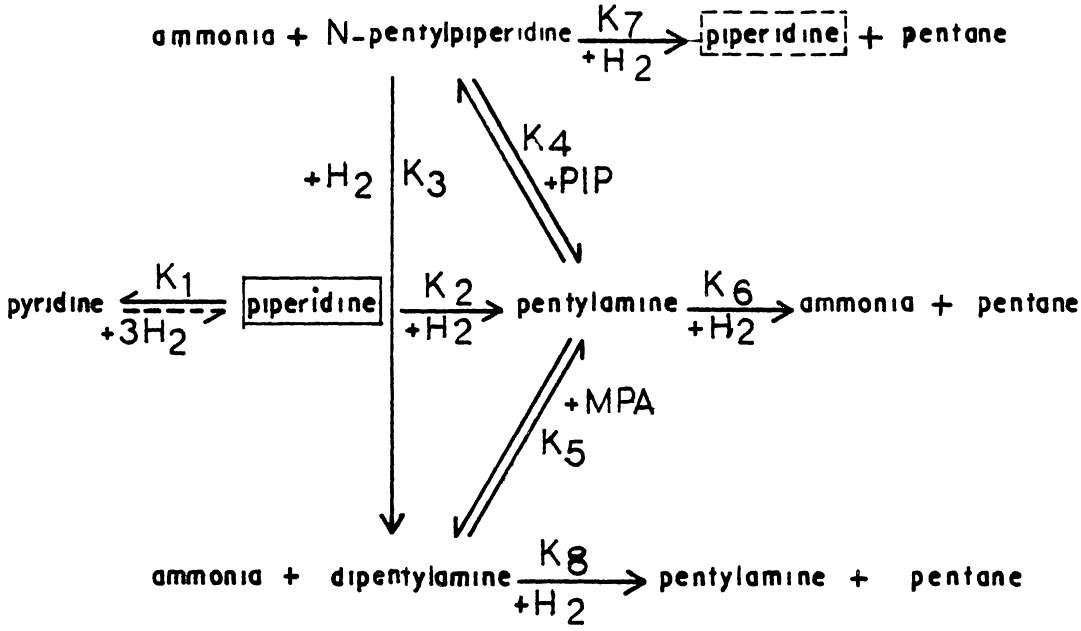

Figure 2. Reaction Network of Piperidine HDN, at 6 1 MPa, Co-Mo/Alumina (33)

have greater hydrogenation-dehydrogenation activity than Co-Mo/alumina catalyst, whereas the latter has greater hydrogenolysis activity, at least at about 300°C and below

Anabtawi et al. (40) studied the vapor-phase hydrogenation of pyridine in an integral flow reactor over a Ni-W/alumina catalyst. The kinetics of the hydrogenation of pyridine to piperidine as well as the effects of various parameters have been investigated. They concluded that hydrogenation of pyridine proceeds through the following main reactions

1 Saturation of pyridine double bonds to form piperidine.

2. Disproportionation of piperidine to form ammonia and n-pentylpiperidine.

3 Formation of n-pentane from n-pentylpiperidine.

In addition, adsorption of hydrogen was found to be the rate-controlling step. Furthermore, the apparent rate constant is inversely proportional to the intial pressure of pyridine. The following rate expression was developed

$$r = -\frac{d[P_p]}{dt} = (P_p)(P_{H_2})\left(\frac{k_s}{[P_{p_o}]} + k_1\right)$$

where $[P_p]$ is the partial pressure of pyridine in N/m^2,

$[P_{p_o}]$ is the initial partial pressure of pyridine in N/m^2,

F is flow rate of feed, moles/hr,

k_1 is reaction rate constant in a plot of k_{ov}

vs $1/[P_{p_o}]$, mole/(g.cat)(hr)(N/m^2),

k_{ov} is the observed rate constant for hydrogenation of pyridine, mole/(g.cat)(hr)(N/m^2),

k_s is the reaction rate constant slope in a plot of k_{ov} vs $1/[P_{p_o}]$, mole/(g.cat)(hr),

and t is W/F, time (g.cat)(hr)/gmole.

Also, the average activation energy was reported to be 57.3 kJ/mol.

Satterfield et al (25), investigating the intereactions between catalytic HDS of thiophene and HDN of pyridine, observed that pyridine inhibits the HDS reaction, whereas sulfur compounds have a dual effect on HDN. At low temperatures, thiophene inhibits the reaction by competing with pyridine for hydrogenation sites which retards the conversion of pyridine to piperidine and hence reduces the overall reaction rate. On the other hand, at high temperatures, H_2S, an HDS reaction product, interacts with the catalyst to improve its hydrogenolysis activity and hence increases the rate of piperidine hydrogenolysis, which is rate controlling under these conditions, leading to an increase in the overall HDN rate.

Satterfield et al. (41) recently studied the simultaneous HDN of pyridine and HDS of thiophene over Ni-Mo/alumina catalysts. Each of thiophene and pyridine had a partial pressure of 12.4 kPa whereas total pressure varied between 1.14 and 7.0 MPa at temperatures of 200-400°C. It was observed that pyridine inhibits thiophene HDS at all

temperatures and pressures studied. On the other hand, pyridine-piperidine equilibrium is attained, in the absence of thiophene, above 350°C at all pressures whereas, in its presence, the equilibrium is not attained because of both pyridine hydrogenation inhibition and enhancement of piperidine hydrogenolysis. Furthermore, the overall conversion of pyridine and piperidine as a pair is increased by the presence of thiophene at pressures of 3.55 and 7.0 MPa as long as the temperature is greater than 300°C.

A.2. Quinoline

Kobe and McKetta (42) reported the following mechanism for quinoline HDN.

Quinoline + H2 --> 1,2,3,4-tetrahydroquinoline -->
(Py-THQ)
amines --> propylbenzene + ammonia
(PB)

Flinn et al. (37), studying the HDN of quinoline over a presulfided Ni-W/Al_2O_3 in a high purity paraffin oil, found that the reaction is first order with respect to quinoline. However, it was reported that the reaction involves ring hydrogenation which is the rate-controlling step, preceeding any nitrogen removal.

Doelman and Vulgter (38) performed their experiments in a fixed bed reactor using a Co-Mo/alumina catalyst. They found that at low temperatures the pyridine ring of

quinoline is hydrogenated resulting in Py-THQ. Around 300°C some 90% of the quinoline is converted into Py-THQ At higher temperature its quantity declines, partly because, above 350°C 5,6,7,8-Tetrahydroquinoline (Bz-THQ) is also formed. Formation of the latter compound is favored by higher temperatures and also by lower feed rates. However, the quantity of Py-THQ present in the reaction products declines more rapidly with increasing temperature than that of the Bz-THQ isomer. The more rapid decline must be attributed to the opening-up of the nitrogen containing ring, which gives rise to various amines. In addition, to the previous compounds, γ-phenylpropylamine was found among the HDN products in most cases, though in small quantities. This compound is expected to result from the breakage of the C-N bond in Py-THQ and it seems likely that NH_2 group splits easily from it. Also, considerable quantities of anilines were found in the HDN products of quinoline. These included aniline, o-toluidine or o-methylaniline (OMA), o-ethylaniline (OEA), and o-propylaniline (OPA). OPA is formed by the breaking of a C-N bond in Py-THQ. The other anilines may have originated either from complete or partial elimination of the alkyl group from OPA, or from breakage of one of the C-C bonds in the nitrogen-containing ring in Py-THQ, giving rise to the formation of an unsubstituted or ortho-substituted N-alkylaniline. However, N-alkylanilines have never been found in the reaction products, but this may be due to their rapid

conversion into an aniline and a hydrocarbon (methane, ethane, or propane). In fact, all of the products of HDN of quinoline can be explained as having been formed from Py-THQ rather than from Bz-THQ, hence they concluded that Bz-THQ is more stable than Py-THQ. Only at very low space velocities, butylpyridine has been observed which must have originated from Bz-THQ. However, the decahydroquinoline (DHQ) formed at these low velocities is probably also derived from this isomer. Furthermore, indole was found in small amounts at the higher HDN temperatures.

Aboul-Gheit et al. (29), working on the HDN of quinoline in paraffin oil over oxidic Co-Mo/alumina catalysts, proposed a mechanism almost similar to that of Kobe and McKetta, with OPA as a reaction intermediate. However, it was assumed that the first step, the hydrogenation, is too fast, whereas the second step, the ring rupture, is rate determining. Also, it was found that the reaction exhibits first order kinetics with respect to total nitrogen content and an activation energy of 125.5 kJ/mol was reported.

Shih et al. (28) also studied quinoline HDN in an attempt to determine the reaction network as well as reaction kinetics Trying to work as closely relevant to practical industrial conditions as possible, they ran their experiments in a 1-liter autoclave using presulfided HDS-9A catalyst and a highly paraffinic white oil as a solvent under a total pressure of 3.4 MPa and a temperature of

342°C. Moreover, an amount of CS_2 equivalent to 0.05 wt.% of the carrier oil was added to the catalyst and quinoline to maintain the catalyst in the sulfided form during the reaction. However, it was concluded that HDN of quinoline is a complex reaction which involves hydrogenation, hydrogenolysis of the resulting piperidine ring and subseqent deamination. Hydrogenation takes place through two routes, the pyridine-ring-hydrogenation route leading to the formation of Py-THQ, and the benzenoid-ring-hydrogenation route leading to the formation of Bz-THQ. Also, these two routes, by subsequent hydrogenation, produce DHQ as another reaction intermediate. Nitrogen removal takes place mainly through the hydrogenolysis of DHQ. The reaction network is shown in Figure 3. It was also reported that the hydrogenation reactions are first order with respect to nitrogen content, whereas they are second order in hydrogen. On the other hand, the hydrogenolysis reactions are first order in nitrogen content. However, the hydrogenolysis of Py-THQ is first order in hydrogen, whereas, the hydrogenolysis of DHQ is zero order in hydrogen.

Satterfield et al. (43) studied the intermediate reactions in the HDN of quinoline in the vapor phase over a sulfided Ni-Mo/alumina catalyst. The experiments were run in a continuous-flow microreactor at 3.4 MPa and 6.9 MPa, and at temperatures of 230 to 420°C, with quinoline partial pressures of about 13 to 110 kPa. It was found that quinoline is rapidly hydrogenated to an essentially equilibrium

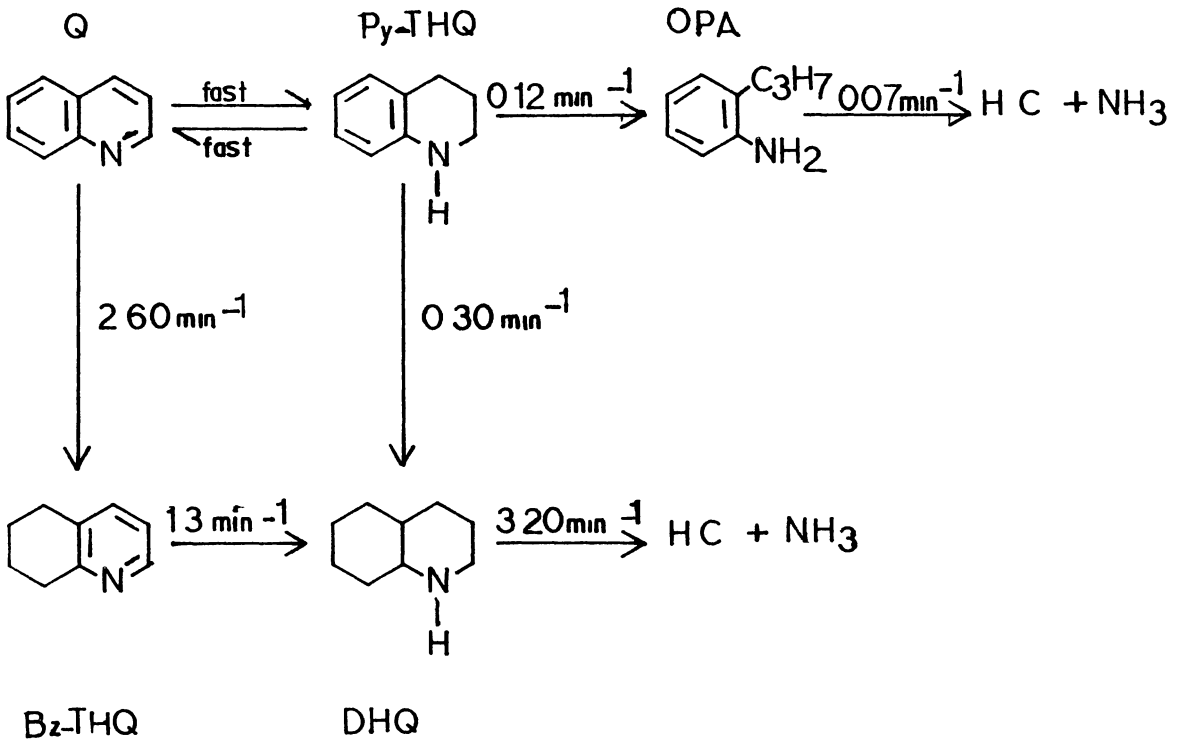

Figure 3. Reaction Network of Quinoline HDN, at 342°C, 13.7 MPa, Ni-Mo/Alumina Catalyst (28)

concentration of Py-THQ. The reaction mechanism is complex, but, considering the previous studies and their experimental results, they suggested the mechanism presented in Figure 4. All the species in the proposed mechanism were identified except for propylcyclohexylamine (PCHA), but it is thought to be a plausible intermediate. However, it was found that the dominating inital reaction pathway varies with temperature. At low temperatures quinoline concentration is much less than that of Py-THQ and thus the latter is converted via the pathways II and VIII, whereas at higher temperatures the equilibrium concentration of Py-THQ is much diminished relative to quinoline and hence reaction path IV becomes significant. On the other hand a significant fraction of quinoline was found to react, under extreme conditions, leading to the formation of various high molecular weight substances including some nitrogen-containing compounds. However, these compounds may be difficult to react further.

Bhinde (44) developed a high-pressure liquid-phase flow microreactor and used it for studying quinoline HDN. Also, the relative reactivites of three dimethylquinolines were determined in a batch autoclave reactor at 350°C and 3.4 MPa over presulfided Ni-Mo/alumina catalyst. Moreover, the interaction effects that occur during simultanous HDN, HDS, and hydrogenation were investigated. For this purpose, HDN of quinoline and indole, HDS of dibenzothiphene and hydrogenation of naphthalene were studied in a batch

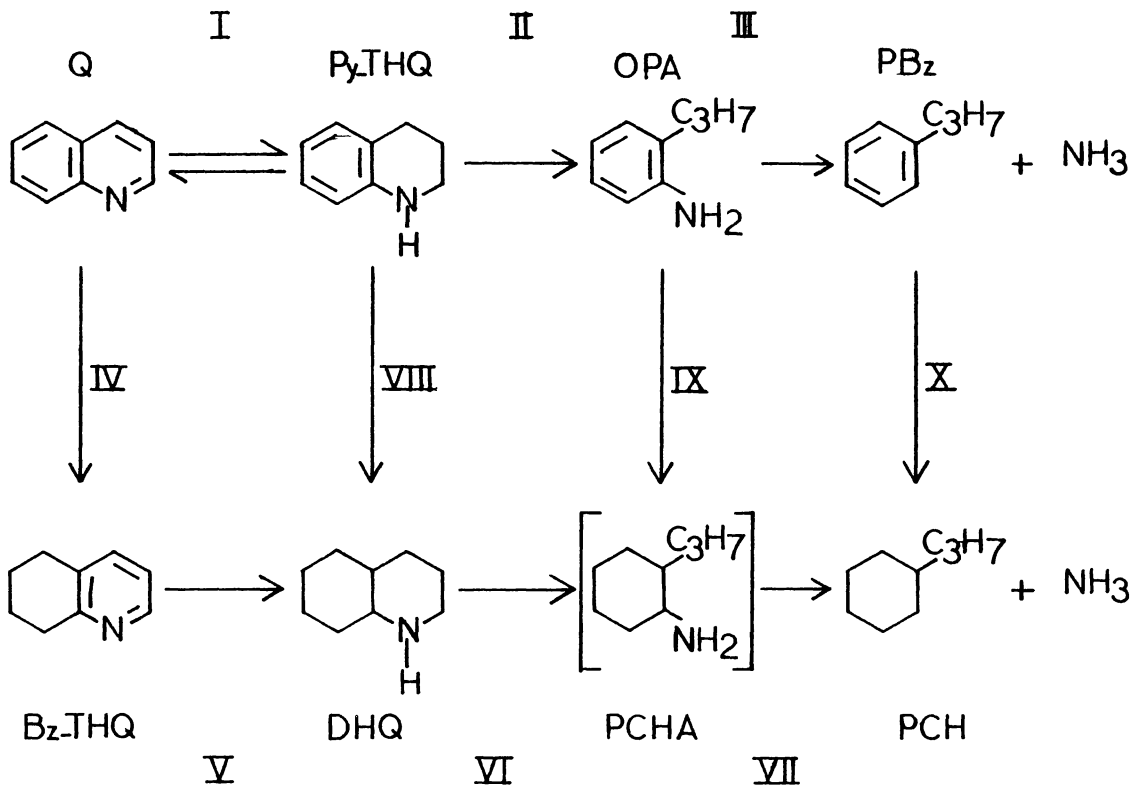

Figure 4. Reaction Network of Quinoline HDN, at 230-420°C, 3.6-7.0 MPa, Ni-Mo/Alumina Catalyst (43)

autoclave under commercial reaction conditions. He proposed a reaction network for quinoline HDN similar to that suggested by Shih et al. He found that quinoline, and Py-THQ rapidly attain thermodynamic equilibrium, and that the rate of total nitrogen removal, the disappearance of the lumped group of quinoline, Py-THQ and other individual reactions follow pseudo-first order kinetics. Also, OPA was found refractory towards HDN and most nitrogen removal occurs through hydrogenolysis of DHQ. In addition, the rate constants in quinoline HDN are reduced by increasing quinoline concentration, whereas the rate of total nitrogen removal increases. Furthermore, it was reported that indole, naphthalene, dibenzothiophene and their reaction products have a slightly negative effect on the kinetics of HDN of quinoline. However, it was found that the reactant molecule is absorbed on one type of catalytic site and hydrogen is adsorbed on a different one.

Cocchetto et al. (45) studied the chemical equilibria in the HDN of quinoline. Equilibrium constants were calculated for significant reaction pathes. It was concluded that HDN reaction pathways, of minimum hydrogen consumptions are not thermodynamically favored under industrial conditions. Thus, the burden of selectively hydrogenating only the hetero-ring is laid on the catalyst. They reported the mechanism shown in Figure 5.

Satterfield et al. (46) investigated reaction network and kinetics of the HDN of quinoline in the vapor phase.

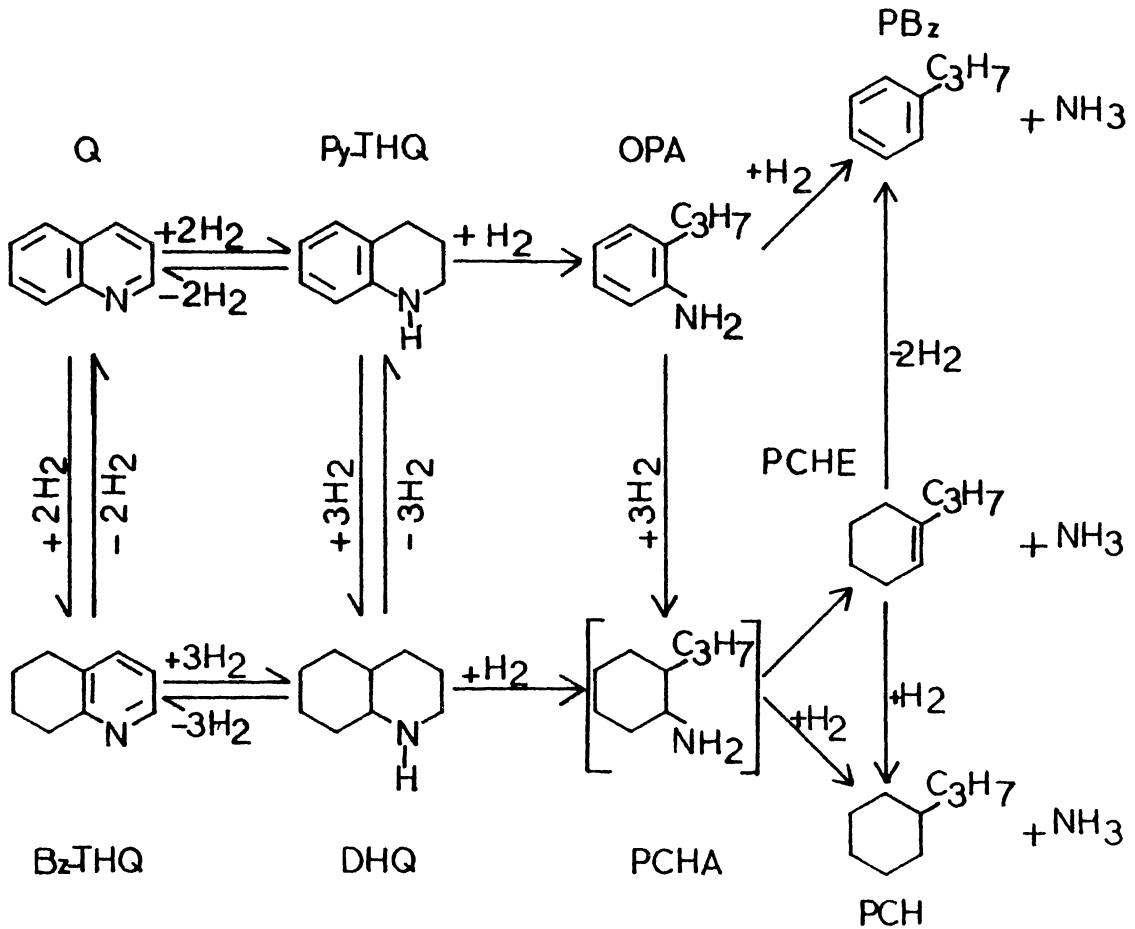

Figure 5 Reaction Network of Quinoline HDN at 330-420°C, 3 6-7.0 MPa, Ni-Mo/Alumina Catalyst (45)

They ran their experiments in a continuous-flow microreactor at 3.55 and 7.0 MPa, 330-420°C, and over presulfided Ni-Mo/alumina catalysts. HDN processes were carried out on quinoline and each of the intermediate HDN products individually. PCH was found to be the predominant product. All the reactions between quinoline and its hydrogenated heterocyclic derivatives were found reversible. However, the complex kinetic behavior, observed in the HDN of quinoline, can be explained by considering the equilibrium limitations on the intial ring hydrogenation reactions as well as the wide variation between the absorptivities of various nitrogen-containing compounds present in the reaction mixture at a certain time. In addition, the following kinetic model was developed for the denitrogenation of OPA.

$$-r_{OPA} = \frac{k'_1 \, P_{OPA}}{P_{OPA} + (K_{NH_3}/K_{OPA})(P_{OPA,o} - P_{OPA})}$$

where, r_{OPA} is the net rate of formation of OPA,

k'_1 is the pseudo-rate constant for OPA denitronation,

K is the adsorption equilibrium constant,

P_{OPA} is the paritial pressure of OPA,

and $P_{OPA,o}$ is the P_{OPA} at the reactor inlet conditions.

If it is assumed that $(K_{NH3}/K_{OPA}) = 1$, equal adsorptivities of OPA and NH_3, a pseudo-first order rate expression results. On the other hand, if $(K_{NH3}/K_{OPA}) = 0$, negligible adsorption of ammonia, zero-order kinetics are developed.

Furthermore, another model was established for the kinetics of the Py-THQ hydrogenolysis to OPA and hence its conversion to hydrocarbons and NH_3. Thus, the net rate of formation of OPA in this case is given by the following expression.

$$r_{OPA} = \frac{k_2' K_{SA} P_{Py\text{-}THQ} - k_1' K_{AA} P_{OPA}}{K_{AA} P_{AA} + K_{SA} P_{SA} + K_{NH_3} P_{NH_3}}$$

where, k_2' is the pseudo-rate constant for hydrogenolysis of Py-THQ to OPA,

AA is a subscript for the aromatic amines, quinoline, Bz-THQ, and OPA,

and SA is a subscript for the secondary amines, Py-THQ and DHQ.

In this expression it is assumed that the secondary amines adsorb equally strongly, with an adsorption equilibrium constant K_{SA} and also aromatic amines are likewise assumed to have equal adsorption equilibrium constant K_{AA}.

Satterfield and Gültekin (47), studying the effect of H_2S on the catalytic HDN of quinoline in the vapor phase, found that H_2S has a slight inhibiting effect on the intermediate hydrogenation steps, whereas it has a marked accelerating effect on the intermediate hydrogenolysis steps. This accelerating effect reached its maximum when the H_2S partial pressure was increased until (H_2S/quinoline) molar ratio is about 1. However, the net effect of H_2S presence

is an increase in the overall HDN rate. In addition, they observed a primary limiting factor on the overall HDN rate, working on commerical Ni-Mo/alumina catalysts. This factor is the very strong adsorption of secondary amines formed as reaction intermediates. Furthermore, rate constants as well as activation energies were reported for most of the intermediate steps for a set of standard conditions in the presence as well as in the absence of H_2S.

In a recent study, Satterfield and Carter (48) investigated the effect of water vapor on the catalytic HDN of quinoline. They ran their experiments at 7 MPa total pressure on a Ni-Mo/alumina catalyst. It was observed that water vapor, at 13.3 kPa partial pressure moderately accelerates certain reactions, whereas it moderately inhibits others. Consequently, there is a little net effect on the overall rate at 330 and 375°C, whereas there is a slight inhibiting effect at 420°C. However, under these experimental conditions, the enhancement effect of H_2S on the HDN rate is not significantly affected.

Satterfield and Yang (49) investigated catalytic HDN in a trickle-bed reactor. The purpose of their work was primarily to compare the reaction network of quinoline HDN with that in the vapor phase, under as nearly identical conditions as possible. Studies were performed over a commercial Ni-Mo/alumina catalyst, HDS-3A at 350,375, and 390°C and 6.9 MPa. Quinoline and various reaction intermediates were used in the experiments. It was reported

that the reaction rate constants for the various HDN reactions, in the presence of an inert paraffin liquid are very similar to those for the same reactions in the vapor phase, although the liquid tends to equalize the adsorptivities of the various nitrogen compounds. In both liquid-and vapor-phase, the overall HDN reaction is zero order under the conditions studied. However, equilibrium is rapidly attained between quinoline and Py-THQ in both cases. In addition, homogenous reactions are negligible except for the hydrogenation of quinoline to Py-THQ. A revised reaction network has been proposed as shown in Figure 6.

Yang and Satterfield (50) reported that the presence of H_2S (generated in situ from CS_2) somewhat inhibits hydrogenation and dehydrogenation reactions in quinoline HDN, whereas, it markedly accelerates hydrogenolysis reactions, for a net increase in the overall rate of HDN. These effects are similar to those observed previously in vapor-phase HDN.

Satterfield and Smith (51), in a more recent study of the effect of water on the HDN of quinoline, ran their experiments at 375°C and 6.9 MPa on a presulfided Ni-Mo/alumina catalyst. They found some conflict between conclusions from their work and previous ones, about the effect of H_2S on the individual reactions in HDN of quinoline. It was reported that H_2S markedly increases hydrogenolysis rates. It increases also hydrogenation rates moderately whereas previously it was concluded that it slightly de-

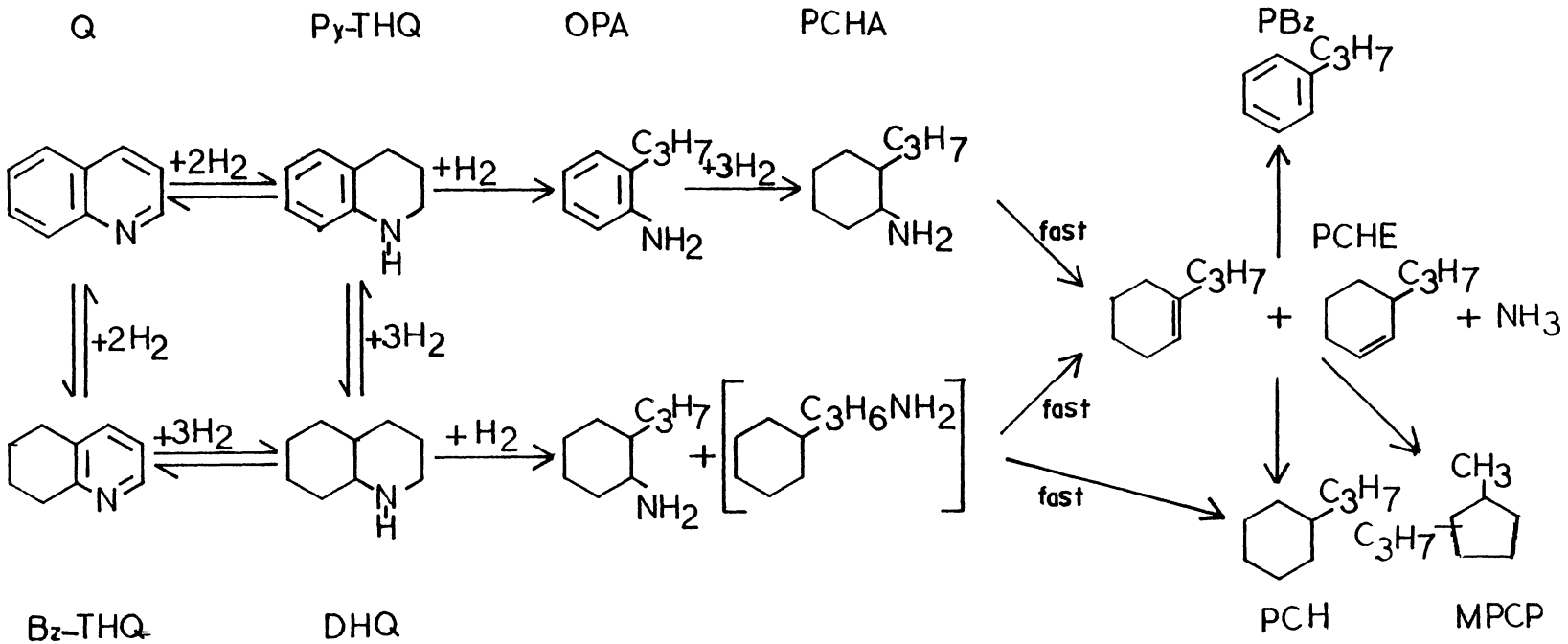

Figure 6. Reaction Network of Quinoline HDN, at 350-390°C, 6.9 MPa, HDS-3A Catalyst (49)

creased hydrogenation rates. However, water vapor was found to moderately increase the HDN rate of quinoline, in either presence or absence of H_2S. Water vapor does not significantly affect hydrogenation reactions but increases hydrogenolysis.

Miller et al. (52) studied the HDN of quinoline over two sulfided Co-Mo catalysts. One catalyst was supported on alumina whereas the other was supported on 50% alumina, 50% ultrastable faujasite zeolite. The purpose of this study was to determine under what conditions non-first-order kinetics can be observed for quinoline HDN and how experimental conditions influence the observed kinetic order. However, it was found that the HDN reaction order determined from a power law kinetic model is not first order, but less than first order with respect to nitrogen concentration. A Langmuir-Hinshelwood kinetic model, in which it was assumed that ammonia is weakly adsorbed on the catalyst, was successful for interpretation of the data. It was concluded that, for low nitrogen feeds, the kinetics are first order. In addition, high reaction temperatures can also lead to first order kinetics by reducing the magnitude of nitrogen adsorption equilibrium constant. This is a function of the catalyst support acid strength. Weakly acidic catalysts have smaller equilibrium adsorption constants and give more nearly first-order kinetics.

A. 3. Isoquinoline

Kobe and McKetta (42) suggested the mechanism presented in Figure 7 for the HDN of Isoquinoline.

A.4. Acridine

Zawadzki et al. (1,20) studied the HDN of acridine at 342°C and 13.8 MPa over a presulfided Ni-Mo/alumina catalyst and developed the mechanism presented in Figure 8. The system showed first-order kinetic behavior with respect to the removal of acridine as well as to total nitrogen content. For this reason, pseudo-first order kinetics was used in modeling each reaction in the reaction network. network. The rate constant for each individual reaction in the network is given on the arrow for the reaction. A carbon-nitrogen bond scission in an aromatic ring does not take place before ring hydrogenation. The nonselective nature of the catalysts for nitrogen removal, is apparent from the rate constants reported in the reaction network. This nonselective nature, in contrast to sulfur removal, in which catalysts show high selectivity towards direct sulfur removal, results in high hydrogen consumption. However, Gates et al. (53) observed that increasing hydrogen pressure results in a non-liner increases in the rate of acridine HDN. Also, it was found that HDN is strongly dependent on temperature with an activation energy of 146 kJ/mol for total nitrogen removal.

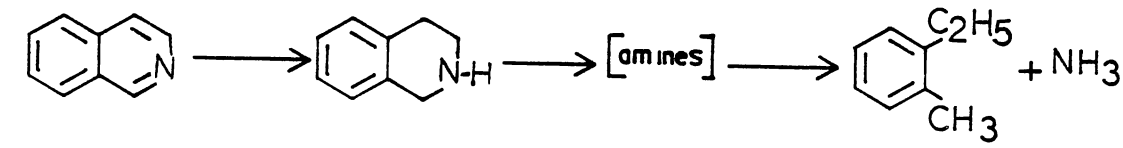

Isoquinoline 1,2,3,8- tetrahydro- isoquinoline o- ethyltoluene

Figure 7 . Reaction Network for Isoquinoline HDN (42)

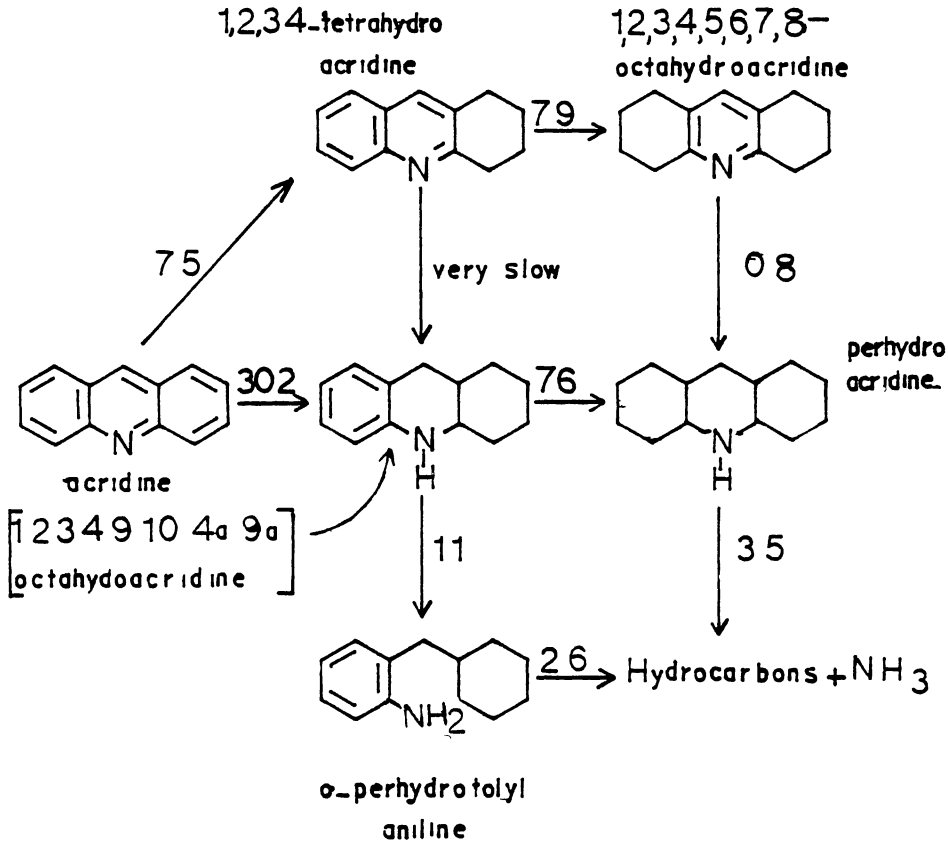

Figure 8. Reaction Network for Acridine HDN at 342°C, 13.7 MPa, Ni-Mo/ Alumina Catalyst (33,20)

Nagai et al. (54) studied the HDN of acridine on a prereduced Mo/alumina catalyst in an attempt to establish the mechanism of the reaction. The experiments were carried out in a flow microreactor using xylene solutions containing 0.1-1.0 wt% acridine at temperatures of 200-350°C, and total pressure of 2.5-14.7 MPa. It was observed that acridine easily hydrogenated to 9,10-dihydroacridine (DHA) even below 200°C. DHA was hydrogenated successively to 1,2,3,4,4a,9,9a,10-octahydroacridine (OHA) and perhydroacridine (PHA), which was denitrogenated to dicyclohexylmethane (DCHM) above 300°C. Their proposed reaction mechanism is presented in Figure 9. The activation energy for the formation of DCHM was found to be 133.9 kJ/mol. The rate equation developed was:

$$r = k \frac{K_{PA} \cdot K_{H_2} \cdot C_{PA} \cdot P_{H_2}}{[1 + K_{PA} \cdot C_{PA} + K_{H_2} \cdot P_{H_2}]^2}$$

where, r is the rate of formation of DCHM,

C_{PA} is the partial pressure of PHA,

P_{H_2} is the partial pressure of H_2,

and k, K_{PA} and K_{H_2} are constants. It was also reported that the hydrogenation of acridine to perhydroacridine is in equilibrium at higher temperatures and the rate-determining step is the transformation of PHA to DCHM.

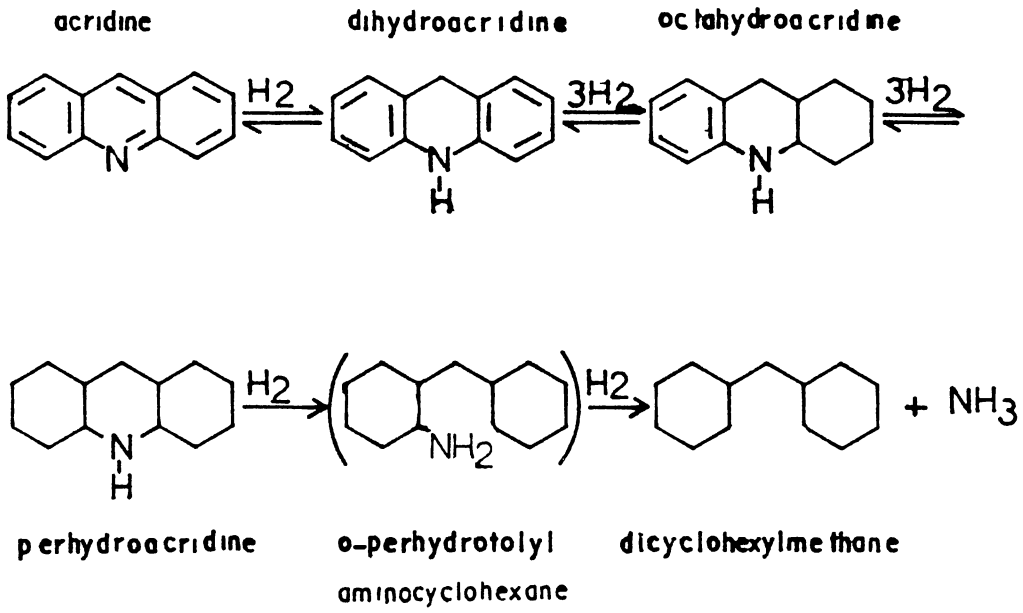

Figure 9. Reaction Network for Acridine HDN, at 200-350°C, 2.5-14.6 MPa, Prereduced Mo/Alumina Catalyst (54)

A.5. Indole

Kobe and McKetta (42) suggested the mechanism presented in Figure 10 for the HDN of indole.

Qader et al. (55) studied the kinetics of the hydroremoval of S,O, and N from a low temperature coal tar They reported that these hydroremoval reactions are all of first order with respect to the heterocyclic molecules and that the rupture of the C-S, C-O, and C-N bonds of these molecules is the rate-controlling step. However, several authors have found that HDN follows first order kinetics (37,55-57). On the other hand, other investigators claimed a first order for HDN of the 6-membered compounds, such as pyridine,and second order for the 5-membered compounds such as indole (38,58).

Aboul-Gheit et al. (29) made a study on the HDN kinetics of some nitrogen compounds over Co-Mo/alumina catalysts. They found that HDN of both basic and non-basic compounds follows a psuedo-first order kinetics. Also, the activation energy for indole HDN was found to be 18.5 kcal/mol Indole HDN was suggested to proceed in the scheme presented in Figure 11 with the first step as the rate controlling step.

Aboul-Gheit (59), in a later study, investigated the kinetics of HDN of indole in paraffin oil over Co-Mo/alumina in a stirred batch autoclave at temperatures between 350-400°C and a hydrogen pressure between 4.1-20.3 MPa.

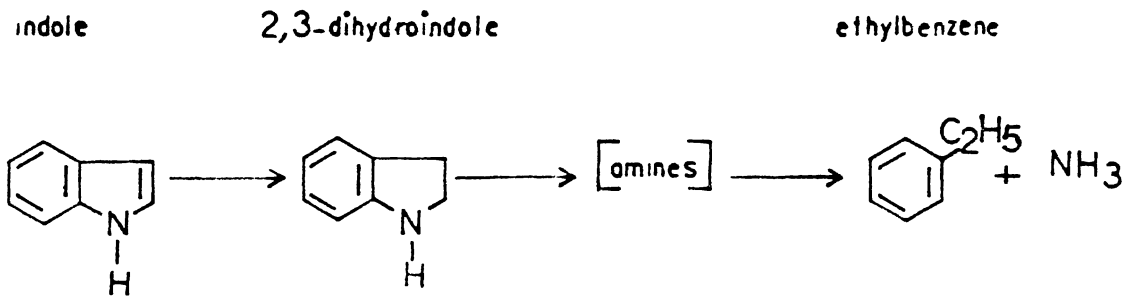

Figure 10. Reaction Network for Indole HDN (56)

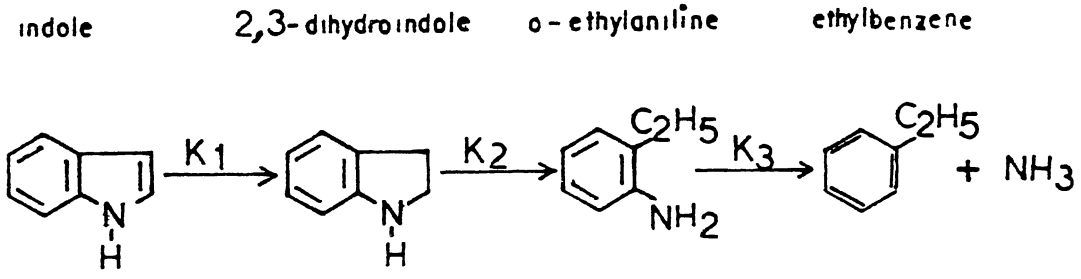

Figure 11. Reaction Network for Indole HDN at 350-400°C, 20.2 MPa, Co-Mo/Alumina Catalyst (29)

The overall rate constant and the rate constants for the three reaction steps were represented by the following equations:

$$k_o = 0.611X10^3 \exp(-20,400/RT) \quad s^{-1}$$
$$k_1 = 0.121X10^2 \exp(-14,865/RT) \quad s^{-1}$$
$$k_2 = 0.590X10^3 \exp(-18,480/RT) \quad s^{-1}$$
$$k_3 = 0.246X10^2 \exp(-14,880/RT) \quad s^{-1}$$

Stern (60) studied the HDN of some nitrogen containing heterocyclic compounds trying to develope the reaction mechanism. The experiments were run in an autoclave at 350°C and 6.9 MPa, using a mixture of 95% H_2 and 5% H_2S The partial pressure of H_2S was maintained during the reaction to keep catalysts in a fully sulfided condition as well as to simulate hydrotreating conditions of heavy feedstocks which contain nitrogen and sulfur simultaneously. However, the indole HDN was found to be a stepwise process with the nitrogen-ring hydrogenation as the first step which leads to the formation of 2,3-dihydroindole and o-ethylaniline (OEA) as intermediate products. OEA is subsequently converted to ethylcyclohexane either through ring hydrogenation and ammonia elimination which is the predominant reaction path or via direct hydrogenolysis which occurs to a lesser extent. This mechanism is shown in Figure 12.

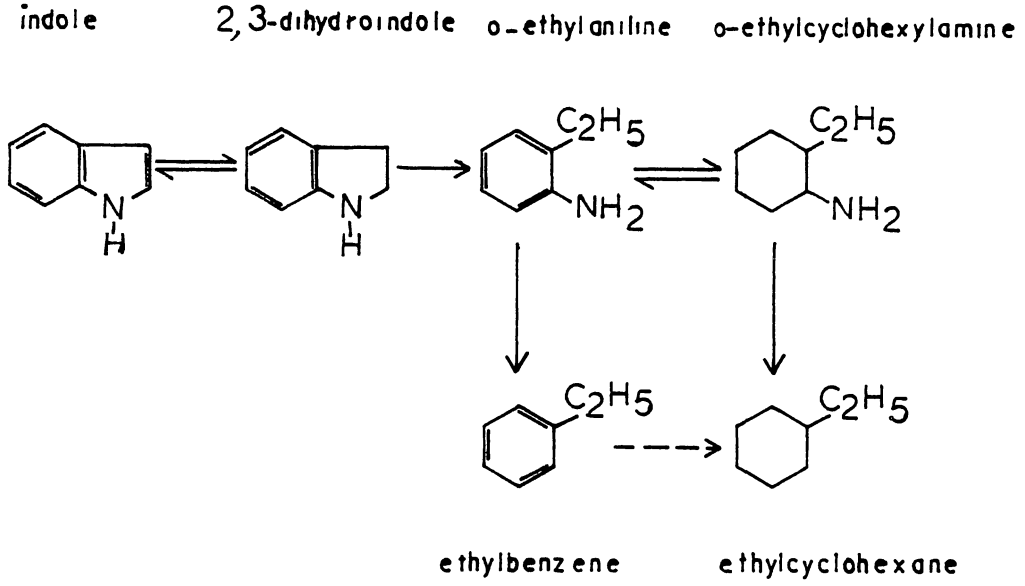

Figure 12. Reaction Network for Indole HDN at 350°C, 6.9 MPa (60)

A.6. Carbazole

Kobe and McKetta (42) suggested the mechanism presented in Figure 13 for the HDN of carbozole.

Stern (60), studied the HDN of carbazole at a temperature of 350°C, under 6.9 MPa, using Harshaw 0402T, Harshaw HT100 and some in house prepared catalysts Re/Al_2O_3 and $Co\text{-}Re/Al_2O_3$. He observed that 1,2,3,4-tetrahydrocarbazole (THC) was the prime product obtained from the HDN of carbozole. In addition, minor amounts of biphenyl and phenylcyclohexane was observed. However, the reason of the absence of hexahydrocarbazole (HHC) the expected intermediate, is not clear. The hydroprocessing conditions may be unfavorable for the formation of such an intermediate or, less likely, its rate of formation is very small compared with its rate of denitrogenation.

Gates et al. (61) investigated the HDN of carbazole under conditions similar to those used for acridine. It was observed that THC is the major intermediate compound present in the product. On the other hand, both cis-hexahydrocarbozole and octahydrocarbazole (OHC) are minor reaction products. However, both carbazole disappearance and total nitrogen removal can be represented as first order reactions. It was also observed that carbazole reactivity is slightly less than that of quinoline and acridine is the least reactive.

Takkar et al. (62) studied the HDN of an SRC-I

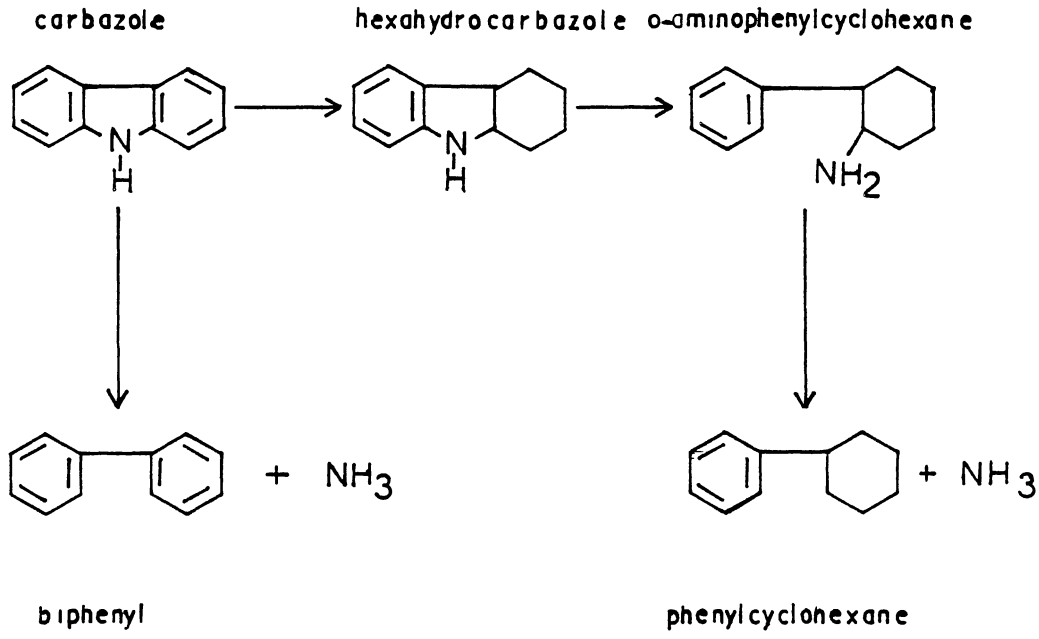

Figure 13. Reaction Network for Carbazole HDN (42)

recycle solvent over a Ni-Mo/alumina catalyst using a trickle-bed reactor. Kinetics of total nitrogen and carbazole removal were examined. They found that nitrogen compounds, other than carbazole, were essentially completely removed or rendered indistinguishable by HDN, hence, concluded that carbazoles are a good model for the less-reactive nitrogen compounds in coal derived liquids. Carbazole HDN was represented by a first order rate equation.

$$-\ln(1-X_C) = k'/LHSV$$

where X_C is the fractional conversion of carbazole,
k' is the first order reaction rate constant, (hr^{-1}),
and LHSV is the liquid hourly space velocity, (hr^{-1}).

Also, the activation energy was estimated to be 51.6 kJ/mol with the frequency factor 3.19 s^{-1}.

Nagai et al.(63), studied the HDN of carbazole in a high pressure flow microreactor over a prereduced Mo/alumina catalyst, using a solution of 0.25 wt% carbazole in xylene. The reaction was performed at 270-310°C under a total pressure of 10.1 MPa. It was observed that carbazole hydrogenates through 1,2,3,4,-THC to perhydrocarbazole (PHC), which denitrogenates to bicyclohexyl. The rate of denitrogenation increases with an increase in temperature. However, bicyclohexyl undergoes isomerization and ring

opening above 300°C to yield ethylbicyclo [4.4.0] decane and hexylcyclohexane. The apparent activation energy for the rate of formation of bicyclohexyl is 126.8 kJ/mol. Furthermore, it was observed that hydrogenation of carbazole to PHC is in a quasi-equilibrium at high temperatures and that the HDN of PHC is the rate-determining step. Suggested reaction scheme is presented in Figure 14.

B. Hydrodenitrogenation of Coal Derived Liquids

Several investigators have studied the kinetics of HDN in coal derived liquids. Two general approaches have been used to model the HDN a power law model often resulting in a first or second order kinetics or a combination of first order models applied to reactive and non reactive oil fractions. Seapan and Crynes (19) have reviewed the hydrotreatment kinetics in the literature. A brief review to the extent of interest of this project is presented here.

B.1 First Order Models.

Qader et al. (55), investigated the kinetics of HDS, HDN and HDO of a low temperature coal tar, boiling range 200-235°C, over a WS_2 catalyst. They reported that heteroatoms can be completely removed at 500°C and a pressure of 10.3 MPa. The data showed that the HDS, HDN, and HDO are all first order with respect to the heterocyclic molecules. Furthermore, HDS was found to follow a true Arrhenius

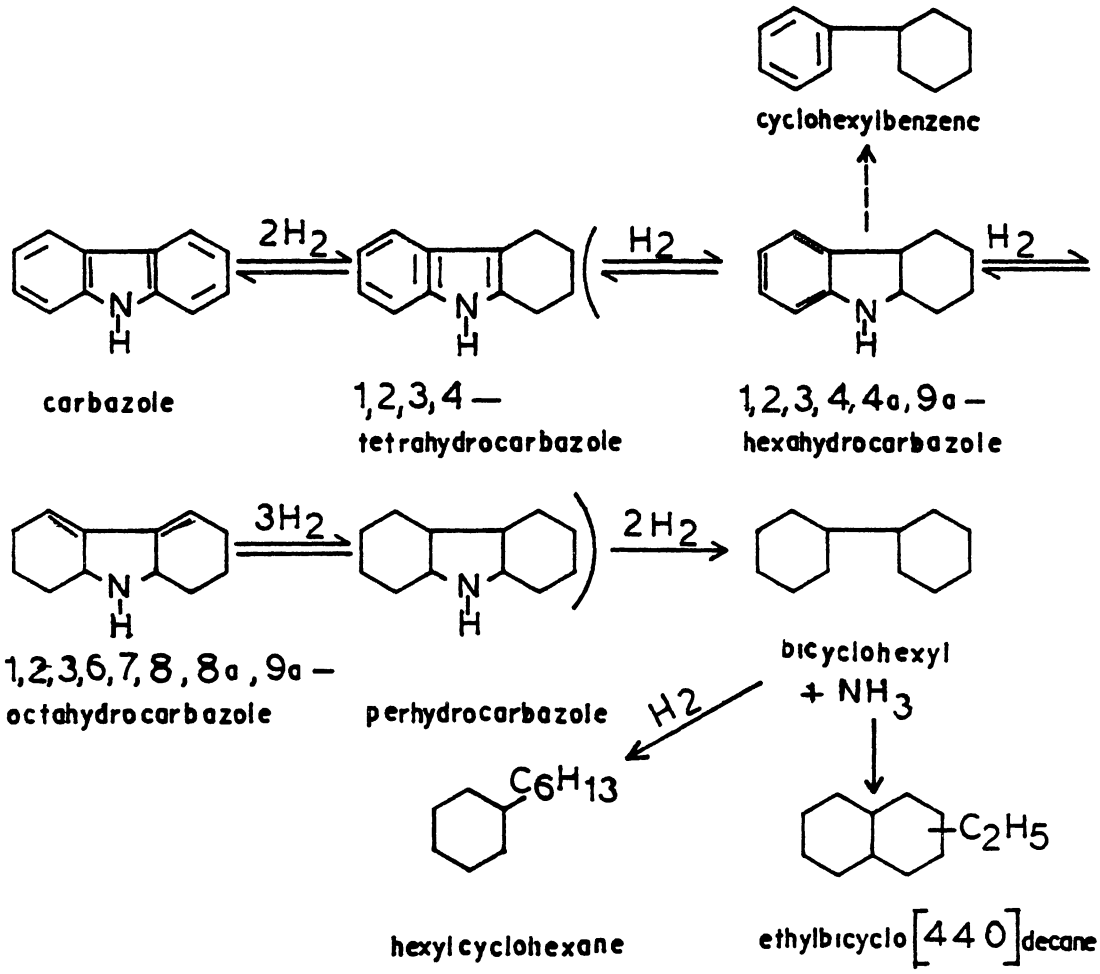

Figure 14. Reaction Network for Carbazole HDN at 270-310°C, 10.1 MPa, Prereduced Mo/Alumina Catalyst (63)

temperature dependence whereas, in the case of HDN and HDO the plots showed slight curvatures which could be resolved into two parts, each approaching linearity with a break at 400°C. These curvatures were attributed either to the presence of two competing reactions with different activation energies, or to the occurrence of the same reaction both thermally and catalytically. A summary of their kinetic results is reported in Table II

In a later study, Qader and Hill (64) investigated the kinetics of hydrocracking of a low temperature neutralized coal tar in a one-liter batch autoclave.
In addition, the neutral tar fraction was hydrorefined over Co-Mo catalyst at 375°C and a pressure of 10.3 MPa to remove S, O and N. Furthermore, a tar fraction boiling between 200°C and 360°C, designated as tar fraction, was prepared. The tar, the neutral tar, the refined tar and the tar fraction were all hydrotreated over a catalyst containing sulfides of nickel and tungsten, supported on silica-alumina, at a temperature range of 400-500°C and a pressure of 10.3 MPa. It was reported that the mechanism of low-temperature-tar hydrocracking involves simaltaneous and consecutive cracking, hydrogenation and isomerization reactions. In addition, cracking reactions involving the breakage of C-C, C-S, C-O and C-N bonds were found rate controlling. The data were described by simple first order kinetics with the rate constants represented by the following Arrhenius equations.

TABLE II

KINETIC DATA FOR COAL TAR HYDROTREATMENT

Compound	Temperature (°C)	Frequency Factor (s^{-1})	Activation Energy (kJ/mol)
Sulfur	300-500	3.3	46.0
Oxygen	300-400	1.0E5	50.2
Oxygen	400-500	5.0E3	33.5
Nitrogen	300-400	1.7E4	41 8
Nitrogen	400-500	5.0E9	58.6

$$k_{gasoline} = 43.528 \exp(-17{,}600/RT) \quad s^{-1}$$
$$k_{oxygen} = 10.033 \exp(-13{,}600/RT) \quad s^{-1}$$
$$k_{sulfur} = 5.9284 \exp(-14{,}500/RT) \quad s^{-1}$$
$$k_{nitrogen} = 13.161 \exp(-15{,}900/RT) \quad s^{-1}$$

Qader et al. (65) studied the rate of tar hydrocracking over a catalyst containing 6% nickel sulfide and 19% tungsten sulfide supported on silica-alumina at 400-475°C. They found that the overall order of the reaction is second order below 10.3 MPa and first order at and above 10.3 MPa. However, the rate of gasoline formation from tar was represented by:

$$k_{1g}=0.14k_{1N.O}+0.16k_{1S}+0.14k_{1O}+0.12k_{1N}+0.08$$

where $k_{1N.O}$, k_{1S}, k_{1O}, and k_{1N} are the first order rate constants for the hydrocracking of neutral oil, and sulfur, oxygen, and nitrogen compounds repectively. The values of k_{1N}, k_{1S}, and k_{1O} can be calculated from the Arrhenius equations, reported in the previous study whereas the rate constant for neutral oil hydrocracking can be calculated from the equation.

$$k_{1N.O} = 66.7 \exp(-16{,}800/RT) \quad s^{-1}$$

Schneider et al. (66), studied the HDN and HDO of SRC-II mid-distillate by catalytic hydrogenation at 350-425°C and under a pressure of 17.2 MPa. It was found that Co-Mo catalyst is the best one for HDO. It is slightly better than Ni-Mo catalyst whereas Ni-W is the poorest of the three. On the other hand, the three catalysts appear to be equal in their HDN activity. The kinetic data, reported for both HDN and HDO, were represented by a simple first order equation. The activation energies and the frequency factors are shown in Table III. In addition, the rate constant for HDN of the KOH raffinate of SRC-II mid-distillate at 400°C was found to be twice that obtained with the middle distillate containing the phenolic compounds, whereas the rate constants for HDO are almost the same. This result leads to the conclusion that the removal of phenolic compounds from coal derived liquids may be the most important step in converting it to refinery charge stock.

TABLE III

KINETIC DATA FOR HYDROTREATMENT OF SRC-II

Reaction	Catalyst	Pre-exponential Factor (s^{-1})	Activation Energy (kJ/mol)
HDN	All Catalysts	0.36E5	106.1
HDO	Co-Mo	6.80E5	122.4
	Ni-Mo	35.36E5	132.6
	Ni-W	218.90E5	145.3

White et al. (67) hydrotreated a COED process coal derived oil over Ni-Mo/alumina catalyst in a continuous downflow system. First order kinetics were assumed in correlating the data on heteroatom removal. An Arrhenius plot for oxygen removal showed a sharp break at about 390°C, giving two different activation energies, 19.7 kJ/mol for temperatures above 390°C and 160.2 kJ/mol for temperatures below 390°C. The low activation energy could be the result of a mechanism change from chemical rate control to diffusion control. On the other hand, the high activation energy would normally be associated with thermal rather than catalytic reactions. A similar behavior was also found for HDN Arrhenius plot but with activation

energies which differ considerably from those found in HDO. The activation energies reported were 111.5 kJ/mol for low-temperature range and 38.1 kJ/mol for the high temperature end. However, the latter activation energy is higher than normally associated with diffusion control.

Jacobs et al. (68) studied the hydrogenation of a COED process coal derived oils over Ni-Mo catalyst in a continuous downflow fixed bed reactor at 20.7 MPa in the temperature range of 343-454°C. The HDS, HDN, and HDO data were correlated by simple first-order kinetics with activation energies of 22.1 kJ/mol, 67.3 kJ/mol, and 34.8 kJ/mol for HDS, HDN, and HDO respectively. However, the break in the Arrhenius plot close to 400°C, reported by White et al. (67), and Qader et al. (55), was not found in this study due to general scatter of the data and the method of determining average temperature.

Ahmed (69) investigated the catalyst deactivation in coal derived liquids hydrotreatment. FMC oil, Synthoil-I liquid, Synthoil-II liquid and Rasyn liquid were hydrotreated over Co-Mo/alumina catalysts in a trickle bed reactor. The experiments were run under 10.3 MPa at a temperature range of 371-454°C. The kinetic data obtained were analyzed assuming pseudo order law models for both HDS and HDN. The HDN data obtained showed that the first order model fits better than the second order model. The activation energies lie between 21-166 kJ/mol. Similarly, HDS data seem to be adequately represented by first order model

with activation energies which varied between 46-113 kJ/mol. Furthermore, the reported low effectiveness factors suggest possible pore diffusional effects.

Sivasubramaniam (70) investigated the effect of catalyst support properties on the HDN of raw anthracene oil and quinoline-doctored raw anthracine oil. Experiments were conducted in a trickle-bed reactor over Co-Mo/alumina catalyst under 10.3 MPa and varying space times. Temperatures of 340,371 and 399°C were used for raw anthracene oil whereas, a temperature of 371°C was used for the doctored feedstock. No catalyst deactivation was observed and the effectiveness factor was assumed to be unity. A simple power rate law expression was initially chosen for data-fitting. It was found that a simple first or n-th order rate expression cannot adequately fit the data. Sivasubramanian examined Satchell's model (71), but it also failed to represent the data satisfactorily. Finally, he tested the reactor models with incomplete catalyst wetting and found that the partial wetting model, based on first order reaction, fits the data better than the partial wetting model, based on the second order reaction. Furthermore, quinoline HDN was found to be a first order reaction.

B 2. Second Order Models

Heck and Stein (72) investigated the kinetics of hydroprocessing of distillate coal liquids with the objective of quantifying the kinetics of heteroatom removal and

aromatic saturation. They hydrotreated distillate coal liquids from H-Coal and SRC processes over Co-Mo/alumina and Ni-Mo/alumina catalysts in fixed bed, continuous flow catalytic reactors. Conditions of 316-427°C, 5.5-17.2 MPa hydrogen pressure, and 0.3-0.4 LHSV, were employed. Both coal liquid distillates had a nominal 160-455°C boiling range, but SRC recycle solvent had a lower hydrogen content and contained more heteroatoms than the H-Coal distillate. It was found that the second-order expression gives a better fit to heteroatom removal data than first-order expression. They also considered n-th order dependency on hydrogen pressure.

Sulfur was found to be more easily removed than nitrogen or oxygen, resulting in a very high percent sulfur removal, more than 99.5%. Therefore, the kinetic constants, reported for HDS, are probably less reliable than those for HDN and HDO. Their kinetic results are reported in Table IV.

Stein et al. (73) conducted experiments on 33 wt%, 90 wt% Monterey SRC and 33 wt% short contact time (SCT) Monterey SRC in recycle solvent to examine the concentration effect as well as to compare the SCT Monterey SRC blend with the regular contact time one. The kinetic data for heteroatom removal was described with a second order model and the kinetic data are presented in Table V.

TABLE IV

KINETIC CONSTANTS FOR HYDROTREATMENT OF COAL LIQUIDS

Process	k_o $(Psig)^{-n}/(wt\%)/hr$	E (KJ/mol)	n	Feed + Catalyst
HDS	1.25E9	129.6	0.96	SRC
HDN	1.23E9	148.5	1.04	Recycle
HDO	2.63E10	159.1	0.71	Solvent + HDS-1441A
HDS	3.76E2	65.9	1.36	SRC
HDN	3.58E9	148.9	0.96	Recycle
HDO	3.46E9	152.8	0.85	Solvent + HDS-9A
HDS	8.52E7	105.9	0.84	H-Coal
HDN	1.90E7	131.7	1.30	distillate
HDO	6.00E7	148.6	1.49	+ HDS-1441A

TABLE V

EFFECT OF BLEND COMPOSITION ON HETEROATOM REMOVAL KINETICS

Process	Blend Type	$(s^{-1})(wt\%^{-1})$ ko,	E,kJ/mol
HDN	33% REG	1.08E5	73.6
	90% REG	3.78E1	76.9
	33% SCT	3.28E3	93.4
HDO	33% REG	1.62E5	119.5
	90% REG	6.78E5	131.9
	33% SCT	1.91E7	147.4
HDS	33% REG	4.83E4	94.9
	90% REG	2.78E1	60.7
	33% SCT	3.75E5	110.1

They concluded that the precent removal of all heteroatoms decreases with increasing SRC concentration. Also, the nitrogen appears to be quite difficult to remove from SRC. However, it was found that, at a given severity of operation, the products from the regular and SCT SRC are very similar.

Soni and Crynes (74), comparing the activities of a Monolith alumina impregnated with cobalt and molybdenum and Nalcomo 474 catalyst, studied the HDS and HDN of Synthoil

and Raw Anthracene Oil. The experiments were conducted in a trickle-bed reactor at 371°C and 10.3 MPa. The global reaction kinetics of HDS and HDN were investigated. The following three kinetic models were considered.

1- A second order reaction

2- Two first order reactions, one for the lighter and the other for the heavier fractions of the feedstock

3- A first order reaction.

The second order model was found to fit the best for both HDS and HDN data. It was observed that HDS activity based on unit surface area is the same for both catalysts, when processing the lighter feedstock, such as Raw Anthracene Oil whereas it is higher for the Monolith catalyst as compared to the Nalcomo 474 catalyst, when processing the heavier feedstock, such as Synthoil liquid. This difference in the activity in the latter case is attributed to the intraparticle diffusion, since the average pore radius and the intraparticle diffusion length of the Monolith catalyst were 80°A and 0.114 mm versus 33°A and 1mm of the Nalcomo 474 catalyst. The effectiveness factors for the Monolith and Nalcomo 474 catalysts were found to be 0.94 and 0.216 respectively for the HDS of Synthoil.

Gary et al. (75) and Thakkar et al (62) studied the HDN of SRC-I recycle solvent over a Ni-Mo/alumina catalyst in a trickle-bed reactor. It was found that a global second-order rate equation fits well the total nitrogen

removal data. An overall activation energy of 36.9 kJ/mol and a frequency factor of 2.06 X 10^3 $(wt\%)^{-1}hr^{-1}$ were reported. In fact, this apparent second order is the overall result of the reactions of several nitrogen compounds, originally present in the feed. In addition, the HDN of most of these nitrogen compounds is governed by first-order kinetics. These facts led Thakkar et al. and Gary et al. to separate the overall second-order model into two coupled first order irreversible steps in parallel. The coupled kinetic model was:

$$-r_N = \alpha_R k_R C_N + \alpha_U k_U C_N$$

This rate equation, upon intergration for a tubular flow reactor, gives·

$$(1-X_N) = \alpha_R \exp(-k_R/LHSV) + \alpha_U \exp(-k_U/LHSV)$$

where k_R is first-order reaction rate constant for reactive nitrogen compounds, hr^{-1},

k_U is first-order reaction rate constant for unreactive nitrogen compounds, hr^{-1},

α_R is the fraction of reactive nitrogen,

α_U is the fraction of unreactive nitrogen,

C_N is the concentration of nitrogen (wt%),

and $-r_N$ is the rate of reaction of nitrogen.

In developing this model, it was assumed that carbazoles are a good model for the less-reactive nitrogen species in

the feed. Therefore the rate constant for less-reactive fraction was assumed to be equal to the reaction rate constant for carbazole. Then the value of α_U was assumed, and k_R was calculated from one of the experimental data points at each reaction temperature. From these assumed and calculated values, k_U, k_R, α_U, and α_R, the nitrogen removal, as predicted by the model, can be calculated and compared by the experimental data. Next, the value of α_U was adjusted and the calculation procedure is repeated to minimize the error between nitrogen removal predicted by the model and the experimental data, and to give the best straight line fit of k_R in an Arrhenius plot. The following values were reported as best fit values·

$\alpha_R = 0.4$

$\alpha_U = 0.6$

$E_R = 41.8$ kJ/mol

$E_U = 51.6$ kJ/mol

$k_{oR} = 2.27\ s^{-1}$

$k_{oU} = 3.19\ s^{-1}$

where k_o is the frequency factor.

Satchell (71) investigated the HDN of anthracene oil over Co-Mo/alumina catalysts. He ran his experiments in a trickle-bed reactor at a temperature range of 316-427°C and under a pressure of 3.4-10.3 MPa. He proposed two models:

a- A simple n-th order rate expression was considered which lead to a third order reaction for the best fit of the data. Such a high apparent order was explained by considering the fact that the feedstock contains various organonitrogen species. The reactivities of these species vary widely. HDN of the more reactive species tends to occur at relatively low space time, leading to a high apparent inital rate constant. On the other hand, at a high space time, only a small fraction of the very reactive species remains, resulting in a smaller apparent reaction rate constant. The only way, that the n-th order rate expression can compensate to this behavior, is to have a large reaction order.

b- Satchell considered the work by Flinn and Beuther (76) who assumed that the reactivity of organic nitrogen species from petroleum feedstocks is a function of boiling point. Based on this idea, he studied the reactivity of these species in anthracene oil by analyzing boiling point ranges of both anthracene oil and its HDN products for organonitronitrogen level. It was found that the weight percent nitrogen remaining in the product generally increases with increasing boiling range. The only reported exception is that of the lowest boiling range which showed a percent nitrogen higher than expected. However, this analysis assumes implicitly that all species remain in the same boiling range in the product as that it occupied in the feed oil. In fact, a substantial amount of cracking,

reduction of molecular weight, and boiling point of the oil take place during the HDN. This leads to coupling the effects of both HDN reactivity and hydrocracking. However, considering the assumption made by Flinn et al. (76) that the assumed first order HDN rate constant is approximately a linear function of the boiling point with a petroleum feed stock, Satchell assumed that the pseudo rate constant, any order, is a linear function of the boiling point. Thus, he developed the following equations for first order and n-th order respectively:

$$k_1 = [\ln(N_{f_1}/N_{p_1})]/\Theta_V$$

$$k_1 = (1/n-1)[1/N_{p_1})^{n-1} - (1/N_{f_1})^{n-1}]/\Theta_V$$

where k_1 is pseudo rate constant for the boiling range 1,

N_{f_1} is the weight percent nitrogen in the feed in boiling range 1,

N_{p_1} is the weight percent nitrogen in the product in boiling range 1,

and Θ_V is the hourly volumetric space time.

In addition, the boiling ranges were numbered from the lowest average boiling point to the highest. Furthermore, it was assumed that the k_1's are independent of both the reactor operating pressure and operating temperature. Thus the model for a whole liquid was derived:

$$N_p = \Sigma\, w_i N_{f_i} \exp(-r_i k_8 \Theta_v) \qquad \text{for } n=1$$

$$N_p = \Sigma \frac{w_i}{[k_8 r_i (n-1)\Theta_v + (1/N_{f_i})^{n-1}]^{1/(n-1)}} \qquad \text{for } n \neq 1$$

where w_i is the mass fraction of the oil in cut i, and r_i is the activity ratio defined as (k_i/k_8). It was found that the second order model gives the best fit for the experimental data. Also, this model was found to be superior to simple power-low model. In addition the effectiveness factor was estimated to be close to one.

Shih et al (77), in evaluating catalysts for upgrading SCT SRC, conducted experiments in a continuous down-flow fixed bed pilot plant under a pressure of 13.8 MPa and at a temperature of 382-413°C. The feedstocks were a 70 wt% (high sulfur) Indiana V regular SRC and a 50 wt% W. Kentucky SCT SRC blends with process recycle solvent. A simple model was used to estimate the catalyst deactivation rate. It is based on the assumptions that catalyst deactivation is independent of reactants and products, and that the deactivation rate is first order with respect to its activity. Thus,

$$dk/dt = -k/\tau$$

where k is the reactant rate constant of the catalyst,
τ is the deactivation time constant,
and t is the age of the catalyst.

Assuming a second order reaction for both heteroatom removal and incorporating it with catalyst deactivation, yields

$$-\frac{dC_A}{d(1/LHSV)} = k_o[\exp-(\frac{E}{RT}+\frac{t}{\tau})]C_A^2$$

where k_o is the pre-exponential factor for fresh catalyst, and C_A is the heteroatom concentration. For a fixed bed reactor, the kinetic equation derived from the above expression is

$$\frac{1}{C_A}-\frac{1}{C_{Ao}} = k_o[\exp-(\frac{E}{RT}+\frac{t}{\tau})]/LHSV$$

Kinetic analysis were performed on the data obtained using the above model, and the estimated catalyst deactivation constants, pre-exponential factors, and activation energies are presented in Table VI

C. Summary of Kinetics Review

Consideration of the work in this chapter leads to the conclusion that most of the previous kinetic studies considered either single model nitrogen compounds or a coal-derived-liquid,whereas little work has been done to relate these two types of studies. Gary et al. (74) approached the problem by assuming that a coal-derived liquid is composed of a fast reacting fraction and a slow reacting one. Satchell (71) considered a coal-derived liquid as composed of several fractions with HDN rate constant for each frac-

TABLE VI

ESTIMATED PARAMETERS FOR CATALYST DEACTIVATION MODEL

Feedstock	k_o,(wt%-hr)$^{-1}$	E,kJ/mol	τ,Days	Process
70wt% (high	2.92E6	124.7	10.6	HDS
Sulfur)Indiana	2.92E1	79.4	17.0	HDN
V regular SRC	3.80E9	180.7	10.4	HDO
50wt% W.	1.85E7	131.4	22.2	HDS
Kentucky	9.36E1	80.4	36.1	HDN
SCT SRC	1.92E6	134.2	8.9	HDO

tion as a function of its boiling point. Bhinde (44) studied the interaction effects that occur during simultaneous HDN, HDS, and hydrogenation reactions. Thus, HDN of quinoline and indole, HDS of dibenzothiophene and hydrogenation of naphthalene were investigated over a pre-sulfided commercial Ni-Mo/alumina catalyst. The reaction kinetics for each reactant was quantitatively determined in the binary mixtures as a function of quinoline concentration under the same conditions as those used for single-componenet studies. It was concluded that indole, naphthalene, dibenzothiophene and their reaction products have a slight negative effect on the kinetics of quinoline

HDN. Quinoline and its reaction products strongly inhibit all hydrogenation reaction. There is clearly a need to develop techniques to predict the kinetics of mixtures from those of pure compounds. However, it is hoped that instrumental analysis will develop in the future to an extent that it becomes simple to determine the exact composition of a liquid fossil fuel. This will help greatly in developing an overall kinetic model for the HDN kinetics. Hence, it is logical to approach to this objective by studying binary mixtures of the single model nitrogen containing compound. As a step in this direction, the HDN of quinoline and acridine and their mixture in n-hexadecane solvent is studied in the project.

It has been established that Ni-Mo catalysts have higher HDN capability than Co-Mo or Ni-W catalysts (78). For this reason, a Ni-Mo/γ-alumina catalyst is used for HDN. Gary et al. (74) conducted screening tests on seven catalysts in a continuous trickle-bed reactor at 10.3 MPa and 371°C. Their results indicated that HDS-9A catalyst is the superior HDN catalyst among the group of catalysts studied. Hence, HDS-9A was selected for study in this work.

A one liter autoclave reactor with glass liner was used for experimental runs. A novel technique to introduce the catalyst into the reactor was developed and successfully implemented. The runs were conducted and the results are presented and discussed in chapters IV and VI.

CHAPTER III

EXPERIMENTAL APPARATUS AND TECHNIQUE

A. Experimental Apparatus

The experimental apparatus used in this project is discussed in three sections

1. Reactor system
2. Catalyst preparation system
3 Analytical instruments

A 1. The Reactor System

A special semi-batch reactor system was designed and constructed to carry out the HDN experiments. This system is composed of the reactor and its accessories for feeding, venting, and sampling as well as temperature and pressure measurment and control devices. A schematic diagram of the reactor system is shown in Figure 15. The specifications of the accessories are listed in Appendix A.

The reactor

The HDN experiments were carried out in a 1-liter special packless, autoclave reactor (Autoclave Engineers, 316 SS) with internal diameter 0.076m. (3 in.) and height of 0.229 m (9 in.). A glass liner of diameter 0.0747 m and

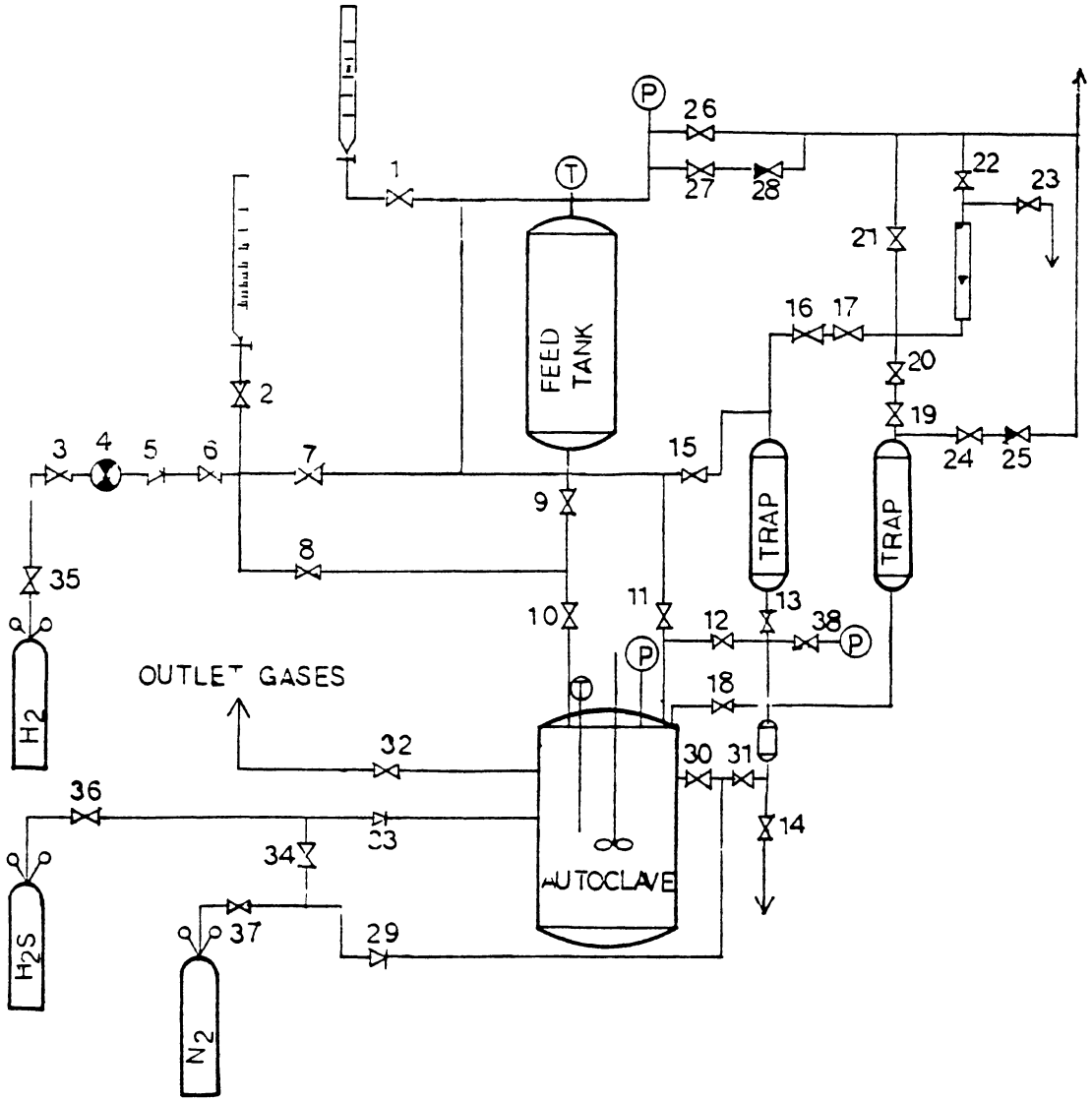

Figure 15. Schematic Diagram of the Reactor System.

length of 0.191 m was employed to minimize the possible catalytic effect of the metallic wall and to protect the reactor wall from any corrosive reactant. The reactor is equipped with an Autoclave Engineers (AE) Dispersimax Agitator. This device is a turbine-type agitator provided with a hollow shaft used in conjunction with a set of removable baffles placed in the vessel. During operation, a low pressure region is created at the turbine impeller. The gases are drawn through the hollow shaft and dispersed through the liquid. The bubbles are broken up by the baffles. This type of agitation can suspend fine solid particles and insure constant circulation of the reactant gases through the liquid. High speed rotary agitation is affected by the rotation of external magnets which actuate internal magnets that are fastened to the shaft. The external drive magnet assembly consists of an outer steel housing containing four rows of permanent magnets spaced at 90° intervals. This outer magnetic housing is placed over a pressure sealed inner housing containing circular, permanent, ceramic, encapsulated magnets mounted on a square rotor shaft. A strong magnetic field makes the inner pressure sealed rotor shaft rotate at the same rotational speed as the outer housing.

The reactor is also equipped with a cooling coil so that a cooling medium can be introduced to quench the system. In addition, two rupture discs with bursting pressures 20.7 and 27.6 MPa (3000 and 4000 psi) are also

installed on the reactor.

Gas Feeding

Gases including nitrogen, hydrogen and a mixture of H_2S/H_2 are brought to the autoclave from their respective gas cylinders through appropriate valves. They enter the autoclave body through special ports. The hydrogen gas from the gas cylinder flows through the main line, where its flow is controlled by a Mity-Mite valve and a check valve It then branches into two subsidery paths, both of these paths lead to the autoclave cover, but in one of these paths, flow is controlled by a micrometering valve.

Liquid Feeding

Liquid is charged into a calibrated 500 ml. buret from where it can flow into the feed tank either from the top or the bottom of the tank. After the liquid in the tank is heated to the required temperature it is allowed to flow into the autoclave through a special port in the reactor cover.

Sampling

A male connector (0.25 in.) is fitted on the tip of the sampling tube through a nut and a ferrule. The tip dips into the reactants inside the autoclve. Another nut and ferrule are fitted on the free end of the male

connector with a piece of 100 mesh SS screen inserted between the nut and the ferrule. The whole system forms an in-line filter. Liquid samples are drawn from the reactor through this filter. The filtered liquid is received in a 30 ml sampling cylinder which is connected to the atmosphere through a rap. The sampling cylinder is equipped with a pressure gauge and a heating tape and is insulated. The heating system is useful especially during winters when the products may freeze in the sampling cylinder.

Venting

The feed tank is connected to the atmosphere through a system of valves including an in-line safety relief valve The reactor is similarly vented to the atmosphere but it is equipped with a trap and a rupture disc

A 2 Catalyst Preparation System

A unique catalyst preparation system is devised and used in this project. The catalyst is handled in a specially designed glass ampoule This ampoule is manufactured from pyrex tubing 14 mm. o.d., 12mm i.d. It is shaped in the form of a closed flat bottomed tube, having a contraction (4 mm. i.d.), 9 cm from the bottom, 2 cm from the top. Figure 16 shows a schematic of the glass ampoule. The open end may be closed with a rubber stopper. The desired amount of fresh catalyst is placed in the ampoule and weighed. Then the catalyst is calcined, sulfided and

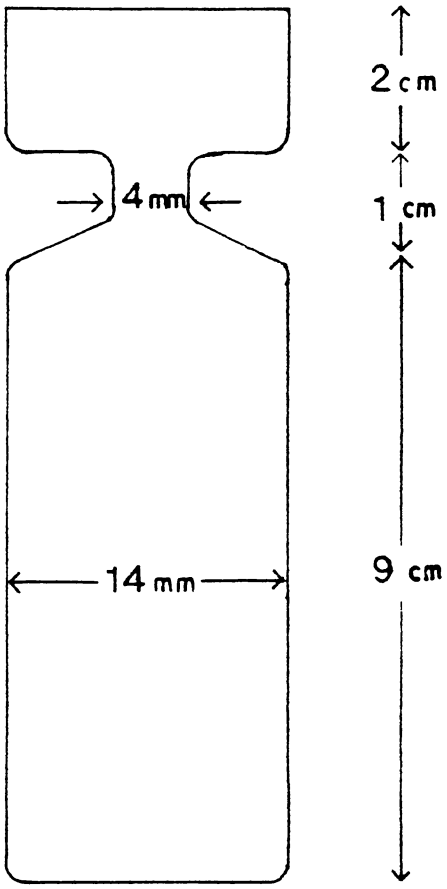

Figure 16. Catalyst Ampoule

the ampoule is sealed.

Calcination

A set of glass ampoules, loaded with 5.4 g catalyst (corresponding to 2 0 wt% of solvent used in experiments), is placed in a furnace. The ampoules are heated for two hours at 500°C At the end of this period the ampoules are transfered out of the furnace to cool

Sulfidation

Sulfidation is carried out in a 1-liter Parr Autoclave which is equipped with auxiliary lines for feeding nitrogen and H_2S/H_2 gases as well as a line for gas vent. In addition, special arrangements are made for temperature measurement and control.

The ampoules, with calcined catalysts are placed in the autoclave and laid in a vertical position. The autoclave is closed and tightened The catalyst samples are then sulfided through the following steps

1 The autoclave is checked for leaks.

2. Heating is started under a flowing stream of nitrogen. When the sulfidation temperature, (260°C) is attained, nitrogen stream is cut off and 5% H_2S/H_2 gas stream is admitted.

3. The temperature is monitored and the heating is rate is controlled by a variac.

4. After two hours, the heater is turned off, H_2/H_2S gas stream is cut off, and nitrogen stream is turned on. The system is left to cool to room temperature.

5 Nitrogen stream is turned off and the autoclave is opened and the ampoules are immediately closed with rubber stoppers.

6. The ampoules are then sealed from their necks The top glass part is shaped into a hook which is later used to hang the glass ampoules inside the autoclave.

A.3. Analytical Instruments

Analytical instruments are comprised of two groups, one for the analysis of liquid samples and the other for the catalyst analysis.

Liquid Analysis

Initially, it was decided to use a Perkin Elmer Elemental Analyzer to determine the nitrogen content in liquid samples. But later, it was found that the elemental analyzer was not suitable for the low nitrogen concentration of this project. This led to the use of a Varian 3700 Gas Chromatograph (GC). For higher sensitivity the GC was equipped with the Thermionic Specific Detector (TSD) The TSD is approximately 50 times more sensitive to nitrogen containing organics than the Flame Ionization Detector (FID) In addition, the TSD supresses the response to car-

bon by three to four orders of magnitude. Details of liquid sample analysis are presented in Appendix B.

Catalyst Analysis

The catalyst is analyzed before and after the reaction to determine both surface area and pore volume. A Quantachrome Autoscan Porosimeter is used for this purpose. In addition, the spent catalyst is analyzed to determine the deposited coke (79).

1. The catalyst is extracted in a Soxhlet apparatus for about three hours until the solvent is clear. Tetrahydrofuran is used as solvent. This step removes the adhering soluble hydrocarbons from the catalyst surface.

2. The catalyst is vacuum dried at 100°C for 12 hrs. This step removes the solvent left in the catalyst pores.

3. The remaining carbonaceous material on the catalyst is considered as coke on the catalyst. This is determined by roasting the catalyst at 600°C in a muffle furnace overnight. The decrease in the catalyst weight is used to calculate the amount of coke deposited. This is corrected for the change of the oxidic form to the sulfide form of nickel and molybdenum.

B. Experimental Technique

In this work a solution of a single model nitrogen compound or of a mixture of two compounds in n-hexadecane is hydrotreated in the reactor over a presulfided HDS-9A

catalyst under a hydrogen pressure of 8.3 MPa (1200 psig) and at a temperature of 357-390°C (675-734°F). Samples of reaction products were taken at specified time intervals and analyzed by the GC. In addition, at the end of the run, the spent catalyst was separated and analyzed.

During this project two experimental techniques were developed and used. In the first method the catalyst was placed in the reactor, sulfided and used in the experiment In the second method, presulfided catalyst in ampoules were placed in the reactor and broken by a pressure surge at the appropriate time. The second technique was found to be more accurate than the first one in defining the starting time for catalytic reactions and was used to collect all the reported data in this project The ampoule technique will be briefly described here and more details are presented in Appendix C.

The catalyst is placed in a specially manufactured ampoule where it is calcined and sulfided, as previously mentioned. It is sealed and placed in the autoclave with the reactants. The autoclave is assembled, purged and inspected for any leaks. Heating is then started under an atmosphere of hydrogen until the required temperature is attained. At this moment hydrogen is admitted to the autoclave raising the pressure inside the system to the required level. This rise in pressure breaks the ampoule and the catalyst dispereses in the reactants. This is the zero time which is recorded as a sudden small jump in the temperature

about (3°C) plot on the temperature recorder. The reaction starts under hydrogen atmosphere, the pressure of which is controlled by a Mity-Mite valve. In addition, the temperature is controlled and maintained at the required level Samples are withdrawn from reaction products at specified time intervals through the sampling cylinder under the effect of pressure difference. Finally, at the end of reaction time, the system is shut down and the reactor is quenched.

This modified method eliminates the feeding problems and gives a precisely defined starting time for the reaction. Furthermore, since about twenty ampoules can be prepared in one batch, all catalyst ampoules are presulfided under identical conditions. The only drawback of the system is that, in some experiments, the ampoules do not break completely and the catalyst may not completely transfer into the liquid This can be checked at the end of the run, in which case the run is considered an aborted one

Another operational problem is the solidification of the solvent, n-hexadecane in the lines during cold days, since the melting point of n-hexadecane is 17°C. This problem is alleviated by heating the feed and sample lines with electric heating tapes.

CHAPTER IV

EXPERIMENTAL RESULTS

In this project, HDN experiments were conducted on quinoline, acridine and their mixtures as listed in Table VII. The run numbers are designated as NQAn, where, N, Q, and A refer to n-hexadecane, quinoline, and acridine, respectively, and n refers to the run number. Whenever a compound is not present in the feedstock, the corresponding letter does not appear in the run number code. The runs, in which the catalyst ampoule did not break or other technical difficulties arose, were discarded and are not listed in Table VII. N-hexadecane was used as the solvent. The pressure in all experiments was 8.3 MPa (1200 psig) and the temperature was varied in the range of 357-390°C (675-743°F). Table VII shows the conditions of these experiments. The samples were generally taken in 30 min. intervals, except in the cases where some technical problems hindered it and in run NQA8 where some samples were taken in 60 or 90 min. intervals.

TABLE VII

LIST OF EXPERIMENTS

Run #	Feed Composition	Temperature (°C)	Duration of experiment,hrs.	Number of Samples
NQ5	4.42% quinoline	357	3.5	6
NQ6	4.45% quinoline	370	3.0	6
NQ9	4.4% quinoline	390	3.0	6
NA1	0.916% acridine	370	3.0	6
NA2	1.814% acridine	390	3.0	6
NA3	1.816% acridine	357	3.0	6
NQA1	1.75% acridine 4.3% quinoline	390	3.0	6
NQA3	1.75% acridine 4.3% quinoline	357	3.0	5
NQA6	1.75% acridine 4.3% quinoline	370	3.0	6
NQA8	1.75% acridine 4.3% quinoline	370	8.5	12

A. Quinoline Hydrodenitrogenation

The major reaction intermediates formed in quinoline HDN are:

1,2,3,4-tetrahydroquinoline (Py-THQ)

5,6,7,8-tetrahydroquinoline (Bz-THQ)

decahydroquinoline (DHQ)

O-propylaniline (OPA)

Other nitrogen-containing compounds that were identified include aniline, o-toluidine, or o-methylaniline (OMA), and o-ethylaniline (OEA). In addition, two primary hydrocarbon products were identified-propylbenzene (PB) and propylcyclohexane (PCH). The abbreviations shown in parenthesis are used in the text while the complete names of compounds are shown in figures. Other hydrocarbons which are expected to result in the process are. benzene, cyclohexene, cyclohexane, and methyl-cyclopentane (80). No attempts were made to identify and measure these hydrocarbons as well as the possible cracking products of n-hexadecane In this project the concentrations of Py-THQ, Bz-THQ, DHQ, quinoline, OPA, OEA, OMA, aniline, PB, and PCH were measured. These concentrations as a function of time are tabulated in Tables VIII, IX, and X and presented in Figures 17-28. In these figures, the curves are generated by a spline method in the SAS-graphics program by connecting the experimental points.

At 357°C quinoline concentration decreases to less than 10% in the first hour of the reaction. It is mainly converted to Py-THQ with the formation of a small amount of Bz-THQ, as shown in Figures 17 and 18. The rate of quinoline conversion decreases with time as well as the rate of formation of Py-THQ. This behavior is due to the chemical equilibrium. But, DHQ concentration increases approximately steadily. OPA shows similar behavior but with lower

TABLE VIII

REACTION PRODUCTS OF RUN NQ5* (357°C)

Compound	Reaction Time, min					
	30	60	90	150	180	210
Quinoline	128.5	34.5	18.0	13.5	13.0	12 1
Py-THQ	164 0	198.1	205.2	196.3	187.2	177.4
Bz-THQ	11 4	13.4	12.8	11.6	11.2	11 2
DHQ	3.9	10 8	21.0	35.3	40.2	50.3
OPA	0.9	1.5	2.0	2.9	3.4	4 0
PCH	0.3	0 5	0.8	2.1	2 8	3.6
PB	0 2	0 2	0.4	0.5	0.6	0.8
OEA	0.2	0.3	0.3	0 3	0.4	0 4
OMA	1 4	1.5	1 5	1.7	1.7	1 8
Aniline	2 1	2.2	2.0	1.8	1 9	1 9
Total Nitrogen	312.4	262.3	262.8	263.4	259.0	259.1

* g-mole/10^6 g n-hexadecane

Initial quinoline concentration =

350.6 g-mole quinoline/10^6g n-hexadecane.

TABLE IX

REACTION PRODUCTS OF RUN NQ6* (370°C)

Compound	Reaction Time, min					
	30	60	90	120	150	180
Quinoline	70 0	30.1	19.2	14.6	12.3	10.6
Py-THQ	136.6	143.2	130.0	116 5	105.9	95 8
Bz-THQ	30 4	33.1	34.0	35 3	35.2	34.0
DHQ	8.9	21.7	32.7	42.9	51 1	54.1
OPA	2.0	3.1	3 9	4.6	4 8	4.8
PCH	2.5	4.0	6.5	8.9	10.3	12.2
PB	0 7	0.8	1.1	1.3	1.4	1.5
OEA	0.7	0.8	0.9	0.9	0 9	0.9
OMA	2.4	2.5	2.5	2.5	2 4	2 4
Aniline**	---	---	---	---	---	---
Total Nitrogen	251.0	234.5	223.2	217.3	212 6	202.0

* g-mole/10^6 g n-hexadecane

Initial quinoline concentration =

345.4 g-mole quinoline/10^6g n-hexadecane.

** Concentration below detection limit

TABLE X

REACTION PRODUCTS OF RUN NQ9* (390°C)

Compound	Reaction Time, min					
	30	60	90	120	150	180
Quinoline	48.6	22.8	14.8	11.4	8.0	7.4
Py-THQ	141.8	132 3	97.9	65 5	41.2	24 2
Bz-THQ	38.8	46.6	47.6	42.8	35.4	27.1
DHQ	10 0	29.8	42 7	42.8	35 3	32.3
OPA	3.4	5.7	7.4	8.3	7.9	8.2
PCH	5 0	12.5	22.0	34.3	47.8	71.8
PB	0.8	1.4	3.5	4 7	6.1	7.6
OEA	1.2	1 4	1.5	1.4	1.2	1 6
OMA	4.0	4.6	3.9	3.5	2.7	2.3
Aniline**	---	---	---	---	---	---
Total Nitrogen	247.8	243.2	215.8	175.7	131.7	103.0

* g-mole/10^6 g n-hexadecane

Initial quinoline concentration =

371.7 g-mole quinoline/10^6g n-hexadecane.

** Concentration below detection limit

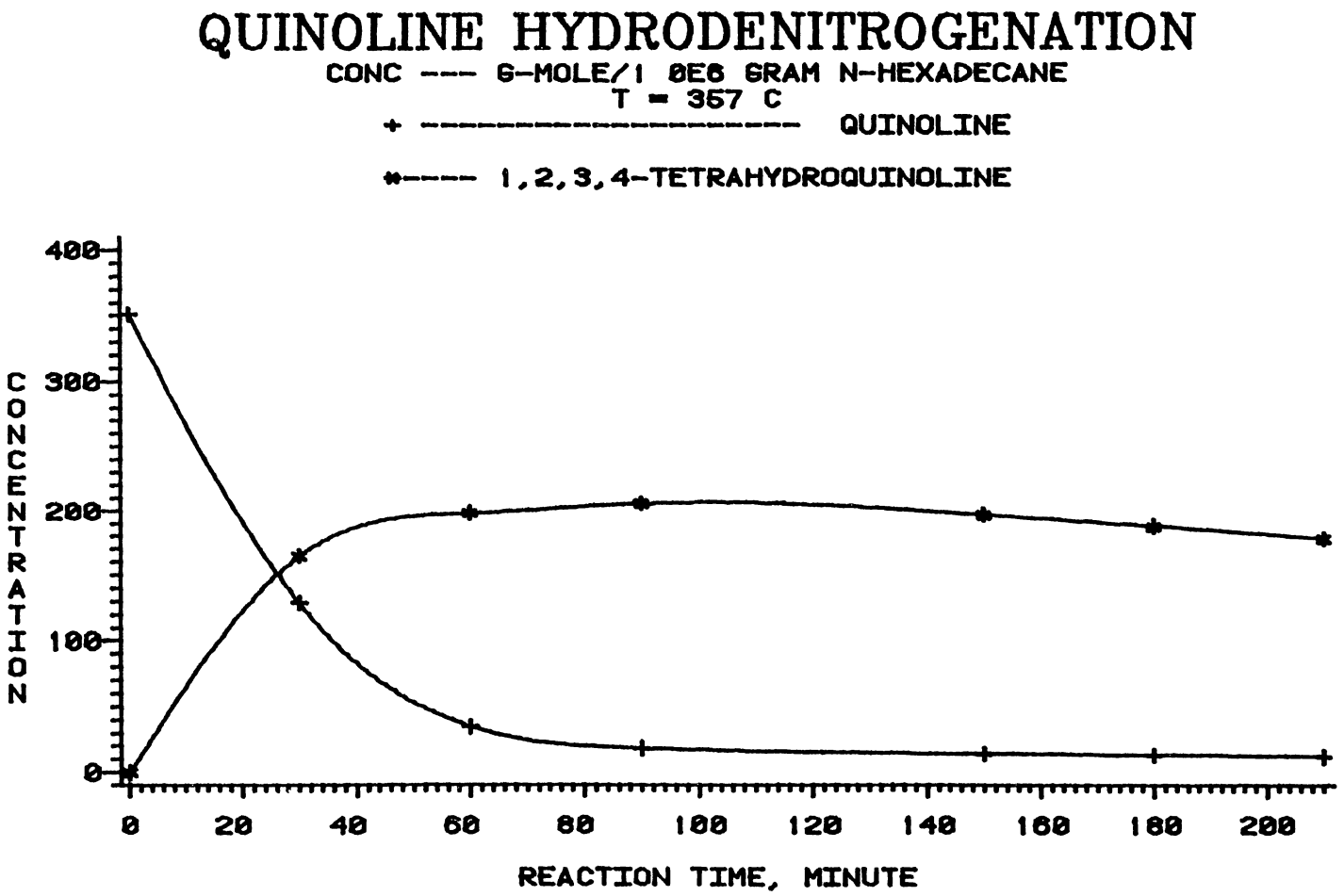

Figure 17 Quinoline HDN Products at 357°C

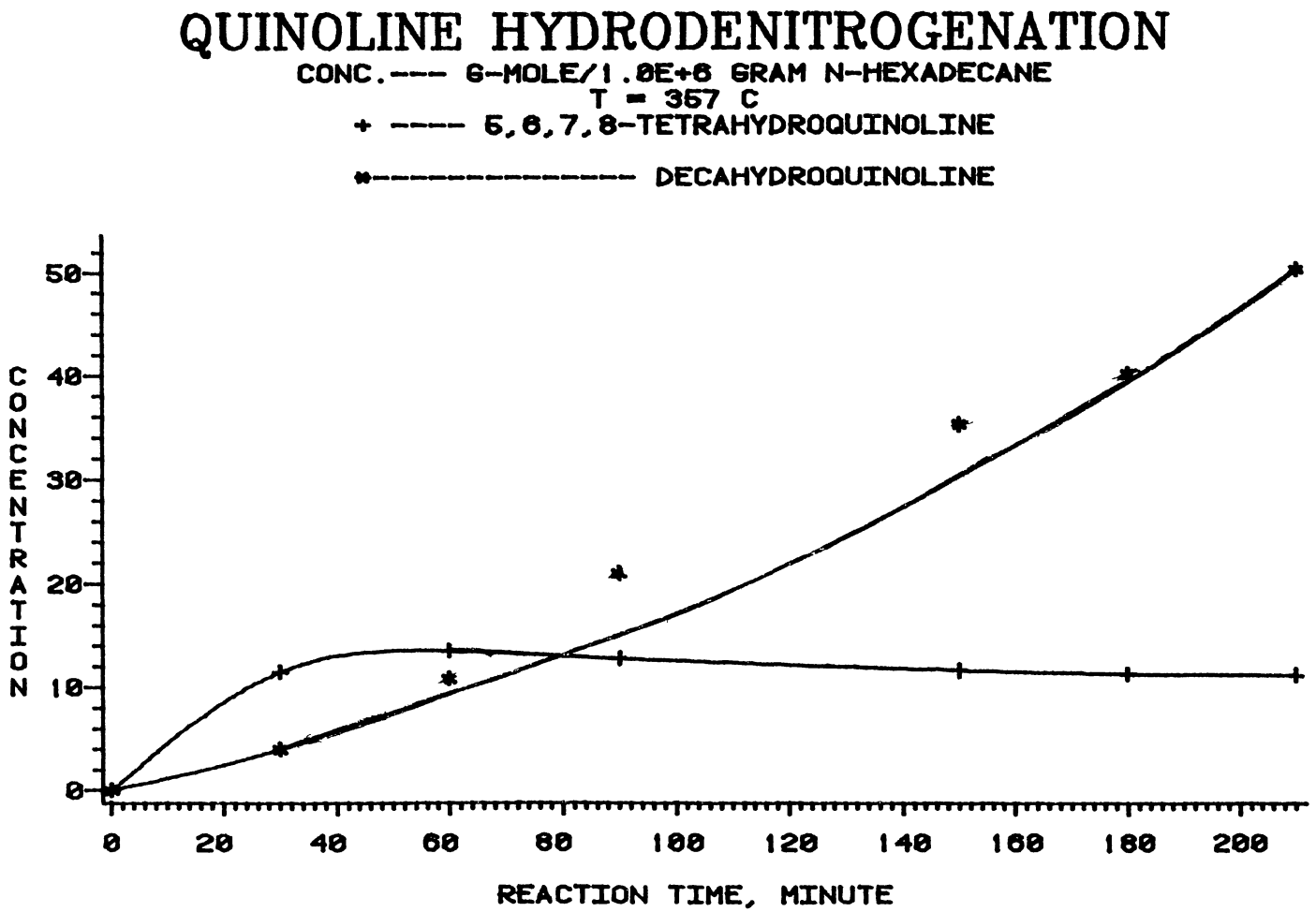

Figure 18 Quinoline HDN Products at 357°C

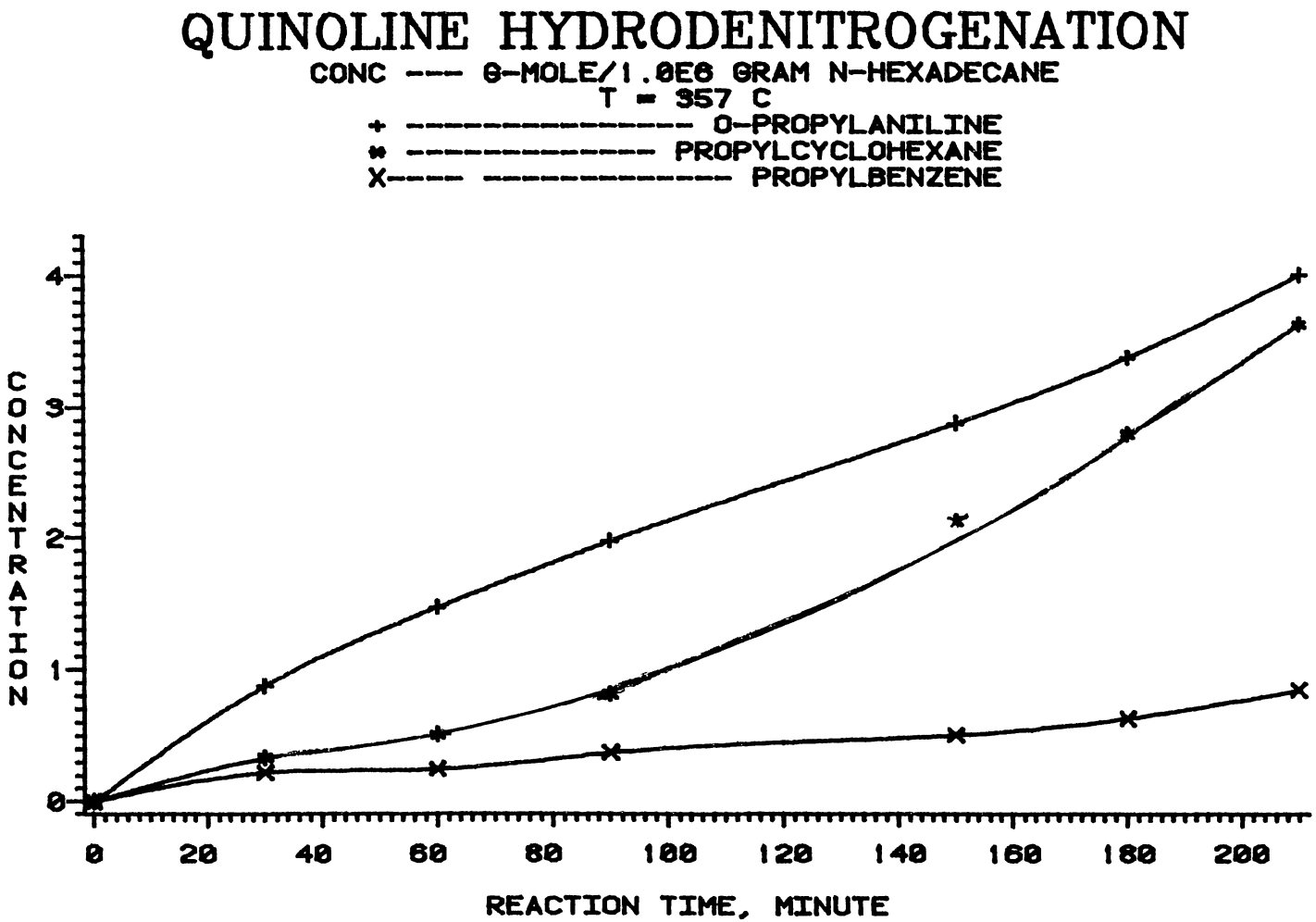

Figure 19. Quinoline HDN Products at 357°C

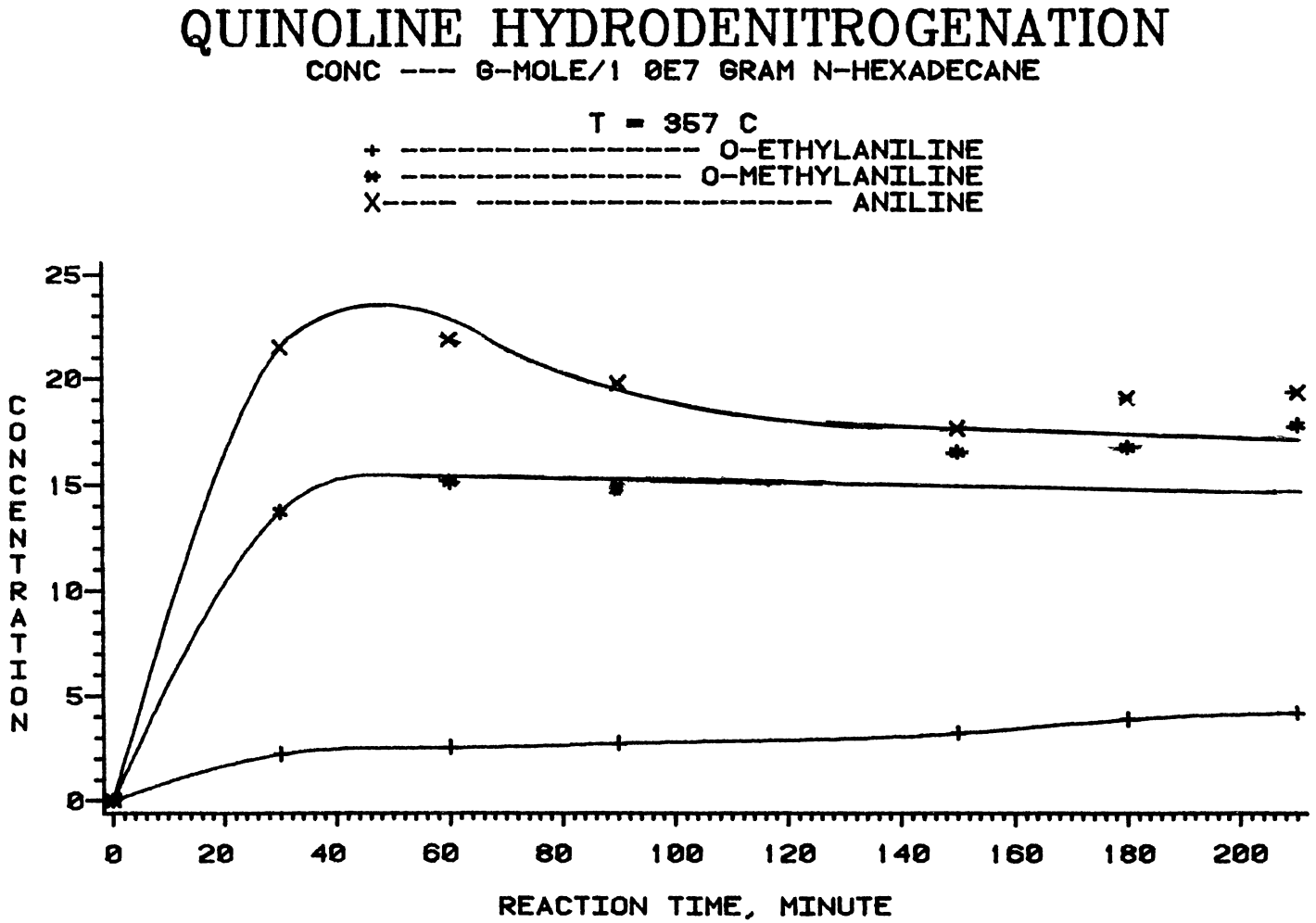

Figure 20. Quinoline HDN Products at 357°C

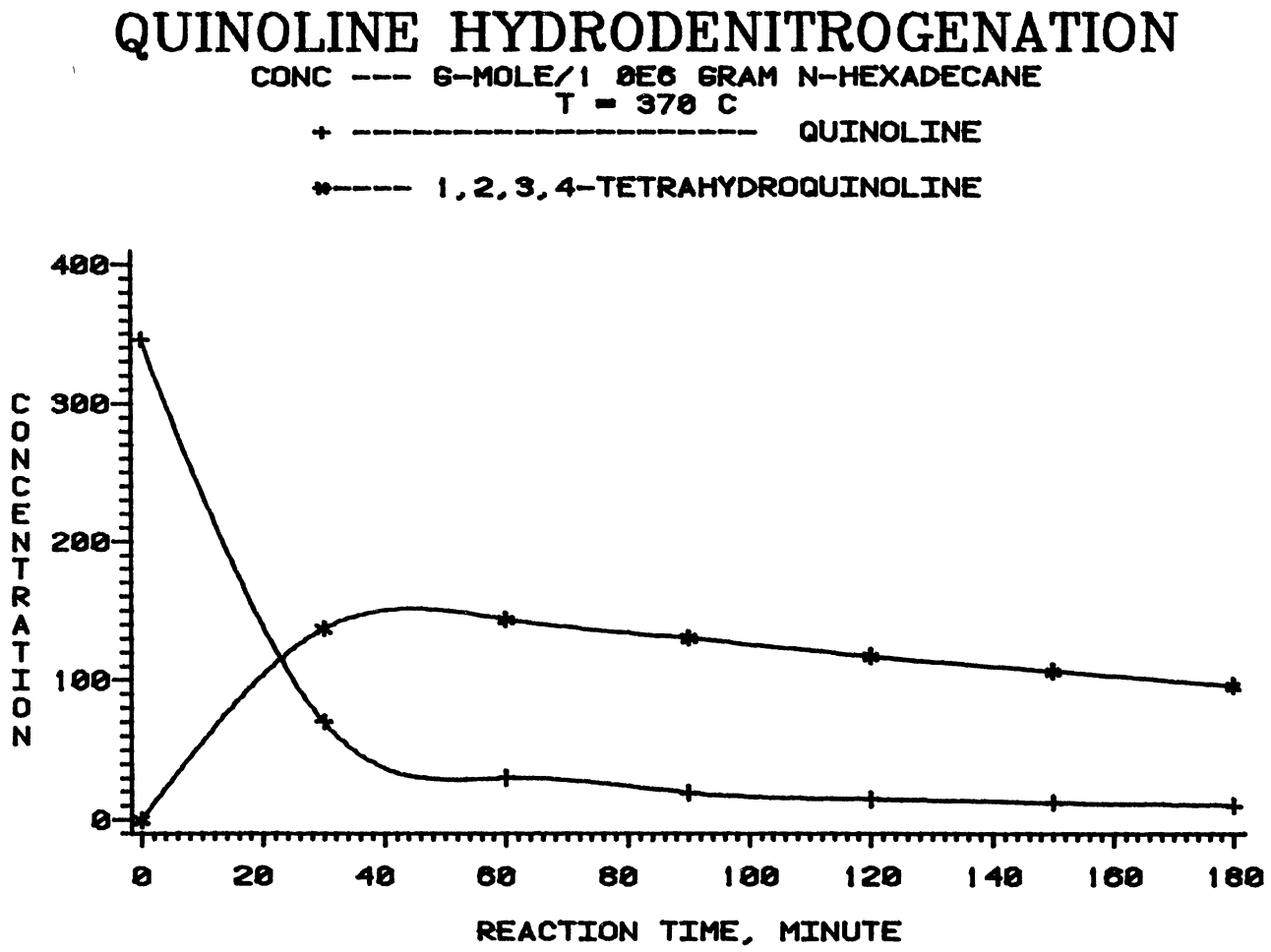

Figure 21. Quinoline HDN Products at 370°C

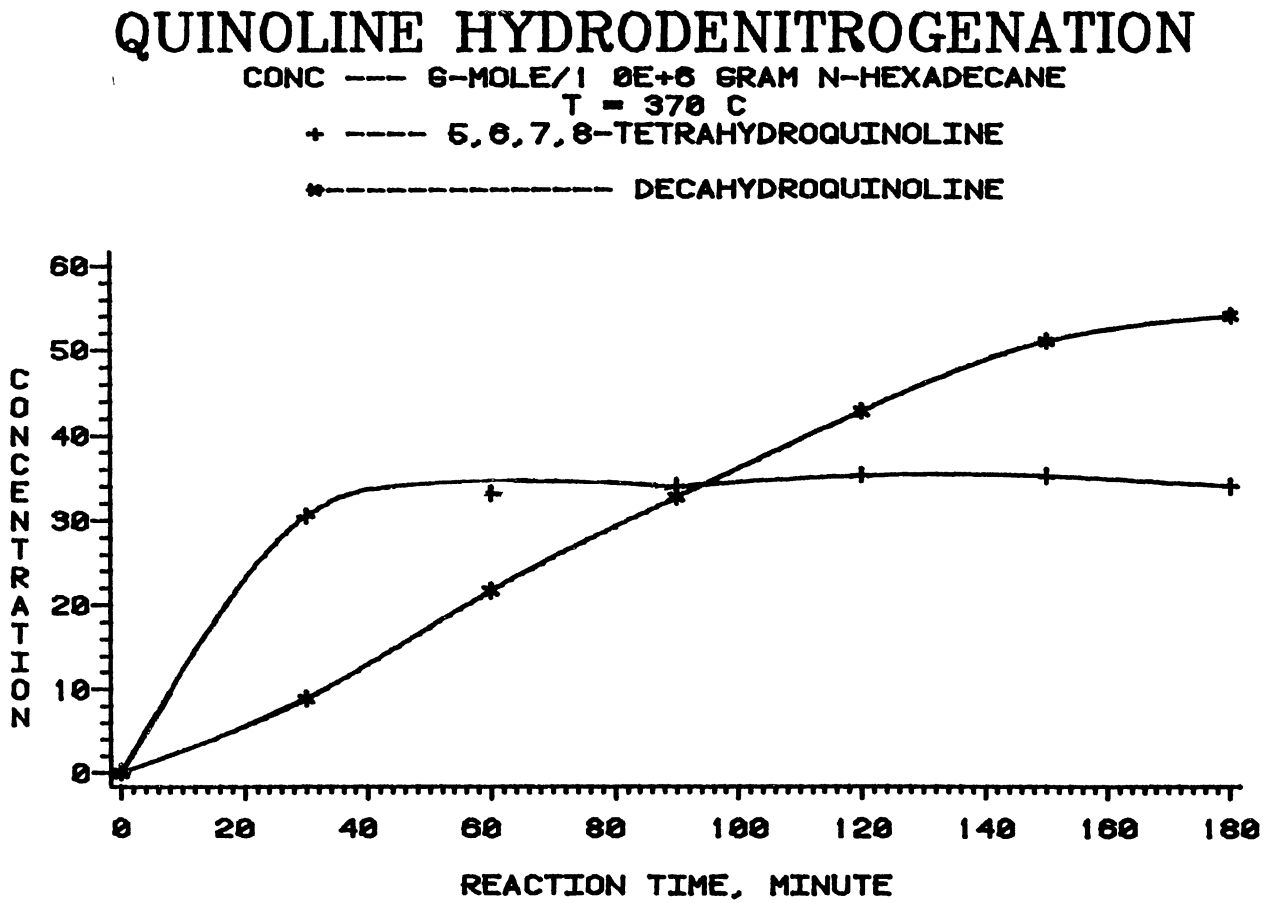

Figure 22. Quinoline HDN Products at 370°C

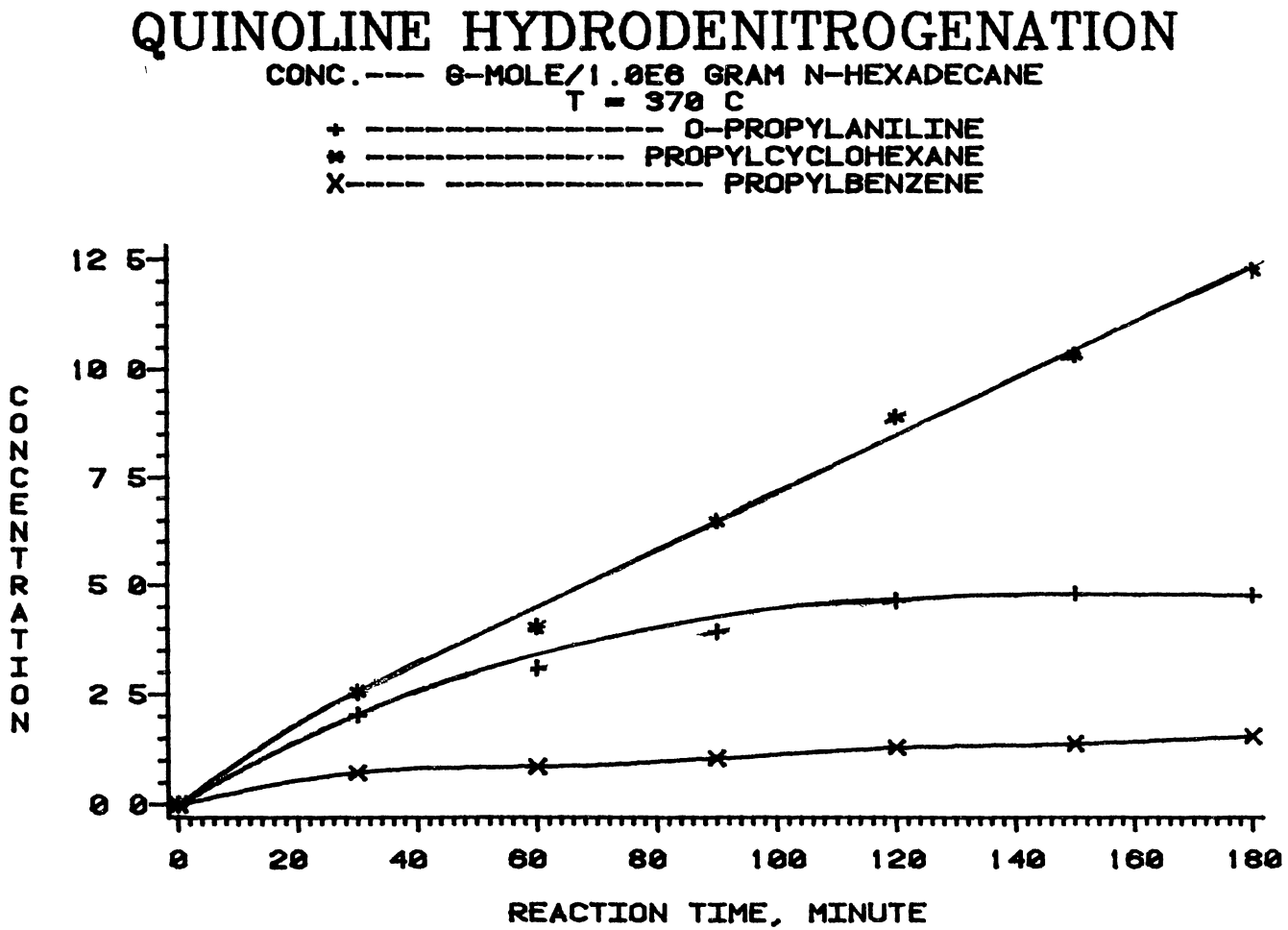

Figure 23. Quinoline HDN Products at 370°C

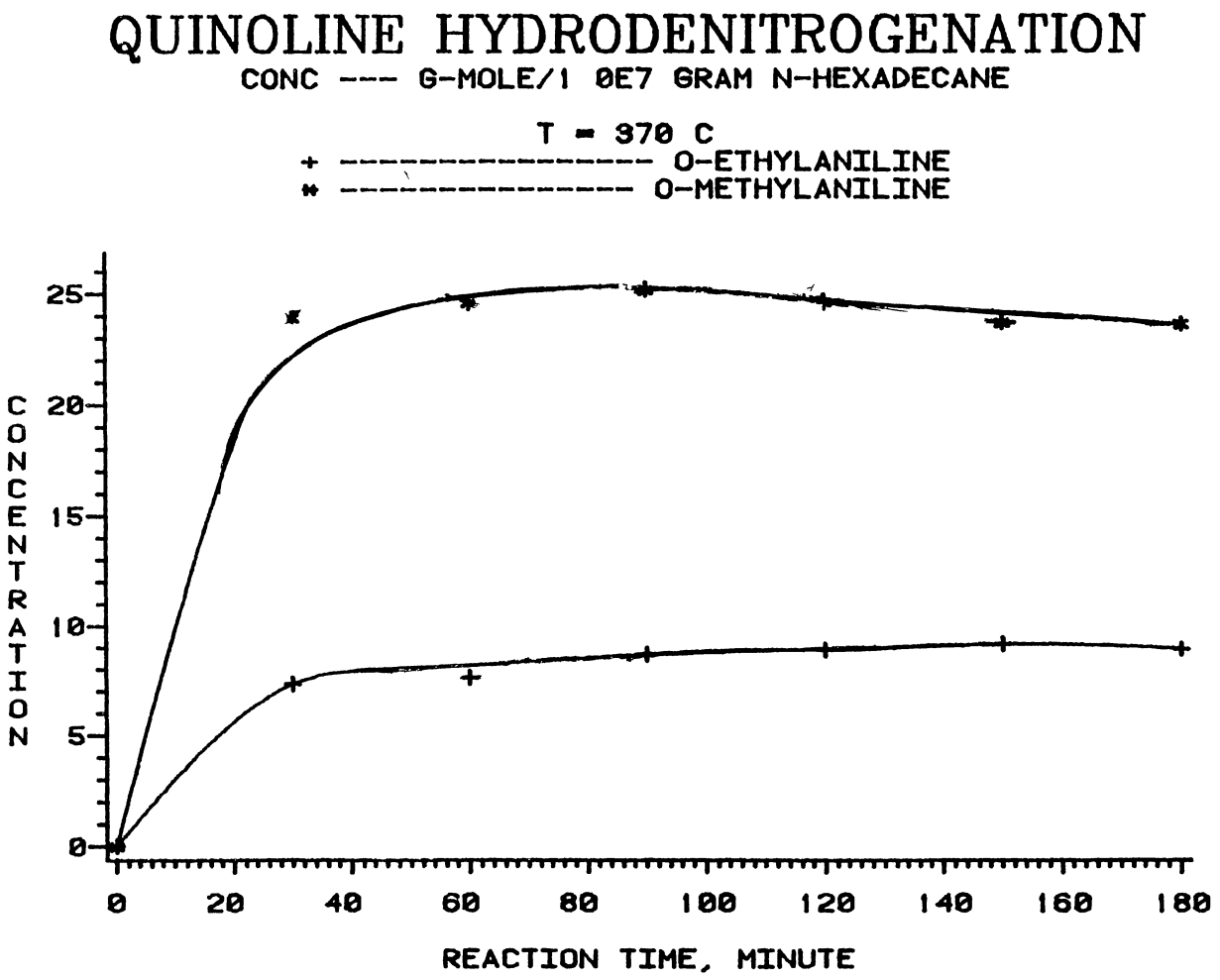

Figure 24 Quinoline HDN Products at 370°C

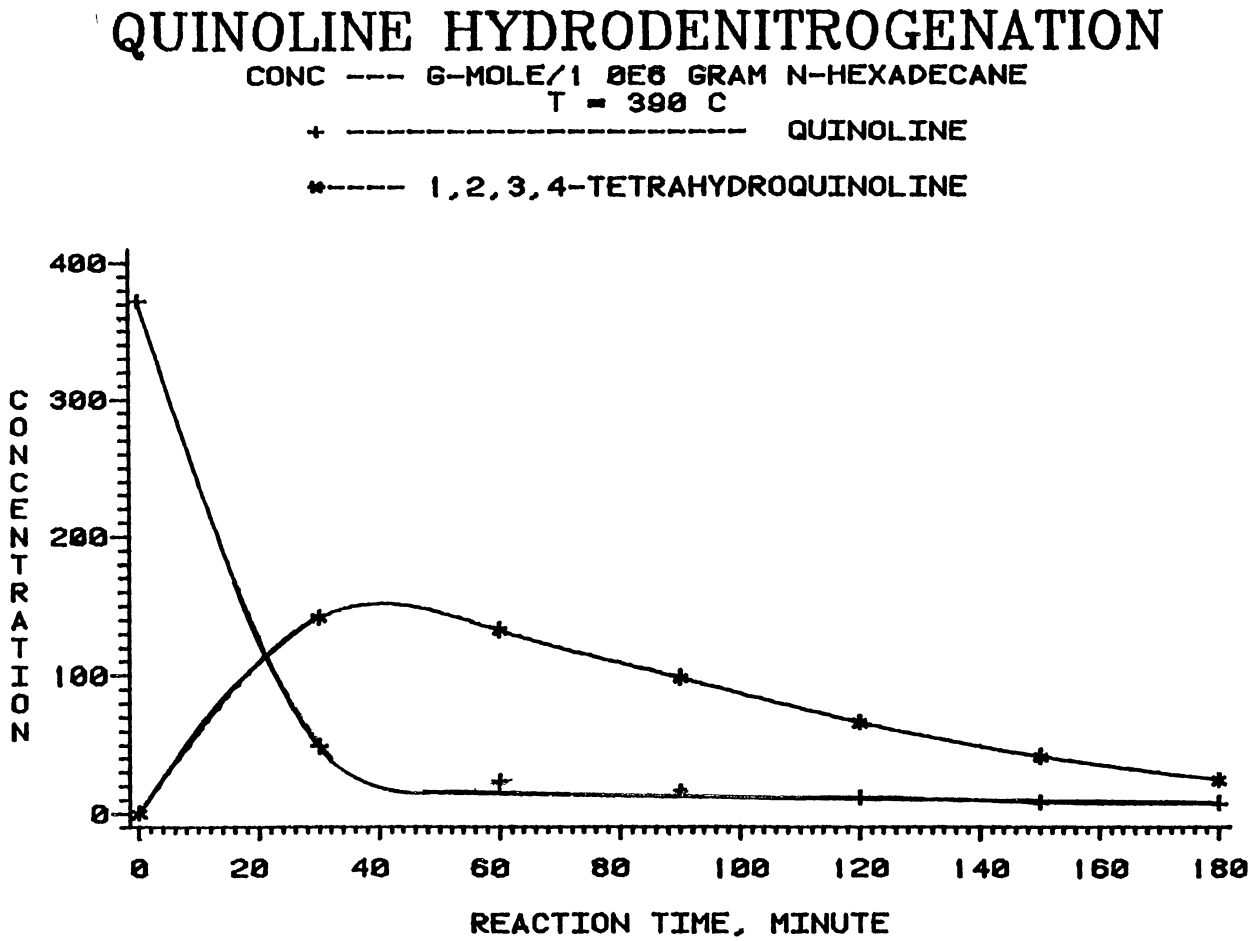

Figure 25 Quinoline HDN Products at 390°C

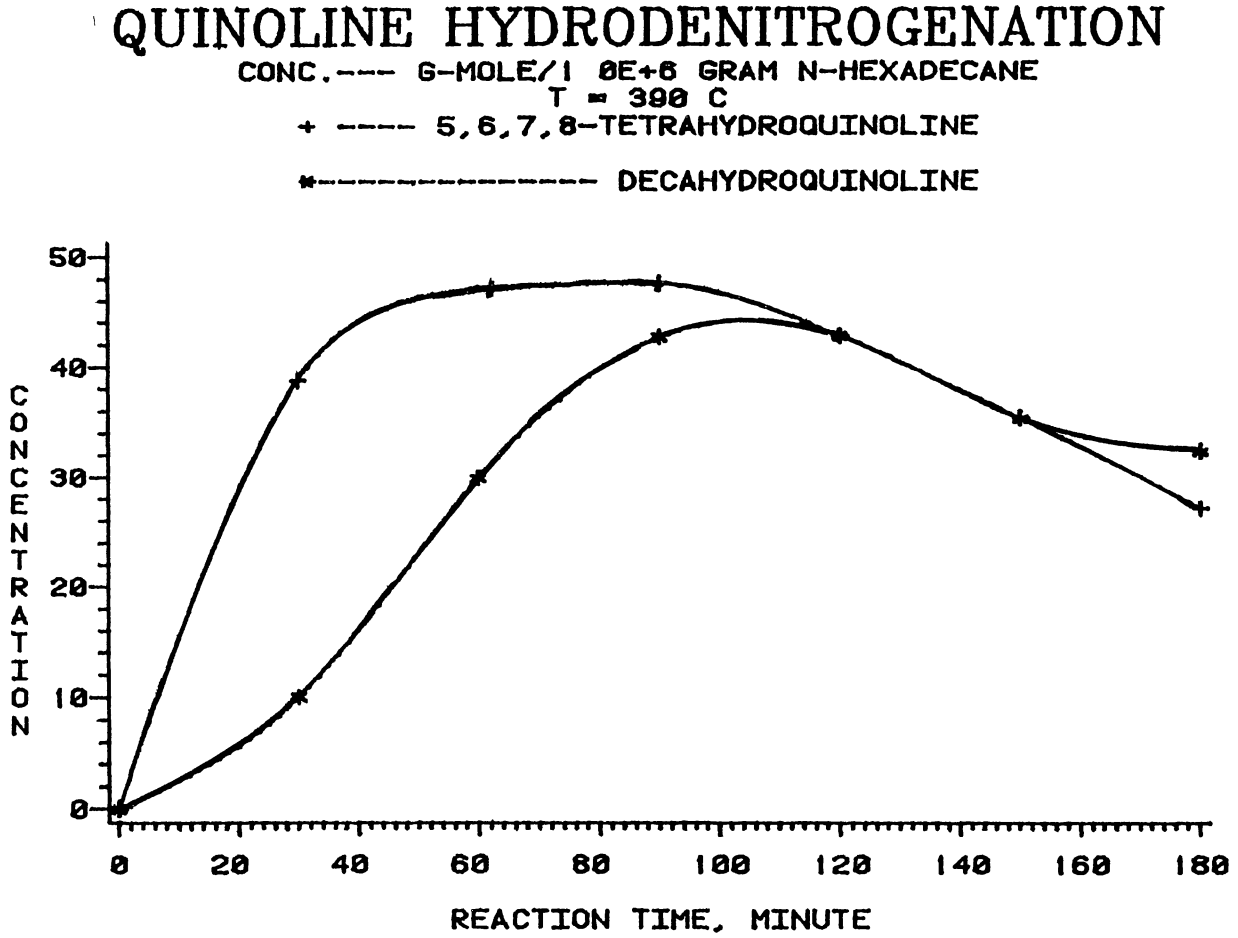

Figure 26. Quinoline HDN Products at 390°C

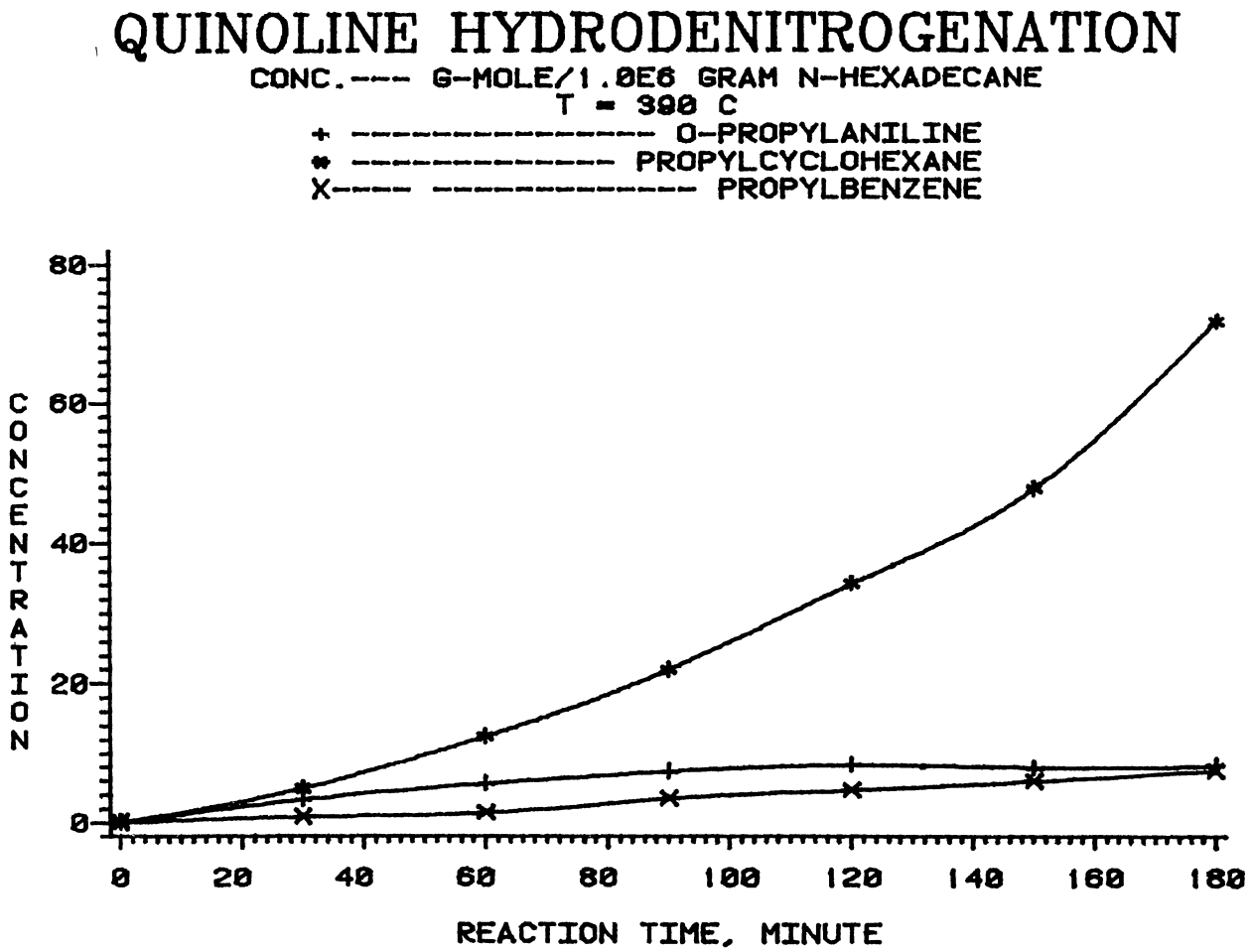

Figure 27. Quinoline HDN Products at 390°C

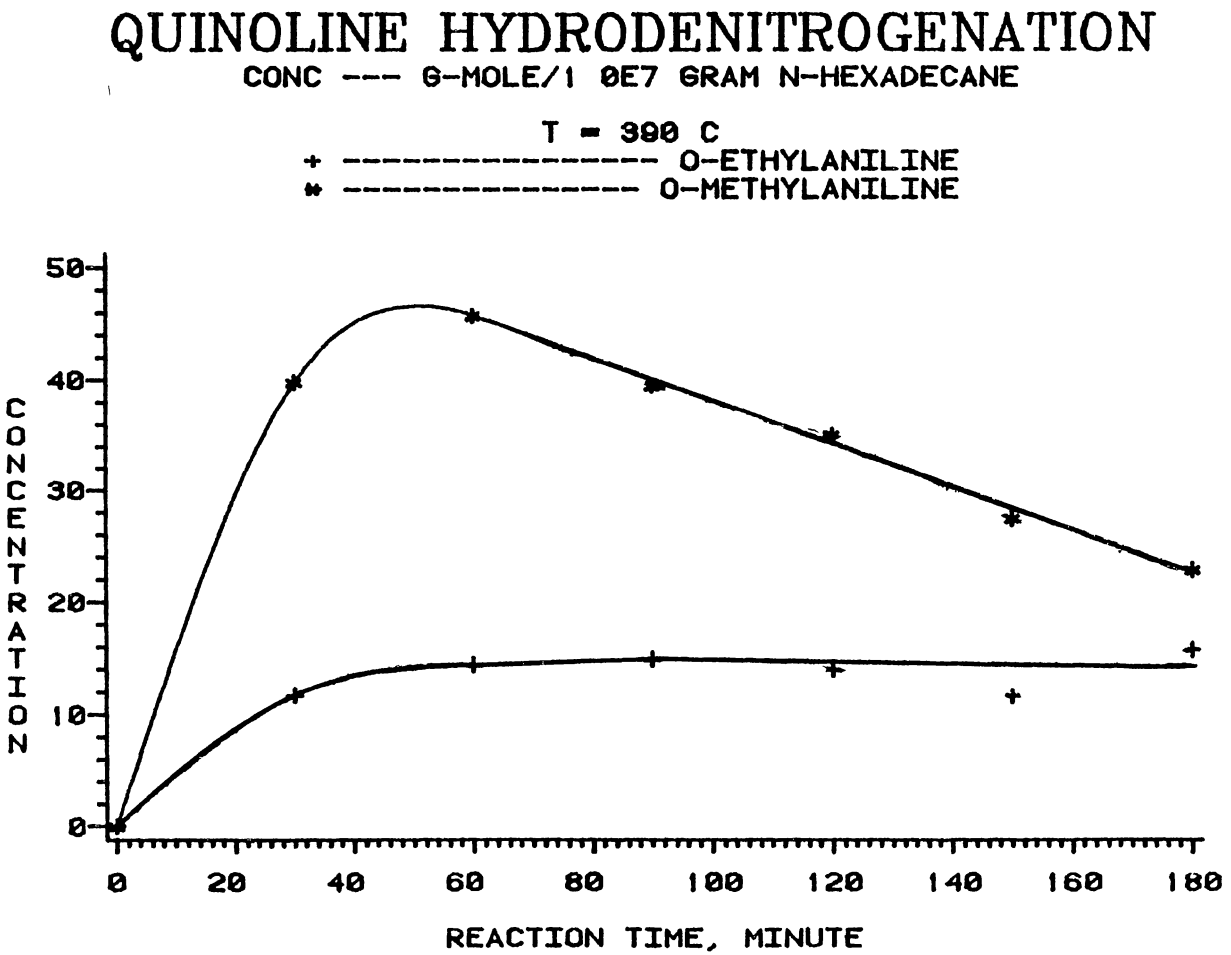

Figure 28. Quinoline HDN Products at 390°C

concentration level as can be seen in Figure 19. Also, concentrations of both PCH and PB are presented in this figure. Aniline shows a maximum concentration at 0.7 hrs., whereas OMA, after an initially fast production, levels off without going through a maximum This can be noticed in Figure 20 The behavior of both compounds gives an indication that they are reaction intermediates and are not the final products OEA appears only in small concentrations and increases very slowly with time.

At 370°C the HDN identified products are the same as before except for aniline which appears to have disappeared rapidly and, hence, not shown in Figures 21-24. The rates of conversion of quinoline are higher and rates of formation of Py-THQ are lower then those at 357°C as can be seen in Figures 21-22, whereas Bz-THQ forms at a higher rate than at 357°C. This confirms the idea that at high temperatures quinoline hydrogenation is shifted towards Bz-THQ formation path. The concentrations of PCH, OEA, and OMA are also higher than those at 357°C. This can be seen in Figures 23-24.

At 390°C 90% of quinoline is converted in about one half an hour Also, clear maxima appeared for Py-THQ, and DHQ This can be seen in Figures 25-26. The concentrations of PCH, OEA, and OMA are higher than those at 370°C Also, OMA goes through a clear maximum. These are shown in Figures 27-28.

A.1 Temperature Effect

In order to clearly show the effect of temperature, concentration versus time plots for each compound are shown in Figures 29-37.

Figure 29 presents quinoline profiles. It is apparent that increasing temperature increases the rate of quinoline conversion and the rate by which the equilibrium is attained. However, the equilibrium conversion seems to be not significantly affected by the temperature.

Figure 30 presents Py-THQ profiles. It can be seen that increasing reaction temperature decreases the rate of formation of Py-THQ, while it increases the rate of decomposition of Py-THQ to both OPA and DHQ

Figure 31 represents Bz-THQ profiles. The rate of formation of this compound increases with temperature. Similarly, its rate of hydrogenation to DHQ increases.

Figure 32 represents DHQ profiles. The effect of temperature on this compound is similar to that of Bz-THQ. Hence, at higher temperatures its rate of hydrogenolysis to PCH increases as shown in Figure 33. The shapes of these profiles lead to the conclusion that PCH is one of the final reaction products.

Figures 34 and 35 show the variations of OPA and PB concentrations respectively. Temperature increases the rate of formation of OPA, as well as the rate of its hydrogenolysis to PB. It is apparent from Figure 35 that PB is,

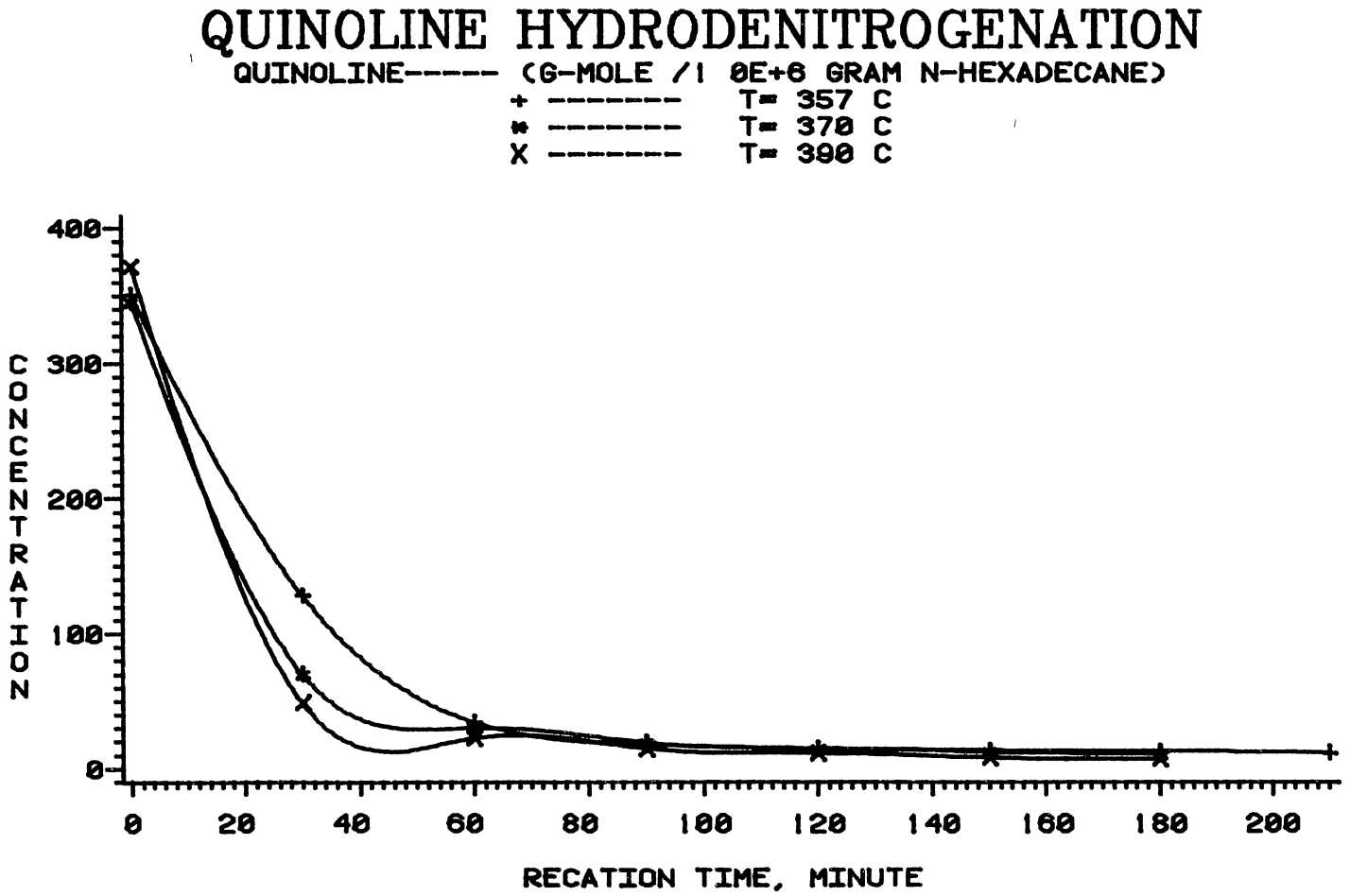

Figure 29. Effects of Temperature on Concentration of Quinoline

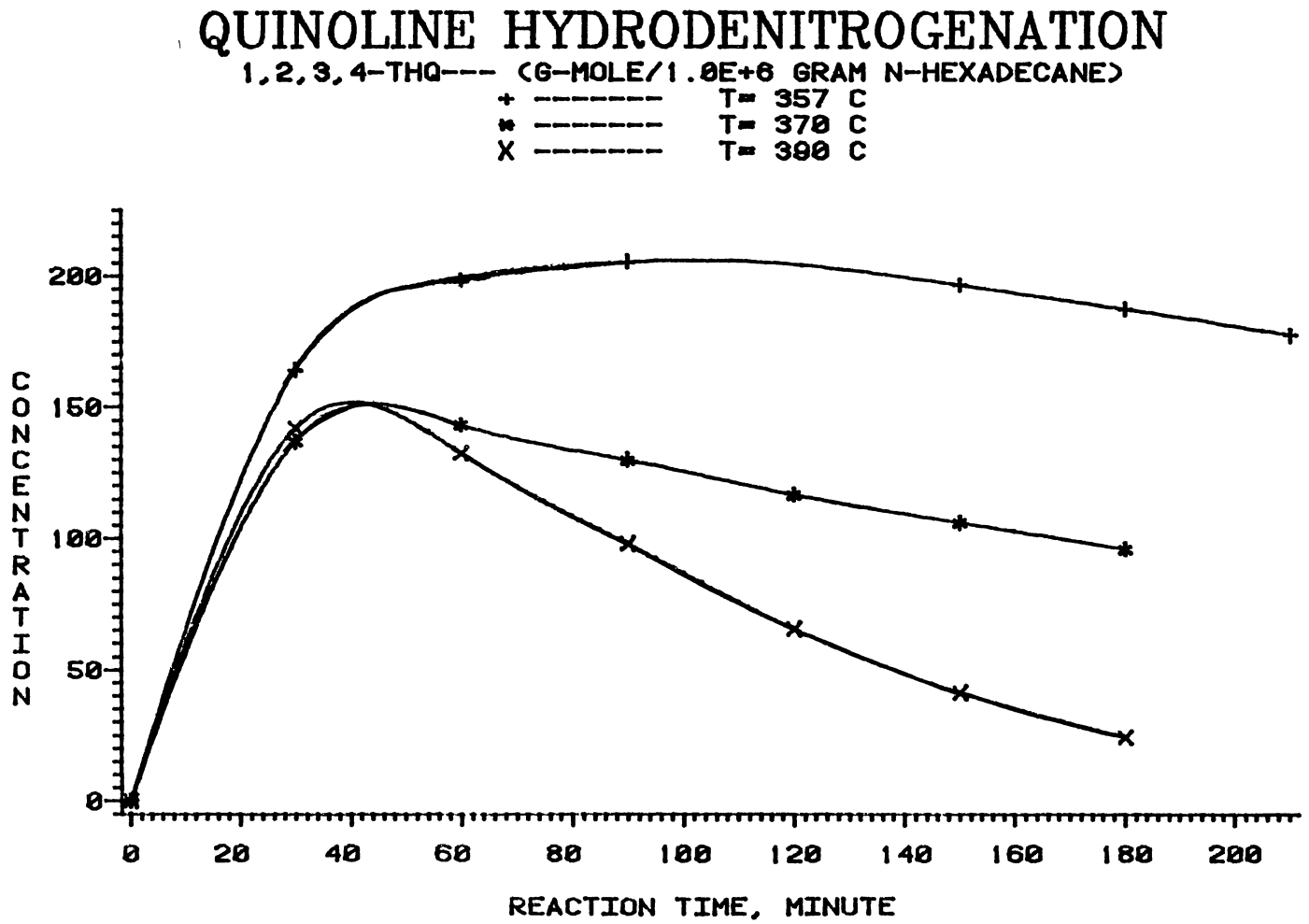

Figure 30. Effects of Temperature on Concentration of 1,2,3,4,-tetrahydroquinoline

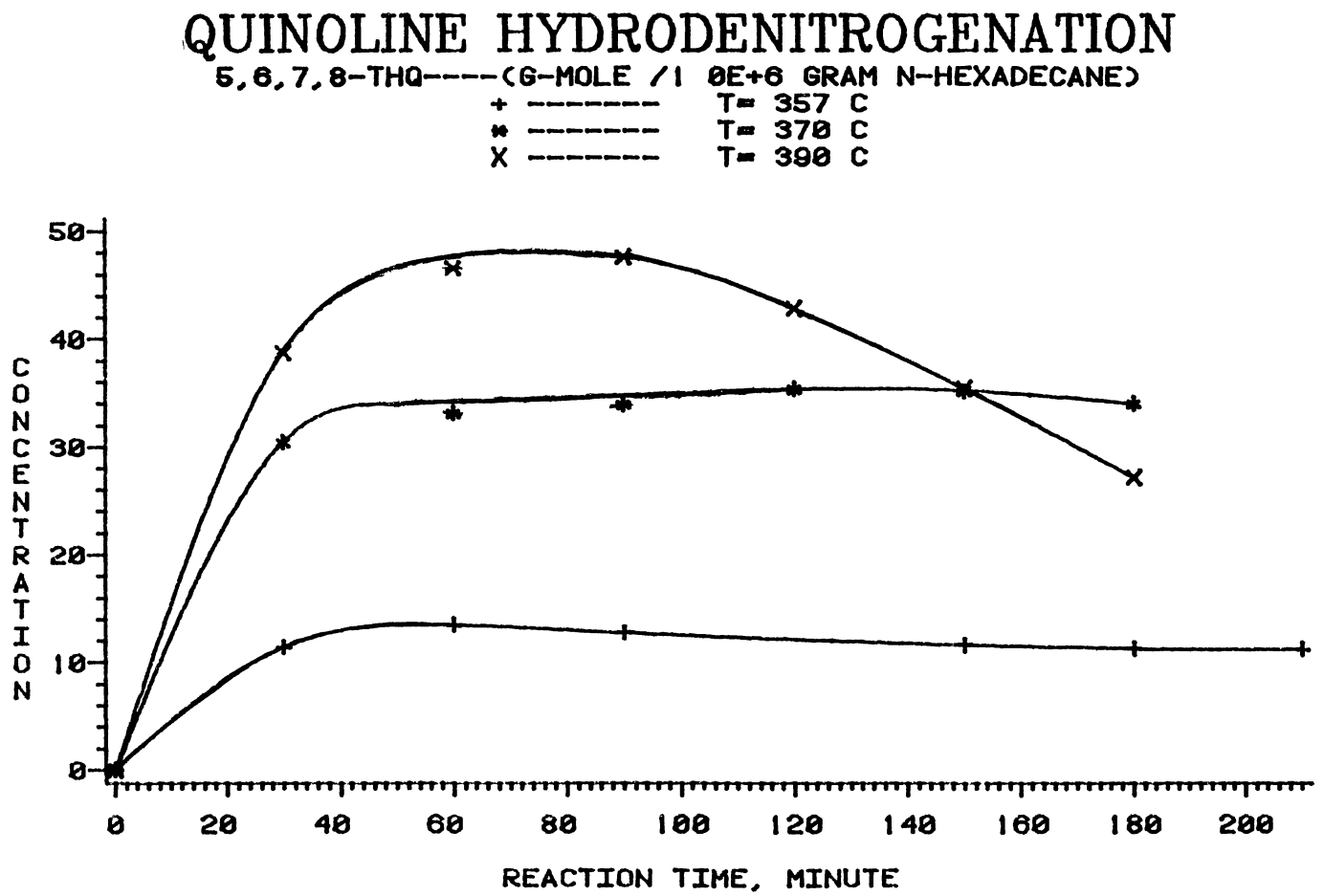

Figure 31. Effects of Temperature on Concentration of 5,6,7,8-tetrahydroquinoline

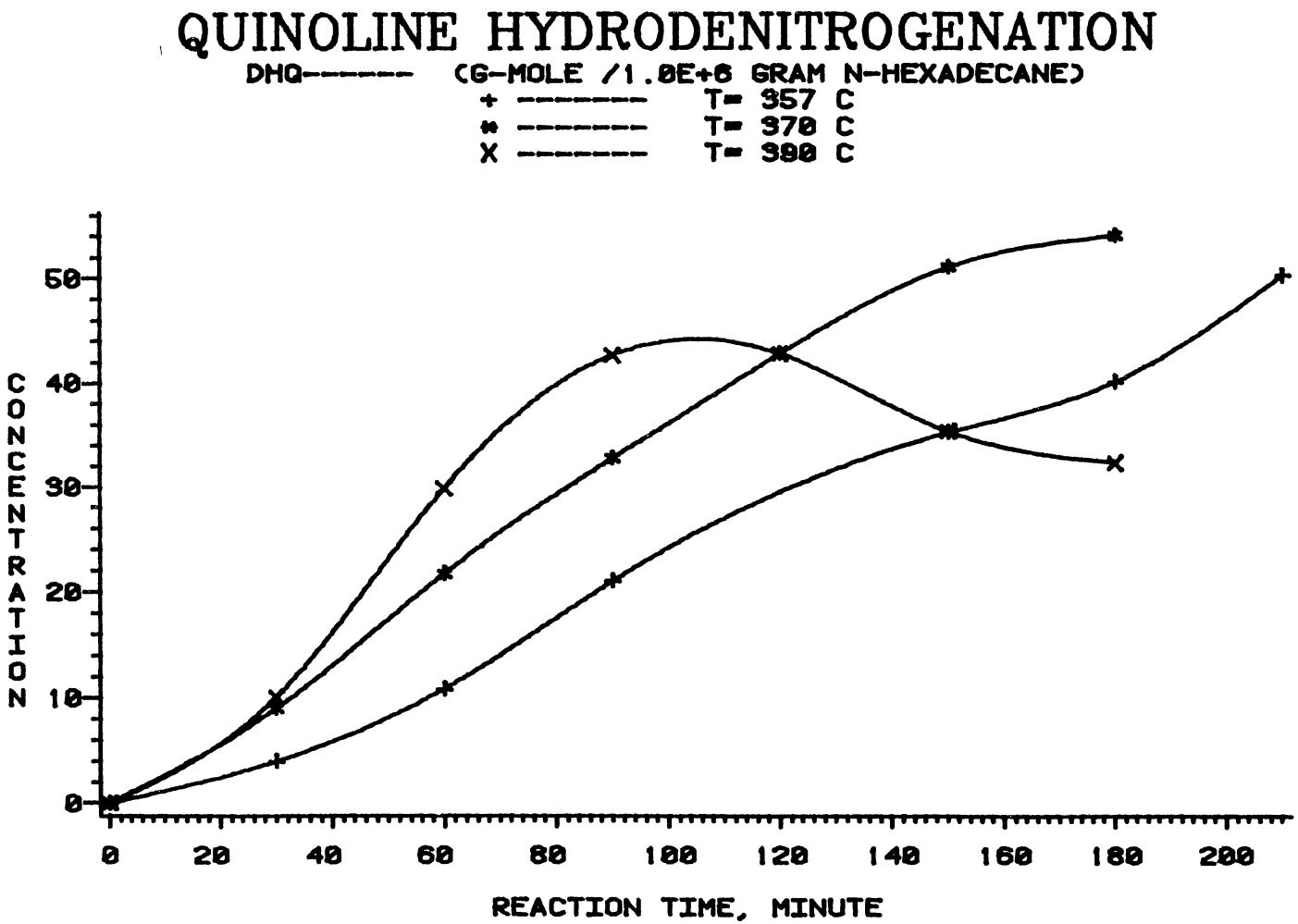

Figure 32. Effects of Temperature on Concentration of decahydroquinoline

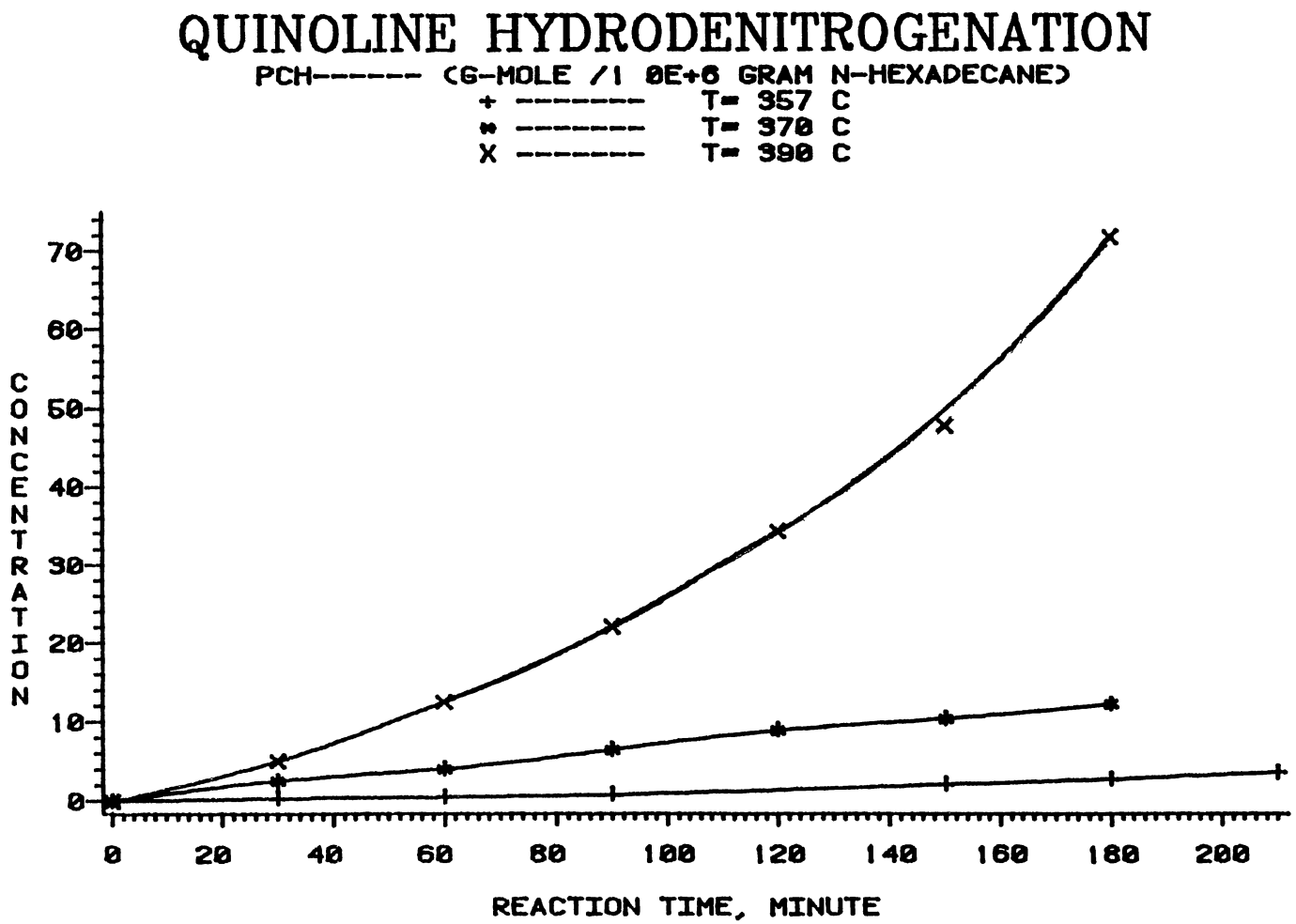

Figure 33. Effects of Temperature on Concentration of Propylcyclohexane

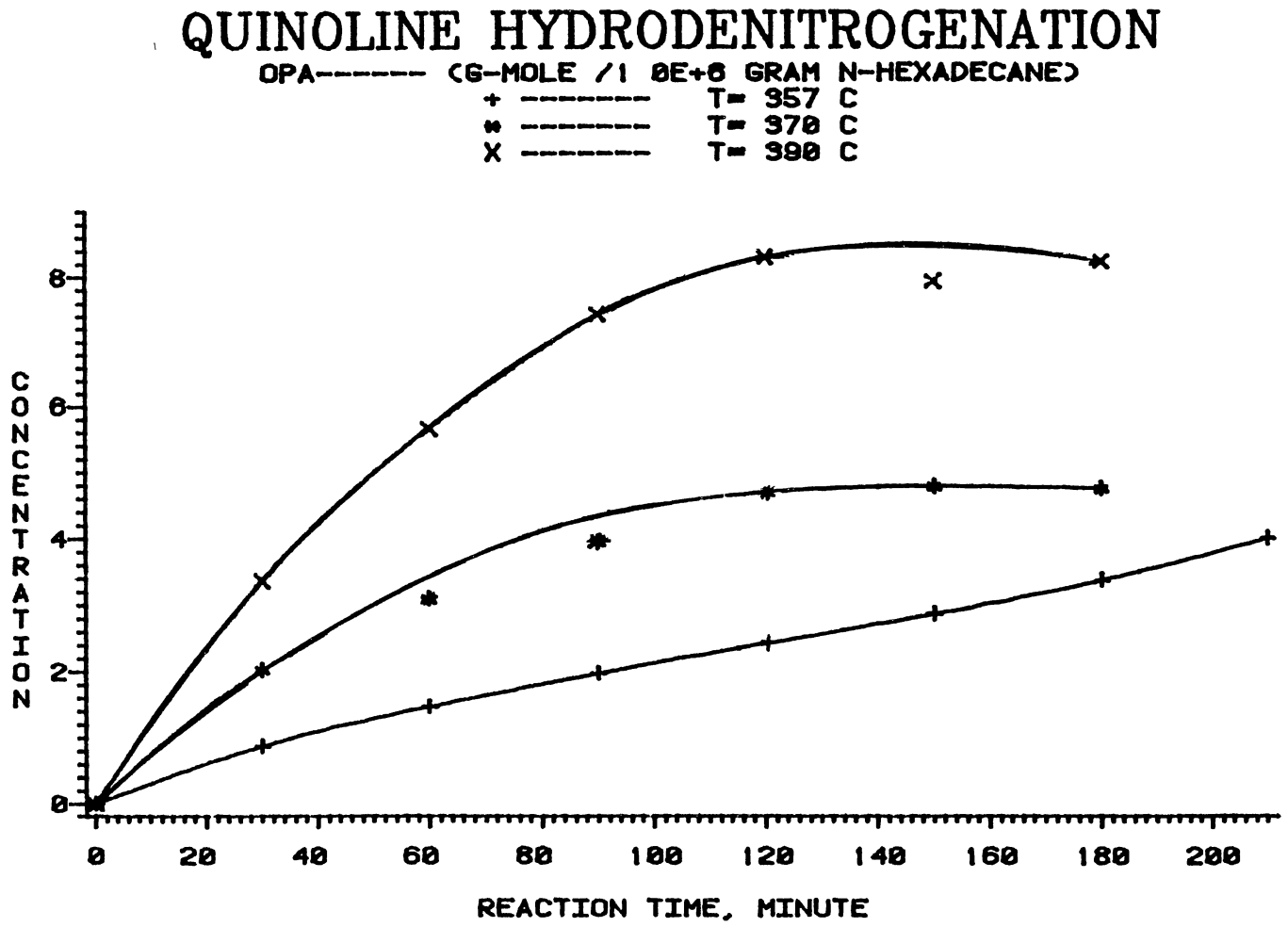

Figure 34. Effects of Temperature on Concentration of O-Propylaniline

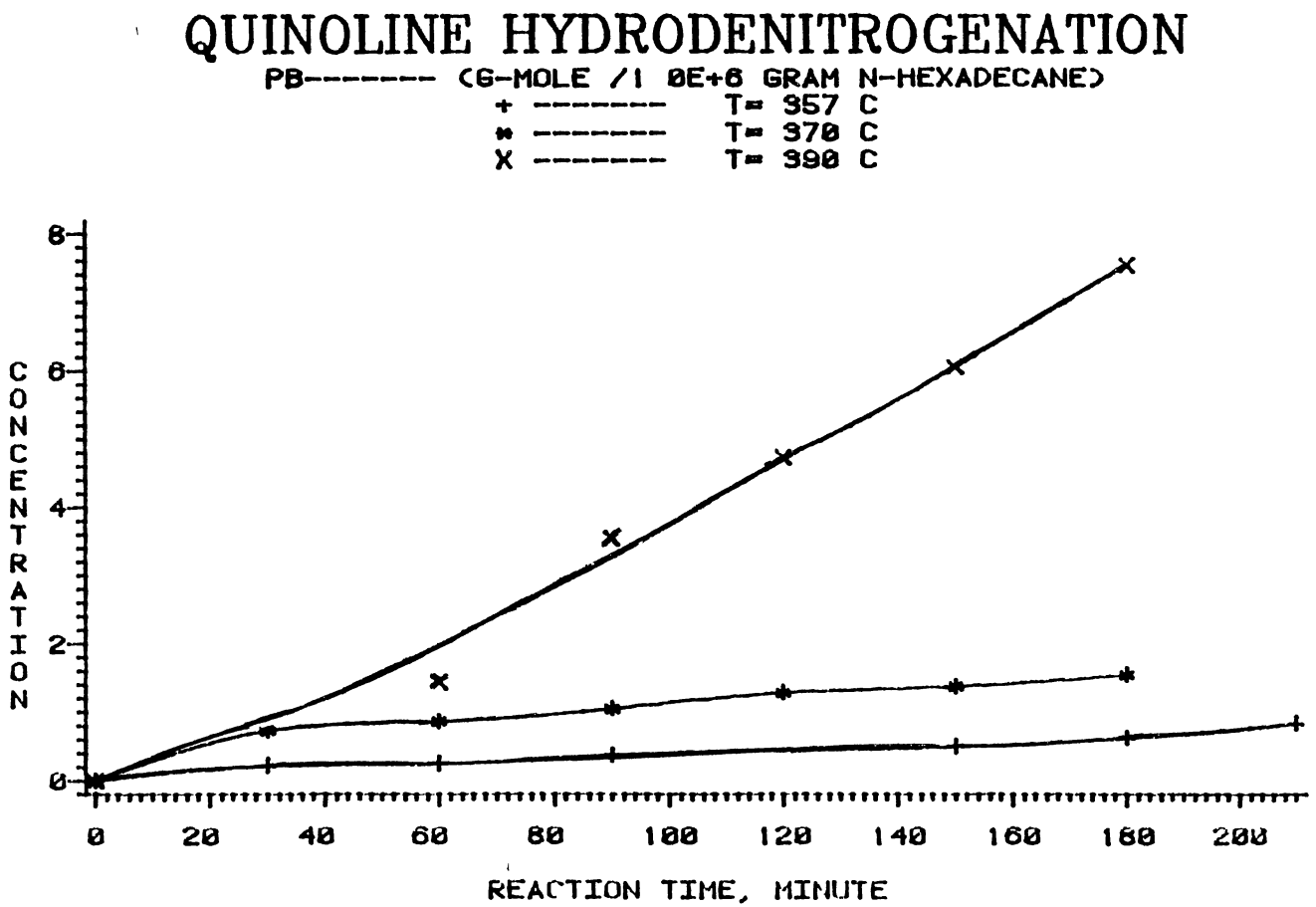

Figure 35 Effects of Temperature on Concentration of Propylbenzene

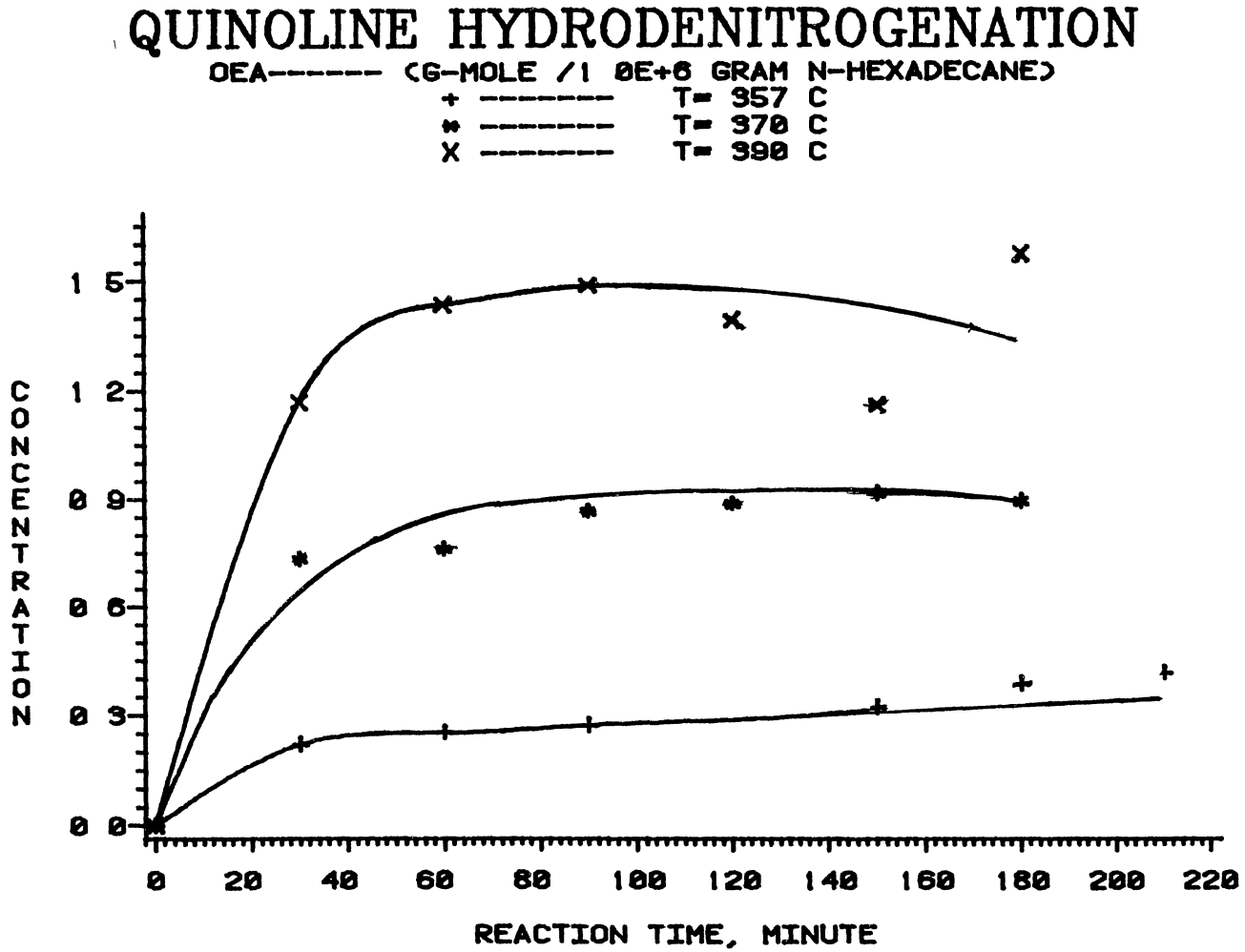

Figure 36. Effects of Temperature on Concentration of O-ethylaniline

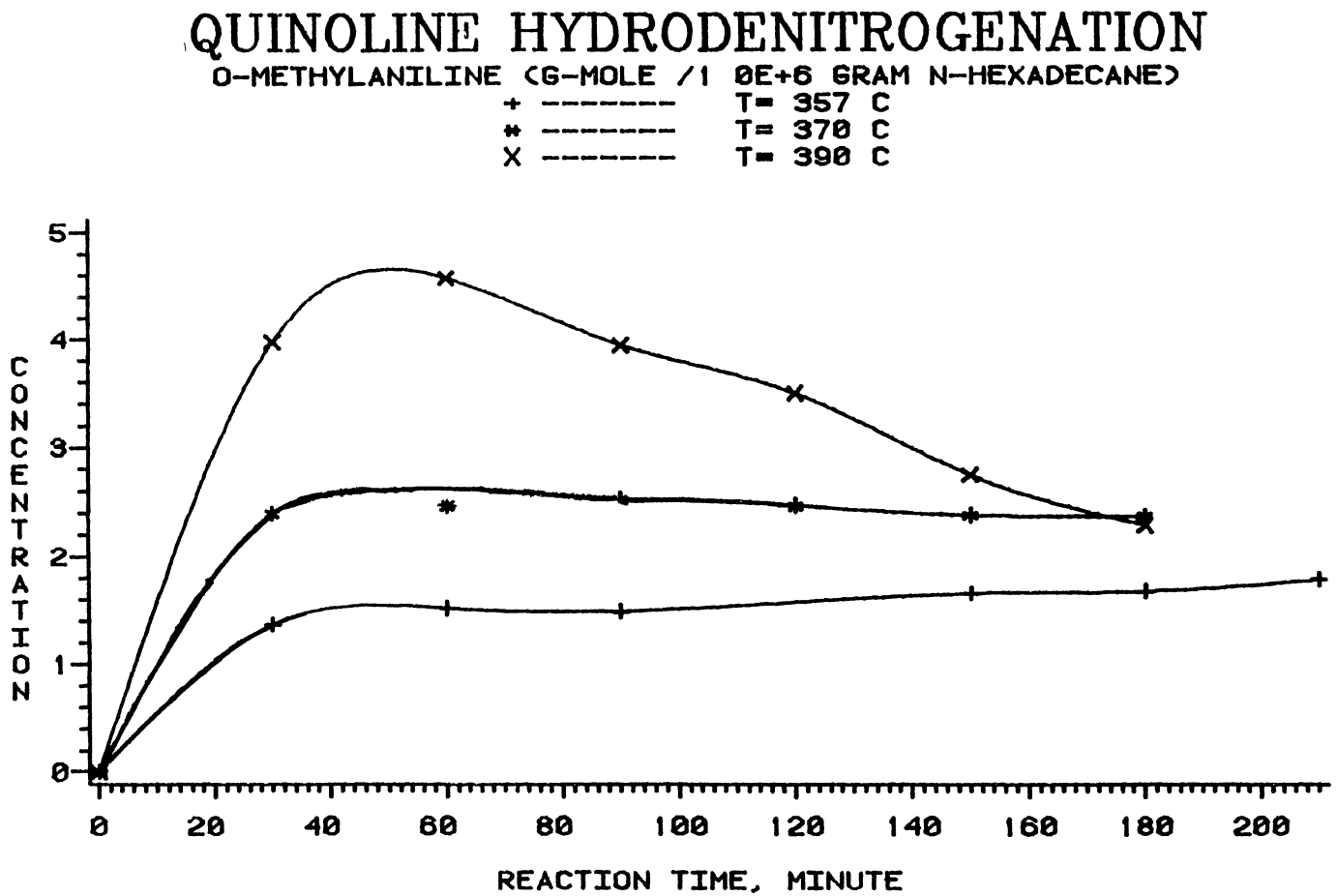

Figure 37. Effects of Temperature on Concentration of O-methylaniline

in fact, also a final reaction product. In addition, the rate of conversion of OPA to OEA and OMA increases with temperature as shown in Figures 36 and 37. Furthermore, these aniline derivatives are not expected to be final products as shown in their profiles specifically for OMA in Figures 37. These two compounds either convert to aniline which is readily converted to benzene and cyclohexcane, or are deaminized to their respective alkyl-benzenes.

A.2. Reaction Network

Several reaction networks have been proposed in the literature for quinoline HDN. The results are affected by reaction conditions, initial concentration, as well as the method of analysis. Considering these networks and the products obtained in this work, a reaction network of Figure 38 is presented. Individual reactions have been observed by other researchers, however the combined network is unique to this project. Each reaction path in this network as well as the investigators who proposed it are listed in Table XI. In fact, the use of a higher initial concentration in this work, as well as the use of a TSD helped greatly in confirming the formation of several reaction intermediates such as OEA, OMA, and aniline.

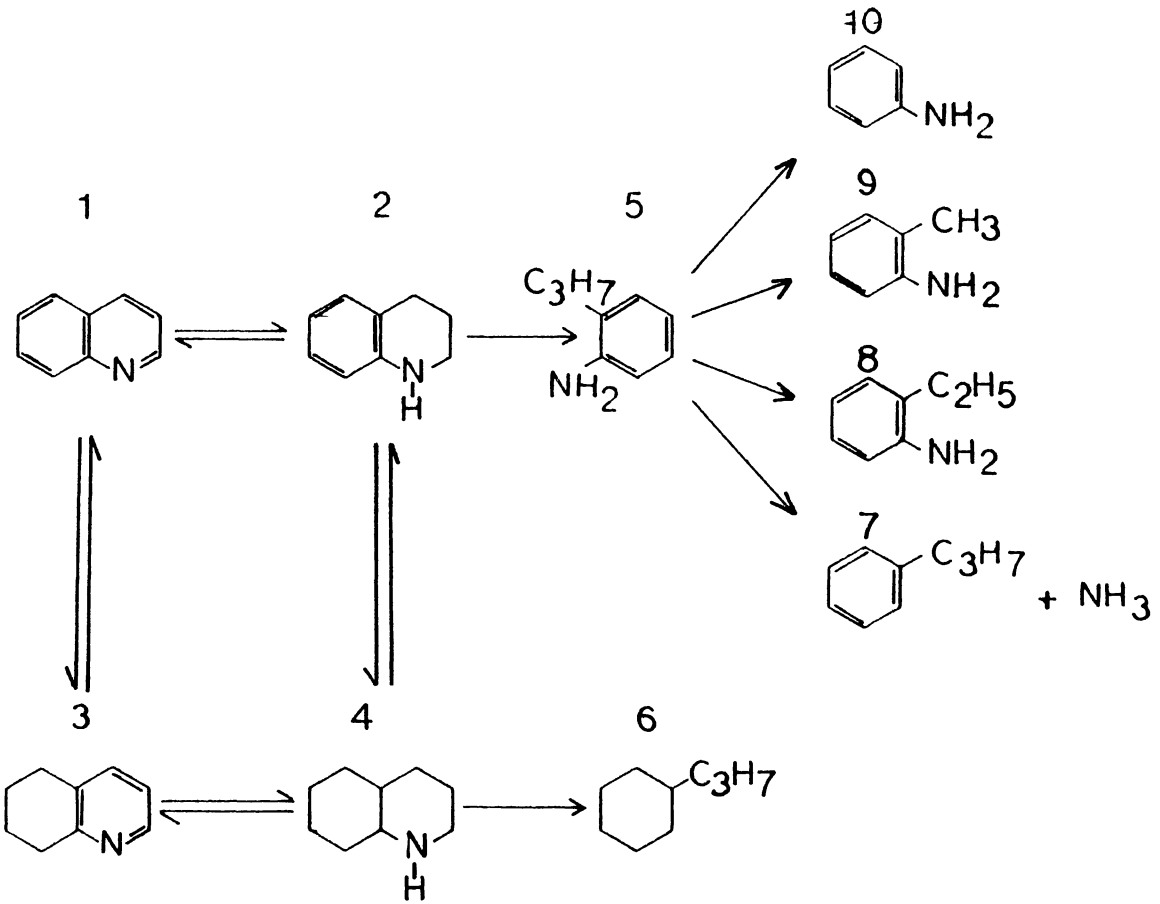

Figure 38. Reaction Network for Quinoline HDN, at 357-390°C, 8.2 MPa, HDS-9A Catalyst

TABLE XI

QUINOLINE HDN REACTION PATHS

Reaction Paths	References
1-->2, 2-->5	28,30,38,43,45,47,49,81
5-->7	28,30,43,45,47
1-->3	28,38,43,45,57,49,52
2-->1 , 2-->4	28,43,45,47,49,52
3-->1 , 4-->2	45,49,52
3-->4	28,38,43,45,47,49,52
4-->3	45,49,52
4-->6	28,43,45,52
5-->8 , 5-->9 , 5-->10	38
4-->7	47 (These paths include other intermediate compounds not shown in Figure 38.)
5-->6	81
7-->6	43

B. Acridine Hydrodenitrogenation

Hydrogenation of acridine results in a series of products. The type of compounds produced depends on the reaction conditions as well as the type of catalyst. Table XII summarize the reported compounds in the literature and their formation conditions. It is apparent from this table that hydrogenation of acridine may produce one or more of

TABLE XII

REDUCED ACRIDINES

Starting Material	Reaction Conditions	Products	Ref.
Acridine	Raney nickel/hydrogen, nickel/hydrogen, conducted at room temperature.	85% acridan	82
	Copper chromite/hydrogen	90% acridan	82
	Ruthenium oxide/hydrogen	98.5% acridan	83
	Raney nickle/hydrogen, at 100°C	16% SOHA	82
	Red phosphorus/iodine	trans-ASOHA	84
	Raney nickel/dioxan, at 100°C	38% ASOHA	82
	Copper chromite/dioxan, at 100°C	70% ASOHA	82
	Lithium/ethanol	STHA	85
	Raney nickel/hydrogen	22% DDHA	82
	Raney nickel/hydrogen, at 240°C	81% α-PHA	82
	Raney nickel/hydrogen, 2.2-4.5 hr, 240-270°C, 75-100 atm.	70-80% α-PHA	86
	Ruthenium oxide/hydrogen, 180°, 110 atm.	Unidentified PHA	82
	Raney nickel/hydrogen, high temparature	1,2,3,4-THA	87

TABLE XII (Continued)

Starting Material	Reaction Conditions	Products	Ref.
9,10-DHA or acridan	Phosphorus/hydroiodic acid.	trans-OHA	88
	Raney nickel/hydrogen	OHA + DDHA	82
1,2,3,4-THA	Tin/hydrocloride acid	Cis-ASOHA +	89,90
	Sodium formate/95% formic acid.	51.6% trans-ASOHA	91
	Platinum oxide/glacial acetic acid.	SOHA + Cis-ASOHA+ trans-	86
	Palladium/Platinum/ Charcoal in methanol.	Cis-ASOHA	92
	Raney nickel/hydrogen, 2.2-4.5 hr, 240-270, 75-100 atm.	70-80% α-PHA	86
STHA	Platinum/acetic acid	SOHA	93
SOHA	Catalytic dehydrogenation, palladium/charcoal 200-250°C.	acridan + acridine	87
	Sodium/ethanol/nickel formate,room temperature.	Unidentified PHA	94
Cis-OHA	Platinum oxide/glacial acetic acid/hydrogen, room temperature and pressure.	20% DDHA + 66% β-PHA + 9% γ-PHA	86
	Raney nickel/hydrogen, 2.2-4.5 hr, 240-270°C, 75-100 atm.	70-80% α-PHA	86

TABLE XII (Continued)

Starting Material	Reaction Conditions	Products	Ref.
trans-OHA	Raney nickel/hydrogen, 2.2-4 5 hr, 240-270°C 75-100 atm.	70-80% α-PHA	86
	Platinum oxide/acetic acid/hydrogen,normal temperature and pressure.	60% α-PHA 15% ß-PHA	95
$\Delta^{4a,10}$-DDHA	Platinum oxide/dioxan/ hydrogen,normal temperature and pressure.	30.5% α-PHA 28% ß-PHA	112

the following compounds

9,10-dihydroacridine or acridan (9,10-DHA)

1,2,3,4-tetrahydroacridine or asymmetric-tetrahydroacridine (1,2,3,4-THA or ASTHA)

1,2,7,8-tetrahydroacridine or symetric-tetrahydroacridine (STHA)

1,2,3,4,5,6,7,8-octahydroacridine or symmetric-octahydroacridine (SOHA)

1,2,3,4,9,10,4a,9a-octahydroacridine or asymmmetric-octahydroacridine (ASOHA)

α - perhydroacridine (α-PHA)

β - perhydroacridine (β-PHA)

γ - perhydroacridine (γ-PHA)

dodecahydroacridine (DDHA)

$\Delta^{4a,10}$-dodecahydroacridine (95,96).

ASOHA also exists in two forms of cis and trans. In addition to the acridine derivatives listed in Table XII, several other compounds have been synthesized, and reported in the literature

1,2,3,4,7,8-hexahydroacridine (97)

1,2,3,4,5,6,7,8,9,10-decahydroacridine or DHA (98)

1,2-dihydroacridine or 1,2-DHA (99)

Furthermore, tetradecahydroacridine or perhydroacridine (PHA) is, in theory, capable of exisiting in five geometric configurations, three of which, α, β, and γ, have been reported in the literature (100). Thus, the hydrogenation of acridine results in a mixture of compounds which may contain a number of hydrogenated acridines. This number, theoretically varies between one and seventeen. In addition, HDN of acridine also results in a hydrocarbon, dicyclohexylmethane (DCHM) (54).

In this project, in order to calibrate chromatogram, it was attempted to obtain these compounds in pure form. However, only two of these compounds were available commercially. 9,10-DHA, and SOHA. DCHM was obtained from Dr. Eisenbraun of the Chemistry Department at Oklahoma State

University. These compounds were used to calibrate the chromatograms. The analysis of the samples showed that 9,10-DHA did not exist in any of our samples SOHA and DCHM were identified and their concentrations were measured. The chromatograms contained several other compounds which had to be identified or predicted. Based on the relative melting points of the suspected compounds, the trends in the variations of their relative concentrations and the results of the previous workers (1,20,54) on acridine, the following compounds are predicted

1,2,3,4-THA

SOHA

ASOHA

α-PHA

DCHM

We also used a gas chromatograph/mass spectrometer for identification of these compounds. However, the mass spectra for most acridine derivatives are not available in mass spectra libraries Based on the mass spectral analysis and the measured molecular weights, we could confirm the existance of the above mentioned compounds. In order to predict the concentrations of the compounds which were not available, we had to resort to approximate techniques, which are explained in Appendix B. The concentrations of these compounds at different times are tabulated in Tables XIII, XIV, and XV, and are presented in Figures 39-44.

TABLE XIII

REACTION PRODUCTS OF RUN NA1* (370°C)

Compound	Reaction Time, min.					
	30	60	90	120	150	180
Acridine	78	14	6	4	1	1
THA	40	64	74	71	66	57
ASOHA	39	36	27	21	17	14
SOHA	219	239	263	219	197	166
PHA	57	36	28	18	15	13
DCHM	22	50	75	117	161	199
Total Nitrogen	433	389	398	333	296	251

* g-mole/10^7 g n-hexadecane

Initial acridine concentration =

513 g-mole/10^7 g n-hexadecane

TABLE XIV

REACTION PRODUCTS OF RUN NA2* (390°C)

Compound	Reaction Time, min.					
	30	60	90	120	150	180
Acridine	164	47	22	8	6	6
THA	28	47	77	80	76	62
SOHA	456	525	614	594	539	481
ASOHA	91	80	73	61	50	42
PHA	185	155	133	110	92	80
DCHM	33	70	116	153	179	228
Total Nitrogen	924	854	919	853	763	671

* g-mole/10^7 g n-hexadecane

Initial acridine concentration =

1081 g-mole/10^7 g n-hexadecane

TABLE XV

REACTION PRODUCTS OF RUN NA3* (357°C)

Compound	Reaction Time, min.					
	30	60	90	120	150	180
Acridine	51	63	76	100	139	177
THA	127	243	253	264	260	240
ASOHA	399	549	503	481	453	398
SOHA	89	74	50	42	39	356
PHA	60	43	30	24	22	20
DCHM	185	37	12	5	3	3
Total Nitrogen	860	946	848	816	777	696

* g-mole/10^7 g n-hexadecane

Initial acridine concentration =

1008 g-mole/10^7 g n-hexadecane

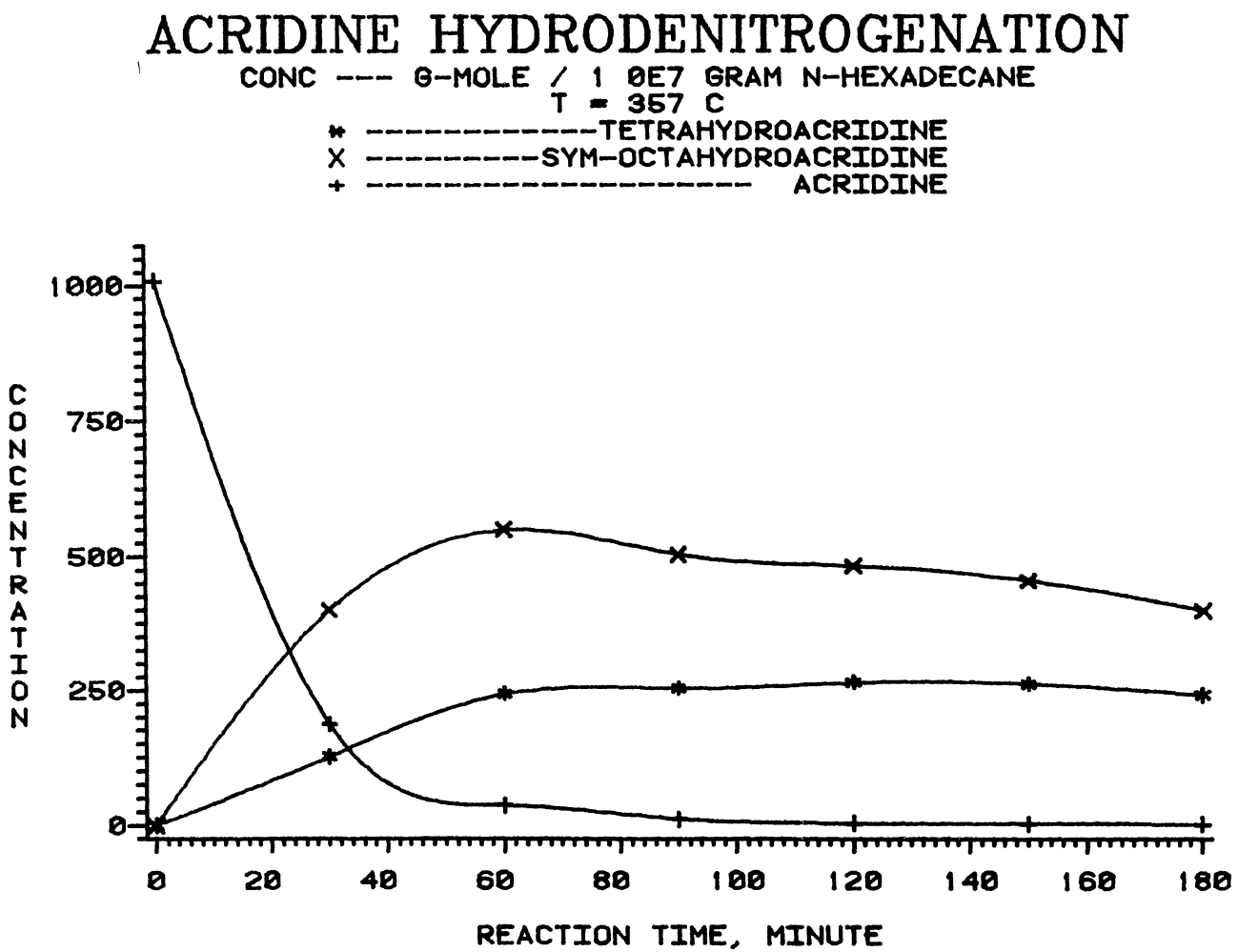

Figure 39. Acridine HDN Products at 357°C

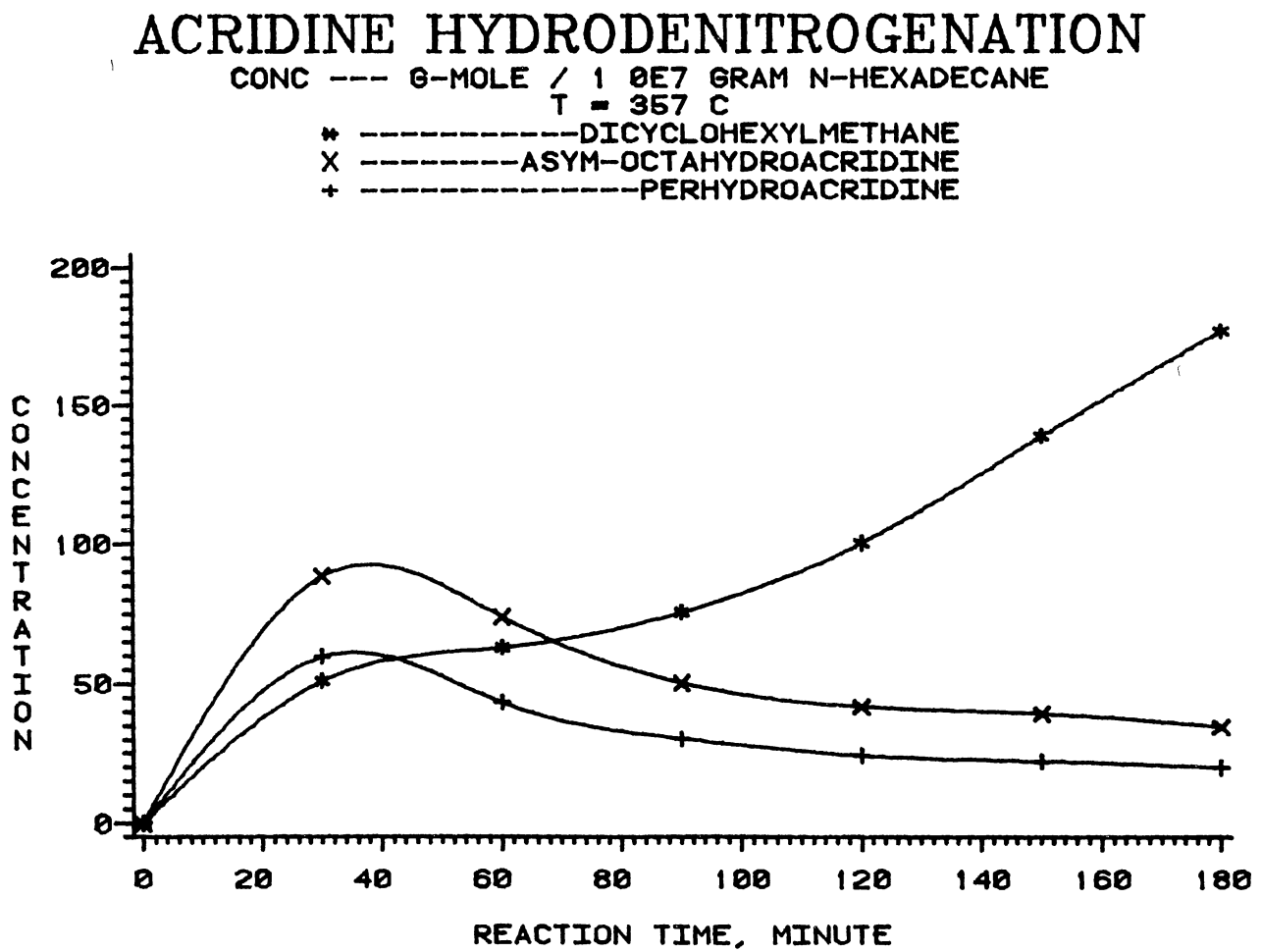

Figure 40. Acridine HDN Products at 357°C

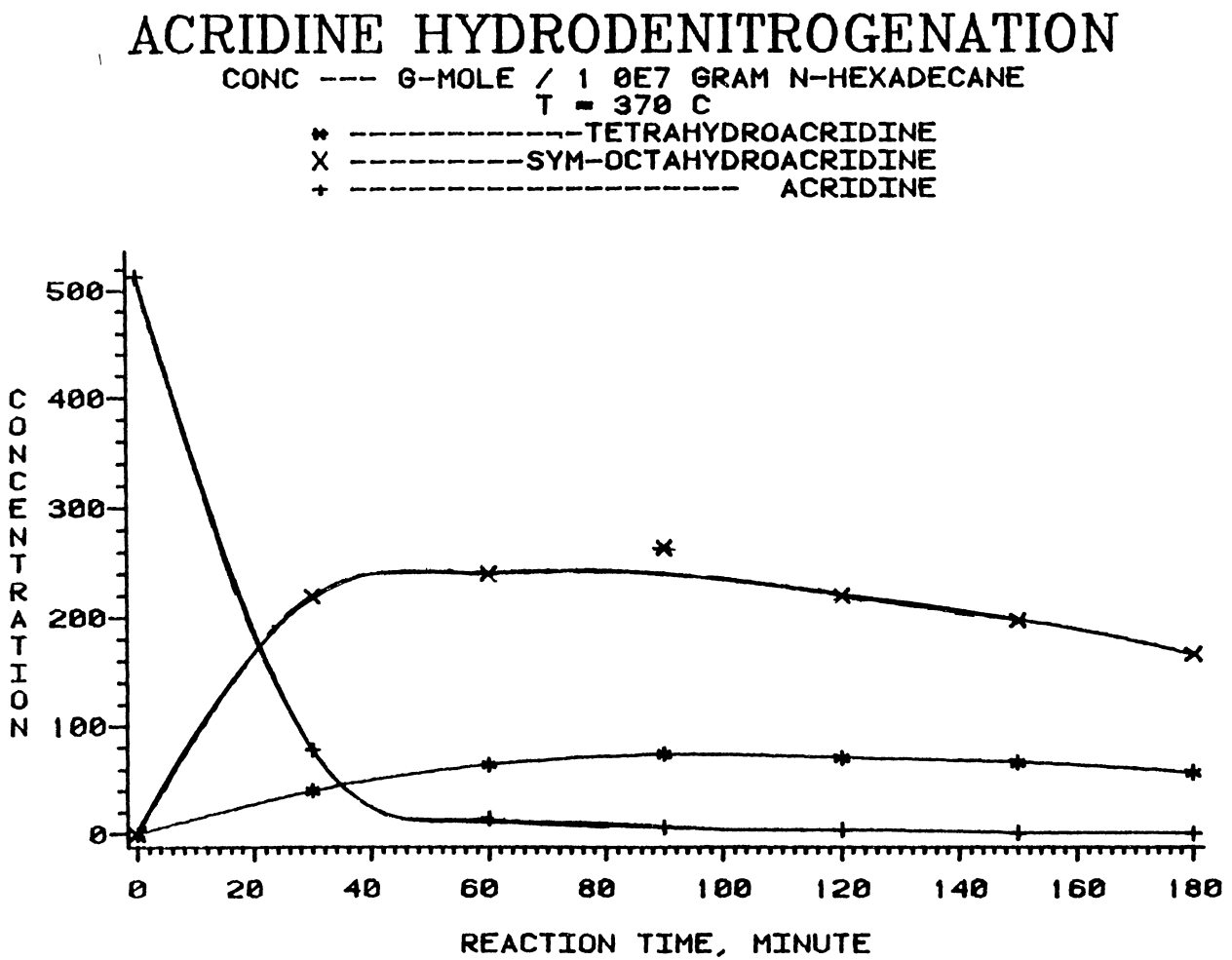

Figure 41 Acridine HDN Products at 370°C

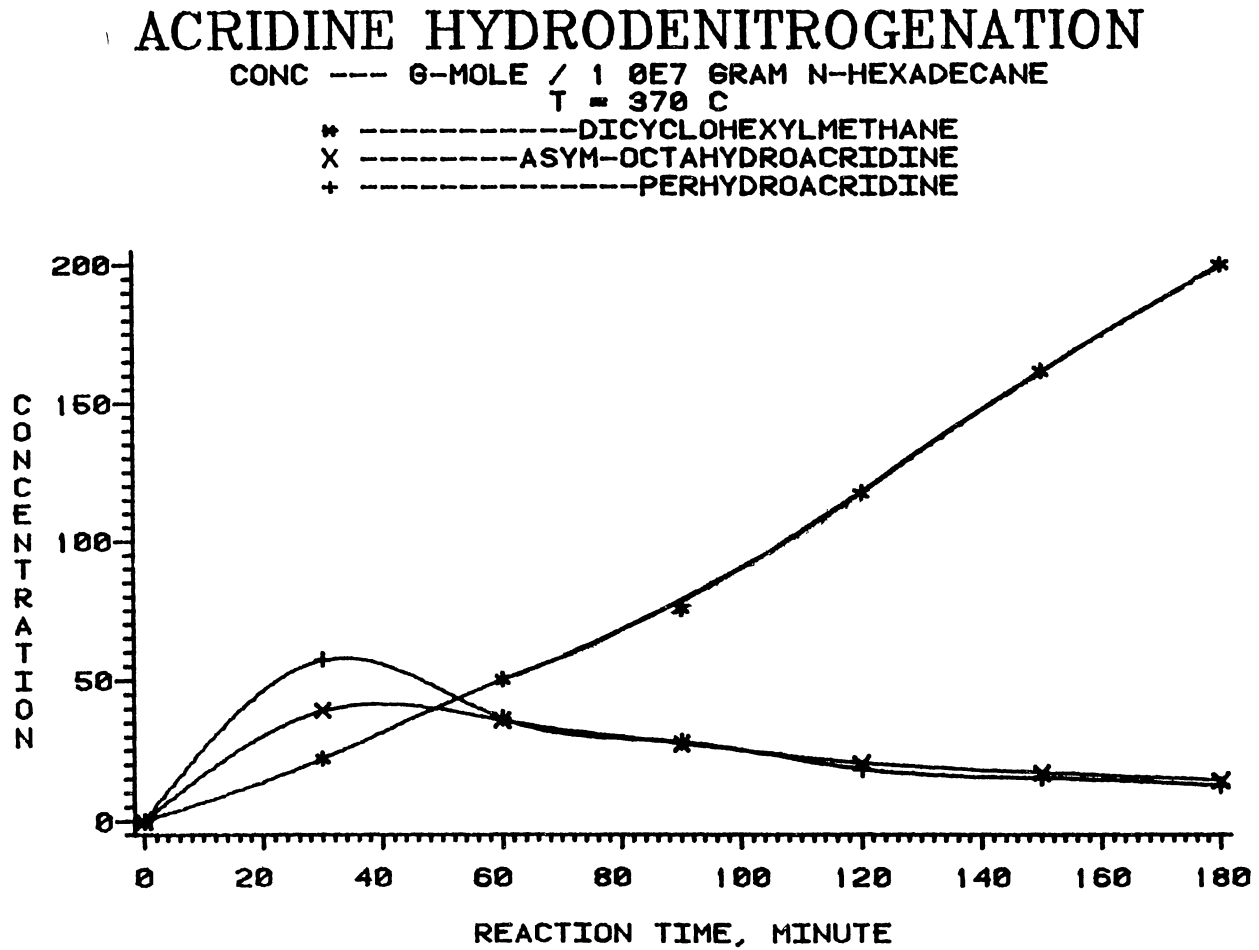

Figure 42, Acridine HDN Products at 370°C

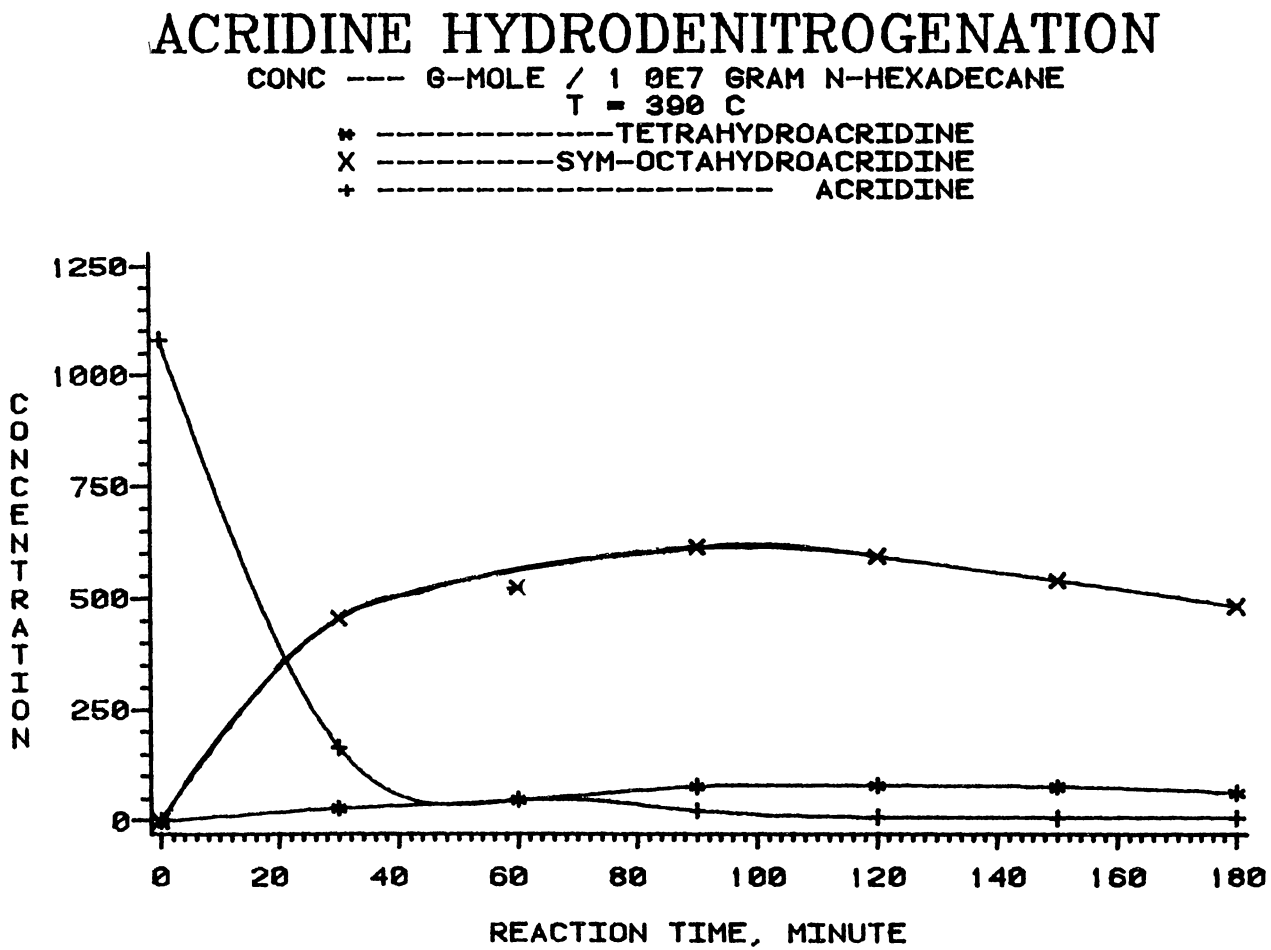

Figure 43. Acridine HDN Products at 390°C

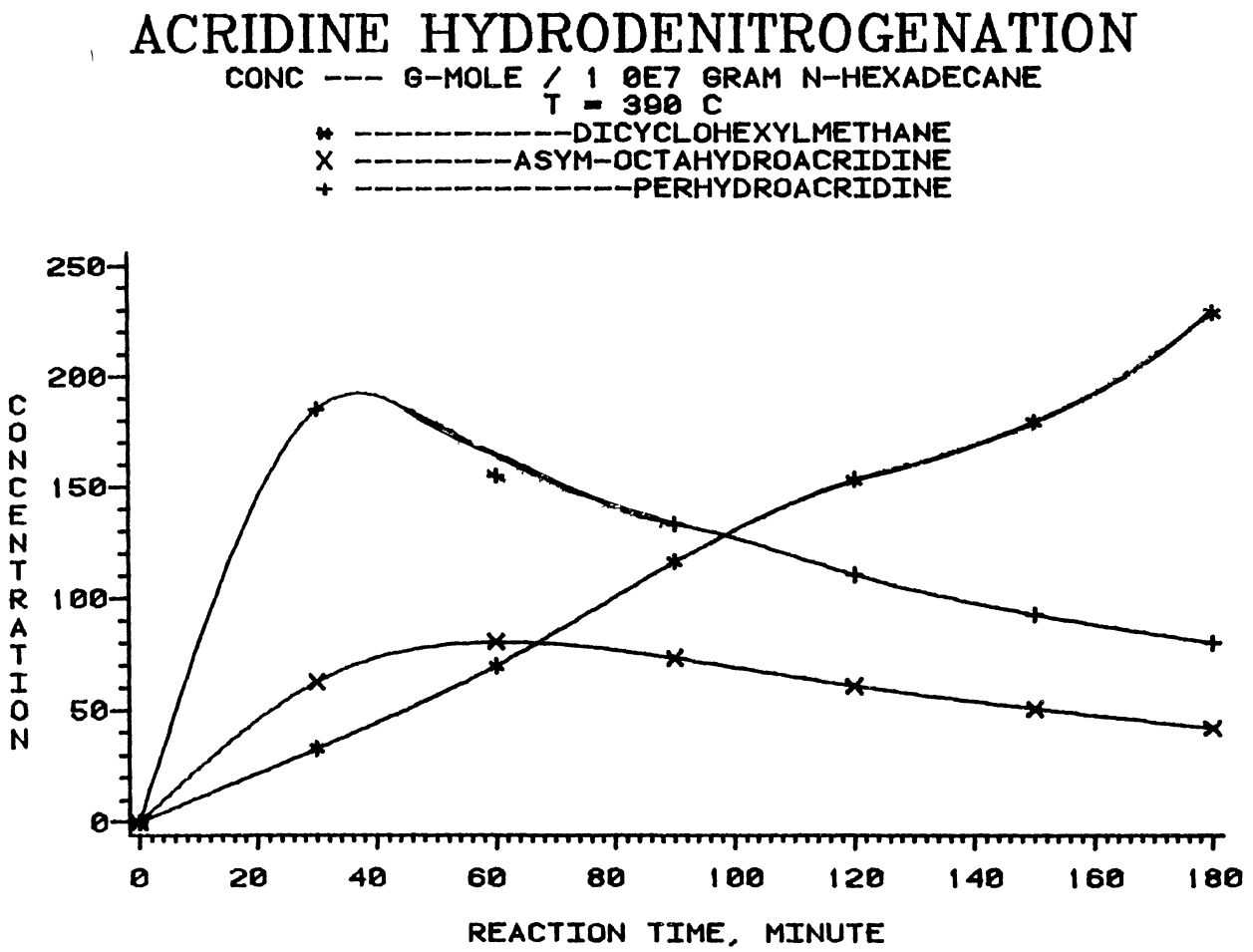

Figure 44. Acridine HDN Products at 390°C

At 357°C acridine concentration decreases to less than 4% in the first hour of reaction. It is converted mainly to THA and SOHA. Small amounts of ASOHA and PHA appear in the reaction products as shown in Figures 39-40. SOHA attains its maximum concentration after about one hour. But its rate of conversion is very slow. Formation of THA is slower than SOHA but after about one hour, its rate of formation is decreased appreciably. After two hours its concentration slowly starts to decrease. In fact the shapes of the plots of THA and SOHA in Figure 39 show that conversion rates are slow and show an equilibrium. On the other hand, DCHM is formed from the hydrogenolysis reaction and its concentration continuously increases with time. These are clearly shown in Figure 42. The rate of total nitrogen removal is slow as is shown in Table XIII. It shows about 51% removal in three hours.

Figures 43 and 44 show the reaction products at 390°C. Acridine, SOHA, and THA show similar behavior as in the 370°C run. This is clear from the comparison between the plots in Figures 41 and 43. However, higher concentration is noticed for THA at 370°C than at 390°C as observed from the comparison of Table XIII with Table XIV, whereas higher maximum concentration of PHA is noticed at 390°C than at 370°C as shown in Figures 41 and 43.

B. 1. Temperature Effect

In order to visualize the effect of temperature,

for each compound, the concentration profiles at different temperatures are plotted together and shown in Figures 45-50 The concentration of each compound at 357°C may be directly compared with its concentration at 390°C, since the initial acridine concentration is approximately the same for both cases Acridine conversion is not significantly affected by reaction temperature as is apparent in Figure 45 On the other hand temperature has a major effect on the rate of conversion of THA as shown in Figure 46. Temperature slightly increases the rate of formation of both SOHA and ASOHA as is apparent in Figures 47 and 48. Finally, at 390°C the rate of formation of PHA as well as the rate of its conversion to DCHM are higher than those at 357°C as shown in Figures 49 and 50 Total nitrogen removal is about 38% at 390°C, whereas it is about 31% at 357°C after three hours of reaction as is indicated in Tables XIV and XV.

B.2 Initial Concentration Effect

The initial acridine concentration at 370°C is about half its concentration at 357°C and 390°C. The total nitrogen removal is about 51% at 370°C, whereas it is 38% and 31% at 390°C and 357°C respectively. It is apparent that reaction rate of nitrogen removal depends on initial concentration. It increases with initial concentration decrease.

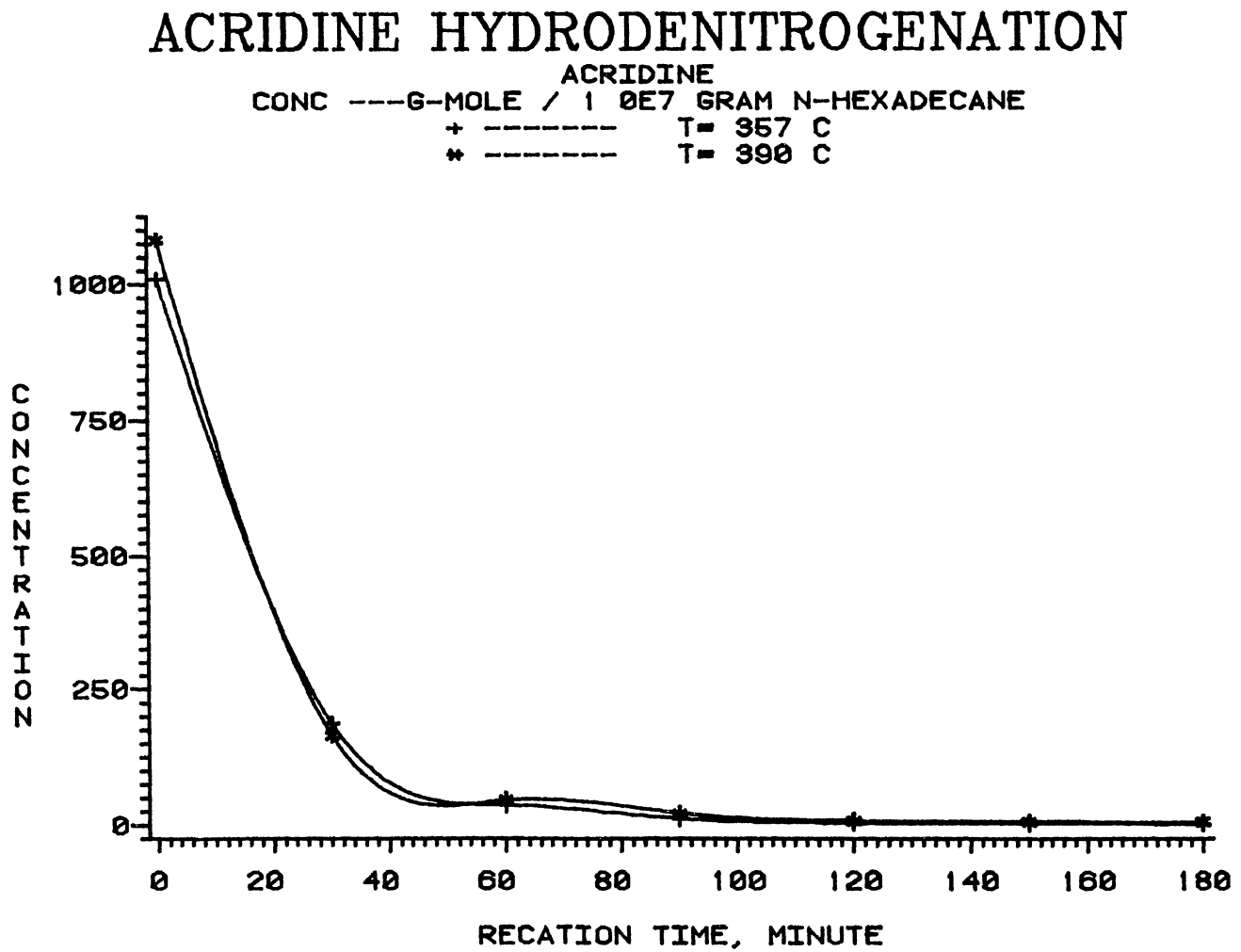

Figure 45. Effects of Temperature on Concentration of Acridine

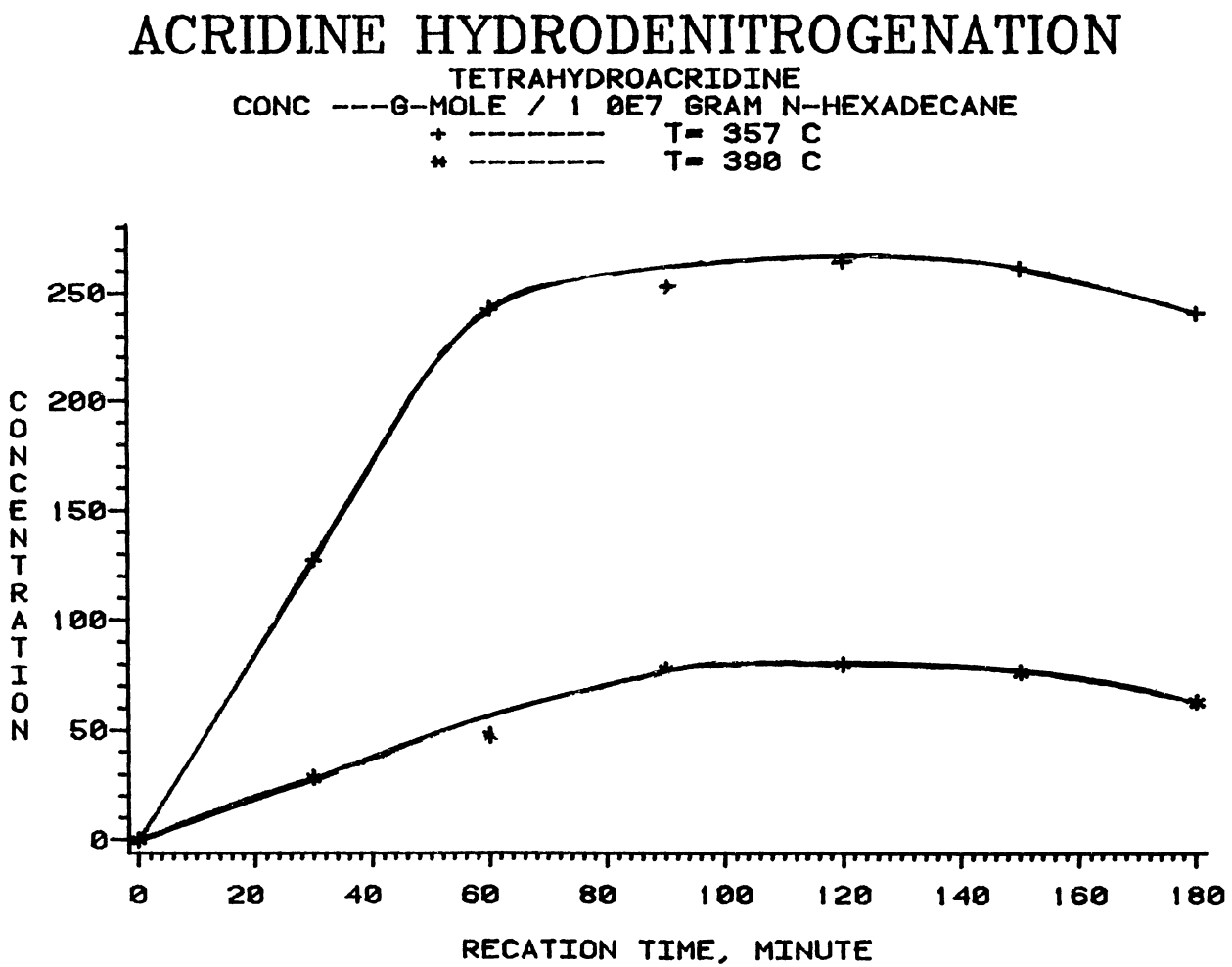

Figure 46. Effects of Temperature on Concentration of Tetrahydroacridine

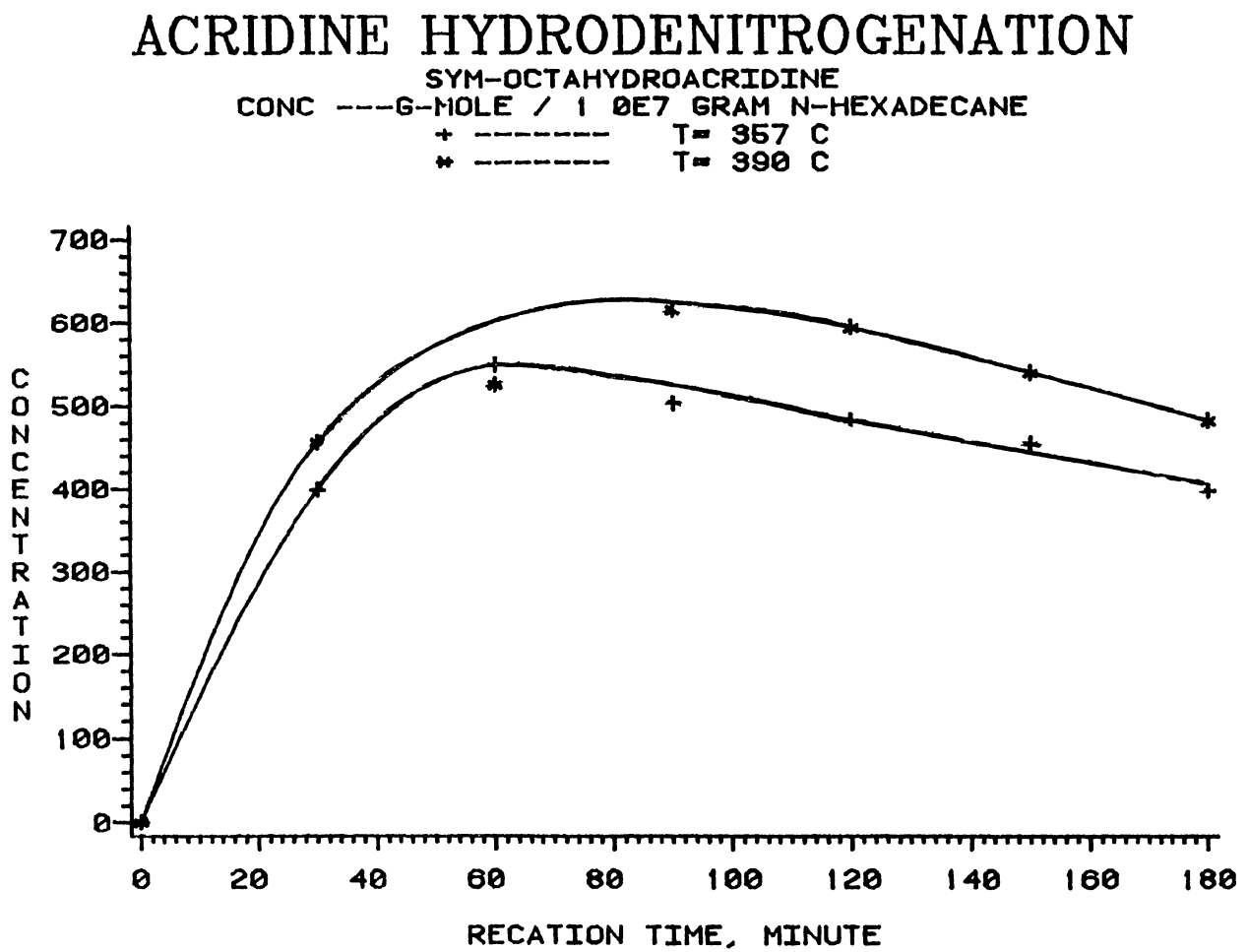

Figure 47. Effects of Temperature on Concentration of Sym-Octahydroacridine

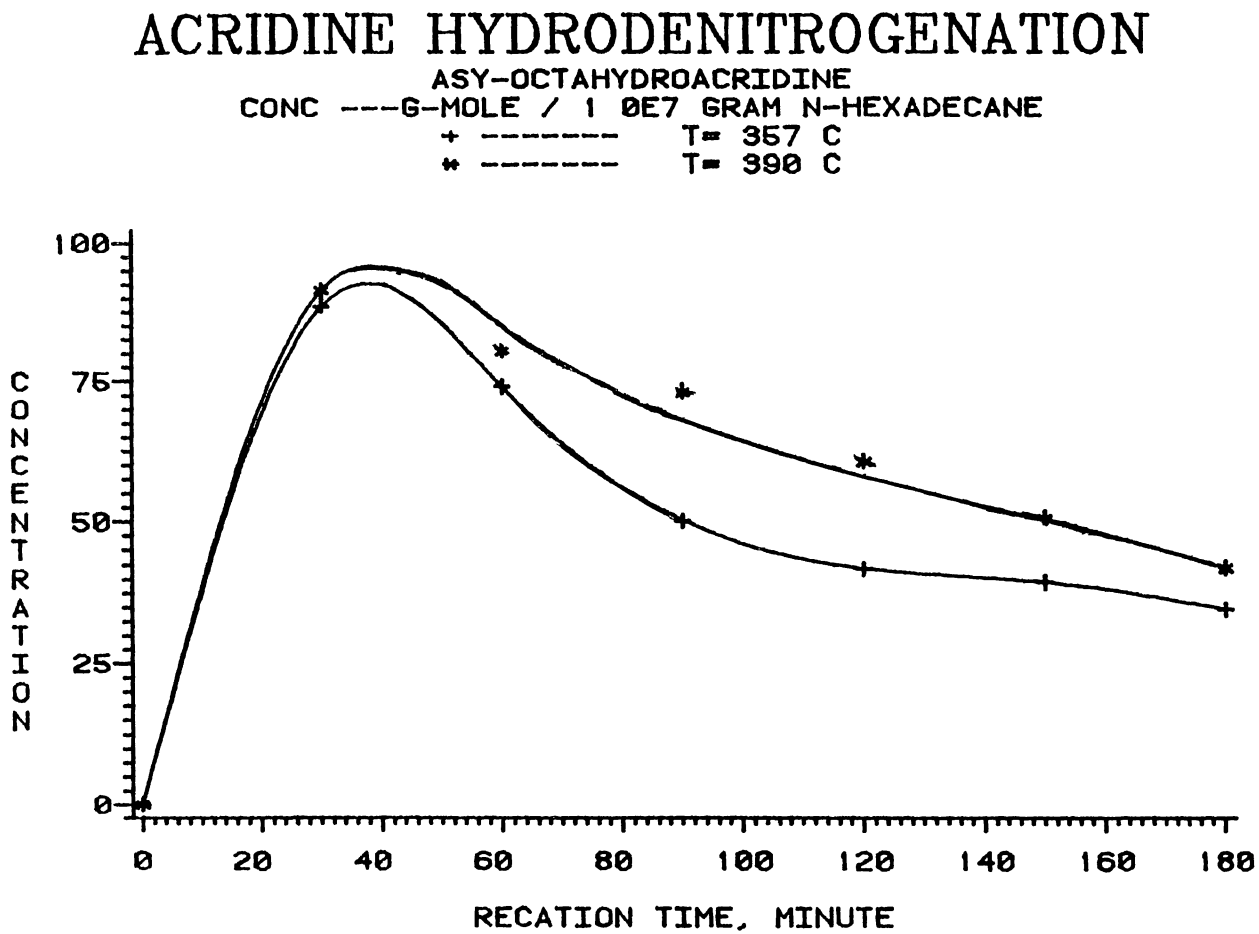

Figure 48. Effects of Temperature on Concentration of Asym-Octahydroacridine

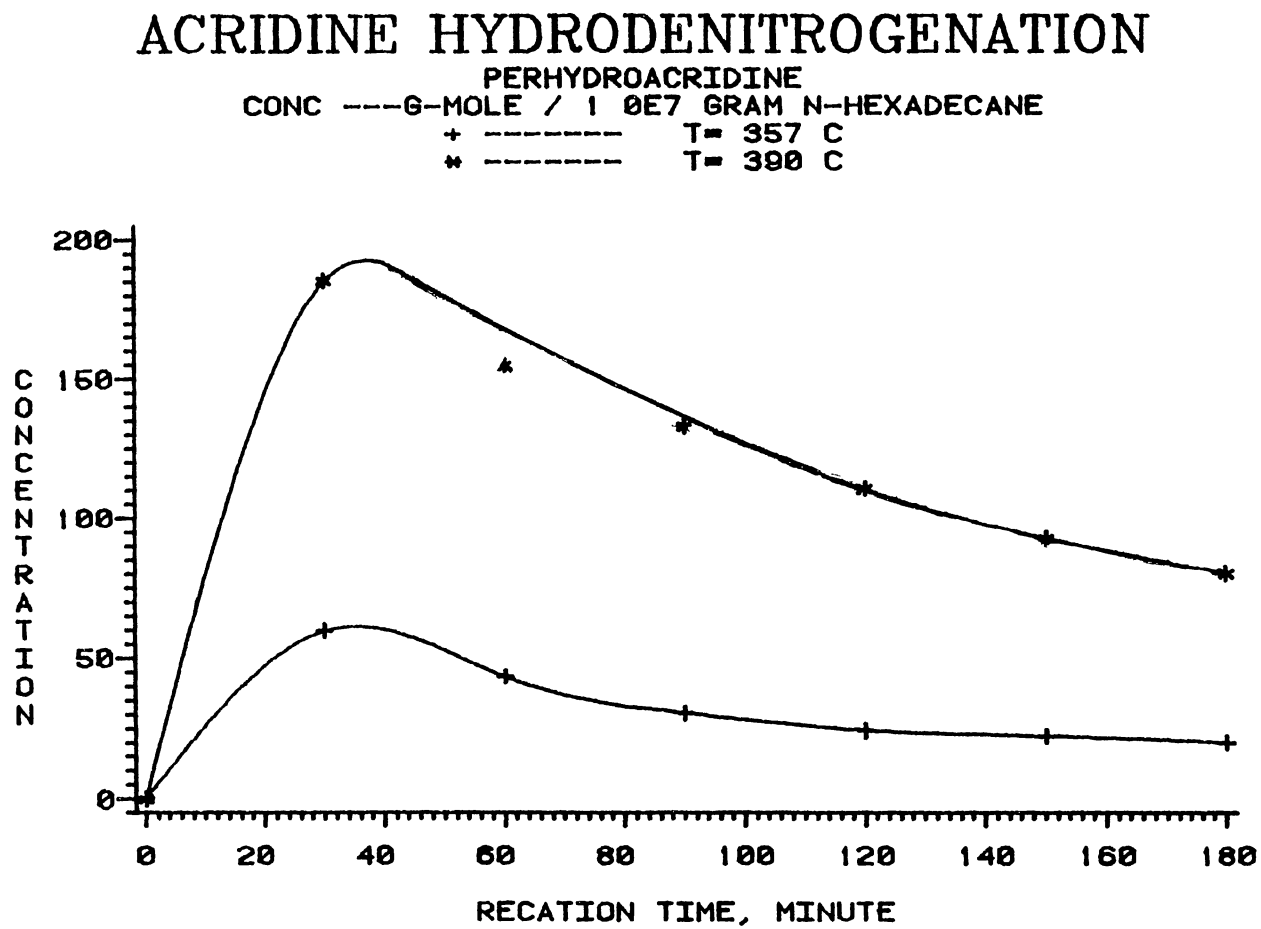

Figure 49. Effects of Temperature on Concentration of Perhydroacridine

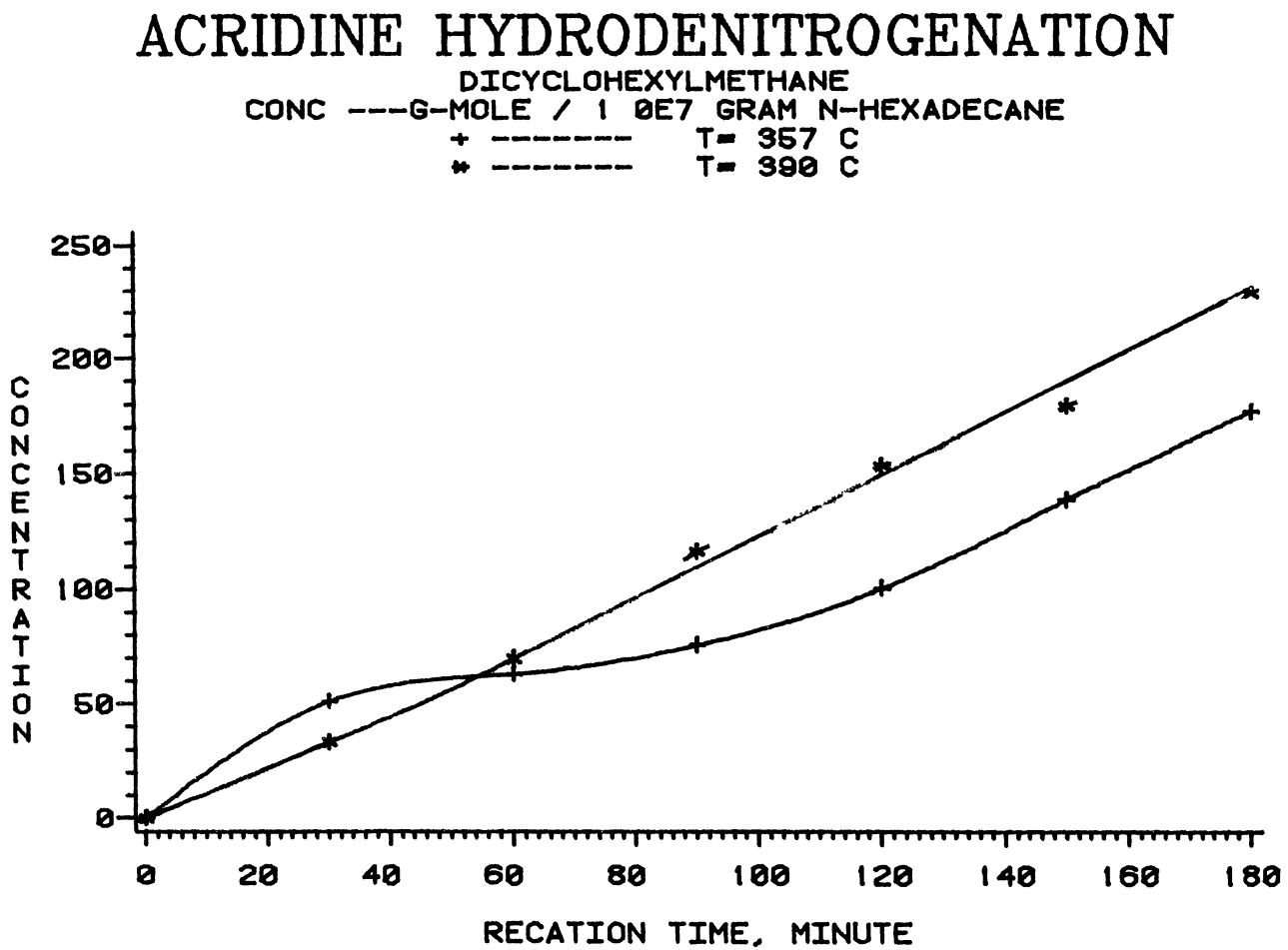

Figure 50 Effect of Temperature on Concentration of Dicyclohexylmethane

B. 3. Reaction Network

Although a wide range of studies has been done on the synthesis of reduced acridines, little work has been reported on the mechanism of its hydrodenitrogenation (1,20,48) Our results indicate that some of the reduced acridines are in chemical equilibria with each other. We believe that acridine is initially converted to ASHOA and THA through two separate routes As indicated by Nagai et al.(54), the formation of ASOHA is accomplished through the rapid hydrogenation of an intermediate, 9-10 DHA, which was not detected in our samples. THA is then converted to SOHA, establishing an equilibrium. Both SOHA and ASOHA are later converted to PHA, which is hydrogenolyzed to DCHM Equilibrium exists between PHA and both SOHA and ASOHA. Based on these discussions, the reaction network of Figure 51 is developed and presented

C. Quinoline-Acridine Mixture Hydrodenitrogenation

Hydrodenitrogenation experiments were carried out on a mixture of quinoline and acridine in n-hexadecane, containing approximately the same amouts of reactants as the single compound runs. The temperatures were identical to those of the single compound runs. The reaction products which resulted from the HDN of a quinoline-acridine mixture are similar to those identified in single compound runs of quinoline and acridine, except for aniline and THA which

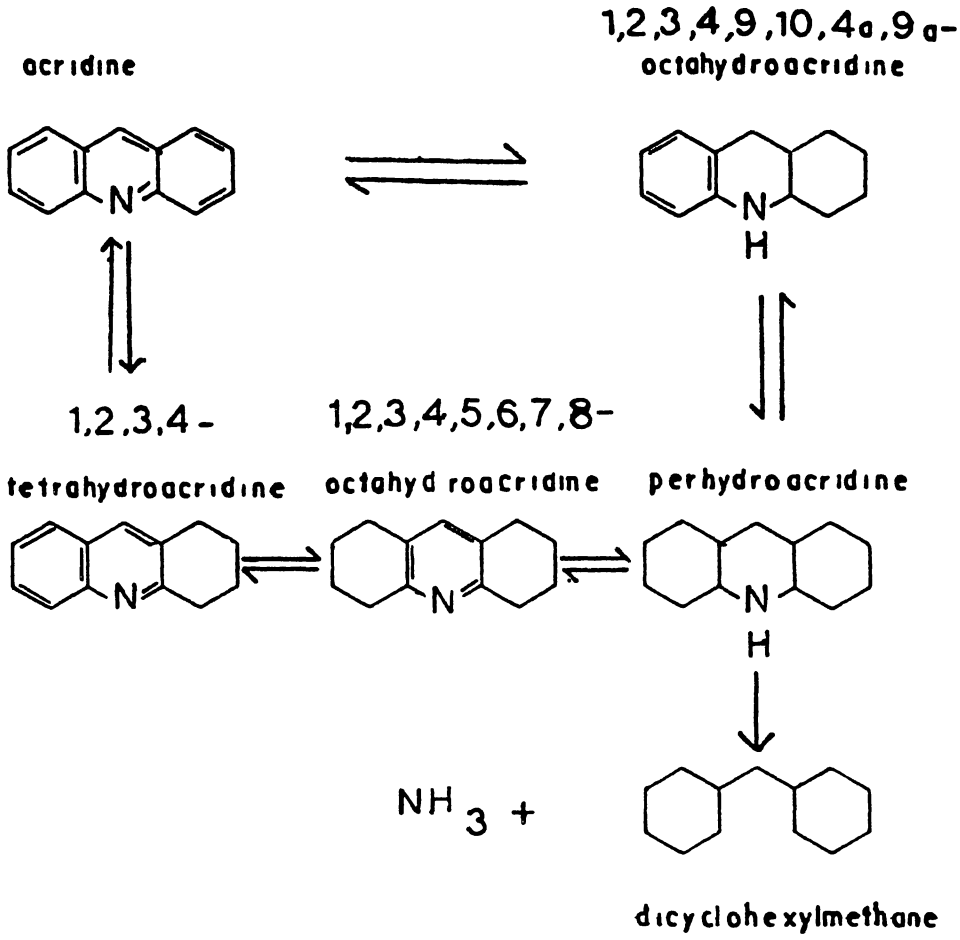

Figure 51. Reaction Network for Acridine HDN at 357-390°C, 8.2 MPa, HDS-9A Catalyst

did not appear in the mixture. Aniline probably had such a low concentration that it could not be detected. THA either reacted quickly or it is not distinguishable from the other products that eluted from the GC and couldn't be identified. The results are presented in the Tables XVI-XIX and plotted in the Figures 52-69. In fact, duplicate runs (NQA6 and NQA8) were conducted at 370°C. However, the NQA6 results were inconsistent with the results of other runs (NQA, NQA3, NQA8) and hence it was considered erroneous, apparently due to some unobserved temperature irregularities.

At 390°C quinoline is rapidly converted to Py-THQ and Bz-THQ. The rate of quinoline conversion is not affected by the presence of acridine, neither is the rate of formation of Py-THQ affected by acridine. But the equilibrium concentration of Py-THQ is somewhat higher in the HDN of the mixture than in the HDN of quinoline, as can be seen from comparison of Figure 52 and Figure 25. The rates of formation of both Bz-THQ and DHQ are similarly not affected by the presence of acridine HDN products, whereas, the rates of conversion of both compounds are slower in the case of the mixture. This can be observed from Figures 53 and 26. Figures 54 shows the formation of OPA and PCH. Comparing the plots from Figure 54 with those of Figure 27 shows that the rate of formation of PCH is about one half of its rate in quinoline HDN, whereas OPA forms at a higher rate in the HDN of the mixture. Hence, we can state that the rate of

TABLE XVI

REACTION PRODUCTS OF RUN NQA1* (390°C)

Compound	Reaction Time, min.					
	30	60	95	120	150	180
Quinoline	47 4	21.5	13.2	13.1	15.7	13.0
Py-THQ	126.7	112 3	83.9	71 5	67 9	65.7
Bz-THQ	41.0	42 9	39 4	36.3	35.6	33.9
DHQ	19 7	32.6	43.0	45.4	44.1	41.7
OPA	6.1	10.4	14.5	16.1	18.0	16.4
PCH	4 2	7.5	15.2	19.8	24.5	33.4
PB	**	**	**	**	**	**
OEA	1.5	1.8	1 8	1.7	1.6	1 4
OMA	3 0	3.4	3.2	3.1	3.1	2.9
Acridine	19.8	11.1	6.5	3.4	1.0	0.7
ASOHA	0.5	0.9	1.5	1 9	2.2	1.9
SOHA	22 6	34 1	46.3	53.9	58 3	54.6
PHA	9 3	11.8	12.4	12 2	10.3	7 2
DCHM	23.2	23.7	23.4	22.5	21.9	20.4
Total nitrogen	297 6	282.8	265.7	258.6	257 8	239.4

* g-mole/10^6 g n-hexadecane

Initial quinoline concentration = 372.1 g-mole quinoline/10^6 g n-hexadecane.

Initial acridine concentration = 102.1 g-mole acridine/10^6 g n-hexadecane.

** Under detection limit

TABLE XVII

REACTION PRODUCTS OF RUN NQA3* (357°C)

Compound	Reaction Time, min.				
	60	90	120	150	180
Quinoline	47 5	19 2	11.3	8.5	7.6
Py-THQ	172.4	167.3	142 1	120 2	98.0
Bz-THQ	18.3	22 6	24.5	25.8	28 1
DHQ	31 0	55.7	75.7	98 3	122.9
OPA	4.6	8.5	13.4	18.5	23.9
PCH	1.3	2 4	6 4	9.4	14.3
PB	**	**	**	**	**
OEA	0.4	0.5	0 5	0.6	0.6
OMA	0.9	1.0	0.9	0.9	0 9
Acridine	34.5	25.8	16 1	11.0	8.6
ASOHA	0 6	1 2	2.1	3.0	4.0
SOHA	15.4	22.5	32.8	39.2	43.5
PHA	12.7	15.2	16.4	16.2	14.2
DCHM	21 9	21 8	20.9	19.8	19.5
Total nitrogen	338.3	339.5	335.8	342.2	352.3

* g-mole/10^6 g n-hexadecane

Initial quinoline concentration = 372.1 g-mole quinoline/10^6 g n-hexadecane.

Initial Acridine concentration = 102.1 g-mole acridine/10^6 g n-hexadecane.

** Under detection limit

TABLE XVIII

REACTION PRODUCTS OF RUN NQA6* (370°C)

Compound	Reaction Time, min.					
	30	60	90	120	150	180
Quinoline	67.8	29.3	18.6	14.1	10.3	9 0
Py-THQ	166.9	188 8	177.4	175.2	167 2	131 9
Bz-THQ	27.9	29 0	27.0	26.2	27.0	26 1
DHQ	10 4	26 4	32.1	45.8	56 9	64 5
OPA	3.3	6.0	9.3	12.2	19.2	22.2
PCH	**	2.0	3.5	5.8	9.1	12.6
PB	**	**	**	**	**	**
OEA	0 9	1.1	1.1	1 2	1.3	1.2
OMA	1 5	1.8	1.7	1 8	1.9	1 9
Acridine	37 3	30 2	22.7	17.0	15 2	12.7
ASOHA	0.3	1.5	0.9	1.5	2.6	2 9
SOHA	11.6	18 1	23.2	29.2	40.9	45.0
PHA	10 3	16.5	18.8	20 3	21.0	19 1
DCHM	11 2	19.00	9.0	8.2	**	7.0
Total nitrogen	363.4	360 4	342 0	314.9	278.0	256 4

* g-mole/10^6 g n-hexadecane

Initial quinoline concentration =
348 4 g-mole quinoline/10^6 g n-hexadecane

Initial acridine concentration =
97.0 g-mole acridine/10^6 g n-hexadecane

** Under detection limit

TABLE XIX

REACTION PRODUCTS OF RUN NQA8* (370°C)

Compound	Reaction Time, min.					
	30	60	90	120	150	180
Quinoline	59 4	21.1	13.0	8.1	4.7	2.2
Py-THQ	176 4	143.4	99.0	61.2	35.1	20.9
Bz-THQ	25.8	35.8	40 6	40.2	35.6	30.3
DHQ	33 7	69.1	94.1	105.8	101.9	95.8
OPA	3.8	10.3	16 2	20.5	23.4	23.6
PCH	1.8	6.8	15.3	24 4	34 0	43.0
PB	**	**	2.2	3.0	3.6	4.1
OEA	0.3	0.5	0.6	0.7	0 7	0.5
OMA	0.7	0.8	1.1	1 0	0.9	0.7
Acridine	31.7	25.4	9 7	4 0	1.5	0 8
ASOHA	0.6	1 7	2.7	3 5	4.1	4.6
SOHA	22 8	41.8	54.9	61.0	62 9	65.1
PHA	8.2	10.5	10 1	8.9	7.2	6.4
DCHM	9.4	8.1	7.5	8 1	7.6	7.6
Total nitrogen	363.4	360.4	342.0	314.9	278.0	256.4

* g-mole/10^6 g n-hexadecane

Initial quinoline concentration = 378.9 g-mole quinoline/10^6 g n-hexadecane.

Initial Acridine concentration = 103.2 g-mole acridine/10^6 g n-hexadecane.

** Under detection limit

TABLE XIX (continued)

Compound	Reaction Time, min.					
	210	240	300	360	420	510
Quinoline	0.4	0.0	0.0	0.0	0 0	3.8
Py-THQ	12 1	7.7	3.6	1.7	6 0	11 9
Bz-THQ	23.7	17.3	9.4	3.9	4.4	11.0
DHQ	76 6	58.6	32.8	13.3	11.5	29 2
OPA	27.9	27.1	24.4	23.8	20.8	14.1
PCH	54.4	56.3	58.2	54 4	55 8	67.8
PB	4.8	4.5	4.1	3.2	2.9	3.8
OEA	0.6	0.4	0.5	0.4	0.4	0.3
OMA	0.5	0.6	0.3	0.2	0.2	0.2
Acridine	0 5	0.4	0.4	0.3	0.3	0 3
ASOHA	4 7	4.8	4 7	4.6	3.7	2.7
SOHA	62.3	60.9	57.4	54.7	47.0	38.3
PHA	5.6	5.3	5.0	4.5	4.3	3 2
DCHM	7.9	8.5	11.4	10.5	10.2	9.9
Total nitrogen	222.8	191.6	138 5	107.4	98.6	111 2

* Initial quinoline concentration = 378.9 g-mole quinoline/10^6 g n-hexadecane.

Initial Acridine concentration = 103.2 g-mole acridine/10^6 g n-hexadecane

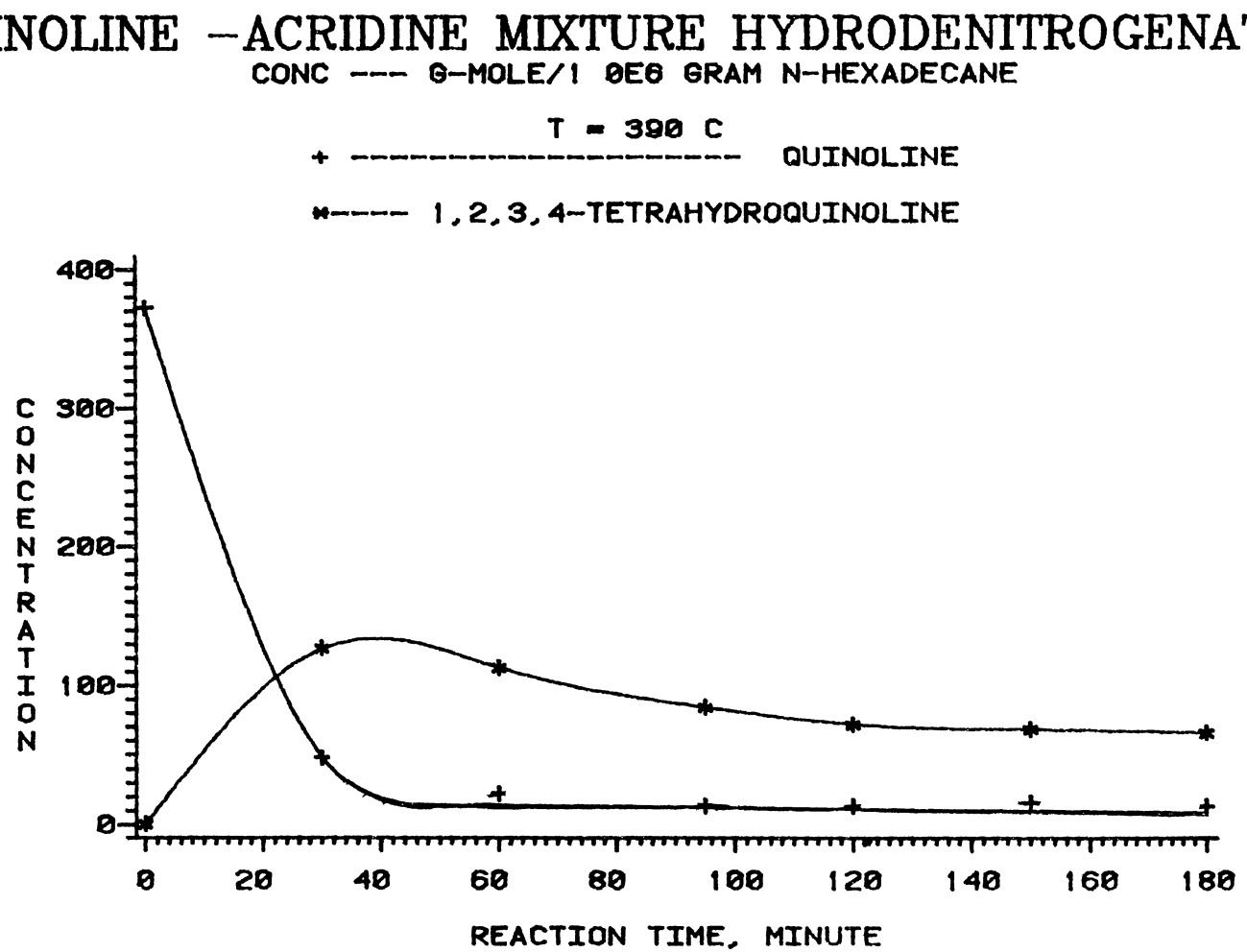

Figure 52 Quinoline-Acridine Mixture HDN Products at 390°C

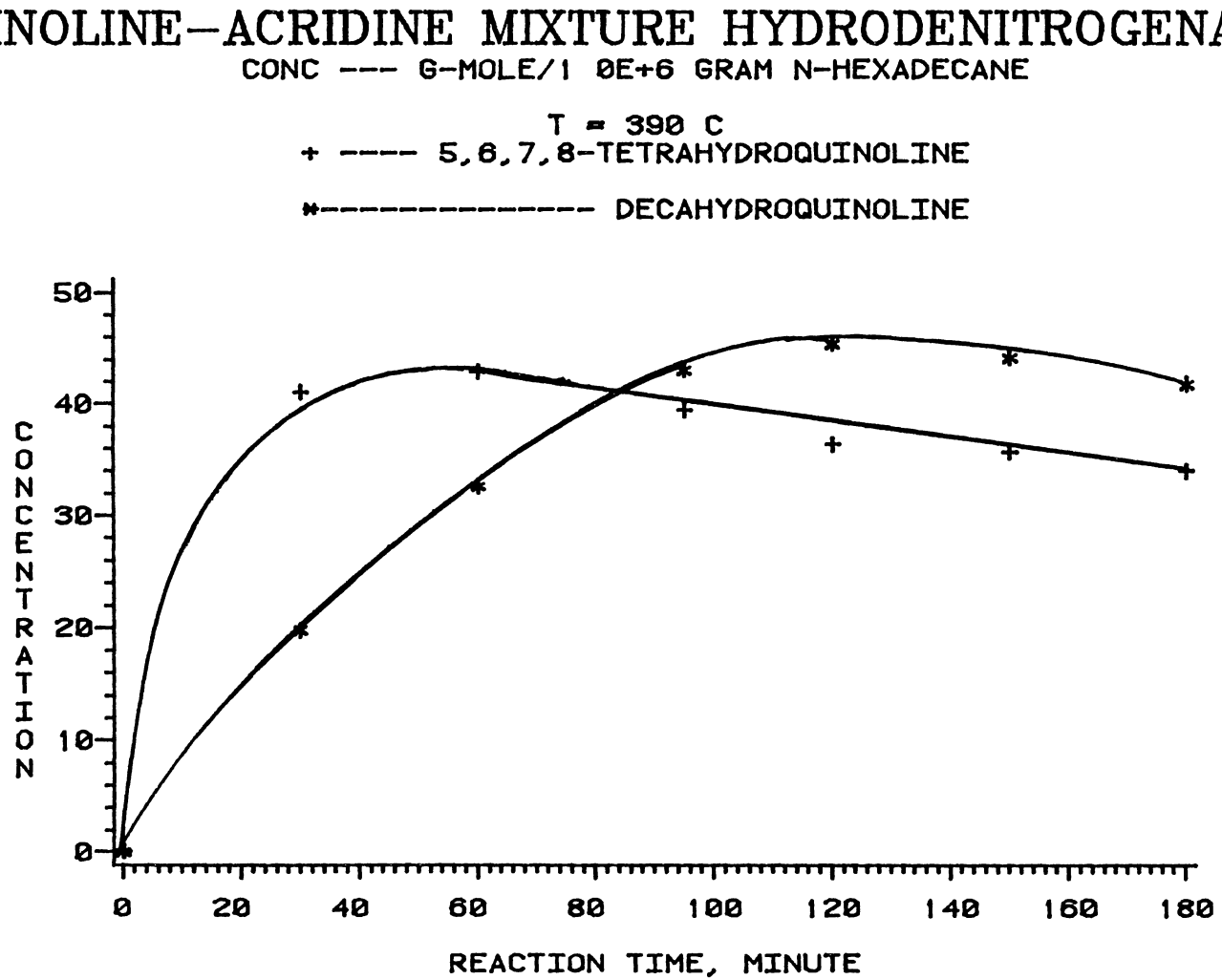

Figure 53. Quinoline-Acridine Mixture HDN Products at 390°C

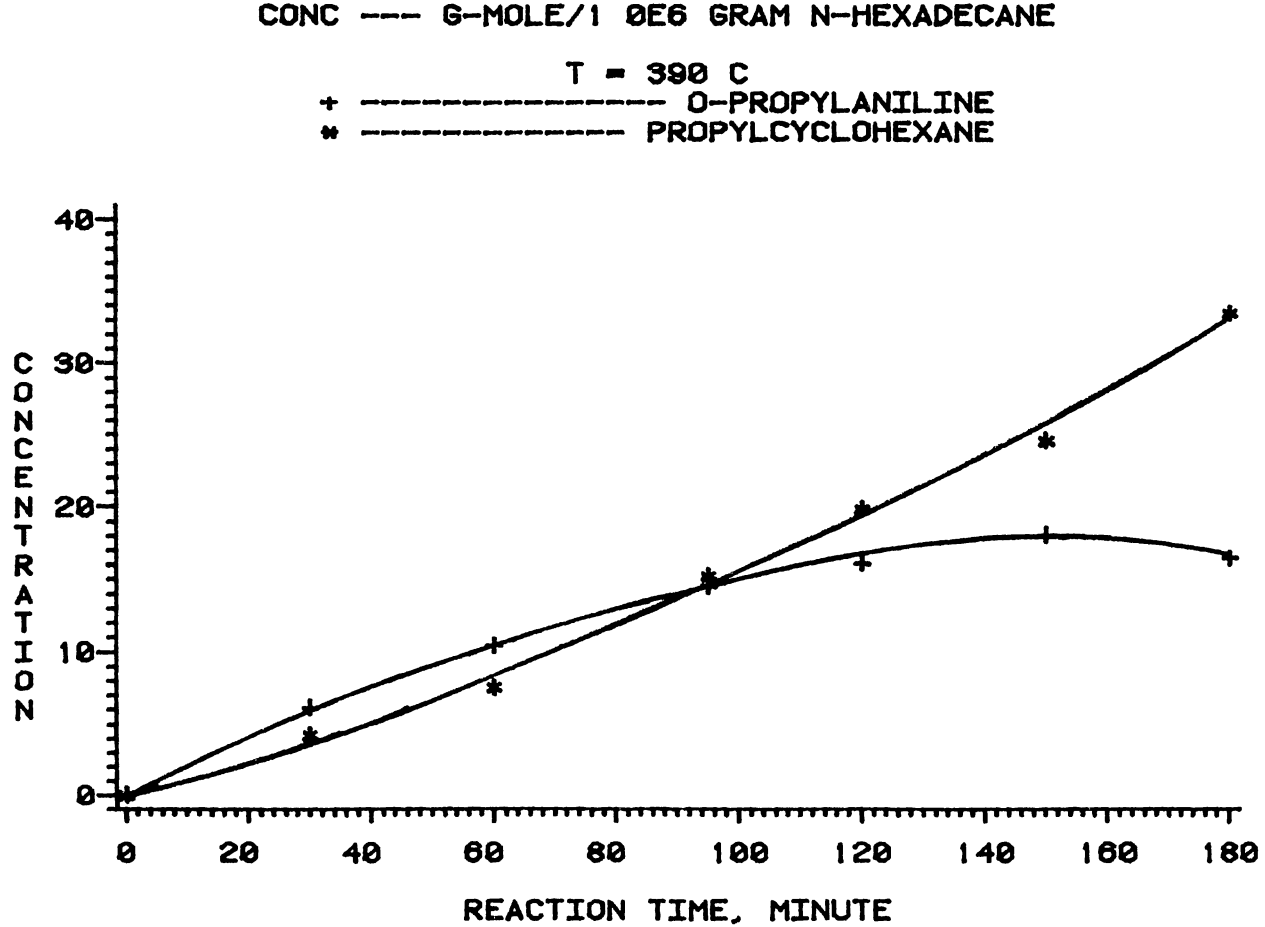

Figure 54 Quinoline-Acridine Mixture HDN Products at 390°C

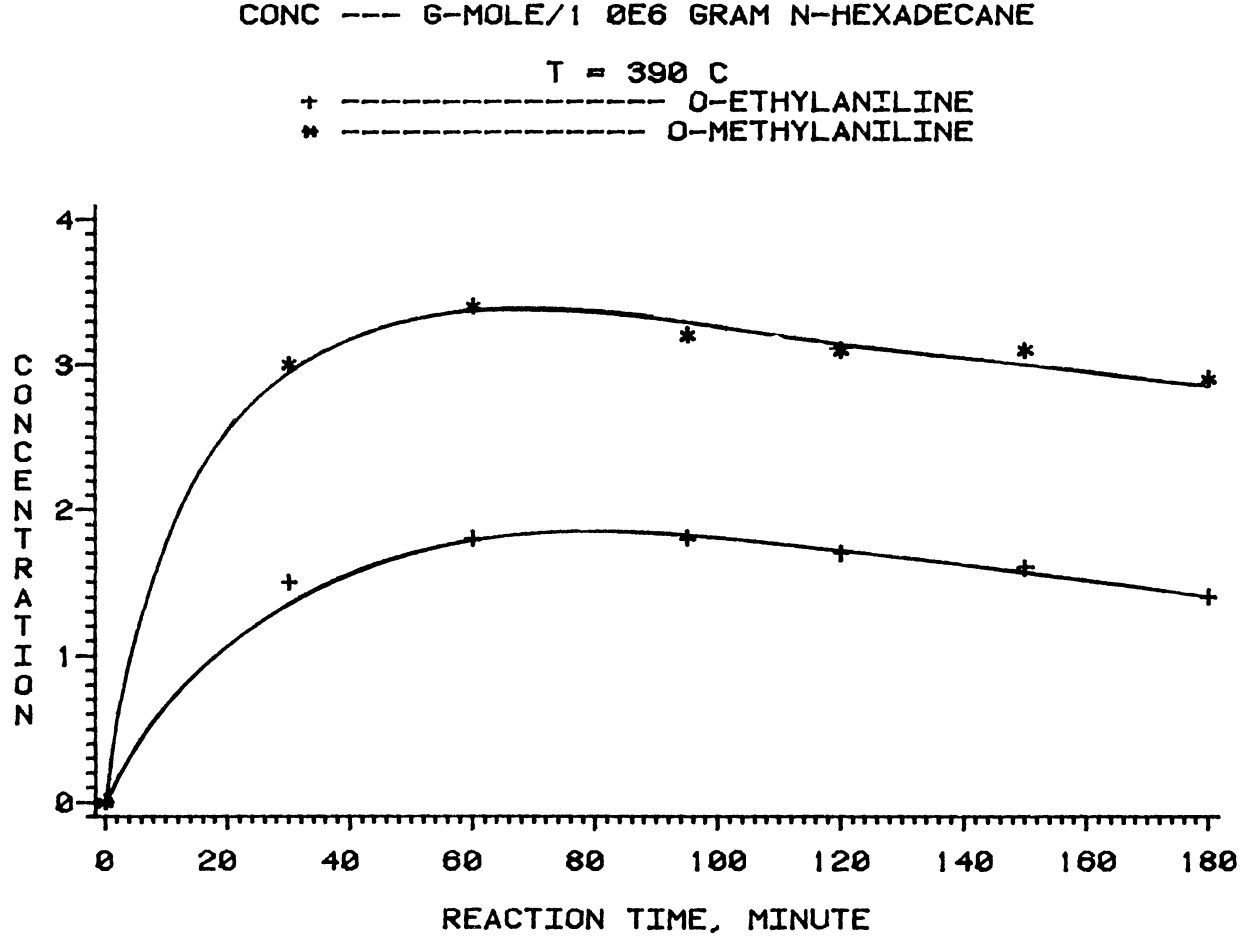

Figure 55. Quinoline-Acridine Mixture HDN Products at 390°C

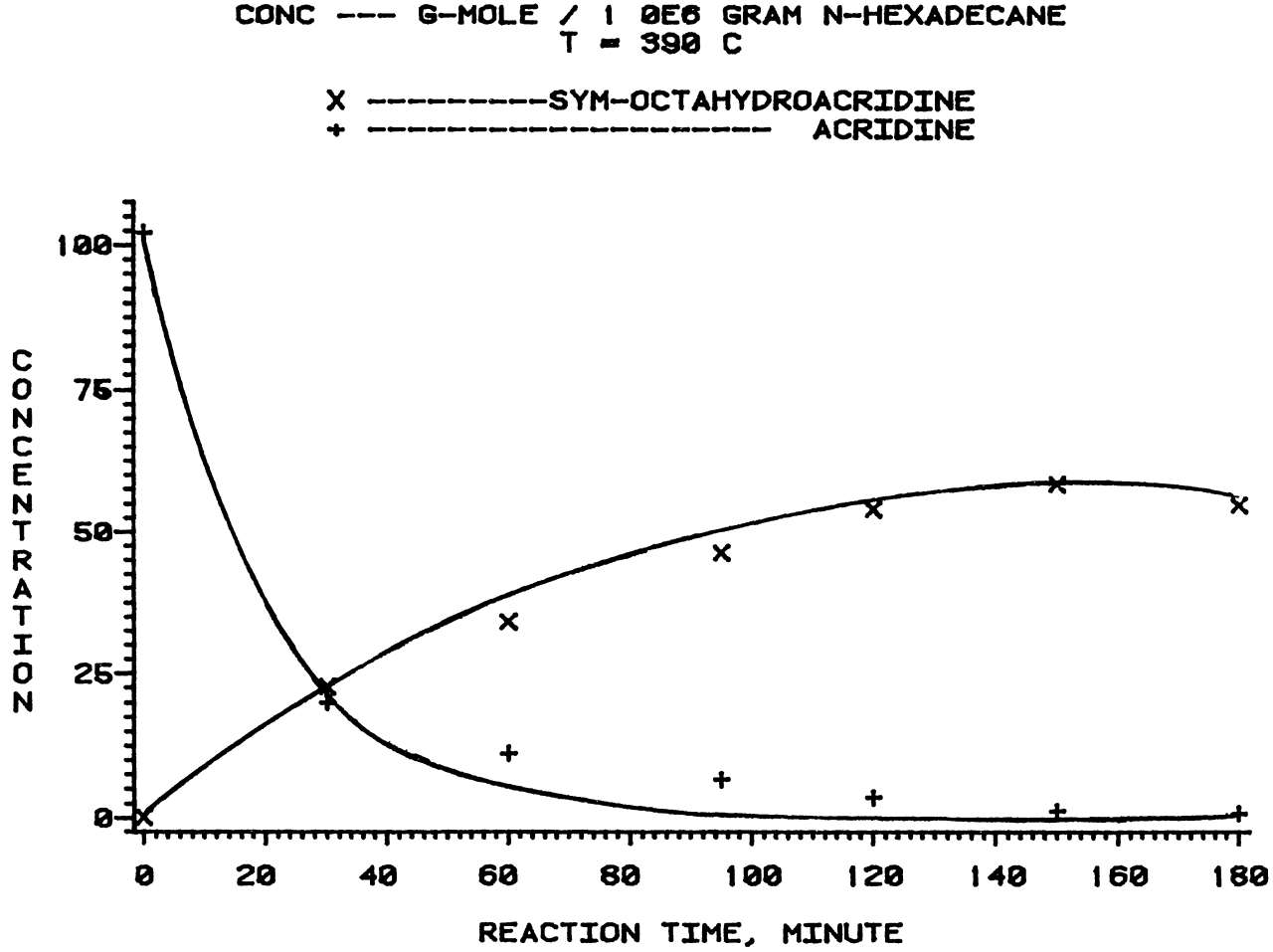

Figure 56. Quinoline-Acridine Mixture HDN Products at 390°C

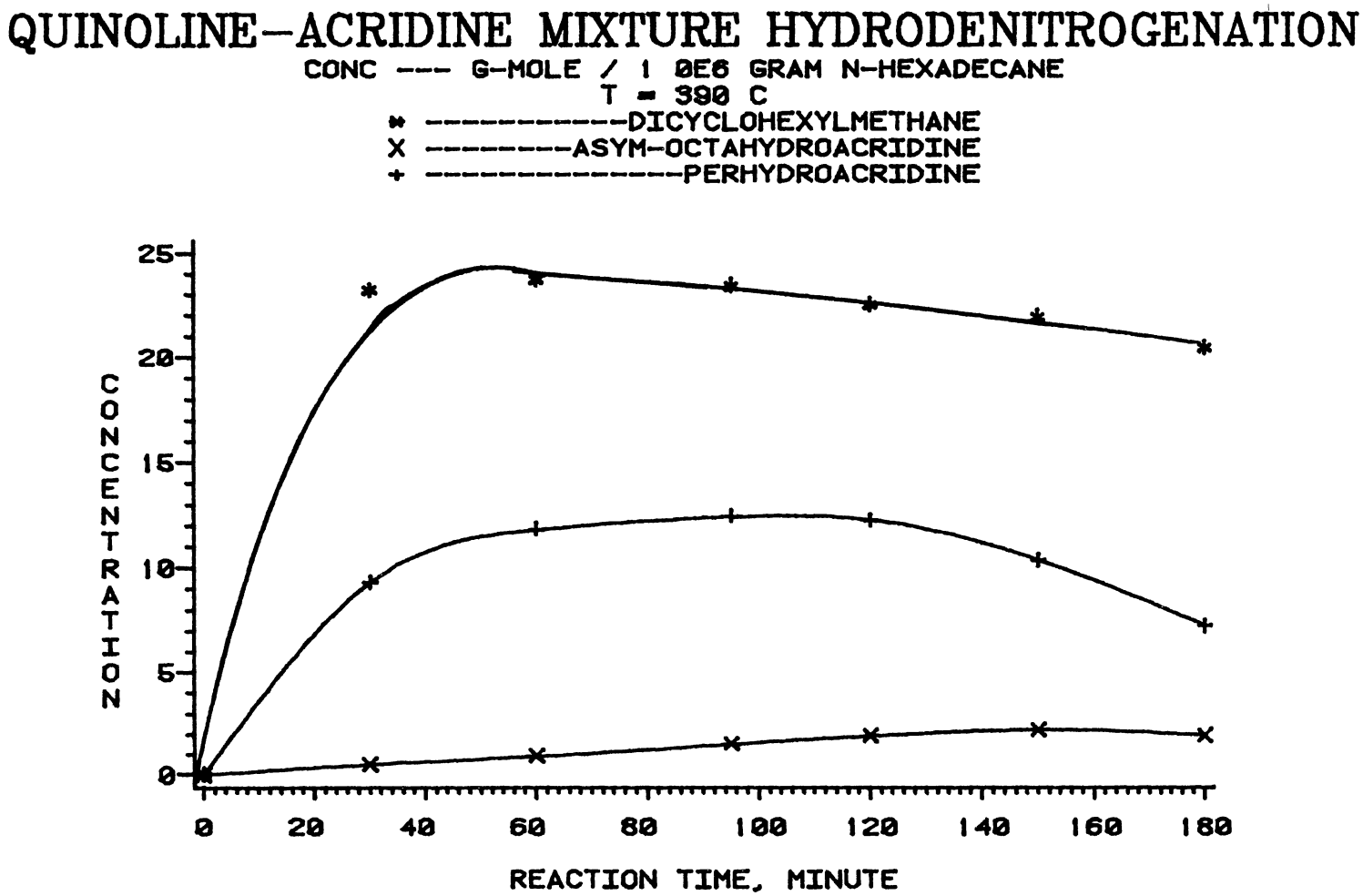

Figure 57 Quinoline-Acridine Mixture HDN Products at 390°C

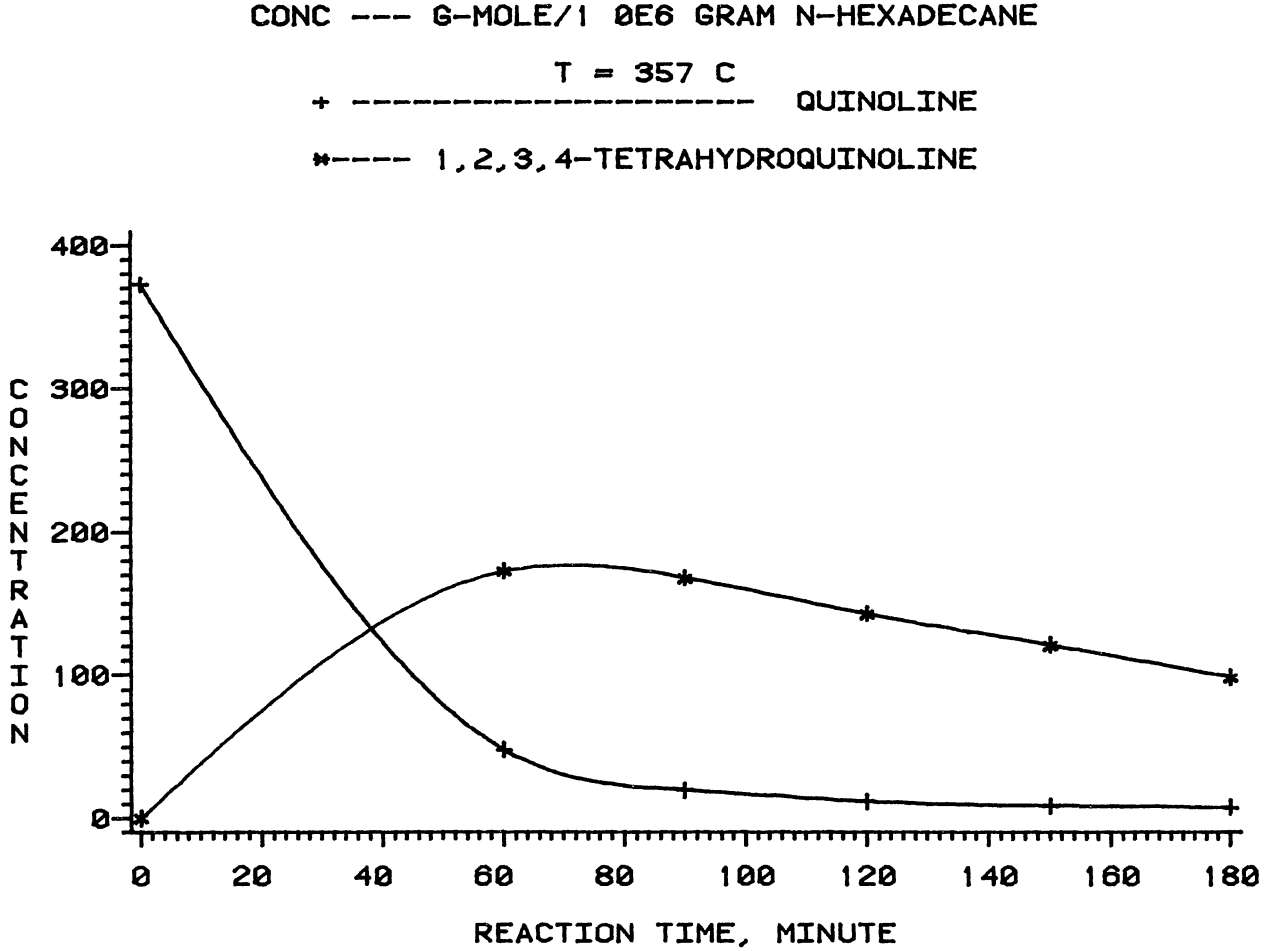

Figure 58 Quinoline-Acridine Mixture HDN Products at 357°C

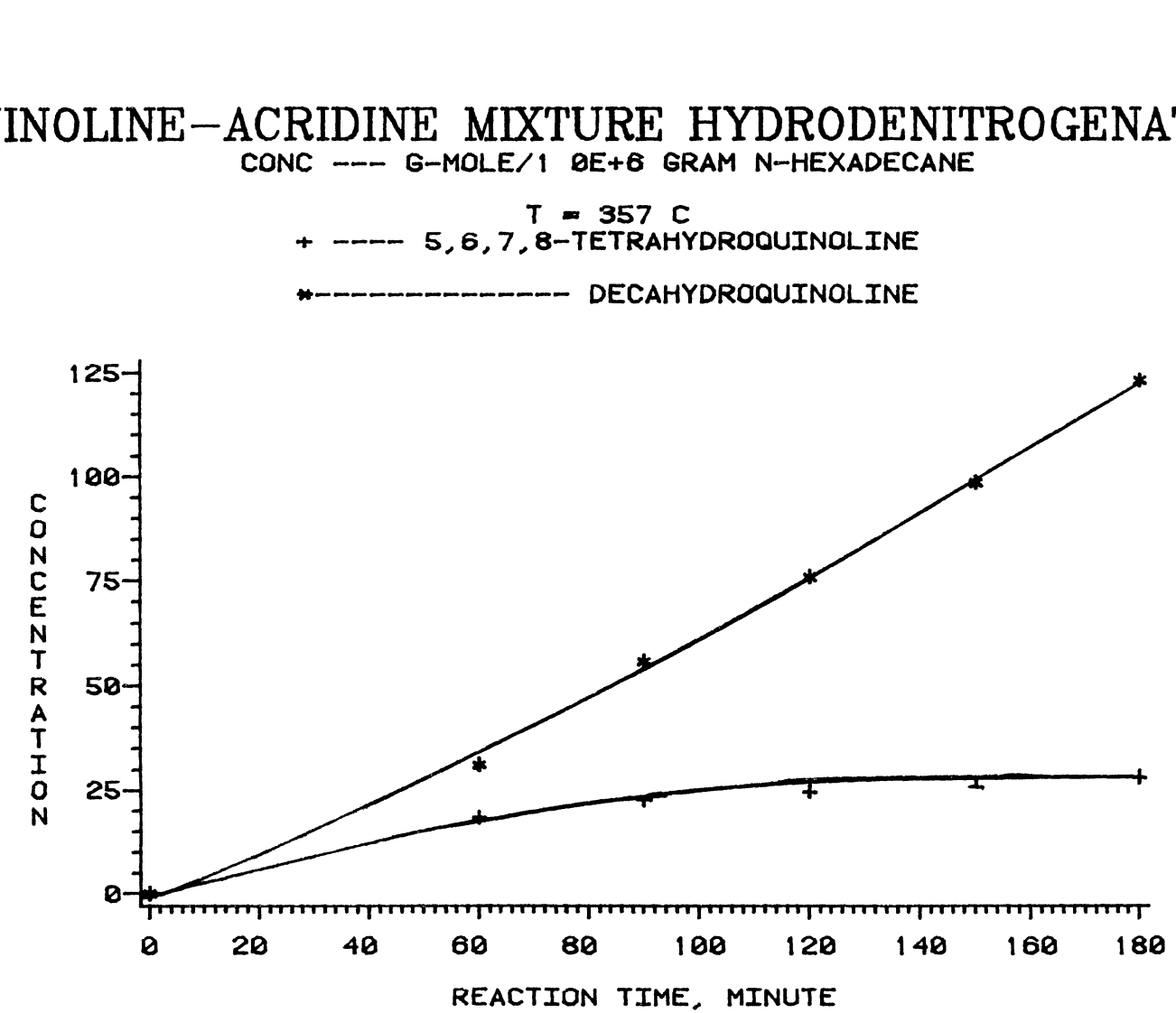

Figure 59. Quinoline-Acridine Mixture HDN Products at 357°C

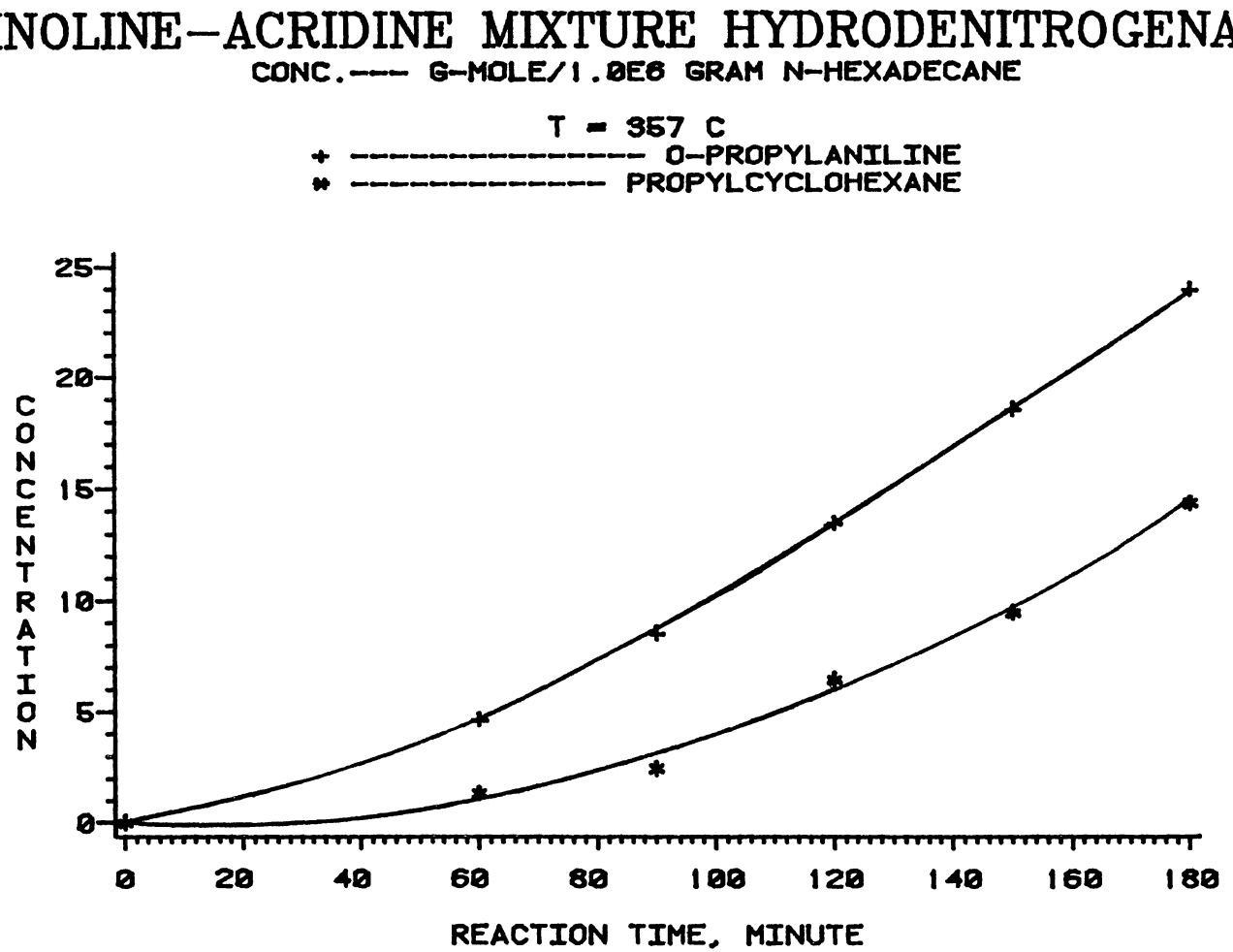

Figure 60. Quinoline-Acridine Mixture HDN Products at 357°C

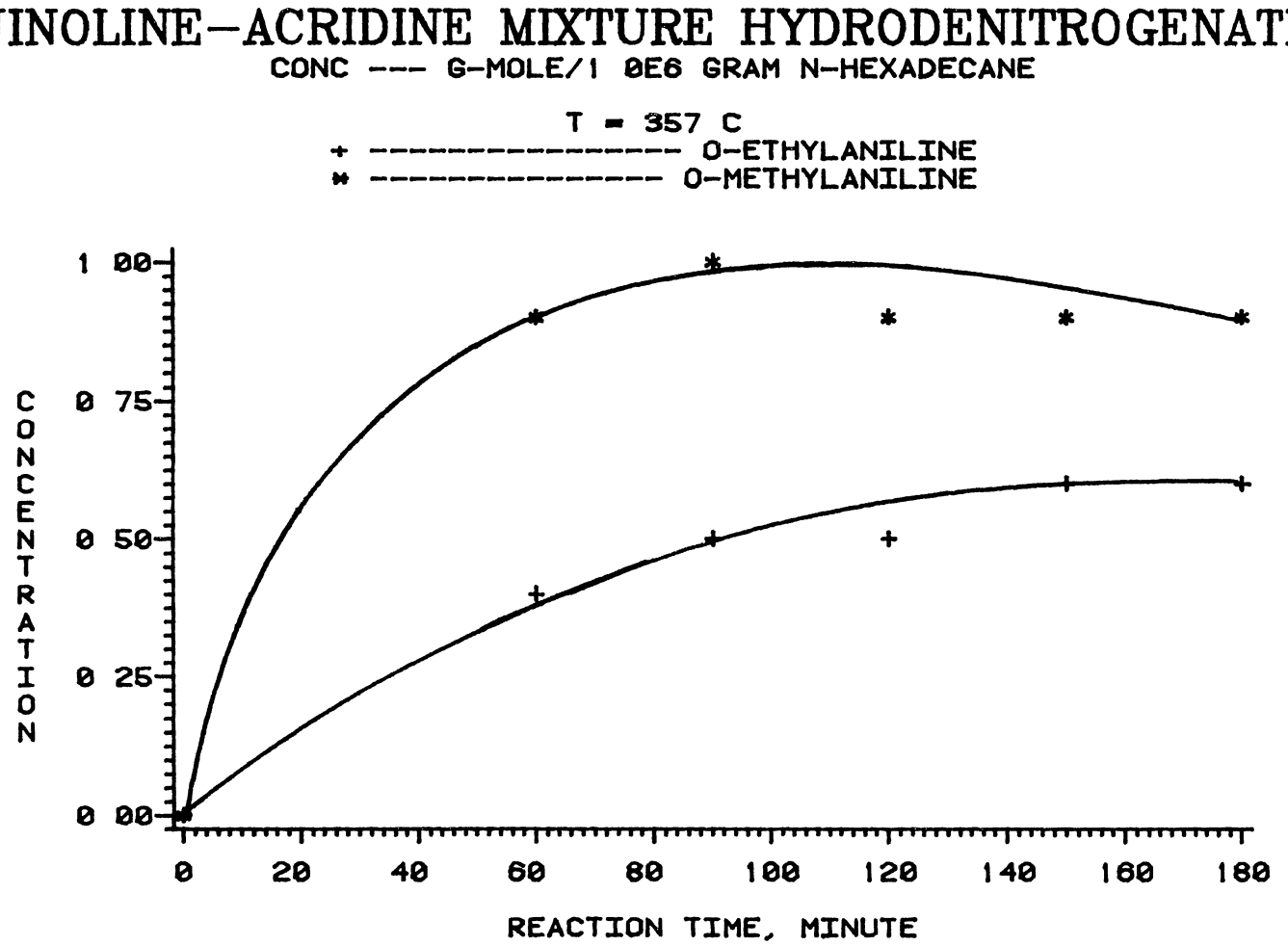

Figure 61. Quinoline-Acridine Mixture HDN Products at 357°C

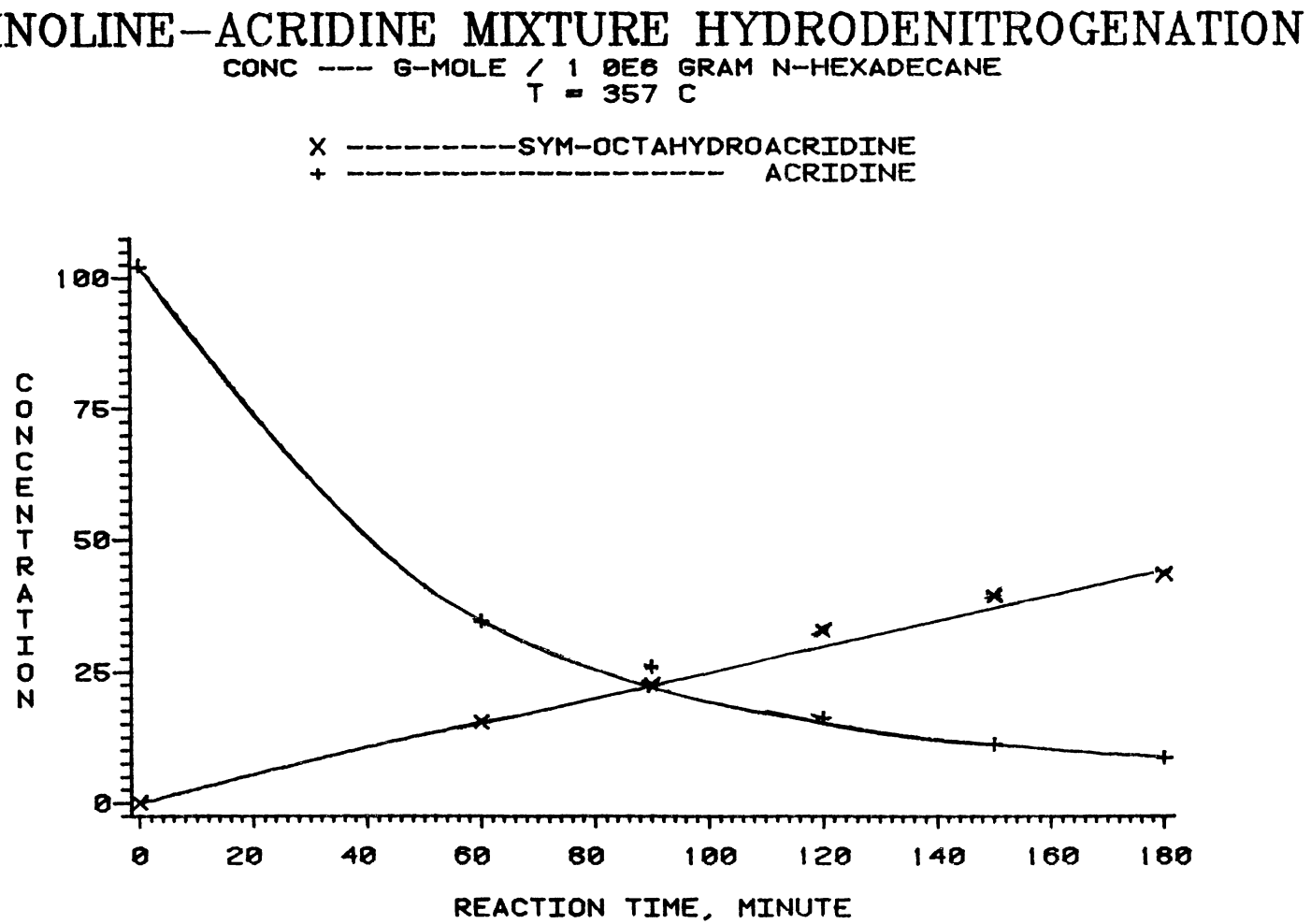

Figure 62 Quinoline-Acridine Mixture HDN Products at 357°C

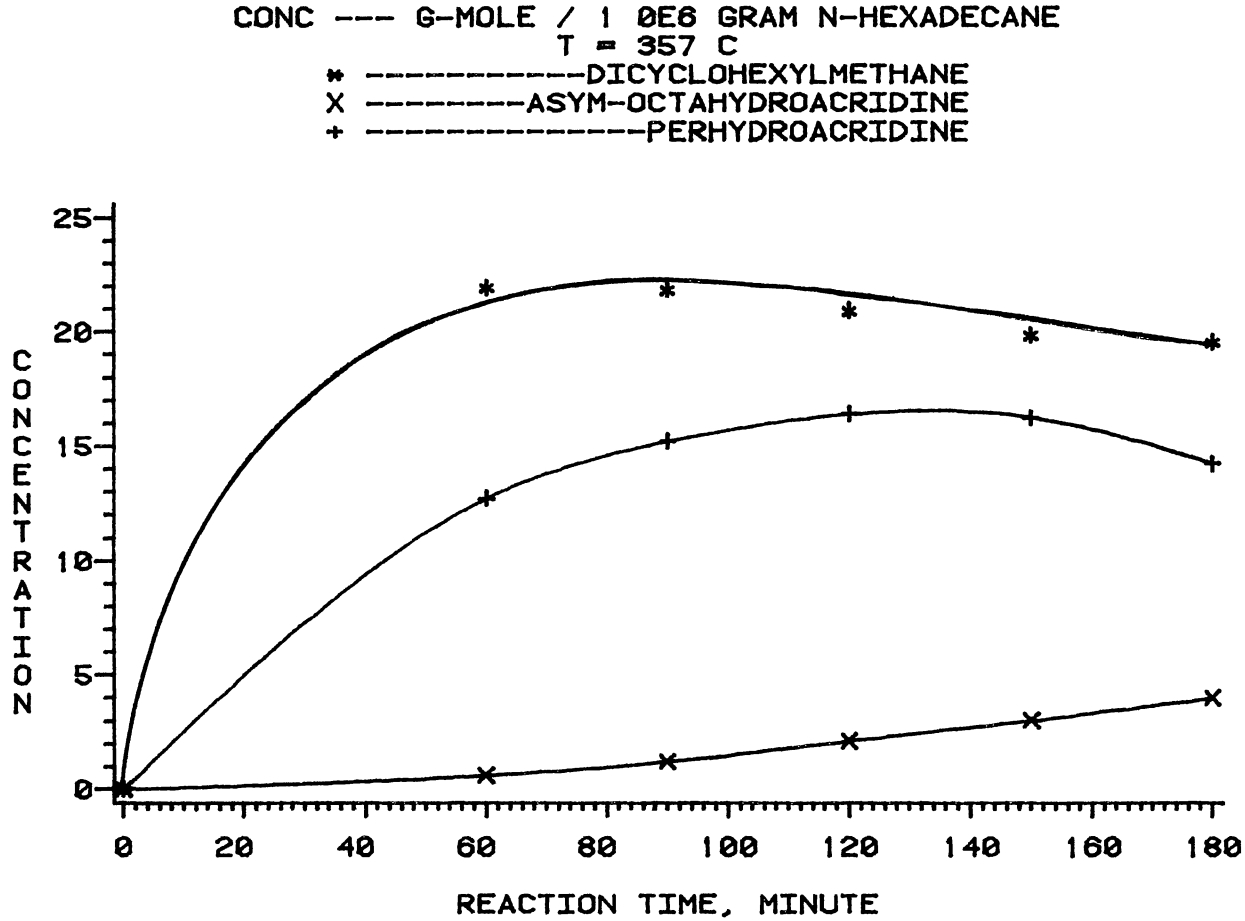

Figure 63. Quinoline-Acridine Mixture HDN Products at 357°C

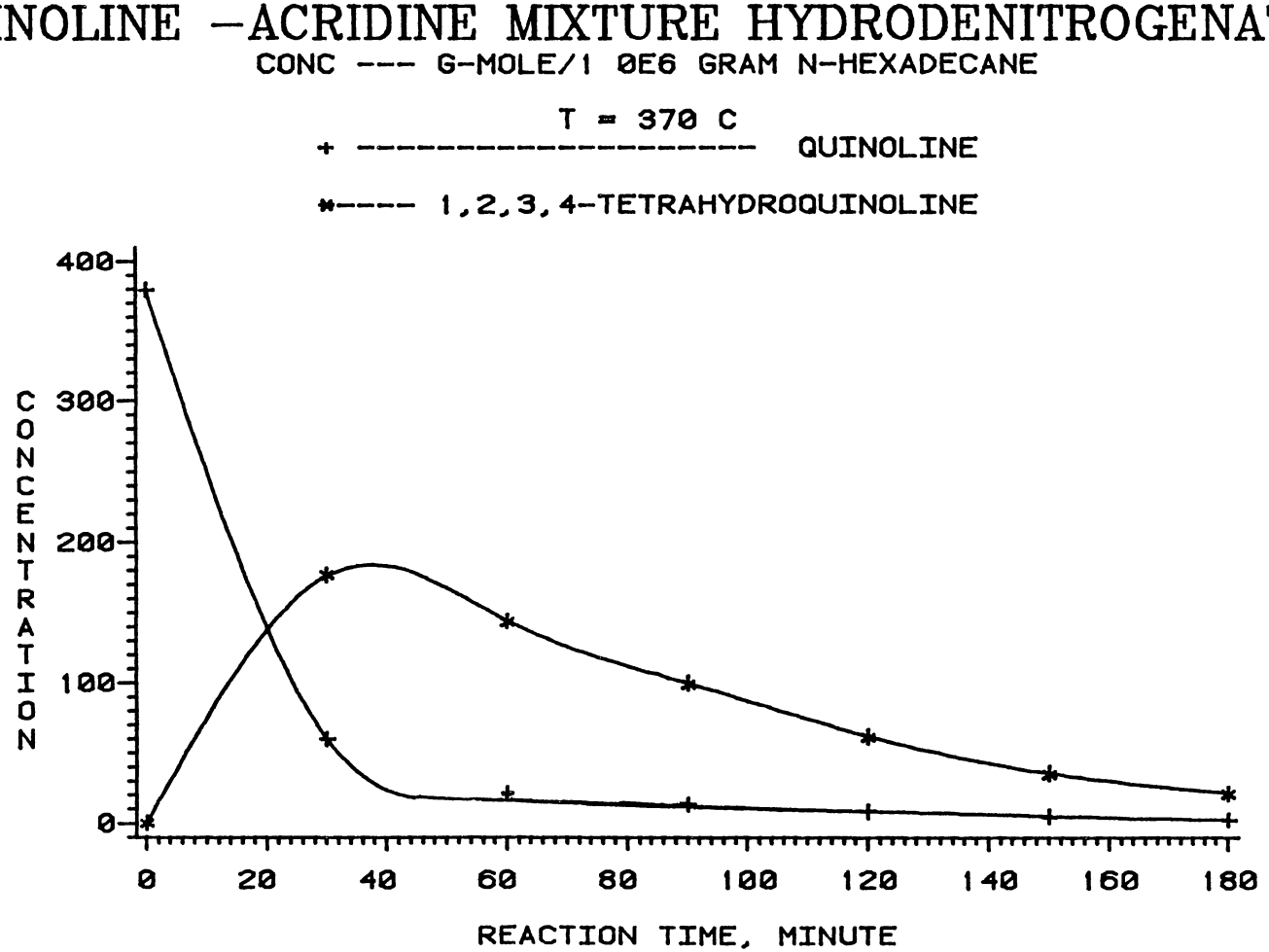

Figure 64. Quinoline-Acridine Mixture HDN Products at 370°C

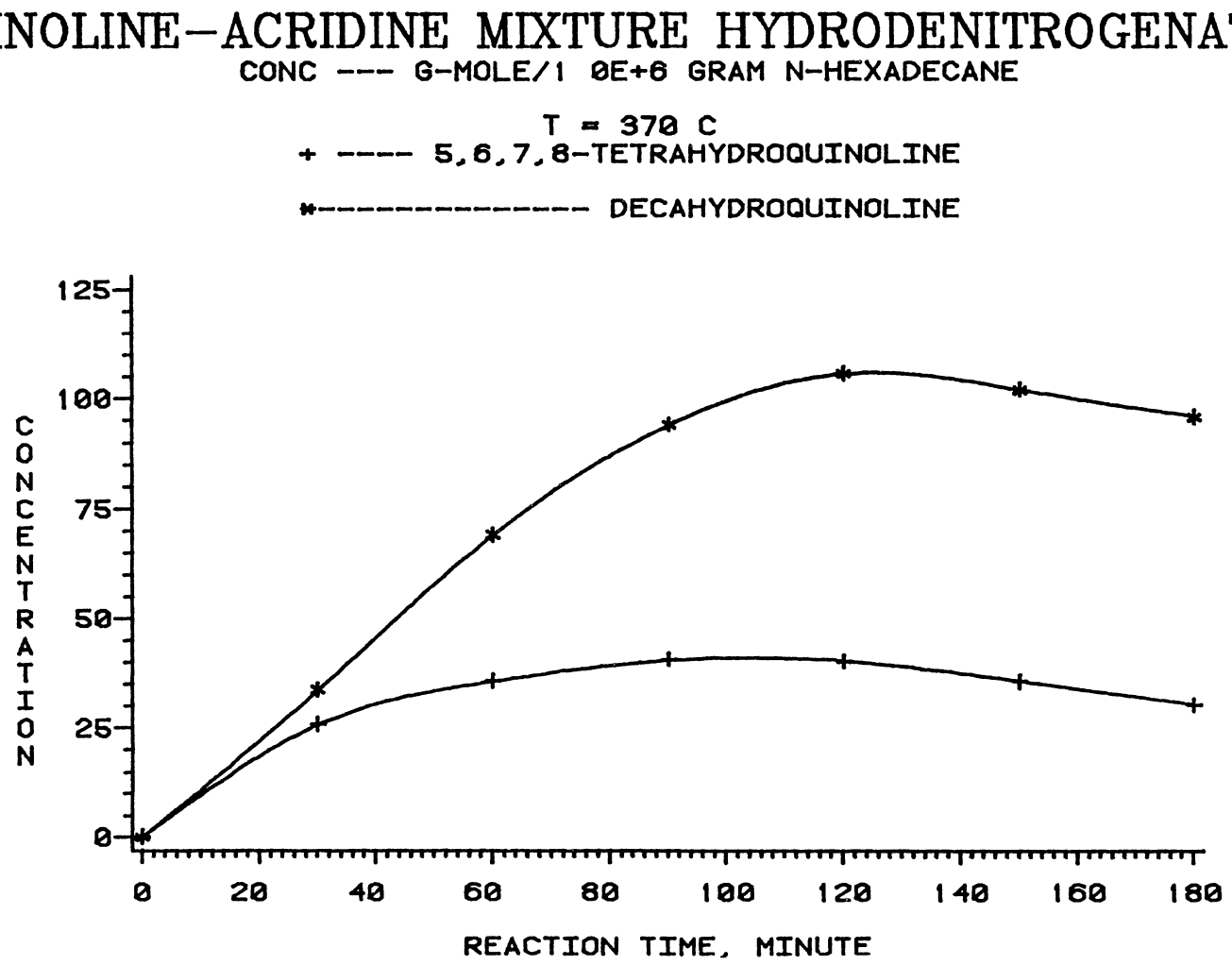

Figure 65. Quinoline-Acridine Mixture HDN Products at 370°C

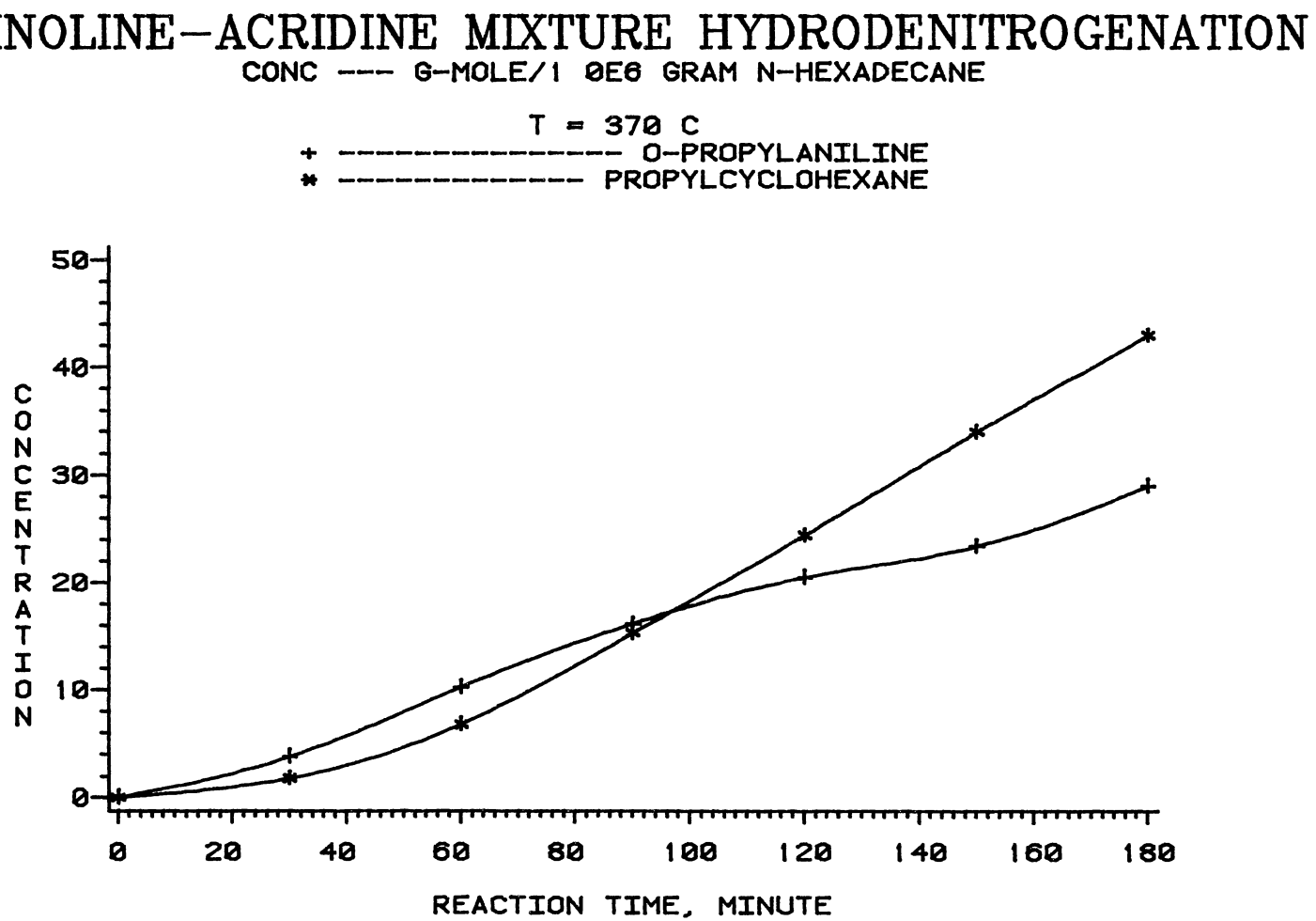

Figure 66. Quinoline-Acridine Mixture HDN Products at 370°C

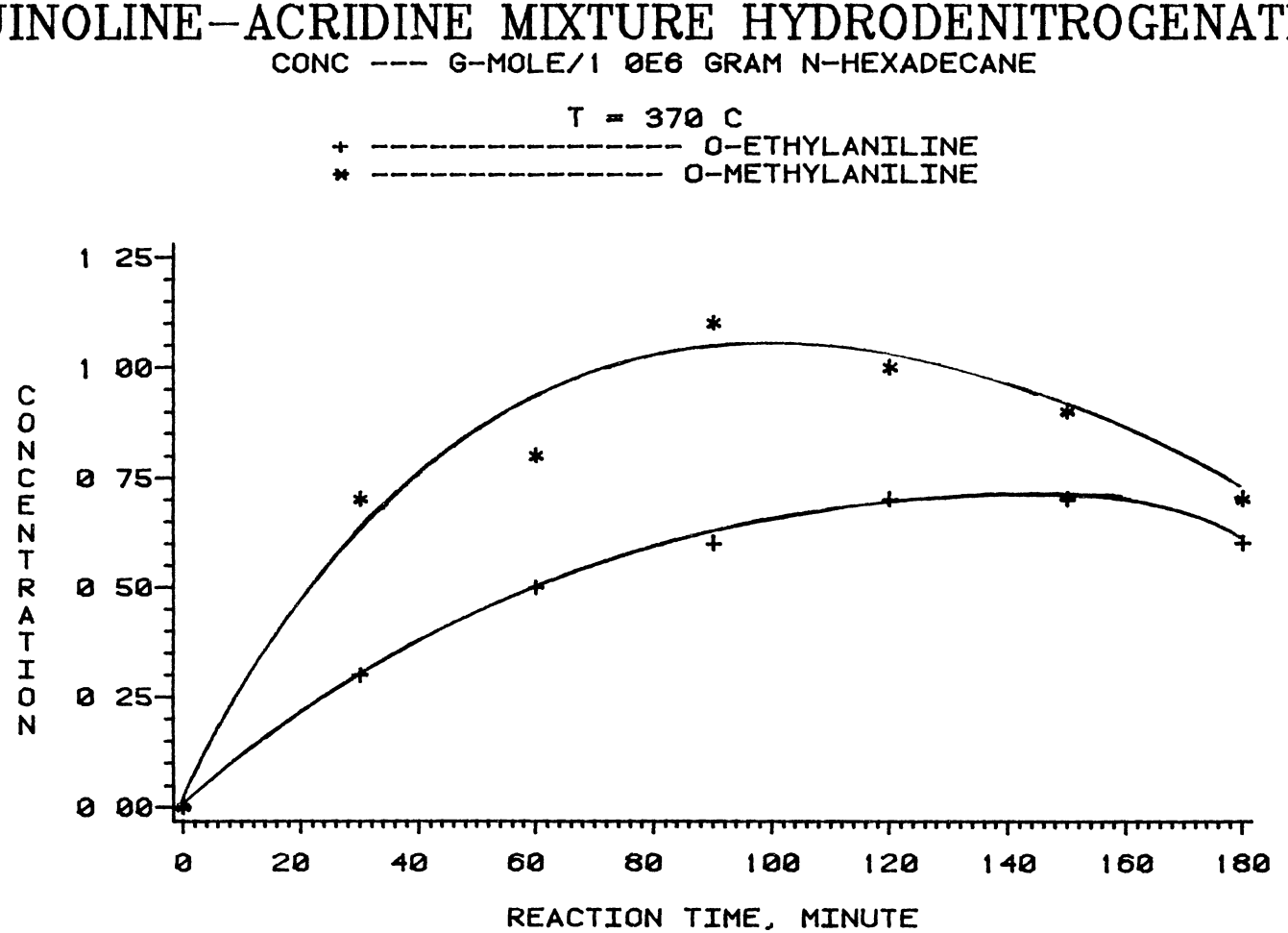

Figure 67. Quinoline-Acridine Mixture HDN Products at 370°C

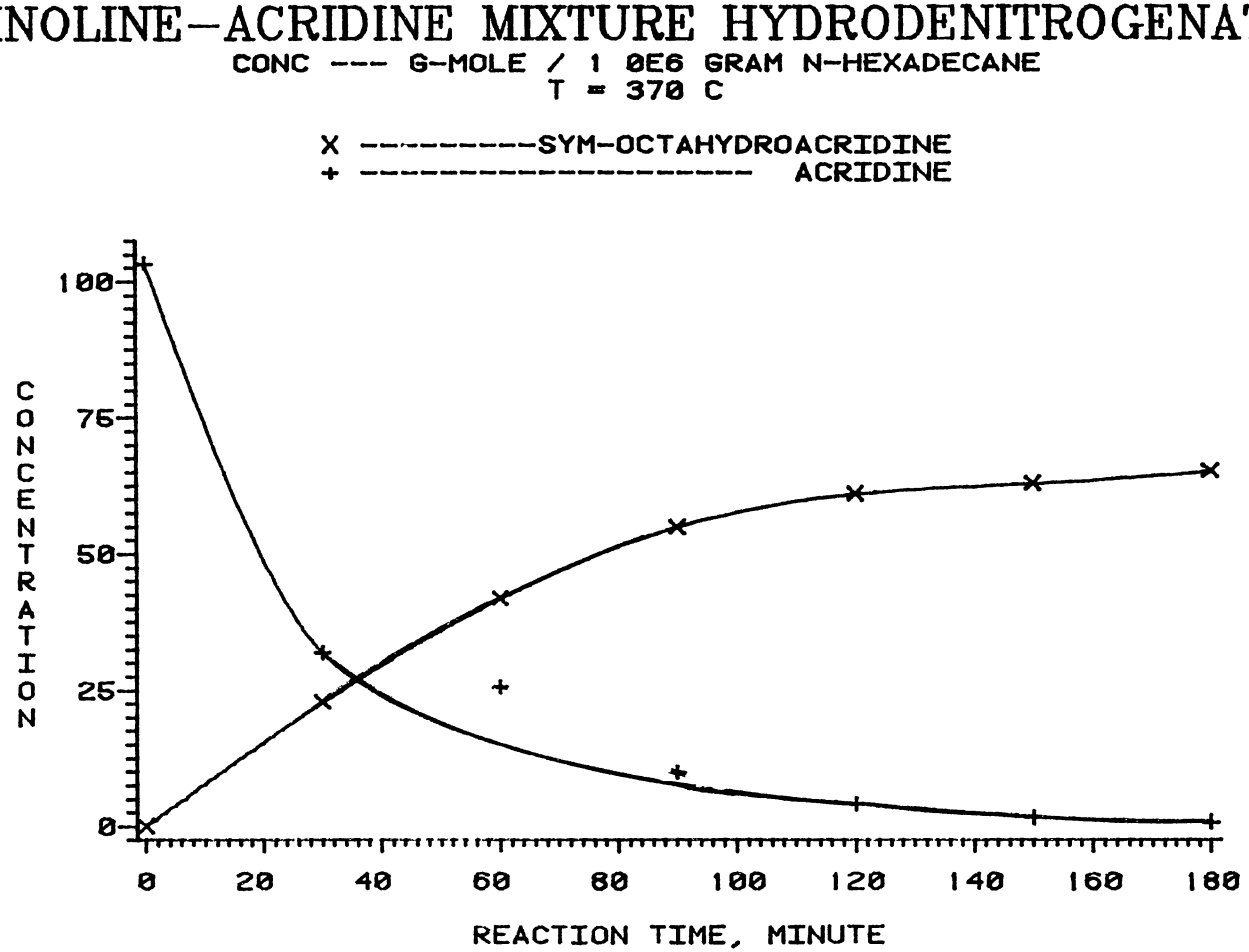

Figure 68 Quinoline-Acridine Mixture HDN Products at 370°C

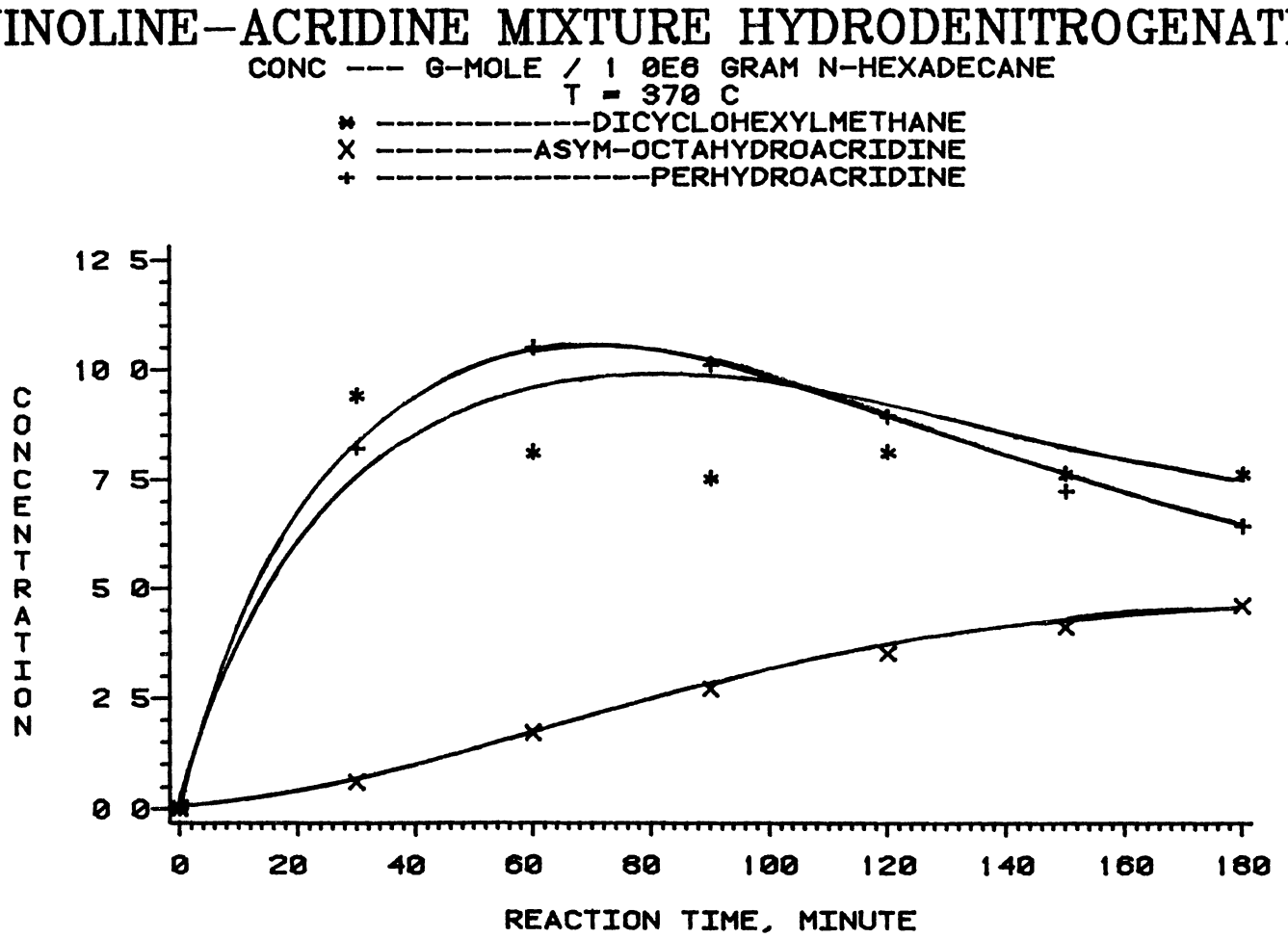

Figure 69. Quinoline-Acridine Mixture HDN Products at 370°C

transformation of DHQ to PCH is somewhat retarded by the presence of acridine. Similarly, the rate of conversion of OPA to OMA is retarded by the presence of acridine HDN products. On the other hand, the formation of OEA is enhanced. This appears from the comparison of Figures 55 and 28

Acridine conversion is decreased by the presence of quinoline HDN products. In the first thirty minutes of reaction about 85% of acridine is converted in acridine HDN, whereas the conversion is slightly decreased to 80.6% in the presence of quinoline HDN products. After 60 minutes the conversion is decreased from 95 7% to 89.1% by the presence of quinoline HDN products. These can be seen from comparing Figures 46 and 59. Also, the rates of formation and conversion of both SOHA and ASOHA are retarded. Similarly, the PHA formation is retarded as may be seen from comparison of Figures 44 and 57. On the other hand, the rate of formation of DCHM is enhanced by quinoline HDN products. Its concentration attains a maximum after about 40 minutes.

At 357°C quinoline conversion is slightly affected by the presence of acridine HDN products. The quinoline conversion, after 60 minutes reaction, decreased from 90.2% to 87.2%. Its conversion to Py-THQ is retarded, whereas its conversion to Bz-THQ is increased. This is apparent when comparing the data and Figures 17, 58, 18 and 59. Also, the rate of formation of DHQ is enhanced. Similarly, the rate of DHQ conversion to PCH and the rate of conversion of

Py-THQ to OPA are enhanced. This can be seen clearly from comparing Figures 19 and 60. Similar to 390°C run, the OPA conversion is affected by the presence of acridine products Its conversion to both OMA and OEA is decreased, and concentrations of aniline and PB are below detection limit. This is apparent from comparison of Figures 20 and 61

Acridine conversion is considerably affected by the presence of quinoline HDN products. After 60 minutes of reaction, 66 2% acridine conversion is attained, while it is 96.4% in the absence of quinoline produts. Also, after 3 hrs., its conversion is 91.6%, whereas it is almost complete in the absence of quinoline HDN products. This observation is similar to the results of 390°C run. In addition, the rate of formation of SOHA is also appreciably decreased. Furthermore, THA did not show up These facts can be seen when comparing Figures 39 and 62. Similarly, the rate of formation of ASOHA is decreased as well as the rate of conversion of PHA. On the other hand, both the rate of formation and the rate of conversion of DCHM are increased which may lead to the conclusion that there is another reaction patn which yields DCHM. These facts are apparent when considering Figures 40 and 63.

At 370°C, quinoline conversion is slightly affected by the presence of acridine HDN products. Py-THQ rate of formation and its rate of conversion are higher. This effect is due to the enhancement of the conversion of Py-THQ to DHQ. The concentration of the latter is increased

appreciably. On the other hand, the rate of formation of Bz-THQ is slightly decreased. These effects are apparent from the Figures 21, 22, 64 and 65 The rates of formation of both OPA and PCH are increased. However, the rates of conversion of OPA to OMA, OEA and PB are decreased, In fact, the last compound did not show up. These facts can be noticed in Figures 23,24,66 and 67.

Acridine conversion is reduced in the presence of quinoline HDN products as can be seen from the comparison of Figures 41,42,68 and 69 Similarly, the rates of formation of SOHA and PHA as well as their rates of conversion are decreased. On the other hand, the rate of formation of DCHM is increased, whereas the rate of formation of ASOHA is dcreased. However, its rate of conversion is increased These are rough estimates of the effects of the presence of quinoline HDN products, since the initial concentration of acridine in the mixture is about double its value in the HDN products.

Run NQA8 was continued for a total of 8.5h to study the long term conversion phenomena. The results until the end of the run are presented in the Figures 70-75. It was expected that both quinoline and acridine, the starting reactants, convert completely after this long reaction time. Also, the reaction intermediates go through maxima and then start to decrease, whereas the final products keep increasing with time. But, some unusual behaviors were observed

1. Quinoline, Py-THQ, Bz-THQ and DHQ reached a

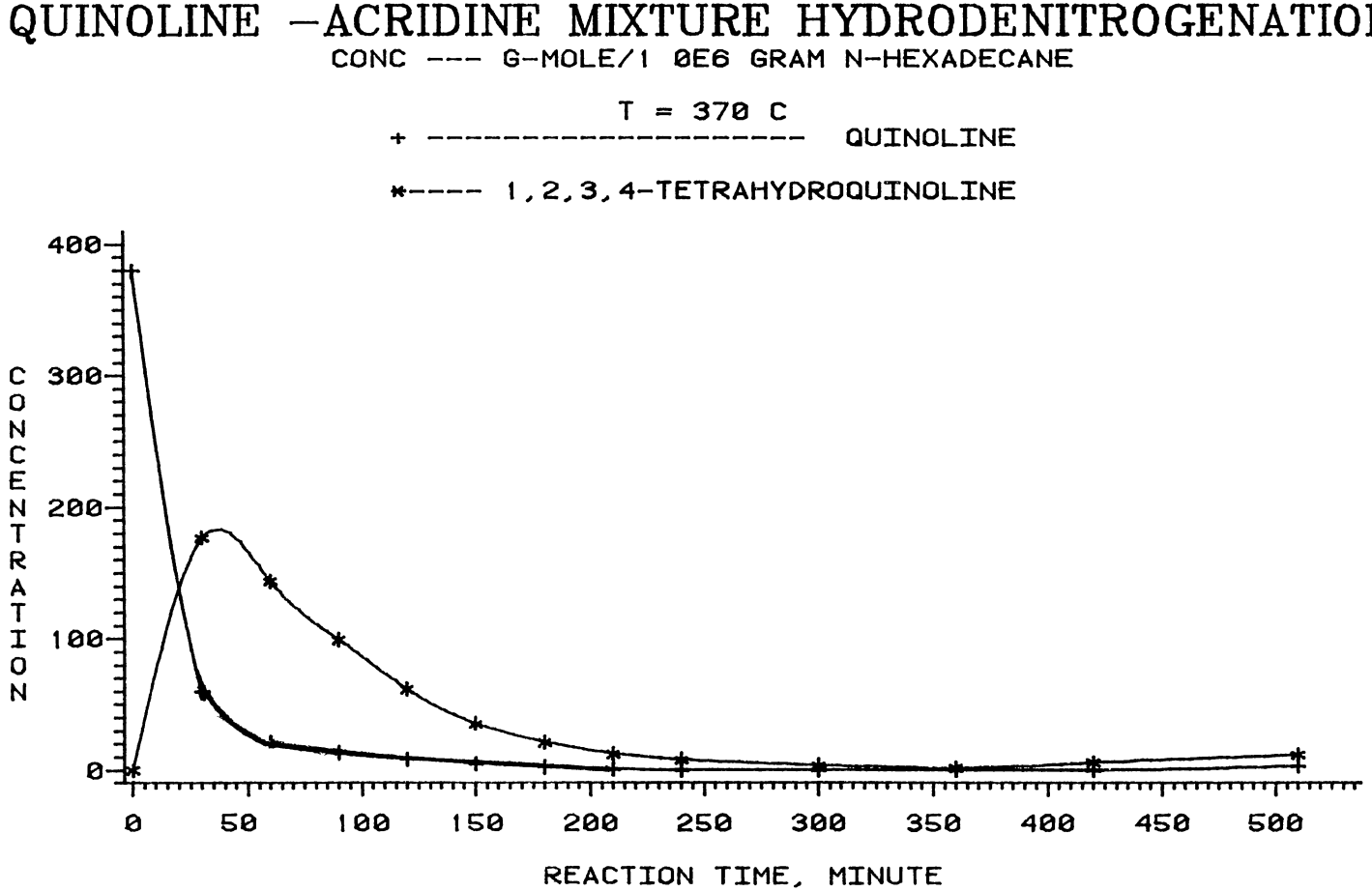

Figure 70 Quinoline-Acridine Mixture Long-Run HDN Products at 370°C

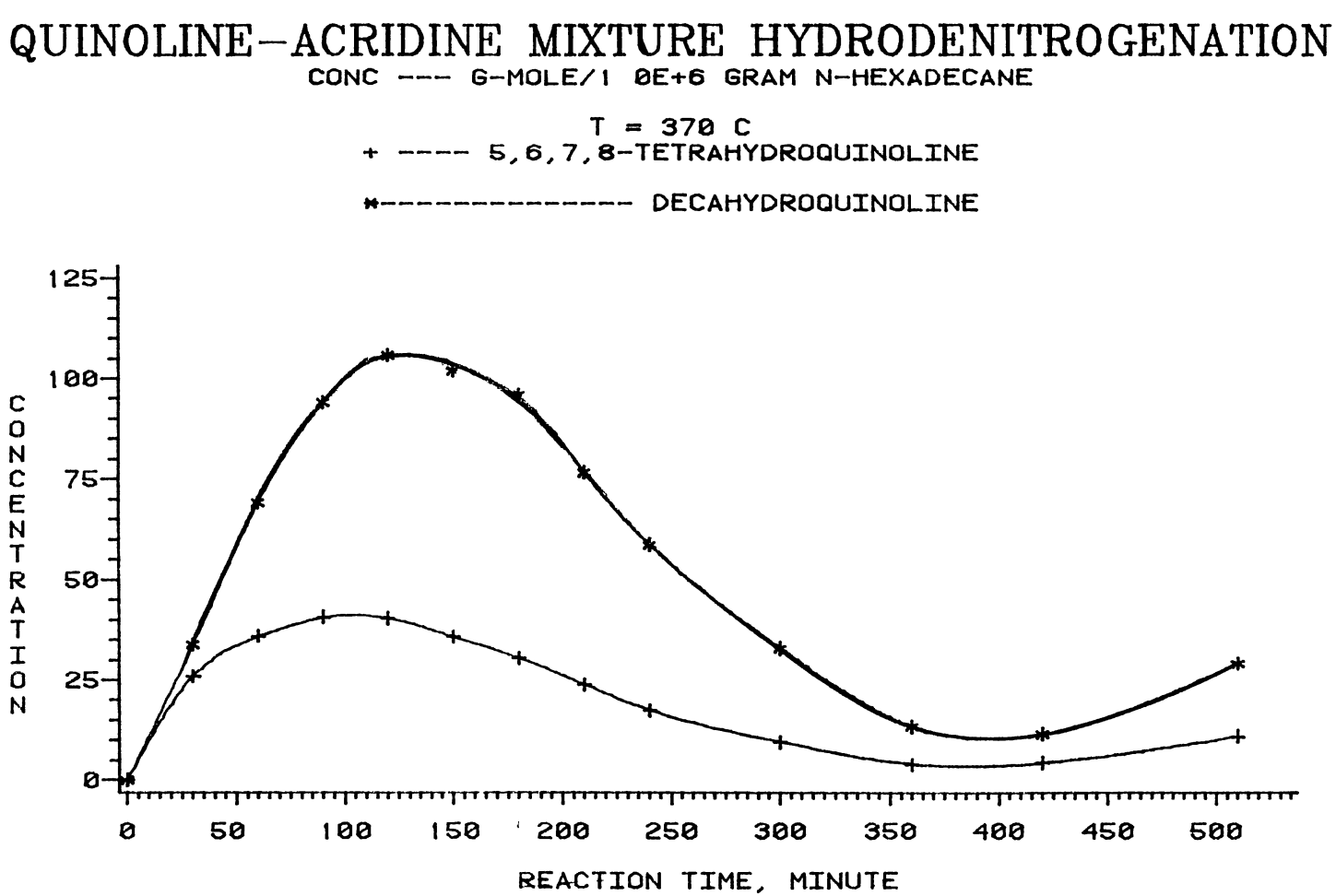

Figure 71 Quinoline-Acridine Mixture Long-Run HDN Products at 370°C

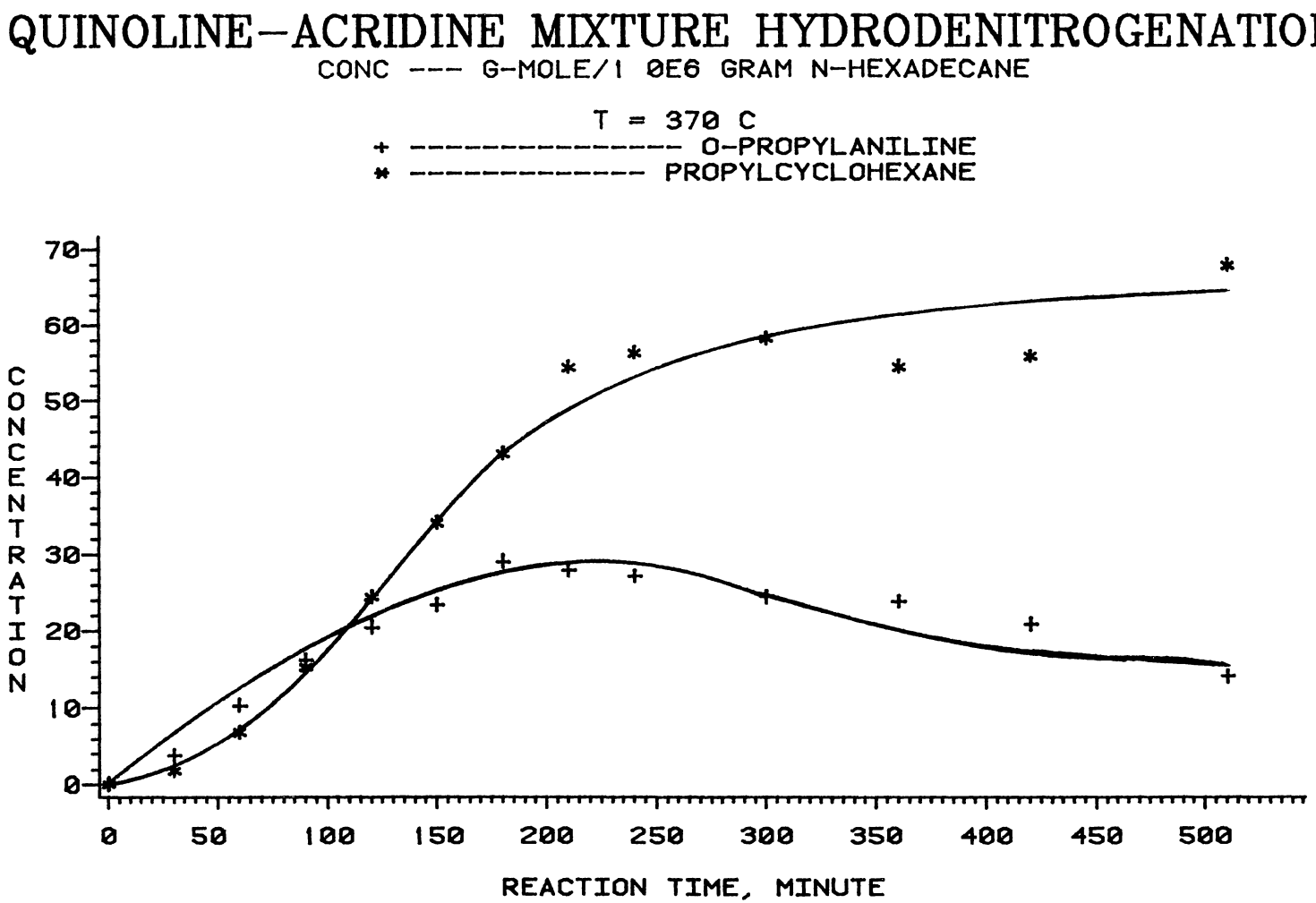

Figure 72. Quinoline-Acridine Mixture Long-Run HDN Products at 370°C

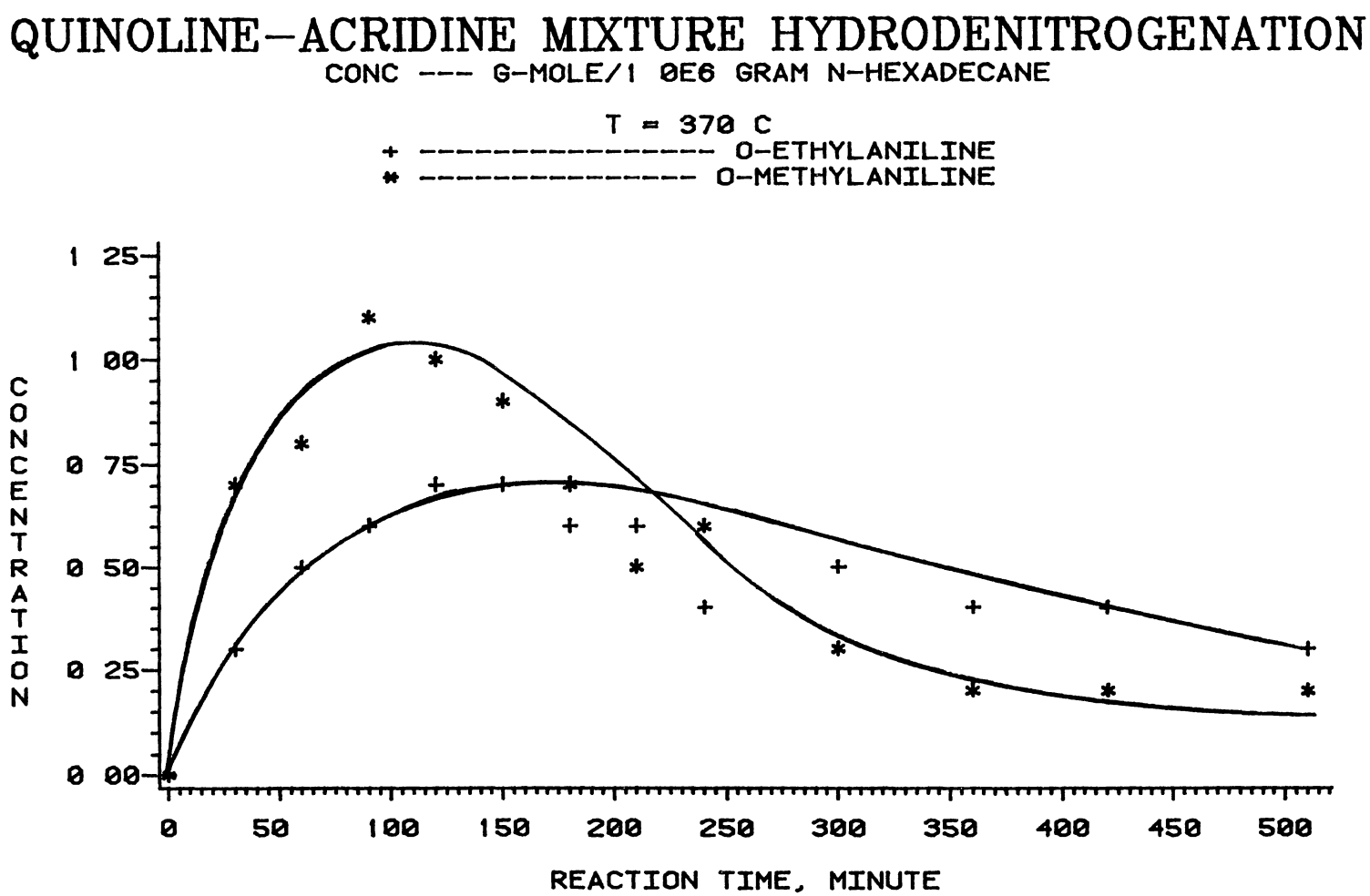

Figure 73. Quinoline-Acridine Mixture Long-Run HDN Products at 370°C

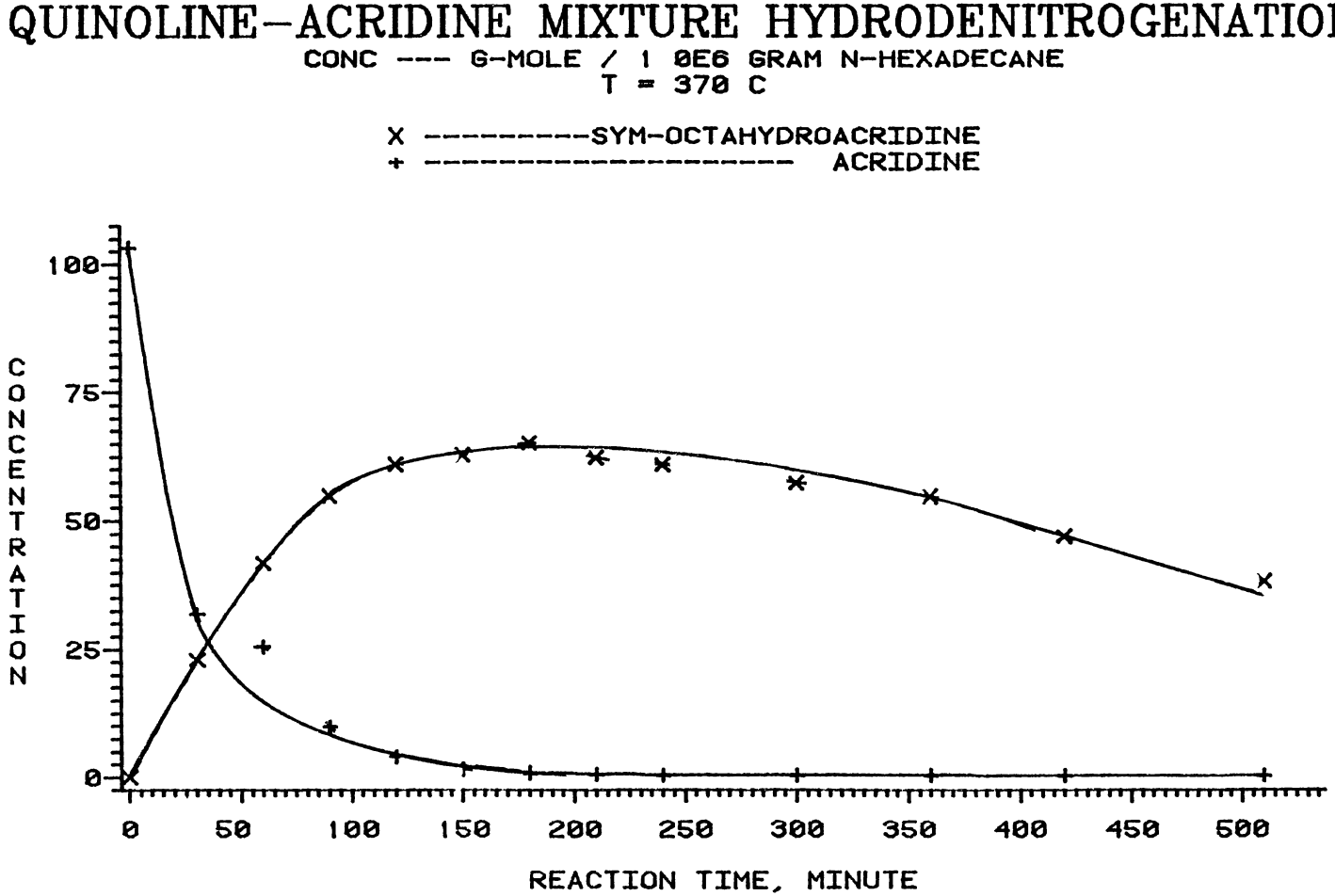

Figure 74 Quinoline-Acridine Mixture Long-Run HDN Products at 370°C

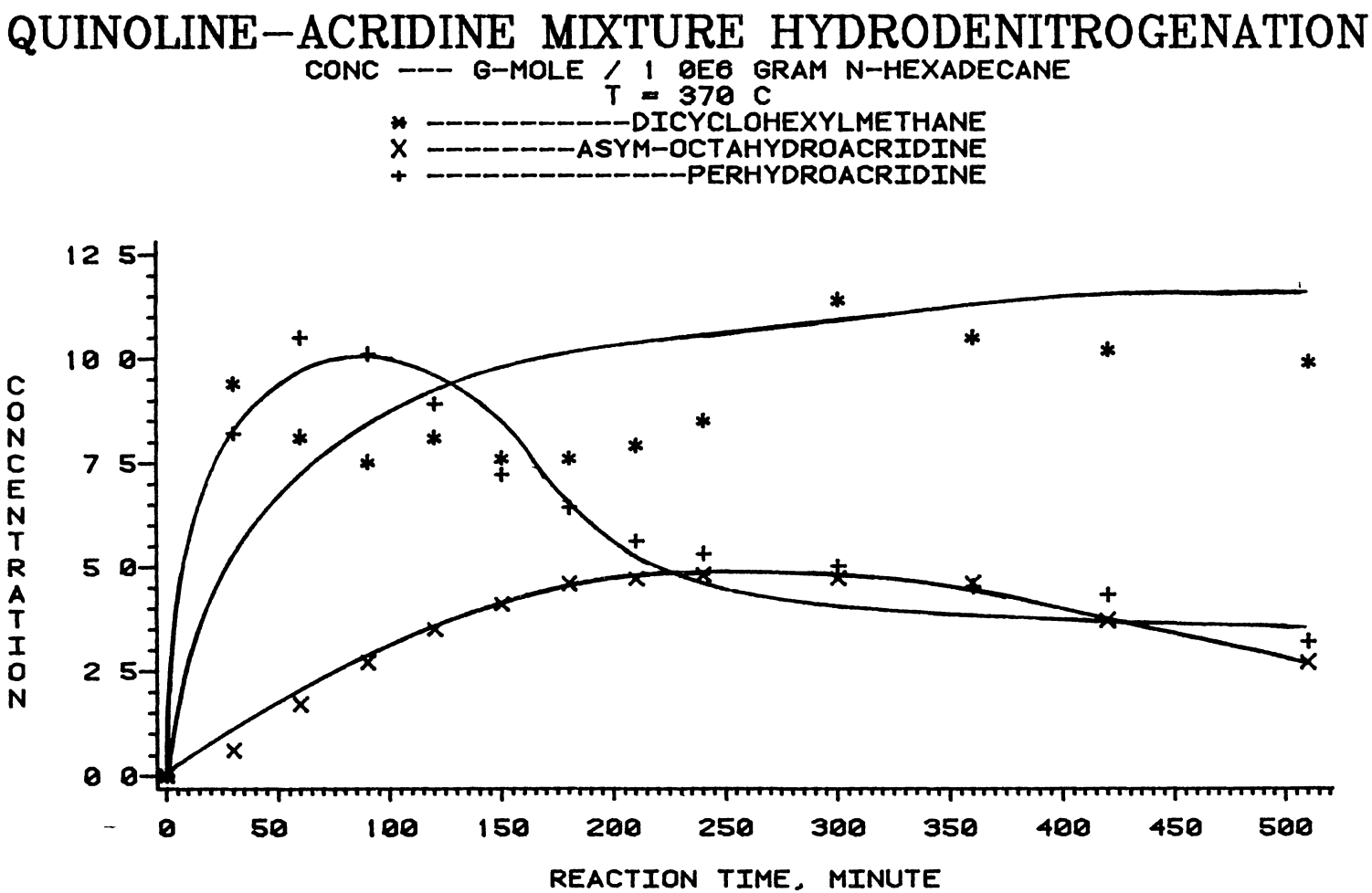

Figure 75 Quinoline-Acridine Mixture Long-Run HDN Products at 370°C

minimum then started to increase. This can be noticed in Figures 70 and 71.

2. PCH, after it started to decrease, it increased. This can be seen in Figure 74.

3 DCHM showed two maxima. This is apparent in Figure 75.

Behavior # 1 may be explained by considering that acridine HDN products, like THA, SOHA, ASOHA and PHA, split to give some of the quinoline HDN products as shown in Figure 76. In fact, Hartung et al. (101-102) have reported a mechanism for HDN of carbazole similar to that suggested here. In addition, butylpyridine was observed by Doleman and Vulgter (38) as one of the products of HDN of quinoline. This compound must have originated form Bz-THQ. This conclusion is confirmed by the fact that SOHA, ASOHA and PHA concentrations are decreasing while DCHM, which is assumed to be the only final product, is also decreasing.

Behavior #2 is, in fact, connected to the previous explanations, since quinoline HDN products yield PCH.

Behavior #3 leads to the suggestion that ASOHA is converted to DCHM through a reaction intermediate, o-perhydrotolylaniline. This reaction path has been reported by Zawadzki et al. (1,20). In addition to these unusual behaviors, it is clear that DHQ is more resistant to HDN than quinoline. Similarly, SOHA is more resistant than acridine.

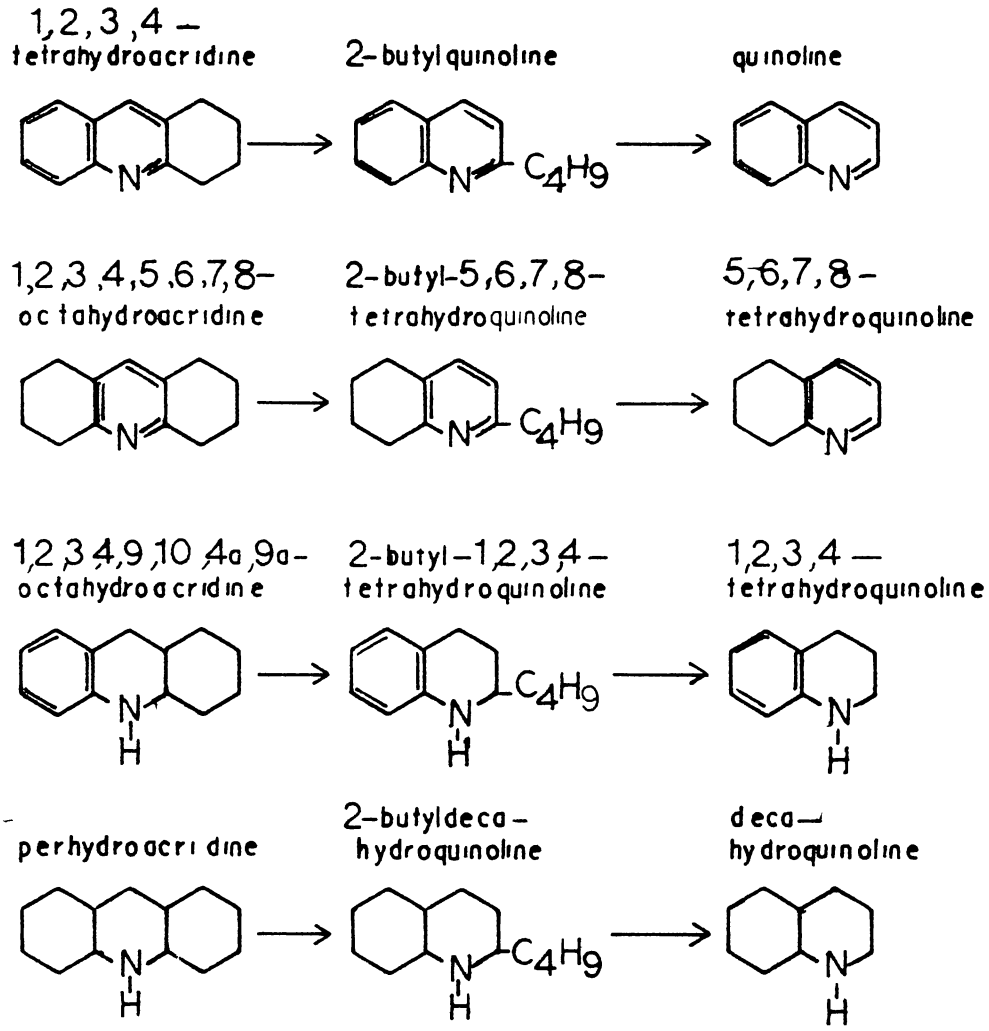

Figure 76. Reactions of some Acridine HDN Products

D. Catalyst Analysis

The properties of the American Cyanamide HDS-9A catalyst used in this project are presented in Table XX. The spent catalysts were analyzed for coke percentage and the regenerated catalysts were analyzed for surface area and pore volume. The results for different HDN runs are presented in Table XXI.

Table XXI shows that the percentage coke deposited on the catalyst is higher in quinoline HDN than in acridine HDN. This may be due to the higher initial concentration in quinoline HDN. In acridine HDN, both runs NA2 and NA3 have almost the same coke, even though they were not performed at the same temperature. On the other hand, coke percentage in NA1 is lower than in NA3 although NA1 was performed at a higher temperature.

This may be due to the lower acridine concentration in NA1. This leads to the conclusion that the reaction temperature in the range of 357°C to 390°C has no significant effect on percentage coke, whereas the amount of coke deposited increases with nitrogen compound concentration. This conclusion is confirmed by the results observed in NQA1, NQA2, and NQA6. However, it is observed that coke in NQA8 is lower than NQA1, NQA2 and NQA6. This may be explained by the fact that coke on the catalyst is composed of two types, a reactive coke which is subsequently converted to reaction products and an unreactive coke which remains

TABLE XX

PROPERTIES OF AMERICAN CYANAMIDE HDS-9A CATALYST*

Loss on ignition at 900°F,Wt %	1.2
Chemical, Wt. % dry basis	
Molybdenum (MoO3)	17.5
Nickel (NiO)	3.2
Sodium (Na2O)	0.03
Iron (Fe)	0.03
Sulfate (SO4)	0.4
Silicon dioxide (SiO2)	0.5
Physical Properties	
Average diamerer, inches	0.061
Average length, inches	0.18
Surface area, m2/gm	170.00 (265)**
Pore volume, cm^3/gm	0.52 (0.46)**

* Vendor's date

** Measured in our laboratory

TABLE XXI

CATALYST ANALYSIS

Catalyst	Surface Area, After Regeneration	Pore Volume After Regeneration	Percentage Coke
	m2/g	cm3/g	
Fresh	205	0.46	-----
NQ5	202	0.49	*
NQ6	214	0 52	*
NQ9	210	0 49	8.90
NA1	207	0.53	6.95
NA2	186	0.52	7.98
NA3	193	0.52	7 90
NQA1	200	0 51	10.99
NQA3	183	0.51	11 39
NQA6	201	0.51	11.07
NQA8	188	0.53	9 65

* The results lost due to mishandeling in the laboratory

unreacted on the catalyst. This assumption was reported by several investigators (103-106). This lower level of coke can be explained by the conversion of reactive coke to reaction products, at the end of the long reaction time of this run, by reaction with hydrogen.

The pore volumes, reported in Table XXI show that the catalysts have recovered their fresh pore volume after regeneration. Similarly, surface area has been almost recovered by regeneration and the variations presented in the table are within the experimental error.

CHAPTER V

KINETIC MODELING

Quantitative interpretation and analysis of the experimental results can only be accomplished through mathematical modeling of the kinetics. In this project two approaches have been taken a lumped compound model and a mechanistic kinetics model Models designated with numbers 1 through 3 below are lumped compound models in which all nitrogen compounds are considered as one reactant "A", whereas models mumber 4-7 are mechanistic models, considering the reactions of each compound separately. Each model results in a set of differential equations. These equations are solved either by analytical integration, whenever possible, or by numerical integration using a Runge-Kutta fourth order method. The parameters of the equations are estimated by a least square regression technique using Marquardt's numerical routine Details of this routine are given elsewhere (106).

Model # 1

The overall HDN reaction is presented by the following lumped equation

$$A+H_2 \text{ ---> hydrocarbon} + NH_3 \qquad [1]$$

where A represents the reacting nitrogen compounds. Assuming that the nitrogen removal can be shown by a first order kinetics model, the rate of HDN can be expressed as

$$-dC_A/dt = k_1 C_A P_{H_2}^n \qquad [2]$$

where C_A is the concentration of nitrogen in weight percent,
k_1 is the rate constant,
P_{H_2} is the partial pressure of hydrogen,
and n is the order of reaction with respect to hydrogen.

Since partial pressure of hydrogen is held constant during the experiments, equation [2] may be written as

$$-dC_A/dt = kC_A \qquad [3]$$

where k is the pseudo-first order rate constant

Integration of this equation results in·

$$\ln(C_A/C_{Ao}) = -kt \qquad [4]$$

where C_{Ao} is the initial weight percent of nitrogen in the oil and C_A is the weight percent of nitrogen in the oil at time t. Based on this model a plot of $\ln(C_A/C_{Ao})$ versus t should result in a straight line with a slope of -k

Model # 2

In this model the overall HDN reaction is assumed as

$$A+H_2 \quad <\!\!---\!\!> \quad D+E \qquad [1]$$

where A is the reacting nitrogen compound,

D is the resulting nitrogen compound,

and E is the hydrocarbon resulting from the HDN of A

It is assumed that hydrogen is adsorbed on one type of sites in atomic form, while all the nitrogen compounds adsorb on a different site. The reaction occurs between the adsorbed hydrogen and nitrogen compounds. The final products of HDN are also adsorbed on the nitrogen compound sites Thus the mechanism of the reaction can be pictured as follows.

$$A+l \quad <\!\!---\!\!> \quad Al \qquad [5]$$

$$H_2+2m \quad <\!\!---\!\!> \quad 2Hm \qquad [6]$$

$$2Hm+Al+l \quad <\!\!---\!\!> \quad Dl+El+2m \qquad [7]$$

$$Dl \quad <\!\!---\!\!> \quad D+l \qquad [8]$$

$$El \quad <\!\!---\!\!> \quad E+l \qquad [9]$$

where m and l represent adsorption sites for hydrogen and nitrogen compounds respectively. Then the rates of the reactions (5-9) can be written as

$$r_5 = k_{51}C_AC_1 - k_{52}C_{A1} \quad [10]$$

$$r_6 = k_{61}C_{H_2}C_m^2 - k_{62}\,C_{Hm}^2 \quad [11]$$

$$r7 = k_{71}C_{A1}C_{Hm}^2\,C_1 - k_{72}C_{D1}C_{E1}C_m^2 \quad [12]$$

$$r_8 = k_{81}C_{D1} - k_{82}\,C_DC_1 \quad [13]$$

$$r_9 = k_{91}C_{E1} - k_{92}C_EC_1 \quad [14]$$

where r_i is the rate of reaction i,

k_{i1} is the rate constant of reaction i in the forward direction,

k_{i2} is the rate constant of reaction i in the backward direction,

C_j is the concentration of compound j,

and C_1 and C_m are the concentrations of the sites 1 and m.

Now the following equilibrium relations are considered

$$K_A = k_{51}/k_{52} \quad [15]$$

$$K_{H2} = k_{61}/k_{62} \quad [16]$$

$$K_{sr} = k_{71}/k_{72} \quad [17]$$

$$K_D = k_{82}/k_{81} \quad [18]$$

$$K_E = k_{92}/k_{91} \quad [19]$$

where K_j is the adsorption equilibrium constant of compound j,

and K_{sr} is the equilibrium constant of the surface reaction.

By substituting the equations 15-19 into the equations 10-14 we get

$$r_5 = k_{51} (C_A C_l - C_{Al}/K_A) \quad [20]$$

$$r_6 = k_{61} (C_{H_2} C_m^2 - C_{Hm}^2/K_{H_2}) \quad [21]$$

$$r_7 = k_{71} (C_{Al} C_{Hm}^2 C_l - C_{Dl} C_{El} C_m^2/K_{sr}) \quad [22]$$

$$r_8 = k_{82} (C_{Dl}/K_D - C_D C_l) \quad [23]$$

$$r_9 = k_{92} (C_{El}/K_E - C_E C_l) \quad [24]$$

Assuming surface reaction, (r_7), to be the rate controlling, then.

k_{51} ---> ∞

k_{61} ---> ∞

k_{82} ---> ∞

and k_{92} ---> ∞

Since r_5, r_6, r_8 and r_9 must remain finite, then the value in parenthesis in each of the equations 20,21,23, and 24 must be equal to zero. This yields the following relations

$$C_{Al} = K_A C_A C_l \quad [25]$$

$$C_{Dl} = K_D C_D C_l \quad [26]$$

$$C_{El} = K_E C_E C_l \quad [27]$$

$$C_{Hm} = (K_{H_2} C_{H_2})^{1/2} C_m \qquad [28]$$

let $$C_{t_1} = C_l + C_{Al} + C_{Dl} + C_{El} \qquad [29]$$

$$C_{t_2} = C_m + C_{Hm} \qquad [30]$$

where C_{t_1} is the concentration of catalytic sites available for both nitrogen compounds and hydrocarbons,

and C_{t_2} is the concentration of catalytic sites available for hydrogen.

Then

$$C_{t_1} = C_l(1 + K_A C_A + K_D C_D + K_E C_E) \qquad [31]$$

$$C_{t_2} = C_m (1 + \sqrt{K_{H_2} C_{H_2}}) \qquad [32]$$

Therefore

$$C_l = \frac{C_{t_1}}{(1 + K_A C_A + K_D C_D + K_E C_E)} \qquad [33]$$

$$C_m = \frac{C_{t_2}}{(1 + \sqrt{K_{H_2} C_{H_2}})} \qquad [34]$$

By substituting from equations (25-28) in equation 22 we get·

$$r_7 = K_{71} C_l^2 C_m^2 (K_A C_A K_{H_2} C_{H_2} - K_D C_D K_E C_E / K_{sr}) \qquad [35]$$

$$= C_l^2 C_m^2 k_{41} K_A K_{H_2} [C_A C_{H_2} - (\frac{K_D K_E}{K_A K_{H_2} K_{sr}}) C_D C_E] \qquad [36]$$

$$\text{But} \quad K = \frac{K_A K_{H_2} K_{sr}}{K_D K_E} \qquad [37]$$

where K is the ordinary thermodynamic equilibrium constant for the overall reaction.

By substitution from [33],[34], and [37], in [36] we get

$$r_7 = \frac{C_{t_1}^2 C_{t_2}^2 k_{41} K_A K_{H_2} [C_A C_{H_2} - C_D C_E / K]}{[1 + K_A C_A + K_D C_D + K_E C_E]^2 [1 + \sqrt{K_{H_2} C_{H_2}}]^2} \qquad [38]$$

Now, making use of Shih, et al. (28) assumption that each nitrogen-containing compound has a comparable adsorption equilibrium constant, the term $[1 + K_A C_A + K_D C_D + K_E C_E]$ can be written as $[1 + K_N C_{No} + K_E C_E]$, where C_{No} is the initial concentration of the nitrogen compound, and K_N its adsorption equilibrium constant.

Then equation 38 can be written as.

$$r_A = \frac{k_A K_A K_{H_2} [C_A C_{H_2} - C_D C_E / K]}{[1 + K_A C_{Ao} + K_E C_E]^2 [1 + \sqrt{K_{H_2} C_{H_2}}]^2} \qquad [39]$$

where $k_A = k_{41} C_{t_1}^2 . C_{t_2}^2$

Model #3

This model is essentially identical to model # 2 except that the reaction of adsorbed hydrogen with adsorbed nitrogen compound results in an intermidiate adsorbed

compound (Pl), which then decomposes to adsorbed hydrocarbon and ammonia The reaction mechanism for this model may be assumed as follows

$$A + l \leftrightarrows Al \quad [5]$$

$$H_2 + 2m \leftrightarrows 2Hm \quad [6]$$

$$Hm + Al \leftrightarrows Pl + m \quad [40]$$

$$2Pl \leftrightarrows Dl + El \quad [41]$$

$$Dl \leftrightarrows D + l \quad [8]$$

$$El \leftrightarrows E + l \quad [9]$$

The rates of the above reactions can be written

$$r_5 = k_{51}C_AC_l - K_{52}C_{Al} \quad [10]$$

$$r_6 = k_{61}C_{H_2}C_m^2 - k_{62}C_{Hm}^2 \quad [11]$$

$$r_{40} = k_{401}C_{Hm}C_{Al} - k_{402}C_{Pl}C_m \quad [42]$$

$$r_{41} = k_{411}C_{Pl}^2 - k_{412}C_{Dl}C_{El} \quad [43]$$

$$r_8 = k_{81}C_{Dl} - k_{82}C_DC_l \quad [13]$$

$$r_9 = k_{91}C_{El} - k_{92}C_EC_l \quad [14]$$

Now consider the following equilibrium equation.

$$K_A = k_{51}/k_{52} \quad [15]$$

$$K_{H_2} = k_{61}/k_{62} \quad [16]$$

$$K_{sr_1} = k_{401}/k_{402} \quad [44]$$

$$K_{sr_2} = k_{411}/k_{412} \quad [45]$$

$$K_D = k_{82}/k_{81} \quad [18]$$

$$K_E = k_{92}/k_{91} \quad [19]$$

By substituting the equations (15,16,44,45,18,19) into the equations (10,11,42,43,13,14) we get

$$r_5 = k_{51} (C_A C_l - C_{Al}/K_A) \quad [20]$$

$$r_6 = k_{61} (C_{H_2} C_m^2 - C_{Hm}^2/K_{H_2}) \quad [21]$$

$$r_{40} = k_{401} (C_{Hm} C_{Al} - C_{Pl} C_m/K_{sr_1}) \quad [46]$$

$$r_{41} = k_{411} (C_{Pl}^2 - C_{Dl} C_{El}/K_{sr_2}) \quad [47]$$

$$r_8 = k_{81} (C_{Dl} - K_D C_D C_l) \quad [23]$$

$$r_9 = k_{91} (C_{El} - K_E C_E C_l) \quad [24]$$

Assuming surface reaction, (r_{40}), to be the rate controlling step then.

k_{51} ---> ∞

k_{61} ---> ∞

k_{411} ---> ∞

k_{81} ---> ∞

and k_{91} ---> ∞

Since r_5, r_6, r_{41}, r_8 & r_9 must remain finite, then the value between parenthesis in each of the equations 20,21,47,23 and 24 are to be equal zero. This yields the following relations:

$$C_{Al} = K_A C_A C_l \quad [25]$$

$$C_{Dl} = K_D C_D C_l \quad [26]$$

$$C_{El} = K_E C_E C_l \quad [27]$$

$$C_{Hm} = (K_{H_2} C_{H_2})^{1/2} C_m \quad [28]$$

$$C_{Pl} = (C_{Dl} C_{El} / K_{sr_2})^{1/2} \quad [48]$$

let $$Ct_1 = (C_l + C_{Al} + C_{Pl} + C_{El} + C_{Dl}) \quad [49]$$

$$C_{t_2} = C_m + C_{Hm} \quad [50]$$

Then

$$C_{t_1} = C_l[1 + K_A C_A + [\frac{(K_D C_D)\ (K_E C_E)}{K_{sr_2}}]^{1/2} + K_D C_D + K_E C_E] \quad [51]$$

$$C_{t_2} = C_m[1 + (K_{H_2} C_{H_2})^{1/2}] \quad [52]$$

The last two equations can be rewritten in the following forms:

$$C_l = C_{t_1} / [1 + K_A C_A + K_D C_D + K_E C_E + \sqrt{K_D C_D K_E C_E / K_{sr_2}}] \quad [53]$$

$$C_m = C_{t_2} / (1 + \sqrt{K_{H_2} C_{H_2}}) \quad [54]$$

By substituting from the equations 25-28,48 in equation 46 we get.

$$r_{40} = k_{401}\, C_1 C_m \left[K_A C_A (K_{H_2} C_{H_2})^{1/2} - \sqrt{\frac{(K_D C_D K_E C_E)}{K_{sr_2}}} / K_{sr_1}\right] \quad [55]$$

Assume $C_D = C_E$

By substituting for C_1 and C_m we get:

$$r_{40} = k_{401} C_{t_1} C_{t_2} [\, K_A C_A (K_{H_2} C_{H_2})^{0.5} - KC_E]/$$

$$[1 + K_A C_A + K_D C_D + K_E C_E + K' C_E]/ [1 + \sqrt{K_{H_2} C_{H_2}}] \quad [56]$$

where, $K = (K_D K_E / K_{sr_2})^{1/2} / K_{sr_1}$ [57]

and $K' = \sqrt{K_D K_E / K_{sr_2}}$ [58]

Now assuming the following.

$$k_A = k_{401} C_{t_1} C_{t_2}$$

$$K_A = K_D$$

$$C_{Ao} = C_A + C_D$$

$$C_E = C_{Ao} - C_A$$

$$K_E = K_E + K'$$

and substituting in equation 56 we get.

$$r_A = r_{40} = \frac{k_A [K_A C_A (K_{H_2} C_{H_2})^{0.5} - K(C_{Ao} - C_A)]}{[1 + K_A C_{Ao} + K_E (C_{Ao} - C_A)][1 + \sqrt{K_{H_2} C_{H_2}}]}$$

Model # 4

This model is based on the reaction network for quinoline, presented in Figure 38 As will be discused in chapter VI, model # 2 shows good estimation for the total nitrogen in quinoline reaction products at different temperatures. The relative errors are less than 5%. This model can be simplified to estimate different reactions in the following style

$$r_A = \frac{k_A K_A K_{H_2} [C_A C_{H_2} - C_D C_E / K]}{[1 + K_N C_{No} + K_E C_E]^2 [1 + \sqrt{K_{H_2} C_{H_2}}]^2} \qquad [39]$$

This model is developed for two product components, D and E. For most of the reactions which will be considered here we can represent the reaction as·

$$A + H_2 \text{ <----> } D \qquad [60]$$

so equation 39 can be rewritten as

$$r_A = \frac{k_A K_A K_{H_2} [C_A C_{H_2} - C_D / K]}{[1 + K_N C_{No}]^2 [1 + \sqrt{K_{H_2} C_{H_2}}]^2} \qquad [61]$$

This equation can be rewritten in a simpler form:

$$(-dC_i/dt) = k_{ij}a_{ij}\,[C_i - C_j/K_{ij}] \qquad [62]$$

where k_{ij} is the specific rate constant for the reaction of the compound i to form compound j. Also the following relations hold

$$K_{ij} = K.C_{H_2} \qquad [63]$$

$$a_{ij} = K_A K_{H_2} C_{H_2}/[1 + K_N C_{No}]^2/[1 + \sqrt{K_{H_2} C_{H_2}}]^2 \qquad [64]$$

C_i is the concentration of the compound i, reacting to produce the compound j,

C_j is the concentration of the product j.

However, each of k_{ij}, a_{ij} and K_{ij} is a function of temperature.

This indicates that a mechanistic model presented in equation 34 reduces to a pseudo-first order reaction for individual steps considered in the reaction network. Now considering the reaction network for the HDN of quinoline, presented in Figure 38, the following mathematical model was developed:

$$(dC_1/dt_1) = -k_{12}a_{12}[C_1 - C_2/K_{12}] - k_{13}a_{13}[C_1 - C_3/K_{13}] \qquad [65]$$

$$(dC_2/dt) = -k_{21}a_{21}(C_2 - C_1/K_{21}) - k_{24}a_{24}(C_2 - C_4/K_{24}) - k_{25}a_{25}C_2 \qquad [66]$$

$$(dC_3/dt) = -k_{31}a_{31}(C_3 - C_1/K_{31}) - k_{34}a_{34}(C_3 - C_4/K_{34}) \qquad [67]$$

$$(dC_4/dt) = - k_{43}a_{43}(C_4 - C_3/K_{43}) - k_{42}a_{42}(C_4 - C_2/K_{42}) - k_{46}a_{46}C_4 \quad [68]$$

$$(dC_5/dt) = - (k_{57}a_{57} + k_{58}a_{58} + k_{59}a_{59} + k_{510})C_5 + k_{25}a_{25}C_2 \quad [69]$$

$$(dC_6/dt) = k_{46}a_{46}C_4 \quad [70]$$

$$(dC_7/dt) = k_{57}a_{57}C_5 \quad [71]$$

$$(dC_8/dt) = k_{58}a_{58}C_5 \quad [72]$$

$$(dC_9/dt) = k_{59}a_{59}C_5 \quad [73]$$

$$(dC_{10/dt}) = k_{510}a_{510}C_5 \quad [74]$$

These ten equations can be rewritten in the following forms.

$$(dC_1/dt) = - (a_{12} + a_{13})C_1 + a_{12}C_2/K_{12} + a_{13}C_3/K_{13} \quad [75]$$

$$(dC_2/dt) = -(a_{21} + a_{24} + a_{25})C_2 + a_{21}C_1/K_{12} + a_{24}C_4/K_{24} \quad [76]$$

$$(dC_3/dt) = -(a_{31} + a_{34})C_3 + a_{31}C_1/K_{31} + a_{34}C_4/K_{34} \quad [77]$$

$$(dC_4/dt) = - (a_{43} + a_{42} + a_{46})C_4 + a_{42}C_2/K_{42} + a_{43}C_3/K_{43} \quad [78]$$

$$(dC_5/dt) = -(a_{57} + a_{58} + a_{59} + a_{510})C_5 + a_{25}C_2 \quad [79]$$

$$(dC_6/dt) = a_{46}C_4 \quad [80]$$

$$(dC_7/dt) = a_{57}C_5 \quad [81]$$

$$(dC_8/dt) = a_{58}C_5 \quad [82]$$

$$(dC_9/dt) = a_{59}C_5 \quad [83]$$

$$(dC_{10}/dt) = a_{510}C_5 \quad [84]$$

where (dC_1/dt) is the net rate of reaction of compound i,

and a_{ij} is a parameter for the reaction starting with compound i to produce compound j.

This set of ten equations with 22 parameters are solved using the Marquardt's routine.

Model # 5

The reaction mechanism for quinoline HDN, presented in Figure 38, may be simplified by assuming that quinoline hydrogenation to Py-THQ is the only reversible reaction. Thus, the set of differential equations developed for model # 4 can be reduced to:

$$(dC_1/dt) = -k_{12}a_{12}\,[C_1 - C_2/K_{12}] - k_{13}a_{13}C_1 \quad [85]$$

$$(dC_2/dt) = -k_{21}a_{21}\,[C_2 - C_1/K_{21}] - k_{24}a_{24}C_2 - k_{25}a_{24}C2 \quad [86]$$

$$(dC_3/dt) = k_{13}a_{13}C_1 - k_{34}a_{34}C_3 \quad [87]$$

$$(dC_4/dt) = k_{24}a_{24}C_2 + k_{34}a_{34}C_3 - k_{46}a_{46}C_4 \quad [88]$$

$$(dC_5/dt) = -[k_{57}a_{57} + k_{58}a_{58} + k_{59}a_{59} + k_{510}a_{510}]C_5 + k_{25}a_{25}C_2 \quad [69]$$

$$(dC_6/dt) = k_{46}a_{46}C_4 \quad [70]$$

$$(dC_7/dt) = k_{57}a_{57}C_5 \quad [71]$$

$$(dC_8/dt) = k_{58}a_{58}C_5 \quad [72]$$

$$(dC_9/dt) = k_{59}a_{59}C_5 \quad [73]$$

$$(dC_{10}/dt) = k_{510}a_{510}C_5 \quad [74]$$

These equations can be written in the following form.

$$(dC_1/dt) = -[a_{12} + a_{13}]C_1 + a_{21}C_1/K_{12} \quad [89]$$

$$(dC_2/dt) = -[a_{21} + a_{24} + a_{25}]\ C_2 + a_{21}C_1/K_{21} \quad [90]$$

$$(dC_3/dt) = a_{13}C_1 - a_{34}C_3 \quad [91]$$

$$(dC_4/dt) = a_{24}C_2 + a_{34}C_3 - a_{46}C_4 \quad [92]$$

$$(dC_5/dt) = -[a_{57} + a_{58} + a_{59} + a_{510}]C_5 + a_{25}C_2 \quad [79]$$

$$(dC_6/dt) = a_{46}C_4 \quad [80]$$

$$(dC_7/dt) = a_{57}C_5 \quad [81]$$

$$(dC_8/dt) = a_{58}C_5 \quad [82]$$

$$(dC_9/dt) = a_{59}C_5 \quad [83]$$

$$(dC_{10}/dt) = a_{510}C_5 \quad [84]$$

This set of ten equations with 13 parameters are solved

using Marquardt's routine.

Model # 6

In this model, the pseudo first order reaction steps, developed earlier in model #4 are applied to the reaction network (Figure 51) of HDN of acridine. Each compound in the reaction network is designated by a number as follows:

Aridine ----> 1

THA ----> 2

ASOHA ----> 3

SOHA ----> 4

PHA ----> 5

DCHM ----> 6

The rate equation for each reaction is given by:

$$(dC_i/dt) = -a_{ij}[C_i - C_j/K_{ij}] \qquad [93]$$

where a_{ij} is a parameter for the reaction starting with compound i to produce compound j. Considering the reaction network for HDN of acridine presented in Figure (51), the following equations can be developed:

$$(dC_1/dt) = -a_{12}[C_1 - C_2/K_{12}] - a_{13}[C_1 - C_3/K_{13}] \qquad [94]$$

$$(dC_2/dt) = -a_{12}[C_1 - C_2/K_{12}] - a_{24}[C_2 - C_4/K_{24}] \qquad [95]$$

$$(dC_3/dt) = -a_{13}[C_1 - C_3/K_{13}] - a_{35}[C_1 - C_5/K_{35}] \qquad [96]$$

$$(dC_4/dt) = -a_{24}[C_2 - C_4/K_{24}] - a_{45}[C_4 - C_5/K_{45}] \qquad [97]$$

$$(dC_5/dt) = -a_{35}[C_3 - C_5/K_{35}] + a_{45}[C_4 - C_5/K_{45}] - a_{56}C_5 \quad [98]$$

$$(dC_6/dt) = a_{56}C_5 \quad [99]$$

This set of six equations with eleven parameters are solved using the Marquardt's routine

Model # 7

This model handles quinoline-acridine mixture HDN It considers the reactions presented in both Figure 38 and Figure 51 In fact, this model is a combination of model # 4 and model # 6. It includes the equations 75-84 and the equations 94-99. Thus, this model results in a set of 16 differential equation with 33 parameters These equations are solved using the previous method as in model # 6

Effect of The Amount of Catalyst

The values of k in these models are in sec^{-1}, which does not consider the relative amount of catalyst to oil. Obviously, if the reactions are conducted with different amounts of catalyst, the observed rates would appear to be different In order to compare the values of rate constants obtained in this work with those obtained with different ratios of catalyst to oil and with those of trickle bed reactors, the rate constants here should be divided by the catalyst concentration (g cat /g n-hexadecane).

CHAPTER VI

DISCUSSION OF RESULTS

In this chapter the results of fitting the experimental data with the models described in Chapter V are discussed

Model # 1

This model considers a pseduo-first order reaction for total nitrogen removal Using the experimental data, the best estimate for k is evaluated by the Marquardt's method.

Quinoline HDN data, presented in Tables VIII, IX, and X, were used to estimate k, the rate constant for total nitrogen removal. The results are presented in Table XXII, and plotted in Figure 77. The percentage relative error (PRE) varies between -22.8% and 13 4% The signs of PRE indicate that this model does not fit the quinoline data satisfactorily. The values of k, predicted by this model, were used to calculate the activation energy Values of ln (k) are plotted versus 1/T in Figure 78. The predicted activation energy is 129.5 kJ/mol. This value is comparable to the value predicted by Shih et al (43), 104 6 kJ/mol, but is closer to the value reported by Aboul-Gheit et al. (44), 126 8 kJ/mol. The rate constants predicted by this model are also close to the values reported by Aboul-Gheit et al (44). They reported the values of 1 3 E-5, 3 4

TABLE XXII

MODEL # 1 - QUINOLINE HDN

k,s^{-1}	Temperature,°C	Time, minute	*Actual Concentration	*Predicted Concentration	Percentage Relative Error
3.3E-5	357	0	351	351	----
		30	312	331	-6.1
		60	262	312	-19.2
		90	263	294	-11 9
		150	263	262	0.4
		180	259	247	4 7
		210	259	233	10.1
6 3E-5	370	0	345	345	-----
		30	251	308	-22.8
		60	235	275	-17.1
		90	223	246	-10 2
		120	217	219	-11 3
		150	213	196	8.0
		180	202	175	13.4

TABLE XXII (continued)

k,s^{-1}	Temperature,°C	Time, minute	*Actual Concentration	*Predicted Concentration	Percentage Relative Error
11 5E-5	390	0	372	372	----
		30	248	302	-21 8
		60	243	245	-10 2
		90	216	199	7 7
		120	176	162	8.0
		150	132	132	0 3
		180	103	107	-3 8

*g-mole/1.0E6 g n-hexadecane

E-5, and 7 5E-5 s^{-1} for 350, 375, and 400°C respectively, whereas they are two orders of magnitude less than the rate constant reported by Shih et al (43), 6 8E-3 s^{-1} at 342°C. In fact, this model is not expected to fit the quinoline HDN results well, because of thermodynamic equilibrium limitations in quinoline HDN process If only the first three data points of each run are fitted with this model, the PRE varies between -10.5 and 9.7 and the values of k will be 0.78E-4, 1.23E-4 and 1.47E-4 s^{-1} for 357, 370, and 390°C respectively which are about one order of magnitude higher than the previous results Then the activation energy is 63 5 kJ/mol (15 2 kcal/ mole). The effectiveness

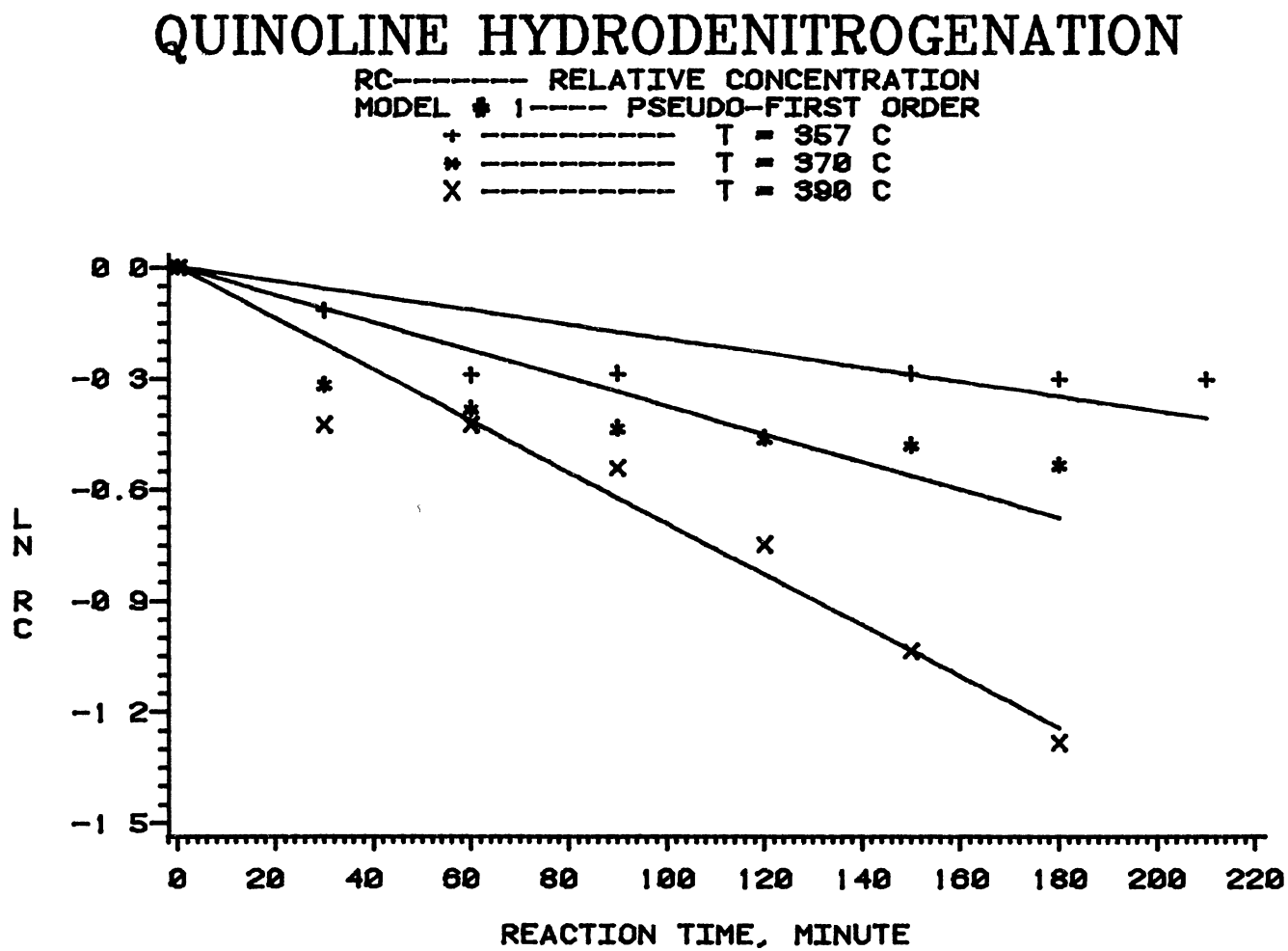

Figure 77 Quinoline Hydrodenitrogenation - Model #1

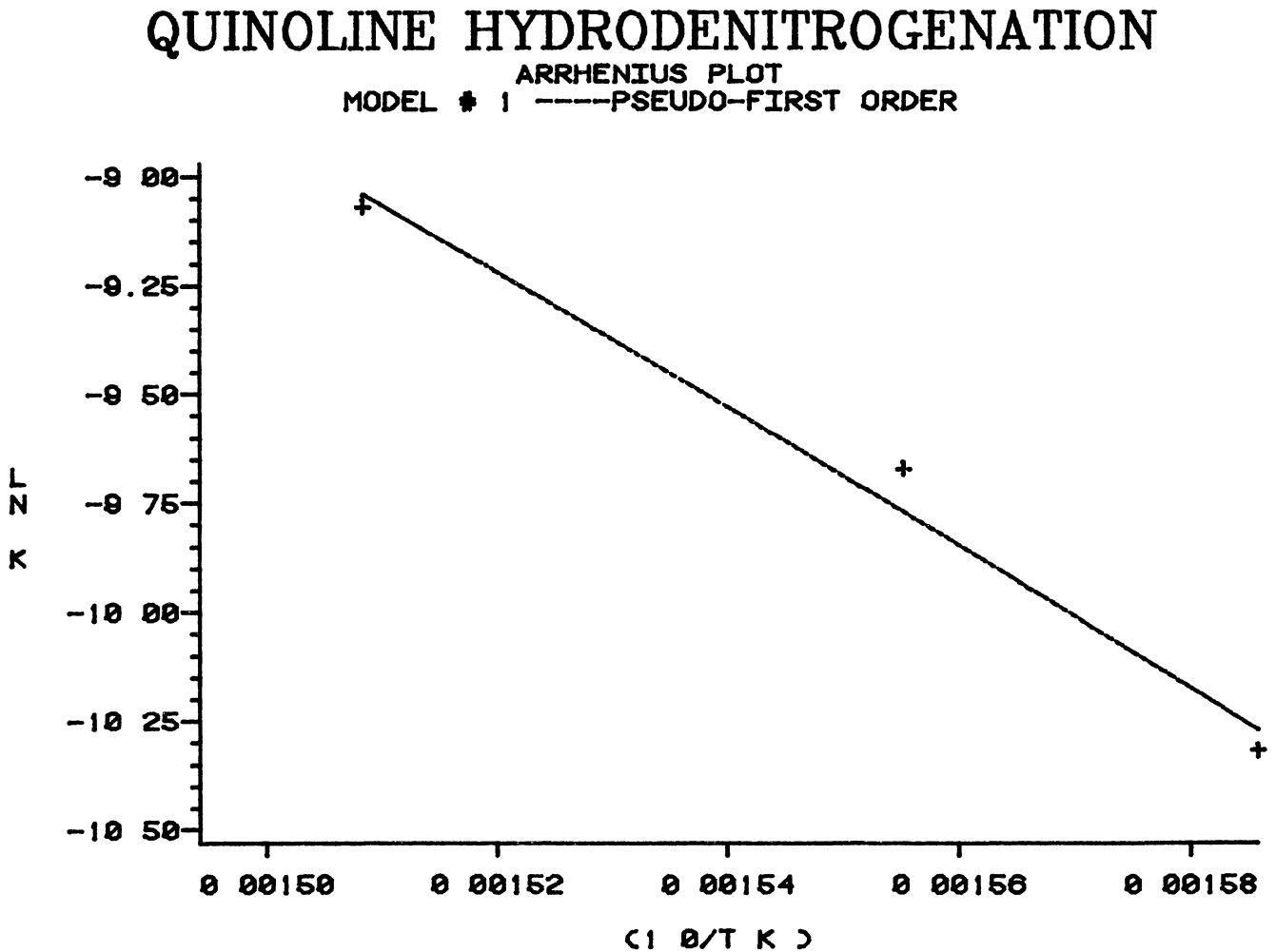

Figure 78 Temperature Dependency of Quinoline HDN Reaction Rate

factor, as calculated in Appendix D, is about 0.98, which indicates that the effect of pore diffusion may be neglected

Acridine HDN data, presented in Tables XIII, XIV, and XV, are fitted with this model to predict the total nitrogen removal. The results are presented in Table XXIII and plotted in Figure 79. The PRE varies between 5.8% and -10.7%, which indicates a better fit than quinoline data Values of ln(k) are plotted versus (1/T) in Figure 80 The activation energy predicted for acridine HDN is 26 1 kJ/mol (6.2 kcal/mol) which is very low compared to the single value reported in literature, 146 kJ/mol (35 kcal/mol) (67). Also, the rate constants predicted here are two orders of magnitude lower than that reported by Gates et. al. (67), (0.83 E-2 s^{-1}) at 342°C.

The HDN data of the quinoline-acridine mixture, presented in Tables XVI, XVII and XIX, were also fitted with this model to predict the total nitrogen removal. The results are presented in Table XXIV and plotted in Figure 81. The range of the PRE shows a poor fit in this case. Figure 82 shows the Arrhenius plot, which predicts an overall activation energy of 67.7 kJ/mol. This may be compared with the average of the activation energies of quinoline and acridine, 77 8 kJ/mol. The pseudo-first order rate constants predicted here are also approximately equal to the average values of the corresponding ones predicted for quinoline and acridine.

TABLE XXIII

MODEL # 1 - ACRIDINE HDN

k,s^{-1}	Temperature,°C	Time, minute	*Actual Concentration	*Predicted Concentration	Percentage Relative Error
3 3E-5	357	30	86.0	95.2	-10 7
		60	94.6	89.9	4.9
		90	84.8	84.9	-0 1
		120	81 6	80.2	1.8
		150	77.7	75.7	2.6
		180	69.6	71.5	-2.7
6 3E-5	370	30	43.3	45.8	-5 8
		60	38.9	40.9	-5.1
		90	39.8	36.5	8 3
		120	33.3	32 6	2.1
		150	29.6	29.1	1 7
		180	25.1	26.0	-3.6
4.1E-5	390	30	92.4	100 4	-8.6
		60	85 4	93.2	-9.1
		90	91 9	86.5	5.8
		120	85.3	80.3	5 8
		150	76.3	74.6	2.2
		180	67.1	69.3	-3.2

* g-mole/1.0E6 g n-hexadecane

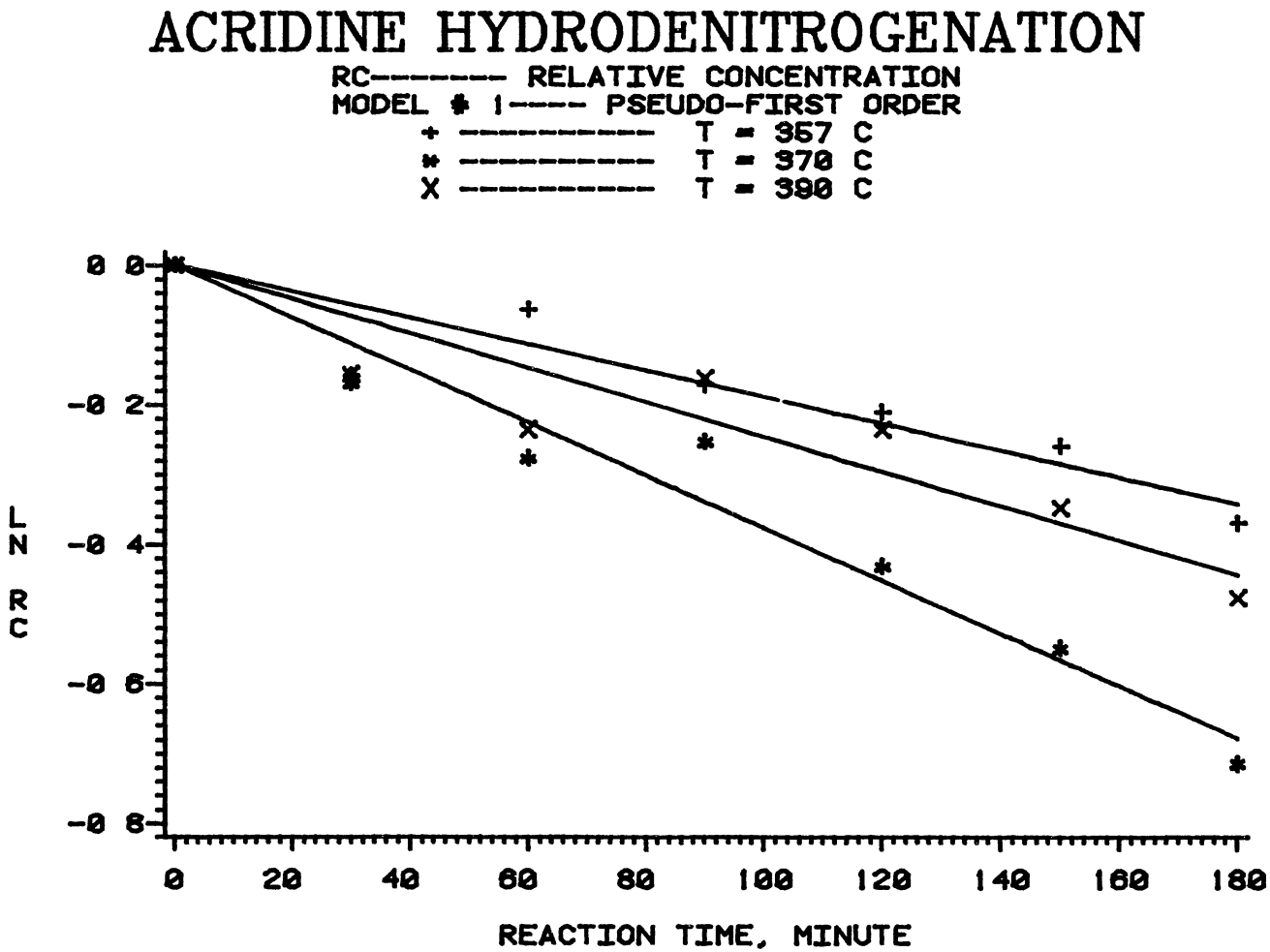

Figure 79. Acridine Hydrodenitrogenation - Model #1

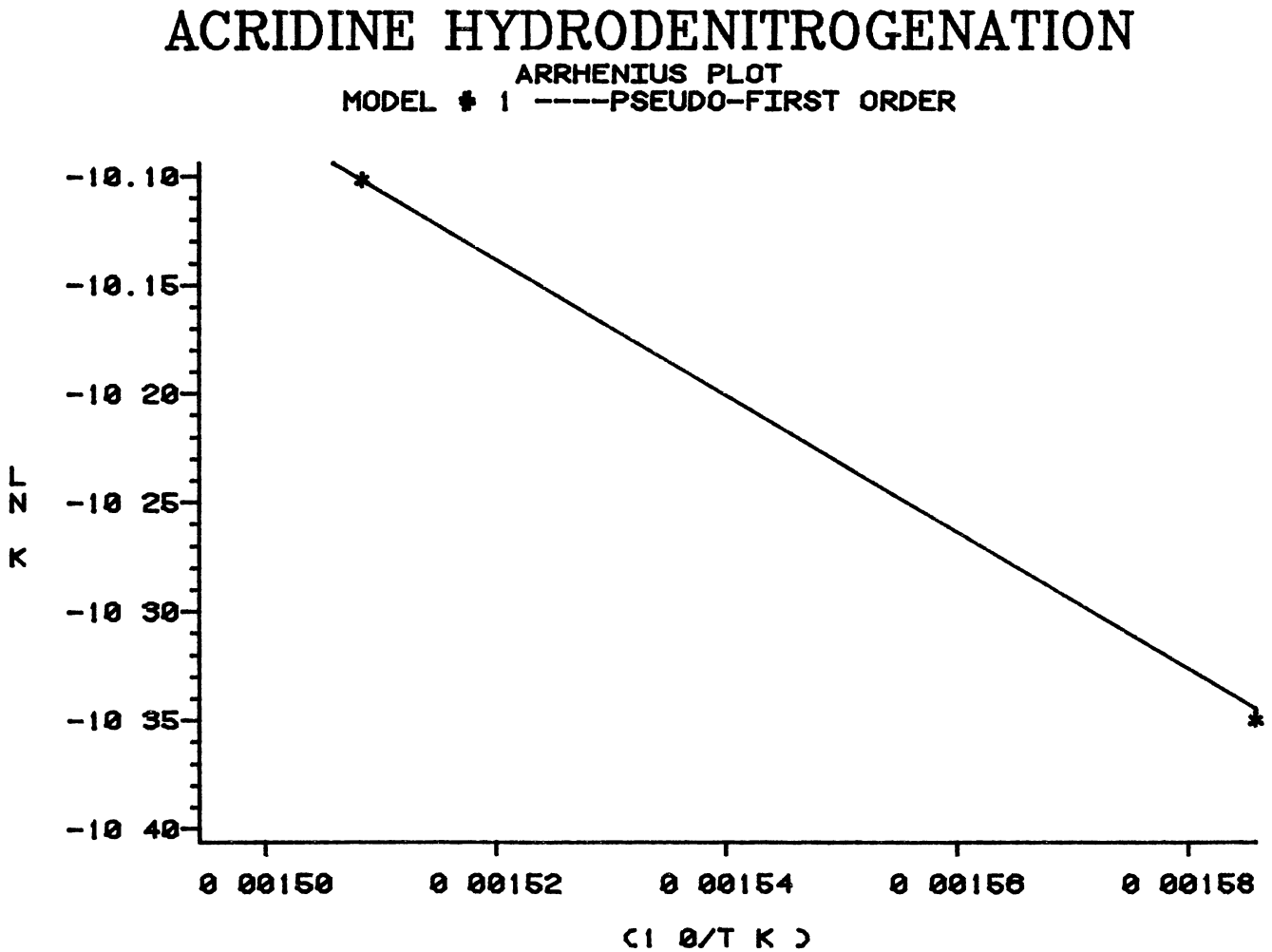

Figure 80. Temperature Dependency of Quinoline HDN Reaction Rate

TABLE XXIV

MODEL # 1 - QUINOLINE-ACRIDINE MIXTURE HDN

k,s^{-1}	Temperature, °C	Time, min.	*Actual Concentration	*Predicted concentration	PRE
4 3 E-5	357	0	474.2	474.2	---
		60	338.3	406.9	-20 3
		90	339.5	377 0	-11 0
		120	335.8	349.2	-4 0
		150	342.3	323 5	5.5
		180	352.3	299.6	14.9
6.2 E-5	370	0	482.1	482.1	----
		30	363 3	430.9	-18 6
		60	360.4	385 1	-6.8
		90	342.0	344.2	-0 6
		120	314.9	307.6	2.3
		150	278.0	274 9	1 1
		180	256 4	245.7	4.2

TABLE XXIV (continued)

k,s^{-1}	Temperature, °C	Time, min	*Actual Concentration	*Predicted concentration	PRE
8 3 E-5	390	0	474.2	474 2	
		30	297 6	408 1	-37 1
		60	282 8	351 2	-24 2
		95	265 7	294 7	-10 9
		120	258 6	260 1	-0 6
		150	257.8	223.8	13 2
		180	239.4	192.6	19 6

*g-mole/1 0E6 g n-hexadecane

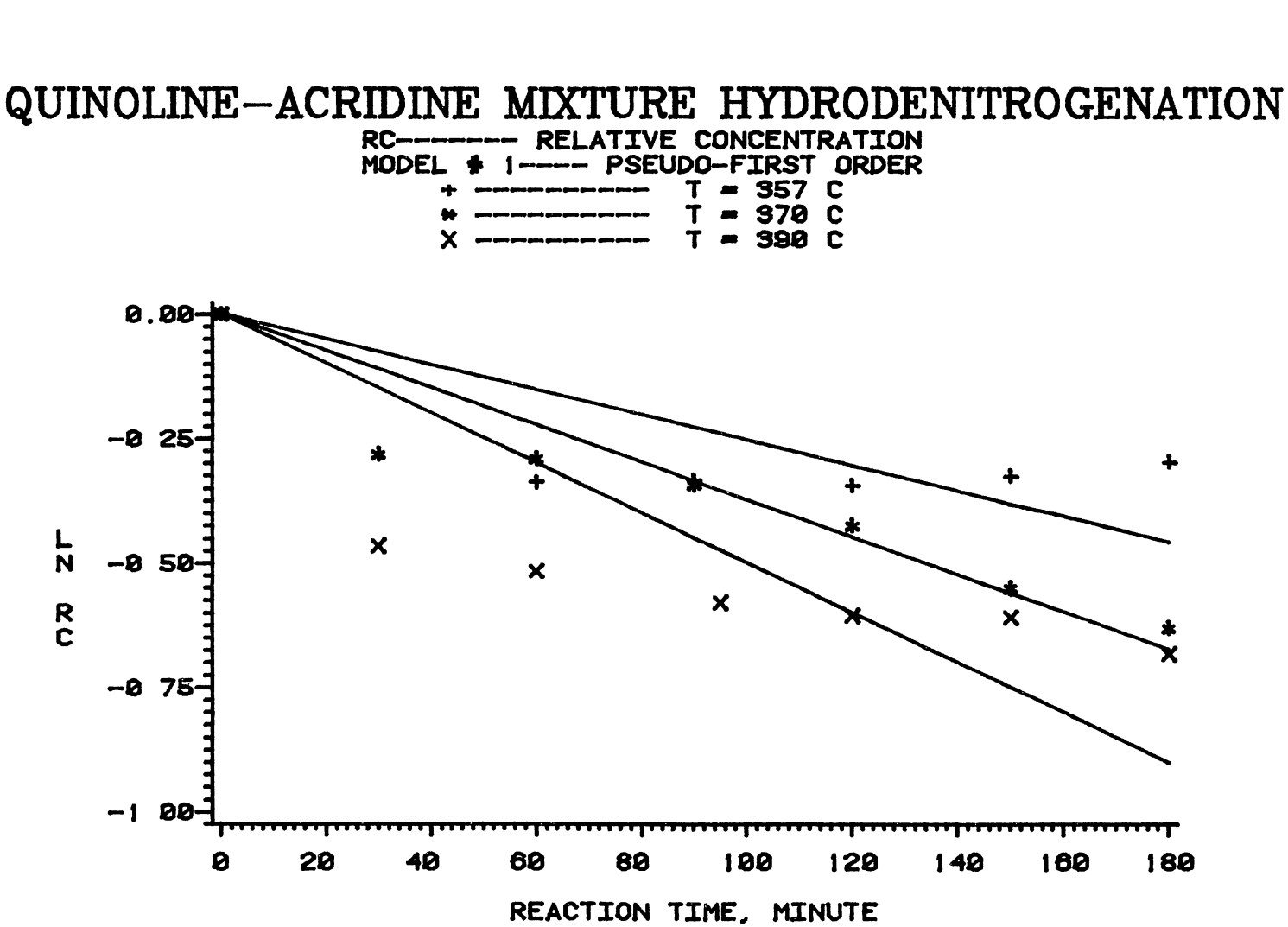

Figure 81 Quinoline-Acridine Mixture Hydrodenitrogenation - Model #1

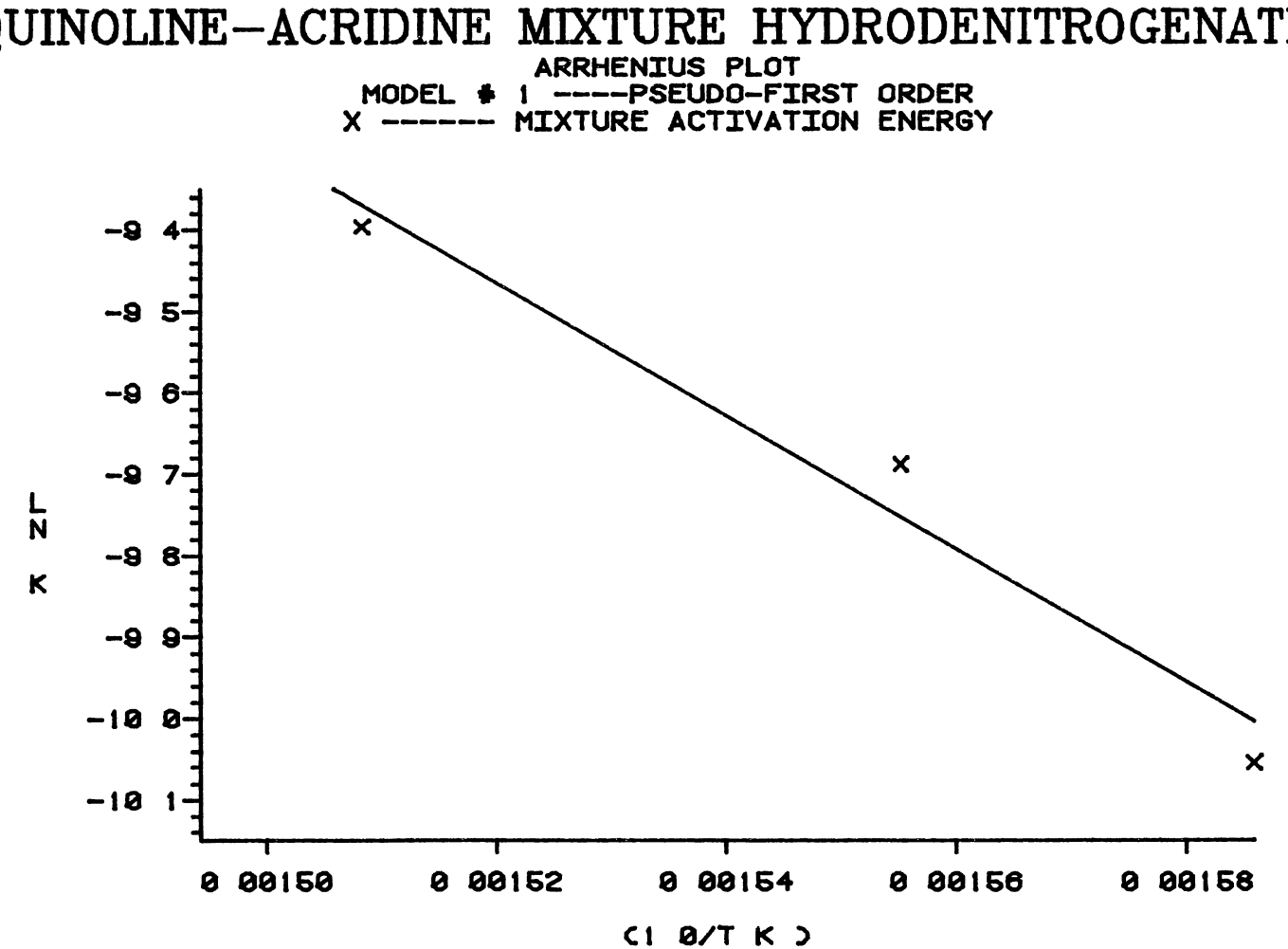

Figure 82. Temperature Dependency of Quinoline -Acridine Mixture HDN Reaction Rate

Model # 2

This model is represented as follows.

$$r_A = \frac{k_A K_A K_{H_2} [C_A C_{H_2} - C_D C_E / K]}{[1 + K_A C_{Ao} + K_E C_E]^2 [1 + \sqrt{K_{H_2} C_{H_2}}]^2} \qquad [39]$$

Marquardt's method was used to get the best estimation for the model parameters and Runge-Kutta method was used to numerically integrate the equation [39].

Quinoline HDN data, presented in Tables VIII, IX, and X, are fitted with this model. The results are presented in Tables XXV and XXVI and plotted in Figure 83. Table XXV shows that the PRE varies between -4.7 and 4.9 indicating an excellent fit From Table XXVI, it is apparent that both k_A and K increase with reaction temperature. The rate constants are utilized to prepare an Arrhenius plot in Figure 84 which gives an activation energy of 56.4 kJ/mol. Then the rate in s^{-1} can be predicted by the following equation when T is in K.

$$k = 0.76 \exp(-6{,}785/T) \qquad [100]$$

Acridine HDN results, presented in Tables XIII, XIV, and XV are also fitted by this model. The results are presented in Tables XXVII and XXVIII and plotted in Figure 85. The PRE varies between 7.1 and -10.5 as shown in Table XXX. This fit is not as good as the fit for quinoline and it is almost as good as model # 1 for acridine. The variations

TABLE XXV

MODEL # 2 - QUINOLINE HDN

Temperature, °C	Time, minute	*Actual Concentration	*Predicted Concentration	Percentage Relative Error
357	0	351	351	----
	30	312	297	4.9
	60	262	274	-4.7
	90	263	265	-0.7
	150	263	259	1.5
	180	259	258	0.3
	210	259	258	0 4
370	0	345	345	----
	30	251	256	-1.8
	60	235	234	0 6
	90	223	223	0 1
	120	217	216	0.6
	150	213	210	1.4
	180	202	204	-1 2
390	0	372	372	----
	30	248**	---	----
	60	243	252	-3 8

TABLE XXV (continued)

Temperature °C	Time, minute	*Actual Concentration	*Predicted Concentration	Percentage Relative Error
	90	216	209	3.4
	120	176	171	2.8
	150	132	136	-3.4
	180	103	102	0.8

* g-mole/1.0E6 g n-hexadecane

** not used in model fitting.

TABLE XXVI

PARAMETER OF MODEL # 2 FOR QUINOLINE HDN

Temperature, °C	357	370	390
k_A, s^{-1}	1.5E-5	2.2E-5	2.6E-5
K_A	3,311	1.165	1,275
K_{H_2}	3,035	4,361	4,816
K_E	75,177	1,931	44,510
K	0 0276	0 0390	0.1447

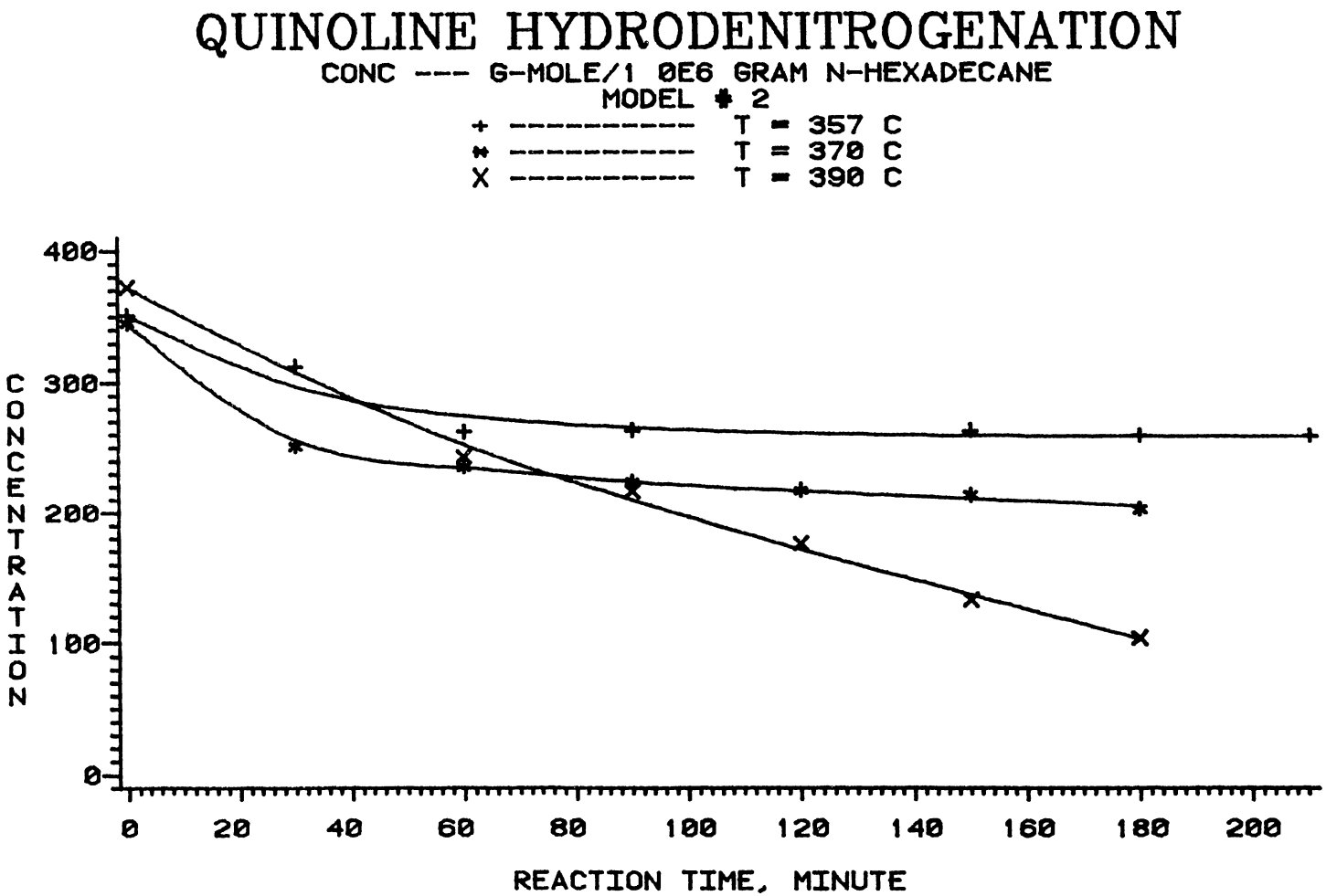

Figure 83 Quinoline Hydrogenation-Model # 2

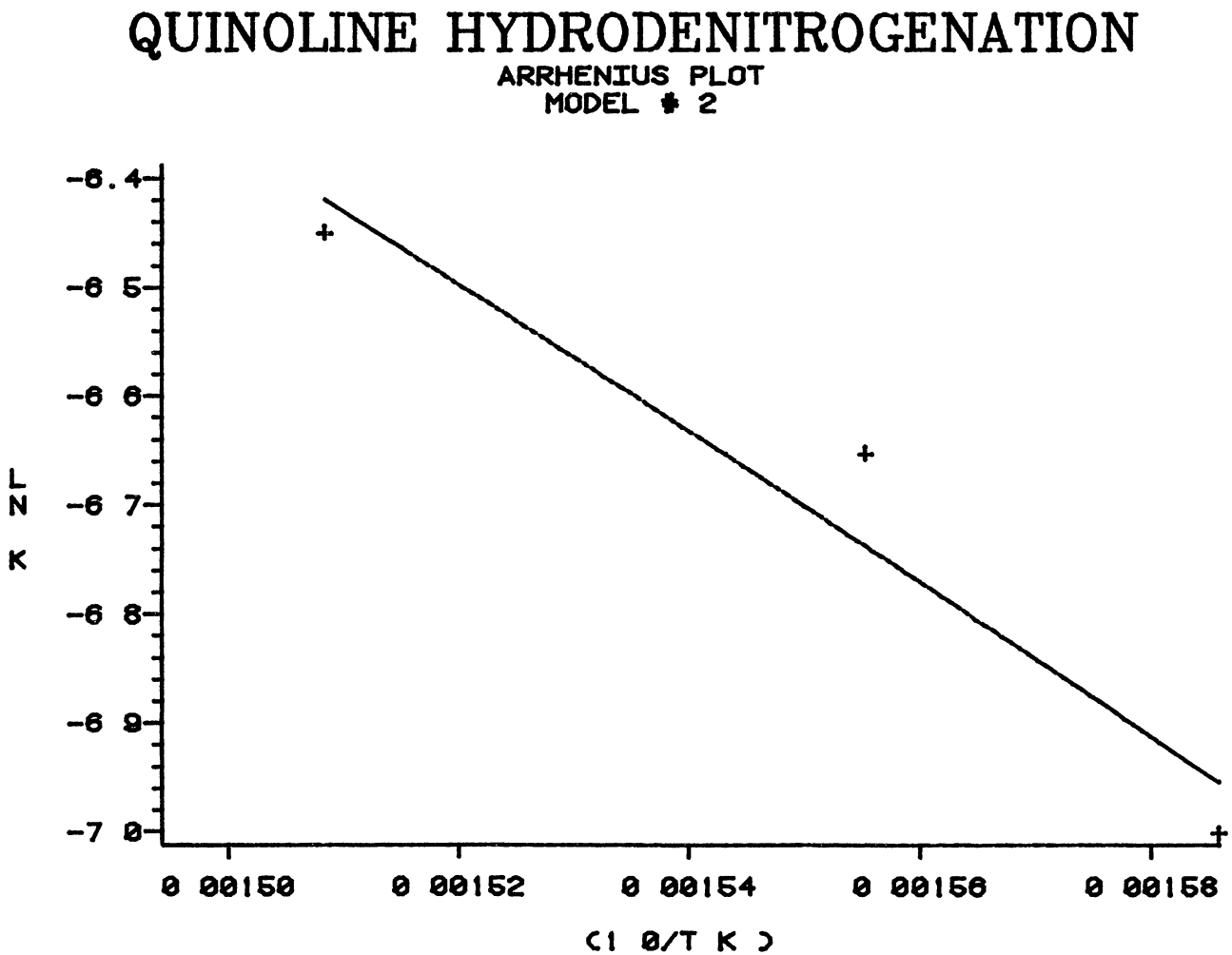

Figure 84. Temperature Dependency of Quinoline HDN Reaction Rate

TABLE XXVII

MODEL # 2 - ACRIDINE HDN

Temperature, °C	Time, minute	*Actual Concentration	*Predicted Concentration	Percentage Relative Error
357	0	100.8	100.8	----
	30	86.0	95.1	-10.5
	60	94.6	89.9	5.0
	90	84.8	85.0	-0.3
	120	81.6	80.4	1.5
	150	77.7	75.8	2.4
	180	69.6	71.1	-2.2
370	0	51.3	51 3	----
	30	43.3	46.1	-6.4
	60	38.9	41.3	-6.3
	90	39 8	37.0	7.1
	120	33.3	33.0	1.0
	150	29.6	29.2	1.4
	180	25.1	25.6	-1.9
390	0	108.1	108.1	----
	30	92.4	98.5	-6.6
	60	85 4	91.4	-7.0
	90	91.9	85.5	6 9

TABLE XXVII (continued)

Temperature, °C	Time, minute	*Actual Concentration	*Predicted Concentration	Percentage Relative Error
	120	85.3	80 3	5.9
	150	76.3	75.1	1.5
	180	67.1	69.7	-3.9

*g-mole/1.0E6 g n-hexadecane.

TABLE XXVIII

PARAMETERS OF MODEL # 2 FOR ACRIDINE HDN

Temperature, °C	357	370	390
k_A, s^{-1}	2.2 E-5	2.4 E-5	2.7 E-5
K_A	1,846	1,756	1,429
K_{H_2}	4,431	5,662	5,317
K_E	46,826	64,448	15,146
K	0.1227	0.4475	0.1419

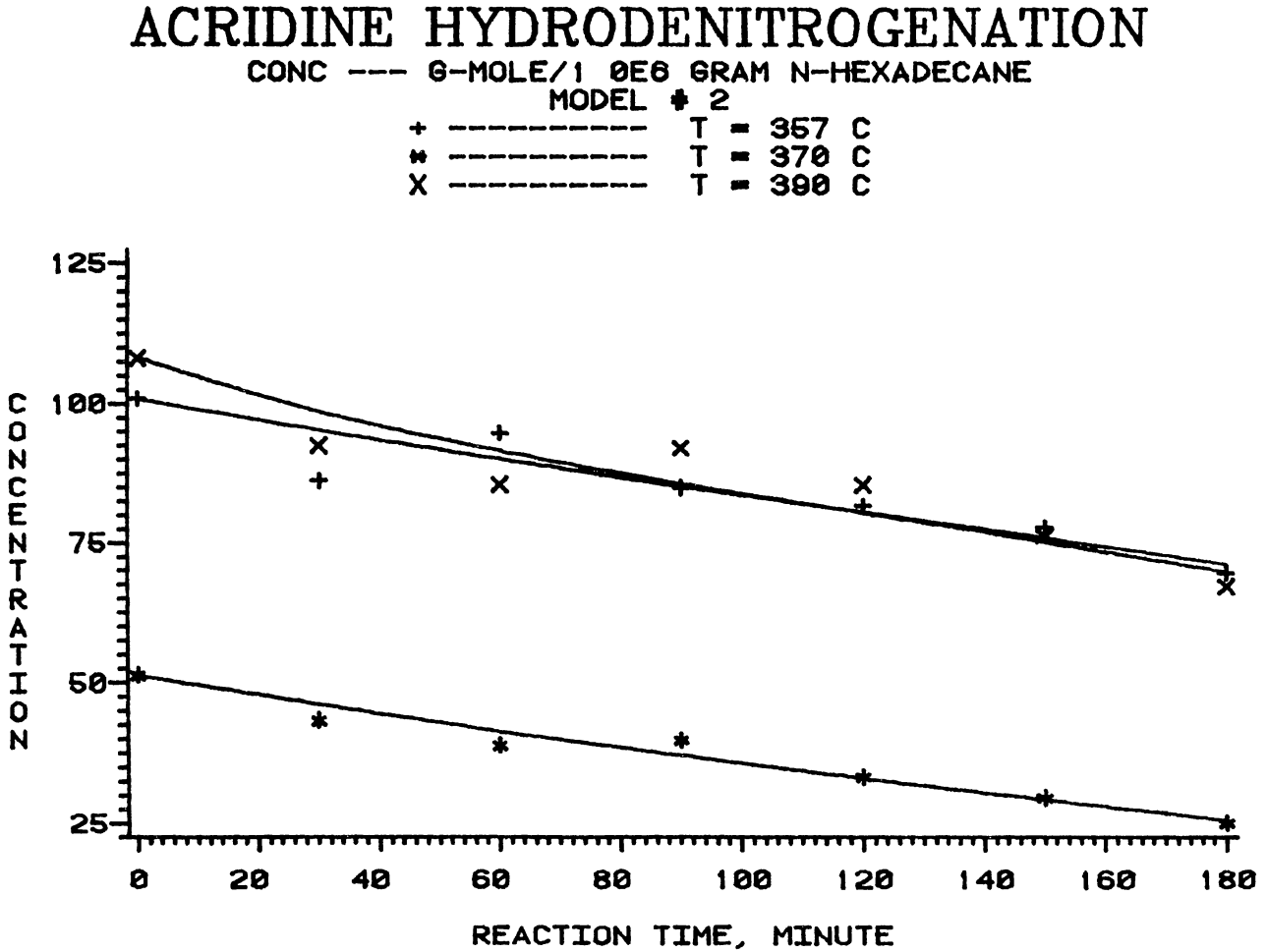

Figure 85 Acridine Hydrodenitrogenation-Model # 2

of both k_A and K are small with temperature as shown in Table XXVIII. The values of K_A result in an activation energy of 21.6 kJ/mol.

The quinoline-acridine mixture HDN data, listed in Tables XVI, XVII and XIX, were fitted here to predict the total nitrogen removal. The results are listed in Tables XXIX and XXX. With the exception of a single data point, having a PRE of -12 6, the PRE values vary between -6 9 and 5 8, indicating a satisfactory fit These results are plotted in Figure 86 The rate constants, presented in Table XXX show a clear rate increase with temperature. These values result in an activation energy of 78 7 kJ/mol. This value is approximately equal to the sum of the activation energies predicted for quinoline and acridine

Model # 3

Model #3 is represented as follows

$$r_A = \frac{k_A[K_A C_A (K_{H_2} C_{H_2})^{0.5} - K(C_{Ao} - C_A)]}{[1 + K_A C_{Ao} + K_E (C_{Ao} - C_A)][1 + \sqrt{K_{H_2} C_{H_2}}]} \quad [59]$$

This model was used to predict the quinoline HDN The results are presented in Tables XXXI and XXXII. The PRE's are generally similar to those of the model #2, the variations of the kinetic parameters with temperature are erratic Therefore, Model #3 was considered unacceptible and no further work was done with this model

TABLE XXIX

MODEL # 2 - QUINOLINE-ACRIDINE MIXTURE HDN

Temperature, °C	Time, minute	*Actual Concentration	*Predicted Concentration	Percentage Relative Error
357	0	474.2	474.2	----
	60	338.3	341.4	-0.9
	90	339.5	341.4	-0.6
	120	335.8	341.4	-1.7
	150	342.2	341.4	0.2
	180	352.3	341.4	3.1
370	0	482 1	482.1	----
	30	363.3	409.2	-12.6
	60	360.4	358.1	0.6
	90	342.0	322.3	5.8
	120	314.9	297.1	5.7
	150	278.0	279.5	-0.5
	180	256.4	267.3	-4.3

TABLE XXIX (Continued)

Temperature, °C	Time, minute	*Actual Concentration	*Predicted Concentration	Percentage Relative Error
390	0	474.2	474.2	----
	30	297.6	306.8	-3.1
	60	282 8	267 1	5.5
	95	265 7	257 8	3.0
	120	258.6	256.4	0.9
	150	257.8	255.9	0.7
	180	239.4	255.8	-6.9

*g-mole/1.0E6 g n-hexdecane.

TABLE XXX

PARAMETERS OF MODEL # 2 FOR QUINOLINE-ACRIDINE MIXTURE

Temperature, °C	357	370	390
k_A, s^{-1}	3 6E-5	5 4L-5	7.7E-5
K_A	435	888	998
K_{H_2}	5,010	6,847	2,399
K_E	24,568	23,249	11,985
K	0 3	1 4	3 6

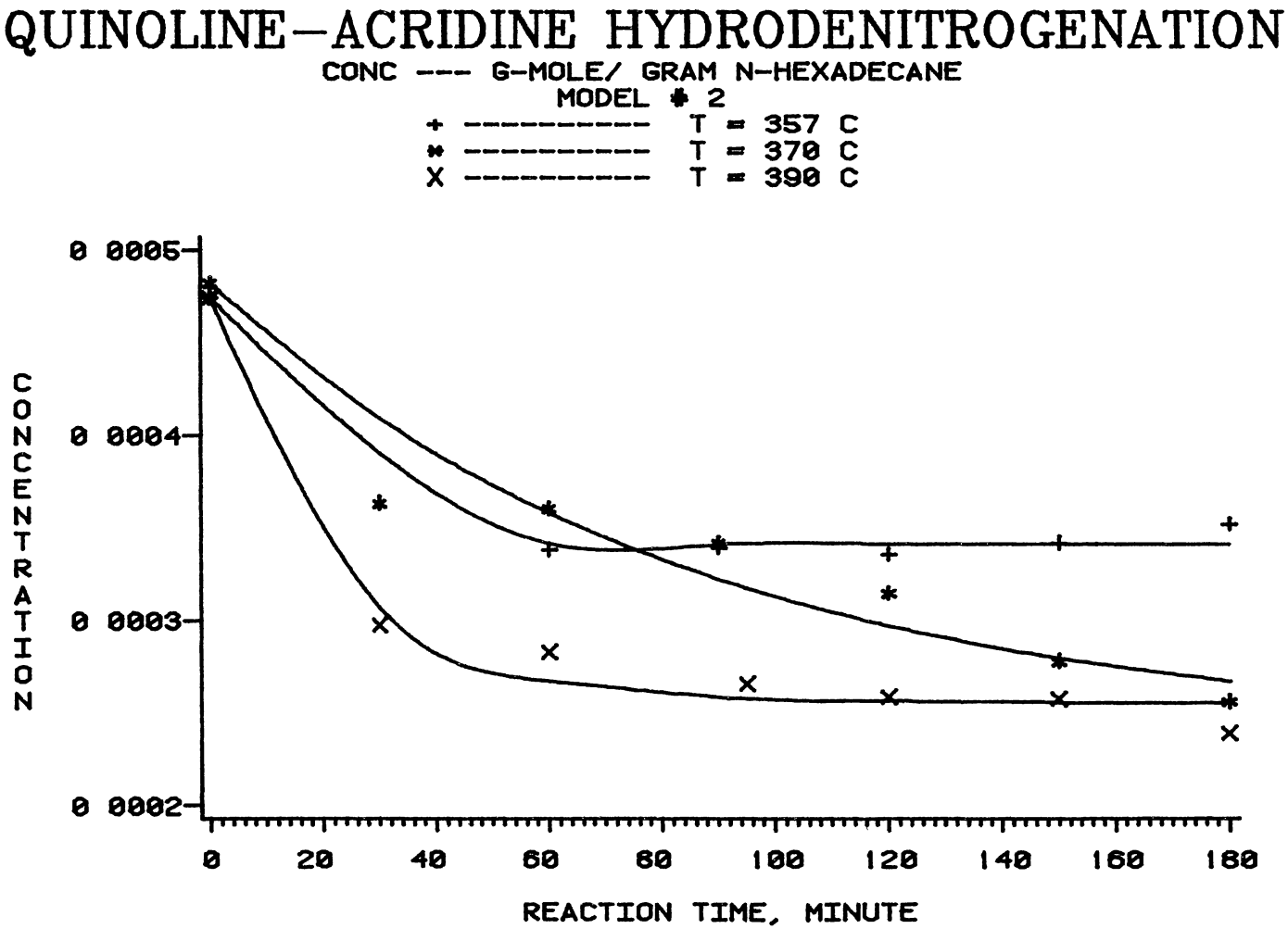

Figure 86 Quinoline-Acridine Mixture Hydrodenitrogenation - Model #2

TABLE XXXI

MODEL # 3 - QUINOLINE HDN

Temperature, °C	Time, minute	*Actual Concentration	*Predicted Concentration	Percentage Relative Error
357	0	351	351	----
	30	312	297	4 8
	60	262	274	-4.7
	90	263	265	-0.7
	150	263	259	1.5
	180	259	258	0.3
	210	259	258	0.4
370	0	345	345	----
	30	251	260	-3.4
	60	235	229	2.7
	90	223	217	2.5
	120	217	213	1.7
	150	213	212	0.6
	180	202	211	-4.5
390	0	372	372	----
	30	248**	----	----
	60	243	257	-5 8
	90	216	210	2 6

TABLE XXXI (Continued)

Temperature, °C	Time, minute	*Actual Concentration	*Predicted Concentration	Percentage Relative Error
	120	176	170	3.6
	150	132	134	-1.6
	180	103	103	-0.2

* g-mole/1.0E6 g n-hexdecane.

** not used in model fitting.

TABLE XXXII

PARAMETERS OF MODEL # 3 FOR QUINOLINE HDN

Temperature, °C	357	370	390
k_A, s^{-1}	2.3E-5	2 5E-5	2.0E-5
K_A	2,191	1,405	1,322
K_{H_2}	5,309	15,430	5,365
K_E	146,933	78,377	576,523
K	0.1E-7	0.1E-6	0.1E-6

Model # 4

This model which consists of ten differential equations with 22 parameters was used to predict the quinoline HDN. Parameters were estimated by Marquardt's method combined with Runge-Kutta integration technique. The results are plotted in Figures 87-98 and the estimated parameters are listed in Table XXXIII OMA concentration profiles predicted by the model are far from actual values as can be seen in Figure 98 This, in fact, resulted from the model assumption that OMA is a final product However, OMA is expected to react further to generate hydrocarbons and ammonia. The concentration of the first sample was used as the starting point for the estimation process. It can be seen from the tables that the percentage relative error (PRE) is less than 7.6% for 91 2% of the points at 357°C and 370°C, and less than 14% for 81.5% of the points at 390°C. This indicates an adequate fit. Some of the parameters do not show consistent behavior with temperature. This was also observed by previous workers (49).

Model # 5

This model is a modified form of the model #4. Some of the reversible reactions in the previous model are considdered to be irreversible. This model is solved in the same manner as model # 4 and fitted for quinoline HDN. The results are presented in Figures 99-110, and the parameters

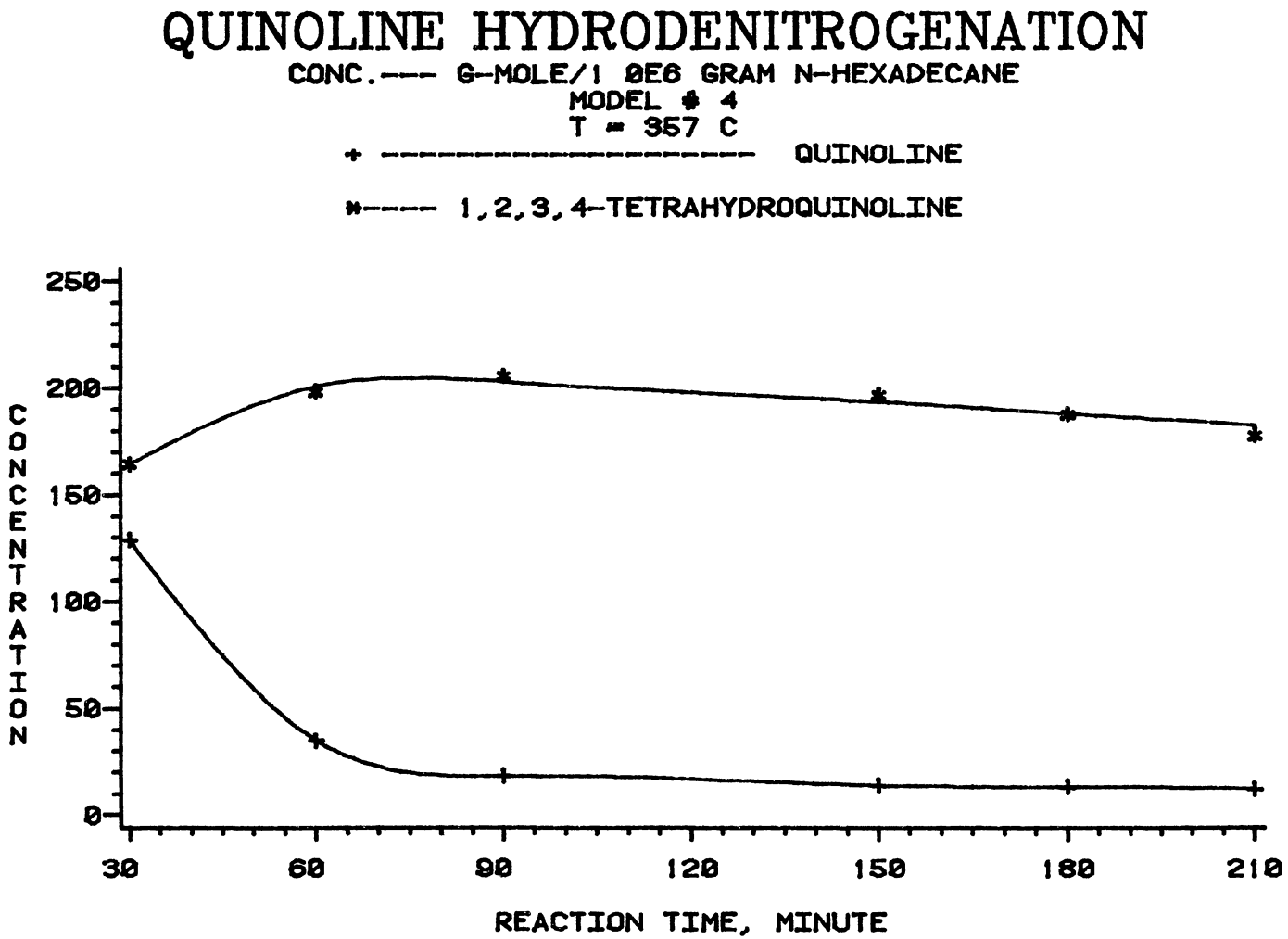

Figure 87 Quinoline HDN Products at 357°C - Model #4

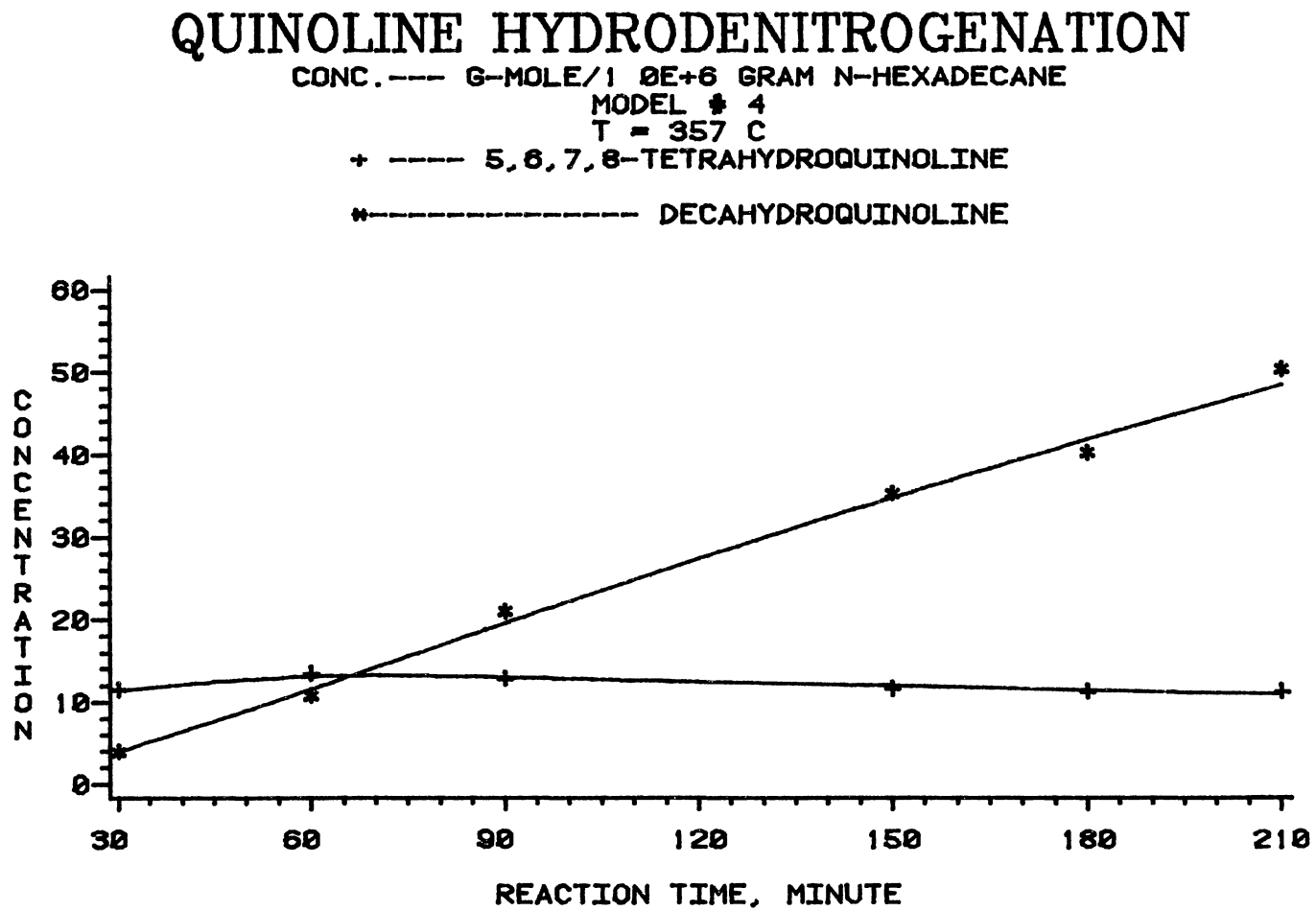

Figure 88. Quinoline HDN Products at 357°C - Model #4

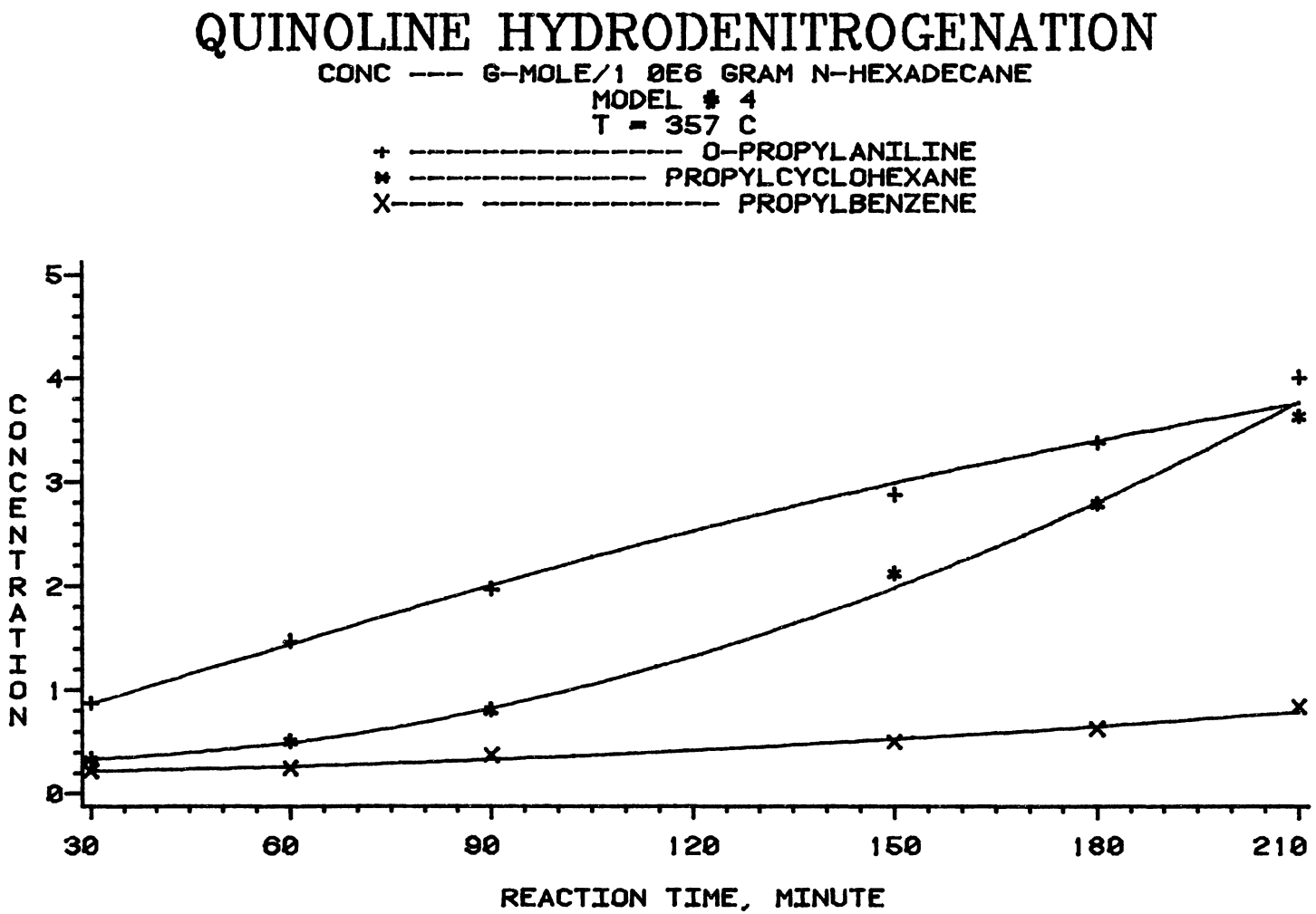

Figure 89 Quinoline HDN Products at 357°C - Model #4

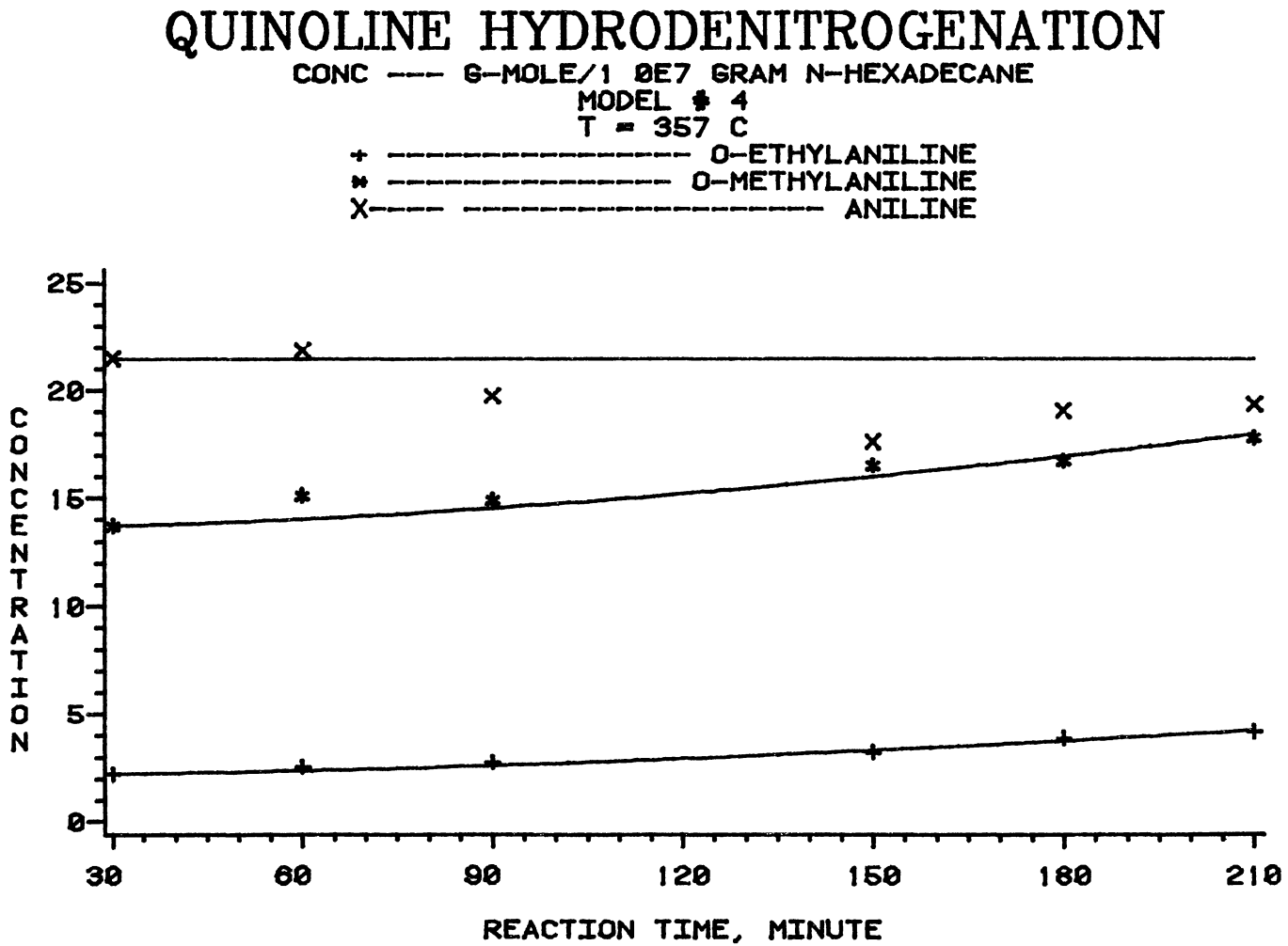

Figure 90. Quinoline HDN Products at 357°C - Model #4

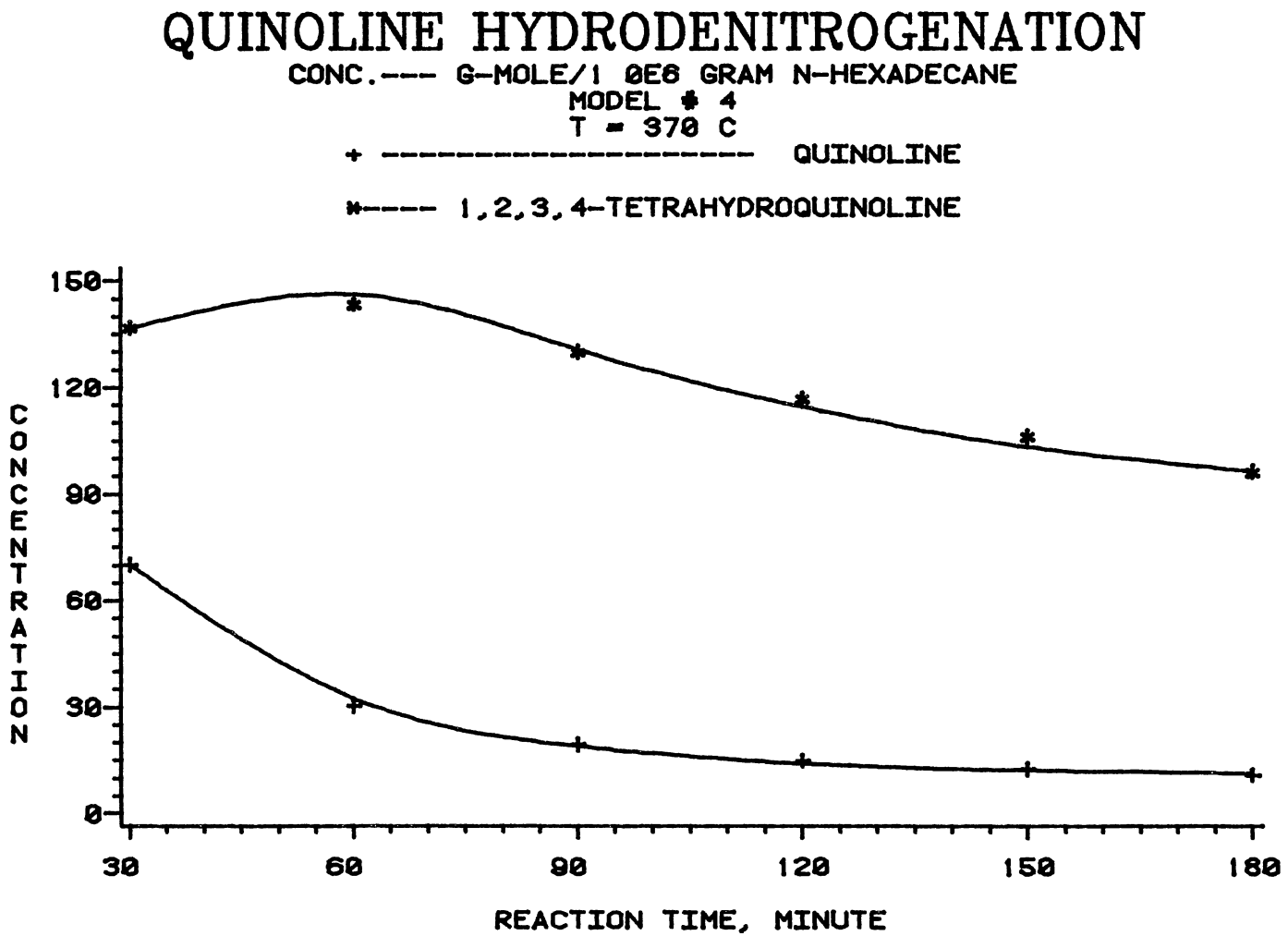

Figure 91. Quinoline HDN Products at 370°C - Model #4

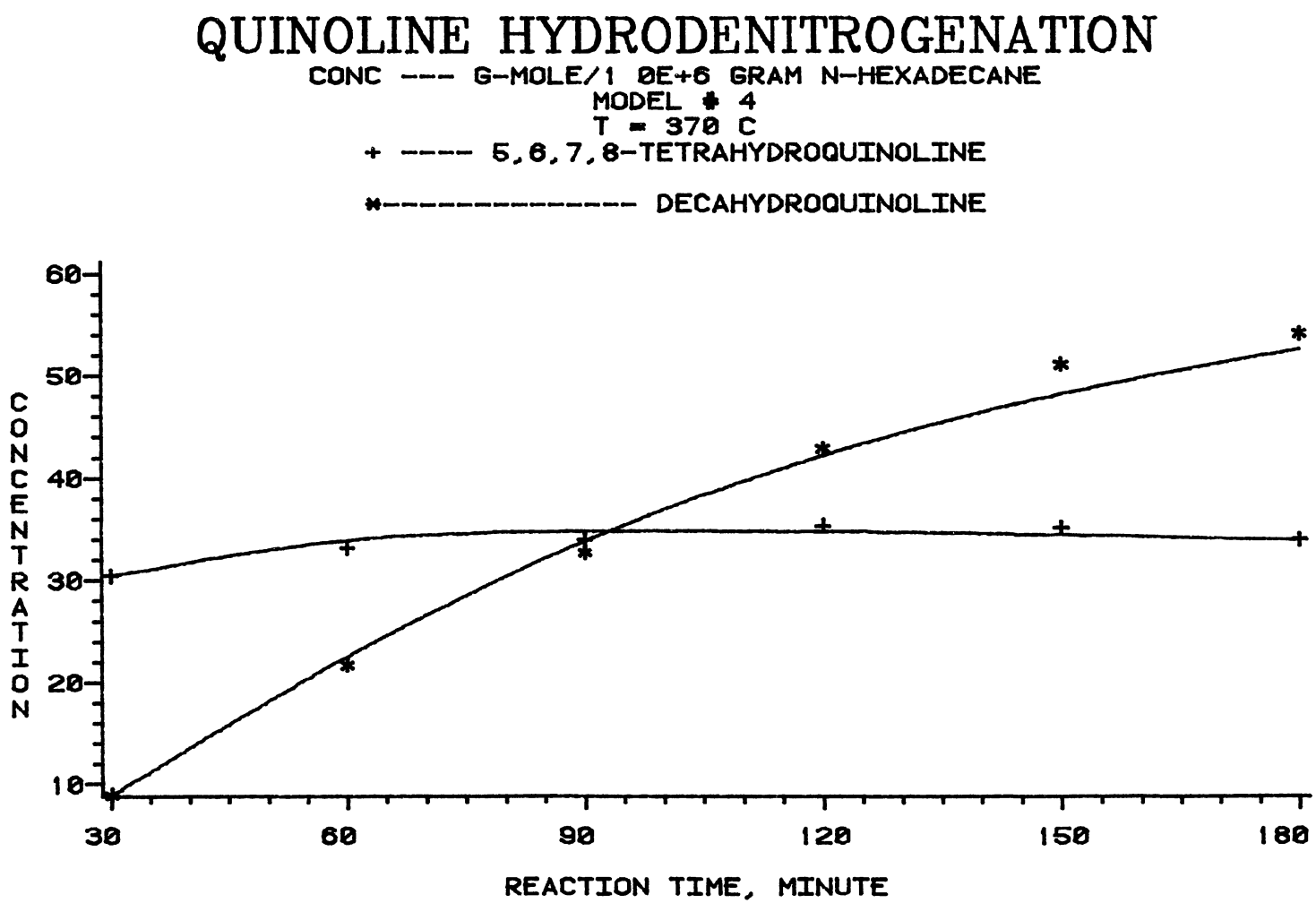

Figure 92 Quinoline HDN Products at 370°C - Model #4

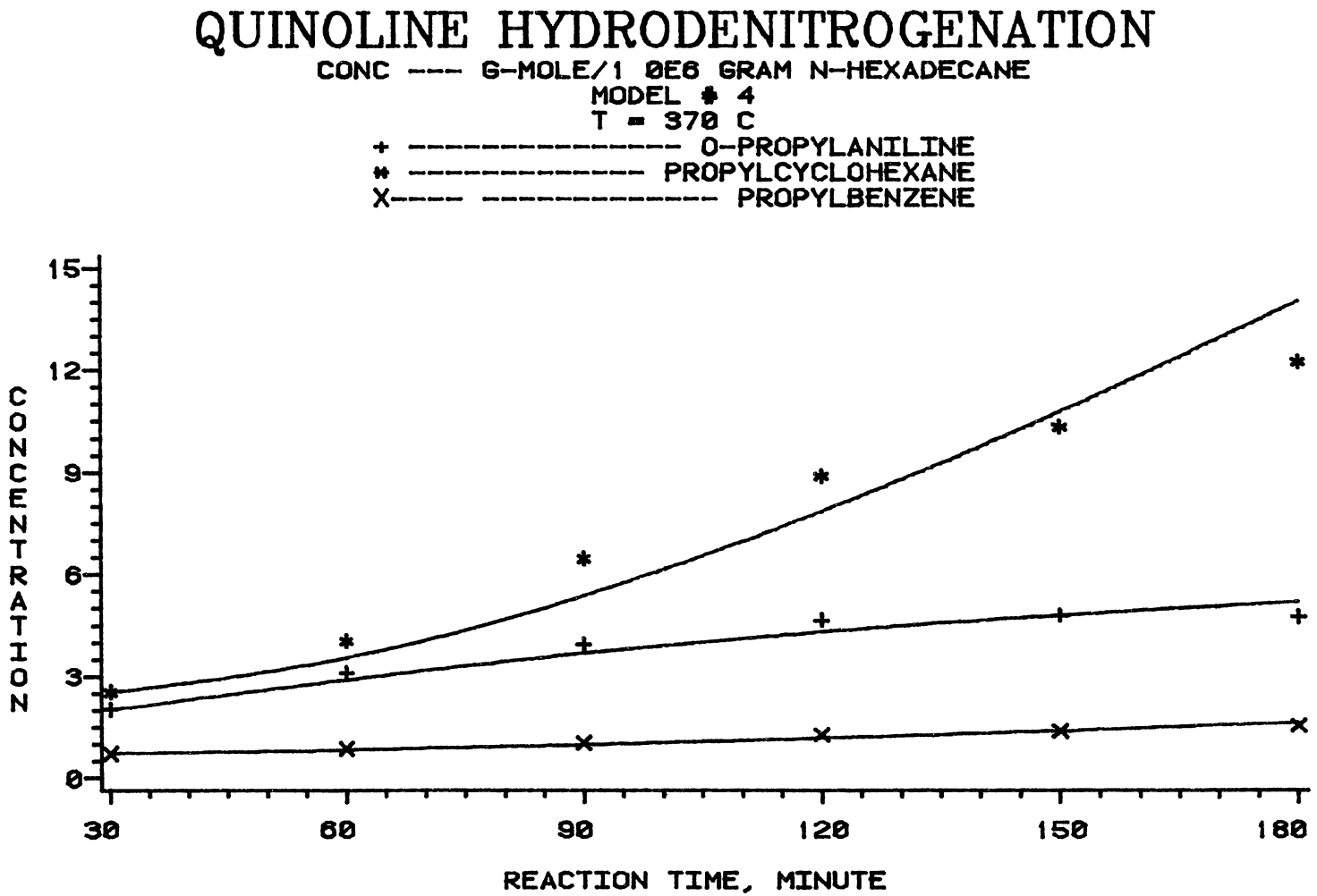

Figure 93 Quinoline HDN Products at 370°C - Model #4

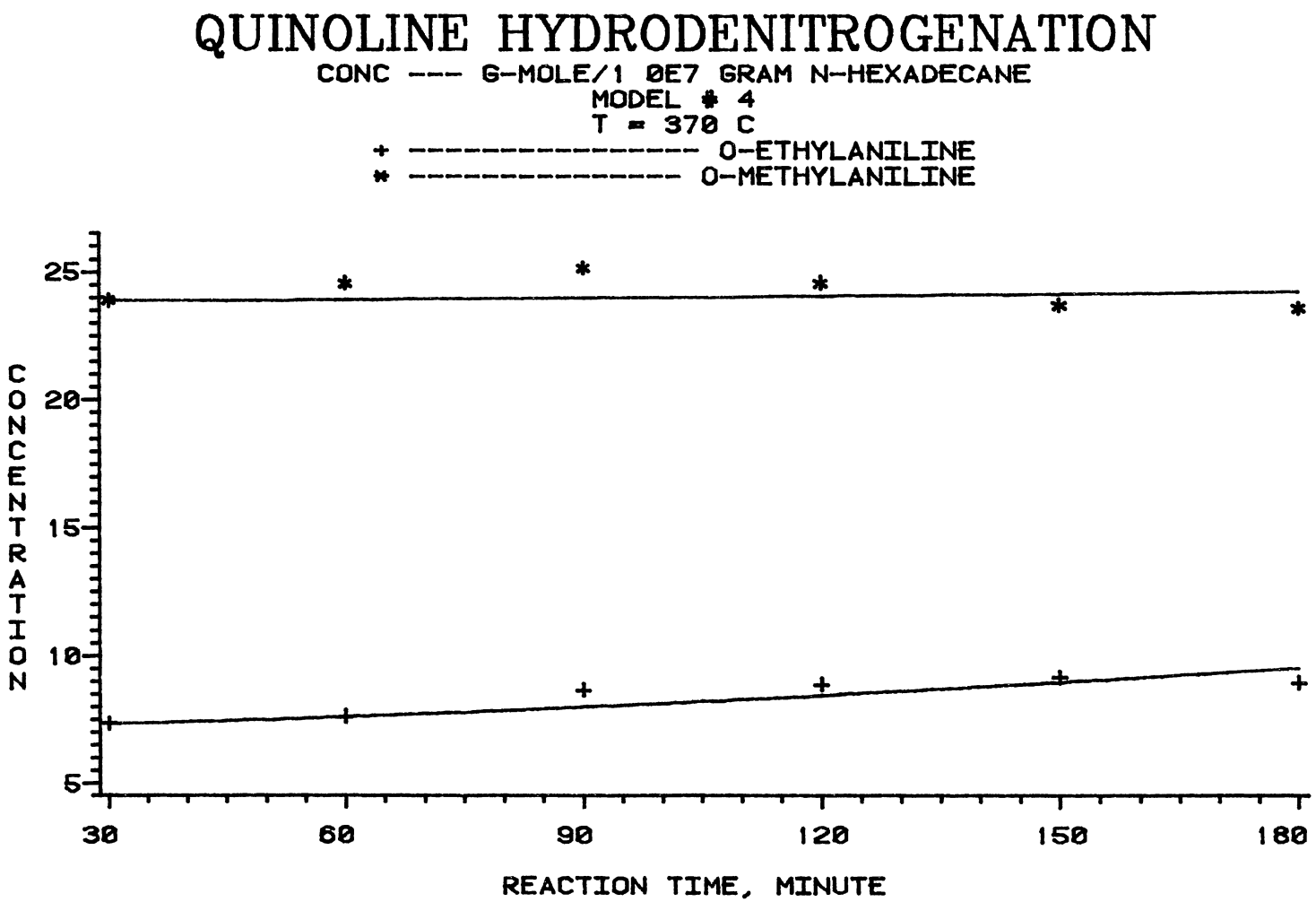

Figure 94. Quinoline HDN Products at 370°C - Model #4

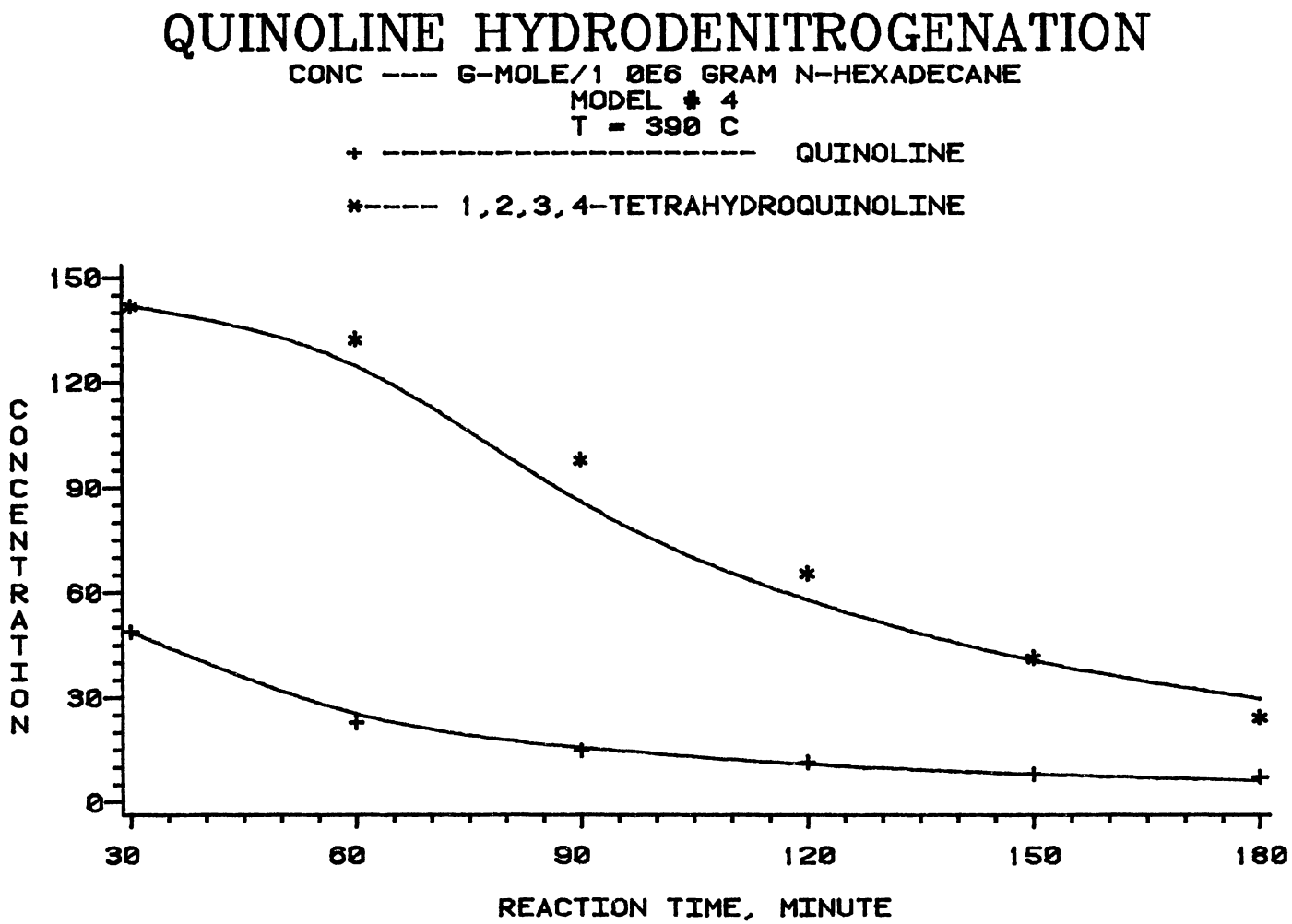

Figure 95. Quinoline HDN Products at 390°C - Model #4

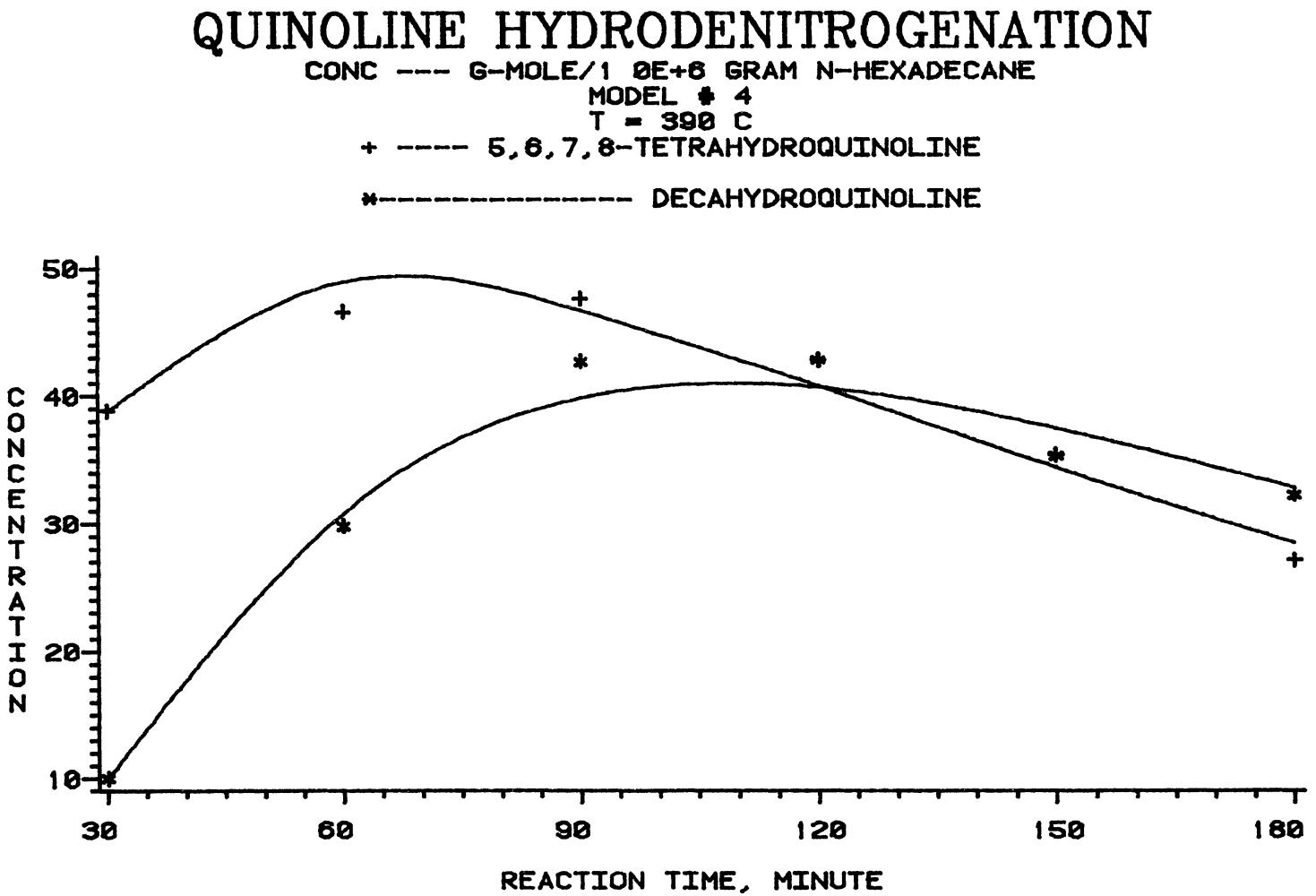

Figure 96. Quinoline HDN Products at 390°C - Model #4

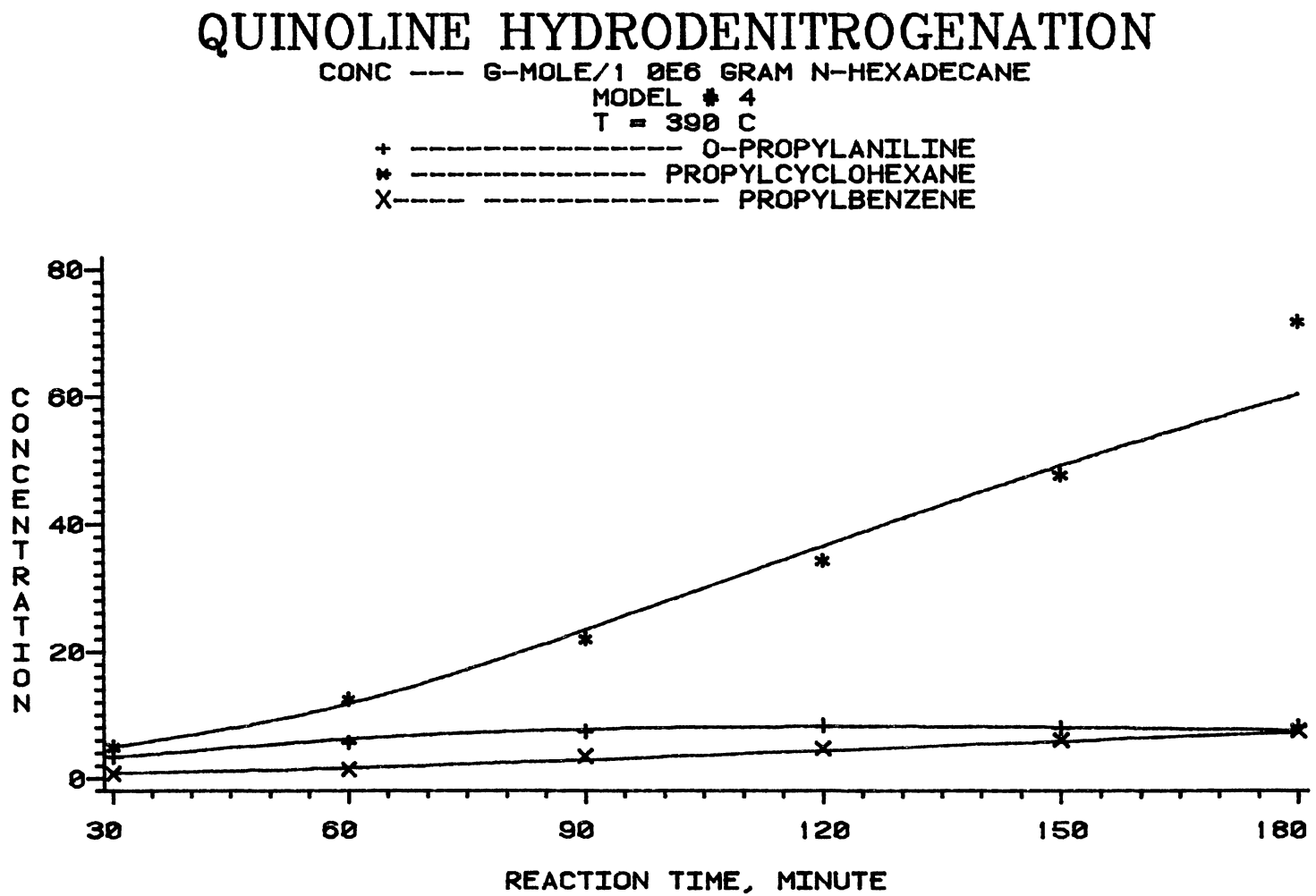

Figure 97. Quinoline HDN Products at 390°C - Model #4

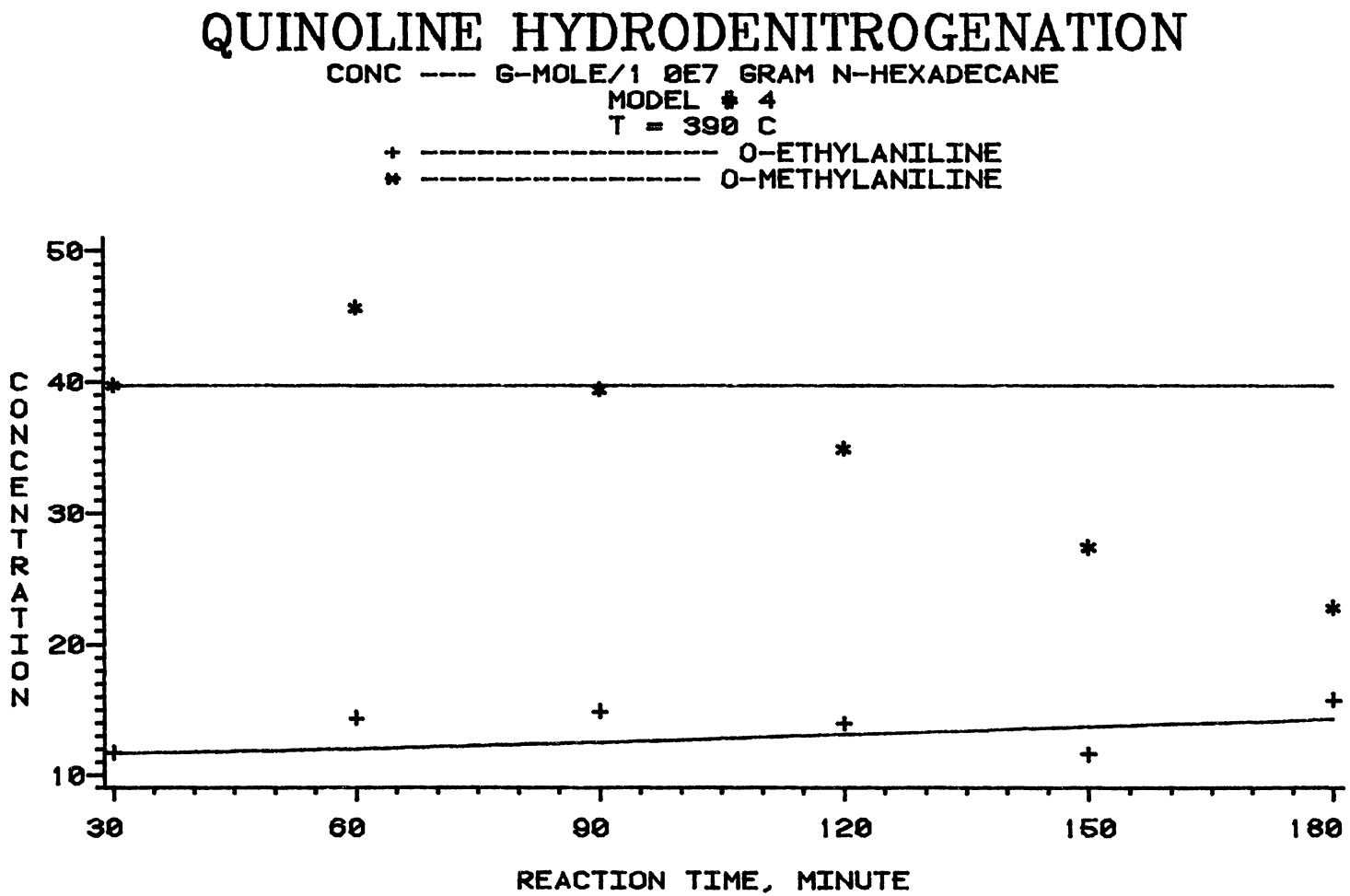

Figure 98 Quinoline HDN Products at 390°C - Model #4

TABLE XXXIII

PARAMETERS OF MODEL # 4 FOR QUINOLINE HDN

Temperature	357°C	370°C	390°C
a_{12}	0.511 E-1	0.209 E-1	0.295 E-1
a_{13}	0.626 E-2	0.125 E-1	0.235 E-2
a_{21}	0.258 E-2	0 110 E-1	0.177 E-1
a_{24}	0.100 E-6	0.385 E-2	0.182 E-1
a_{25}	0.118 E-3	0.237 E-3	0.920 E-3
a_{31}	0.307 E-2	0.168 E-2	0 191 E-2
a_{34}	0.100 E-15	0.100 E-10	0.100 E-1
a_{42}	0.692 E-4	0.189 E-2	0.263 E-3
a_{43}	0.100 E-13	0 100 E-20	0.100 E-15
a_{46}	0.710 E-3	0.215 E-2	0.107 E-1
a_{57}	0.130 E-2	0.159 E-2	0.602 E-2
a_{58}	0.466 E-3	0.382 E-3	0.243 E-3
a_{59}	0.976 E-3	0.648 E-4	0.100 E-8
a_{510}	0.100 E-12	-----	-----
K_{12}	0.100 E+15	0.100 E+20	0.261 E+2
K_{13}	0.995 E-1	0.119 E+1	0.596 E+0
K_{21}	0.102 E+0	0.230 E+0	0.137 E+0
K_{24}	0.100 E+10	0.271 E+0	0.100 E+13
K_{31}	0.221 E+1	0.470 E+0	0.758 E-1
K_{34}	0.100 E+5	0.100 E+12	0.100 E+12
K_{42}	0.500 E-1	0.532 E+0	0.394 E-1
K_{43}	0.100 E+8	0.100 E+3	0.100 E+3

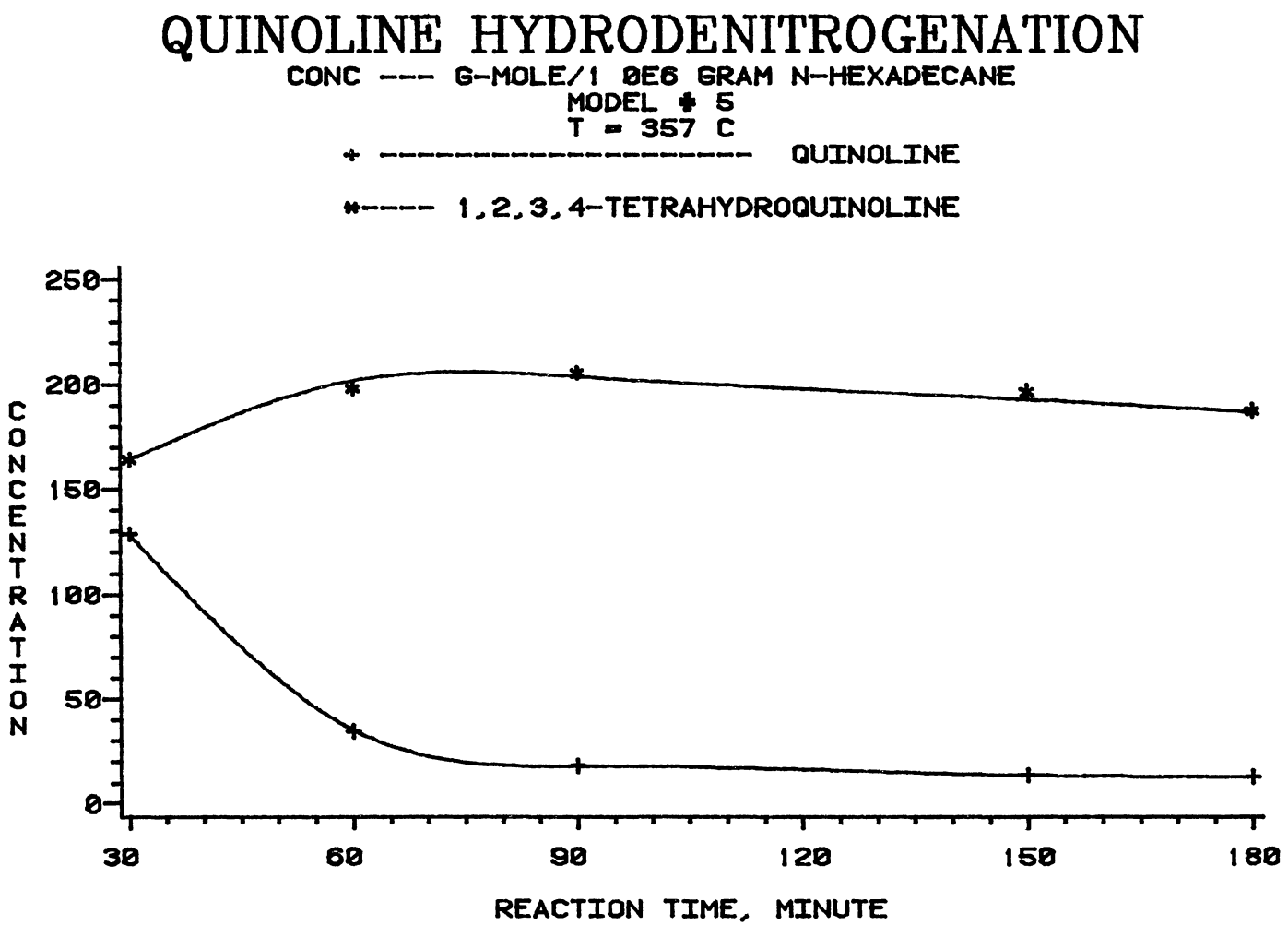

Figure 99. Quinoline HDN Products at 357°C - Model #5

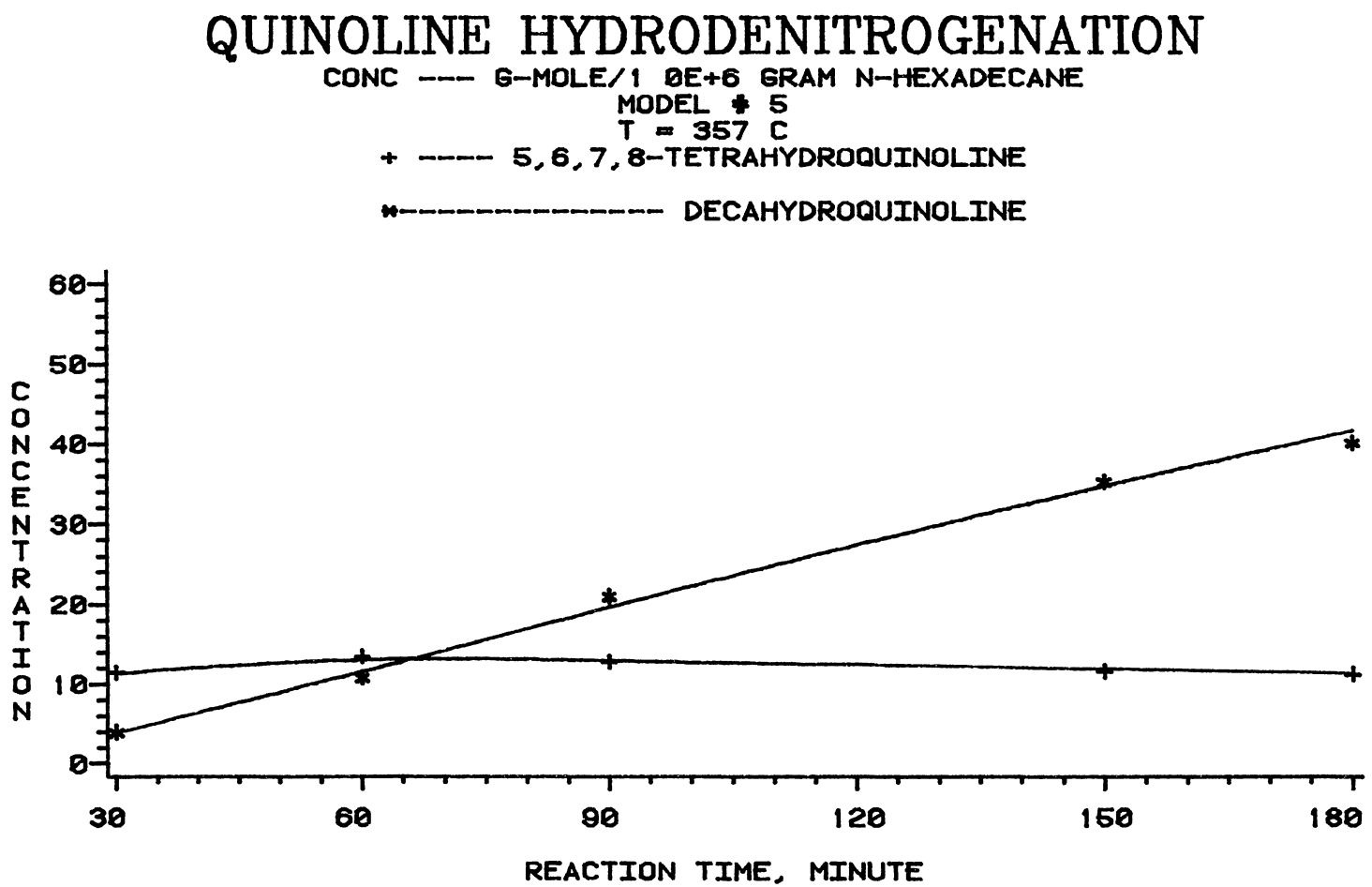

Figure 100. Quinoline HDN Products at 357°C - Model #5

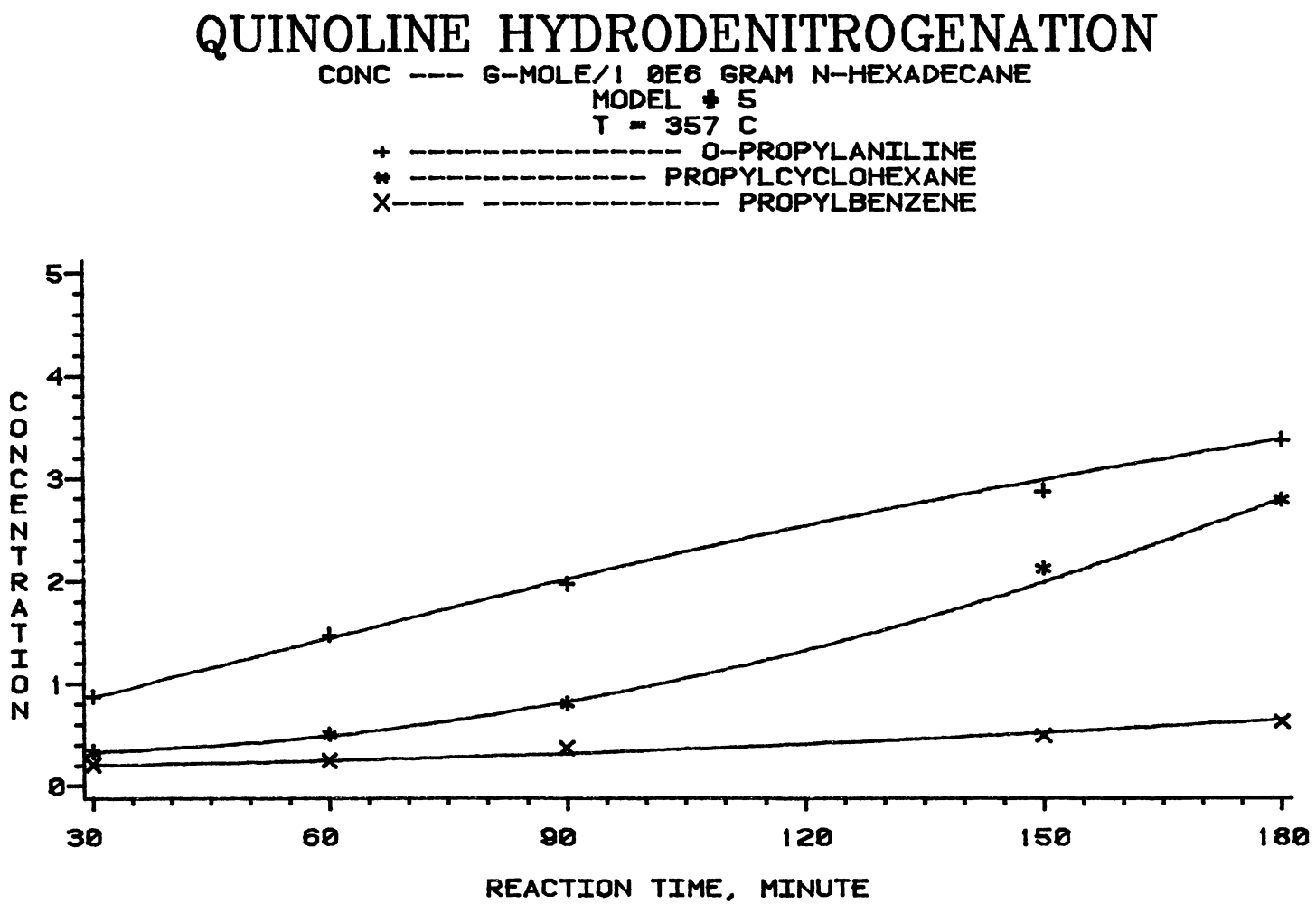

Figure 101. Quinoline HDN Products at 357°C - Model #5

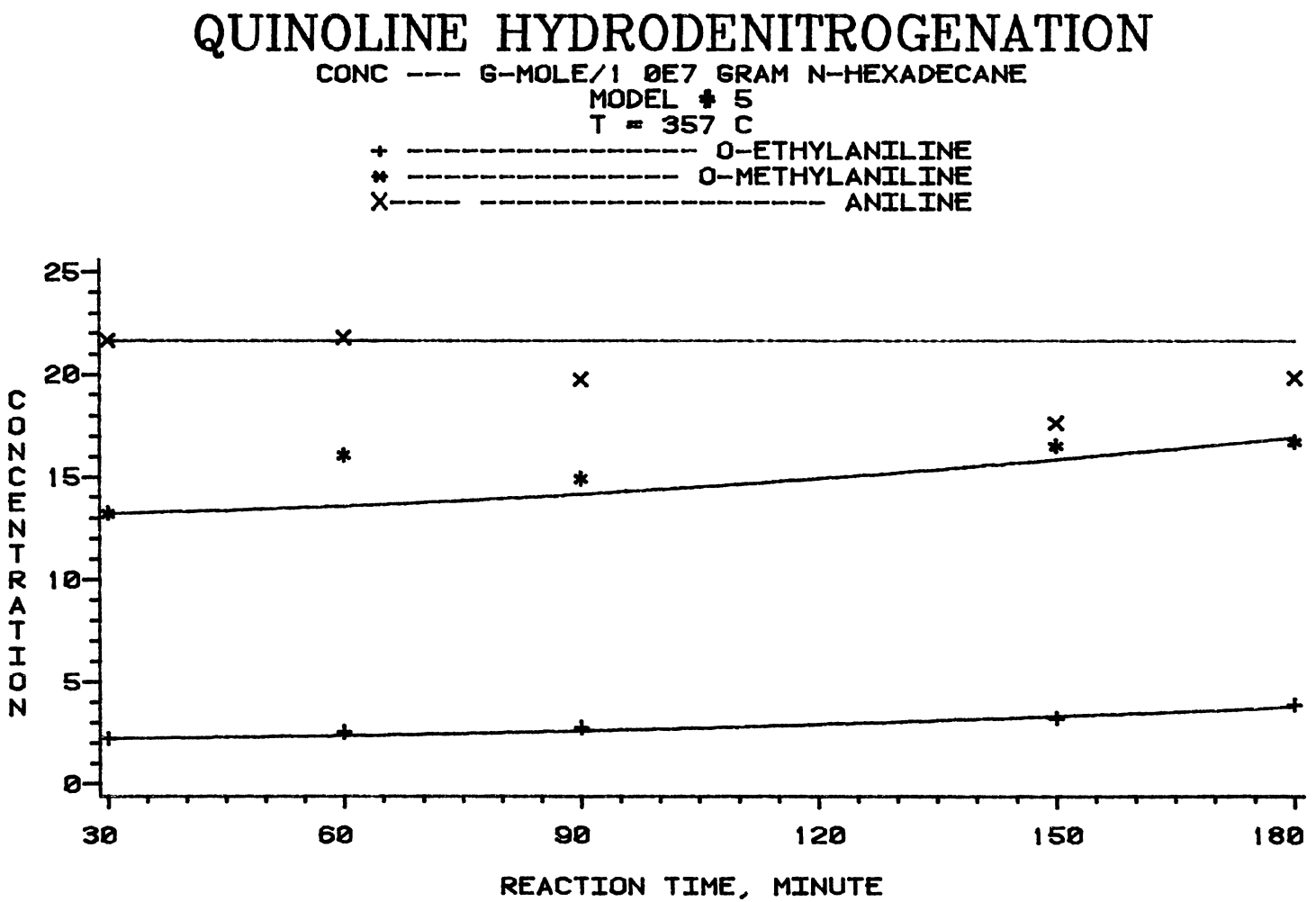

Figure 102. Quinoline HDN Products at 357°C - Model #5

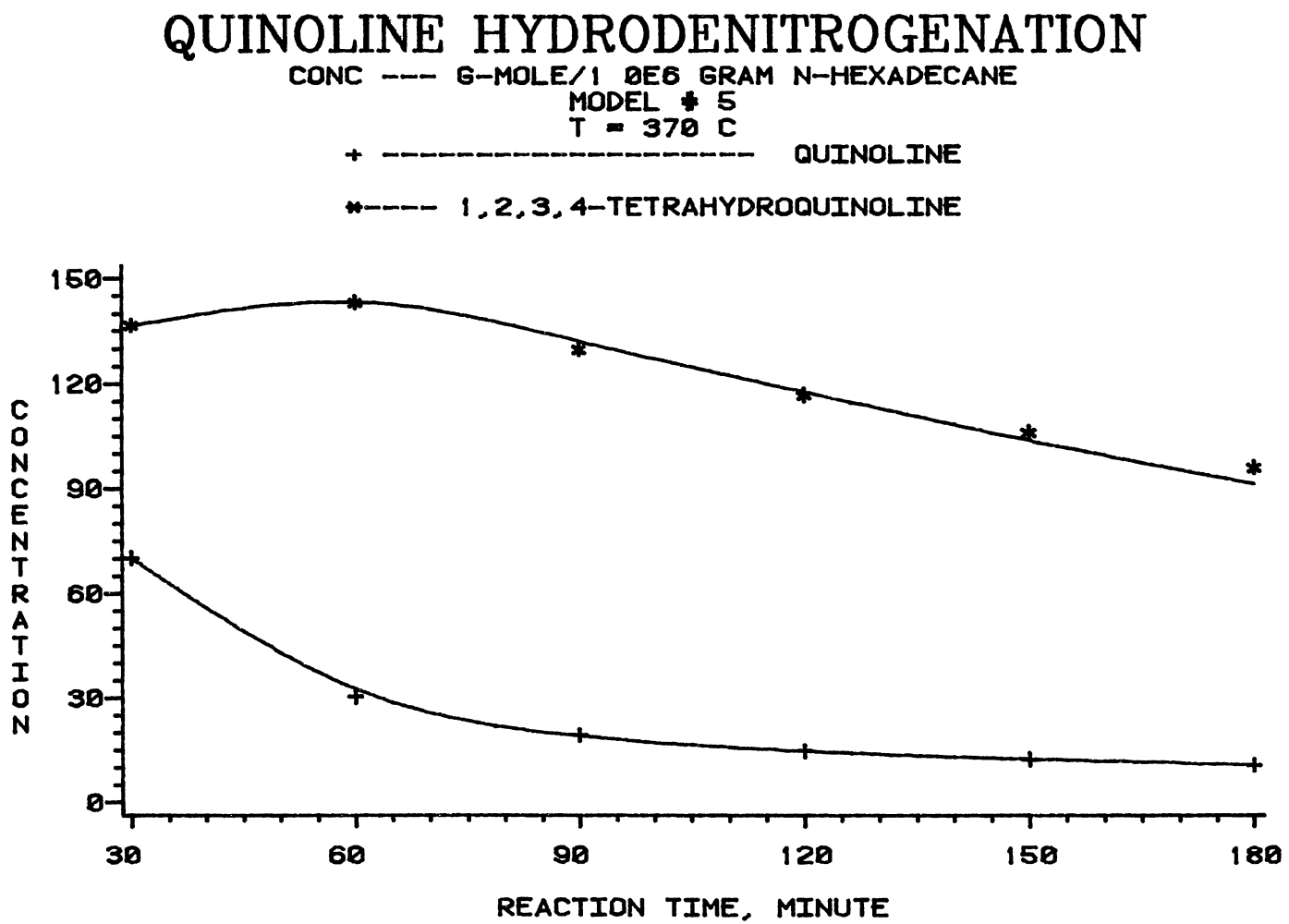

Figure 103. Quinoline HDN Products at 370°C - Model #5

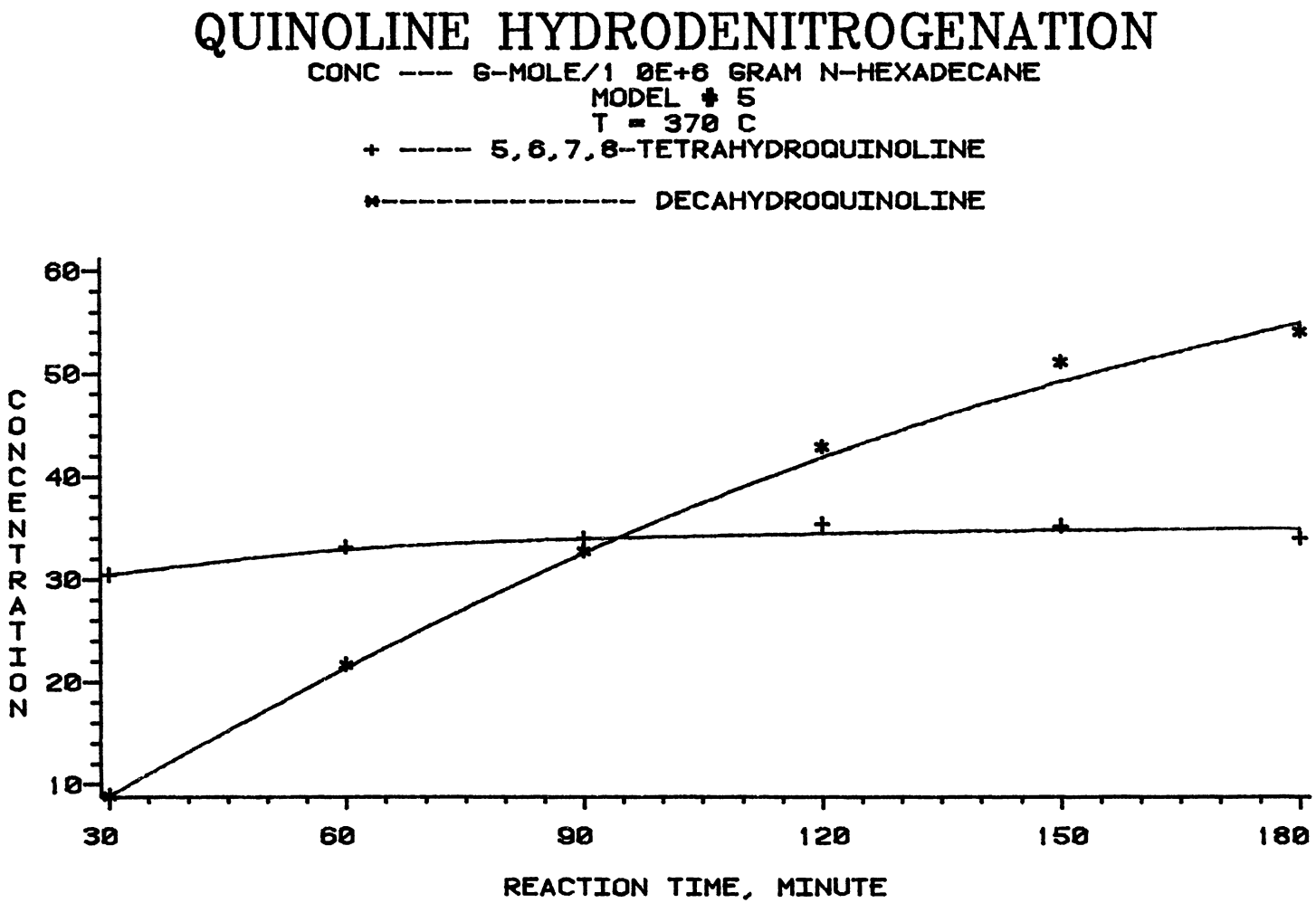

Figure 104. Quinoline HDN Products at 370°C - Model #5

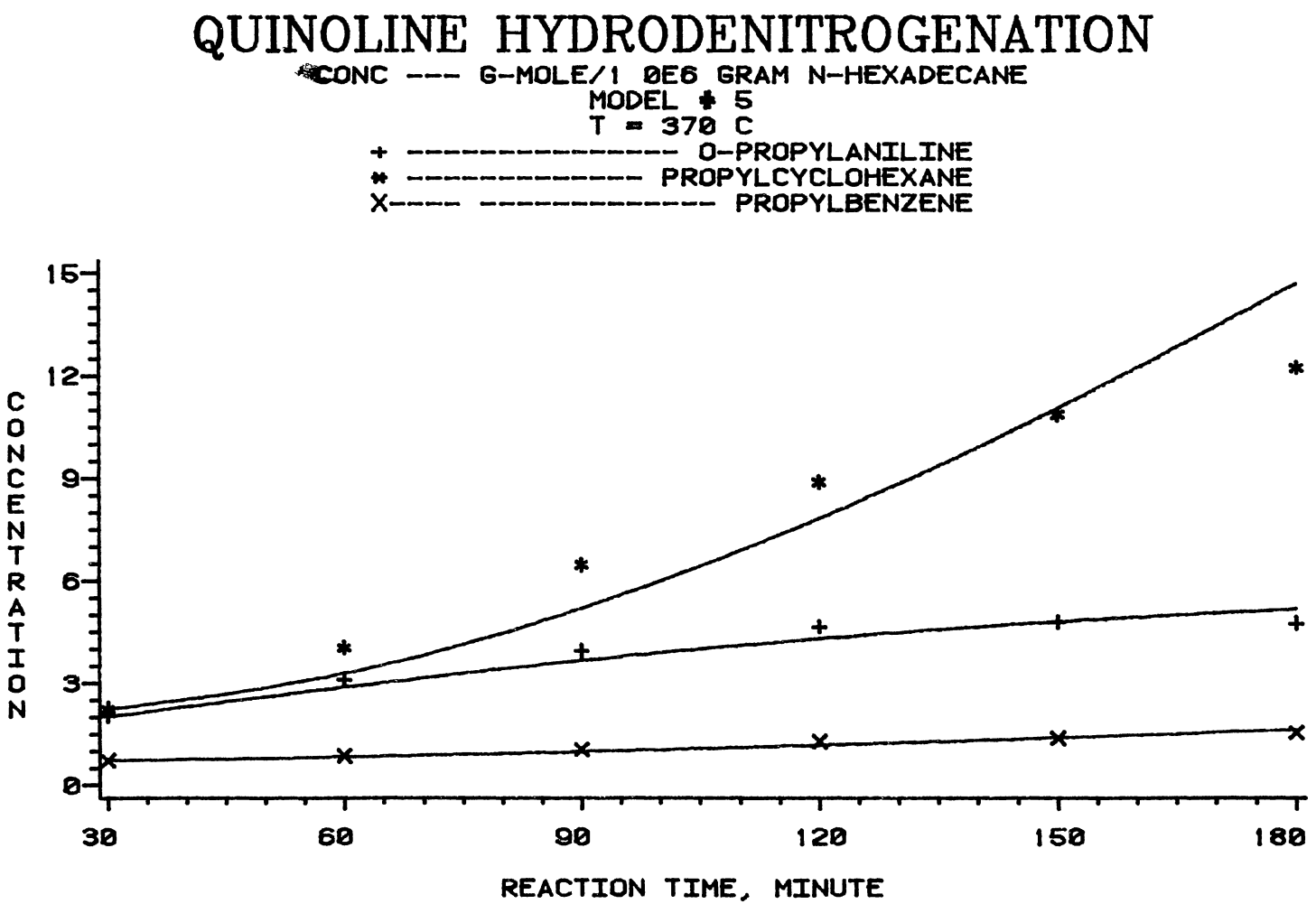

Figure 105. Quinoline HDN Products at 370°C - Model #5

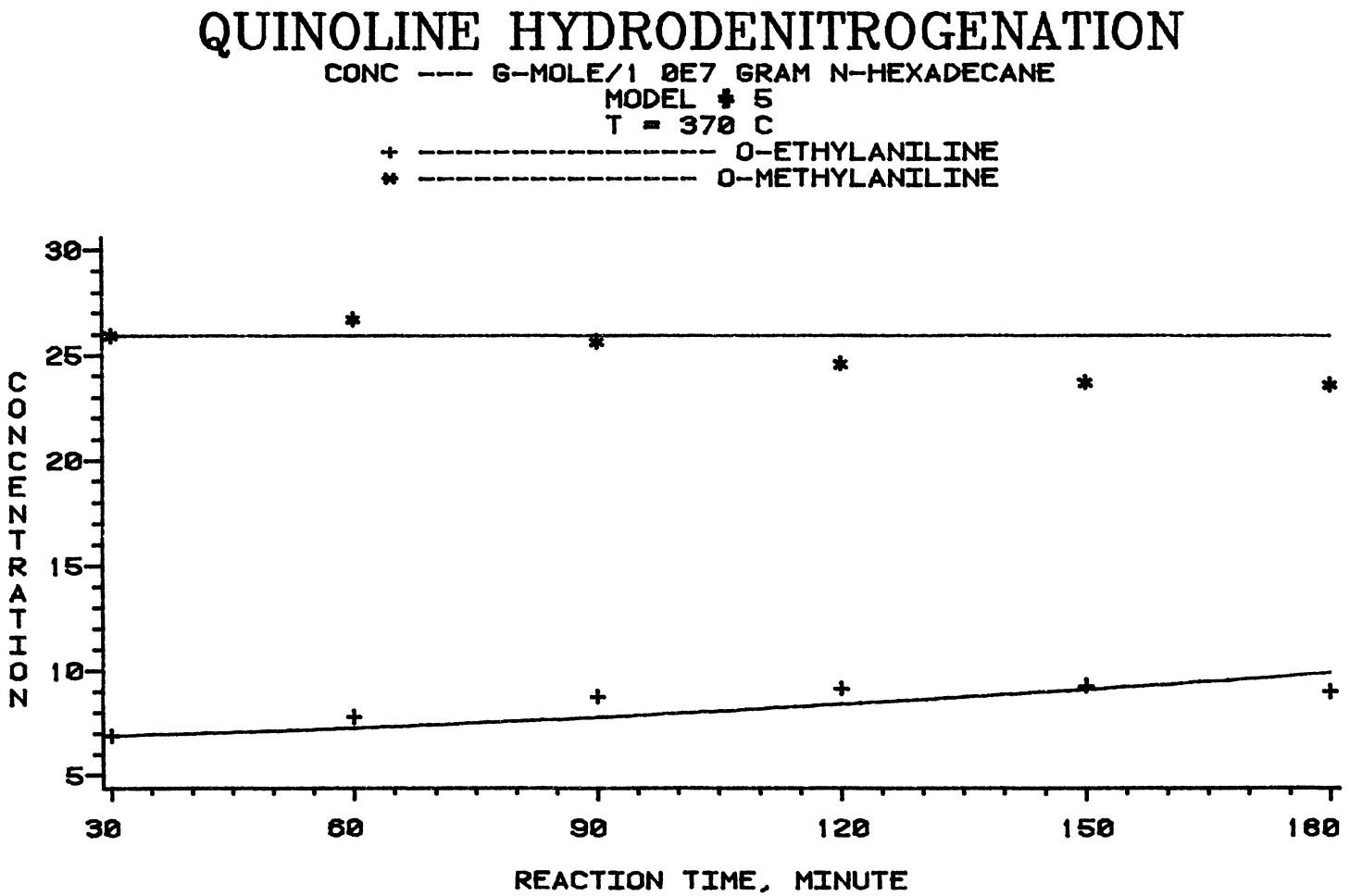

Figure 106. Quinoline HDN Products at 370°C - Model #5

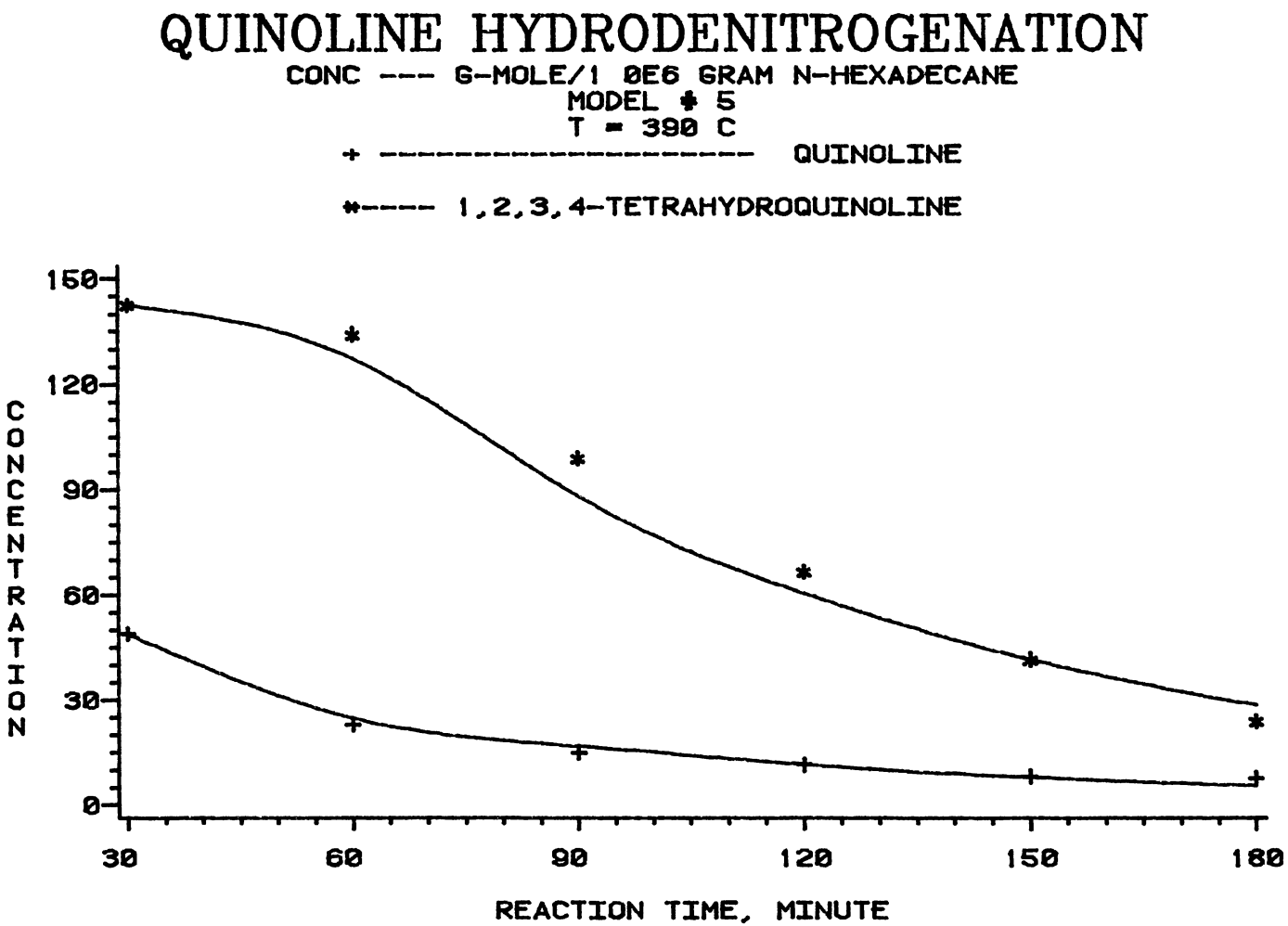

Figure 107. Quinoline HDN Products at 390°C - Model #5

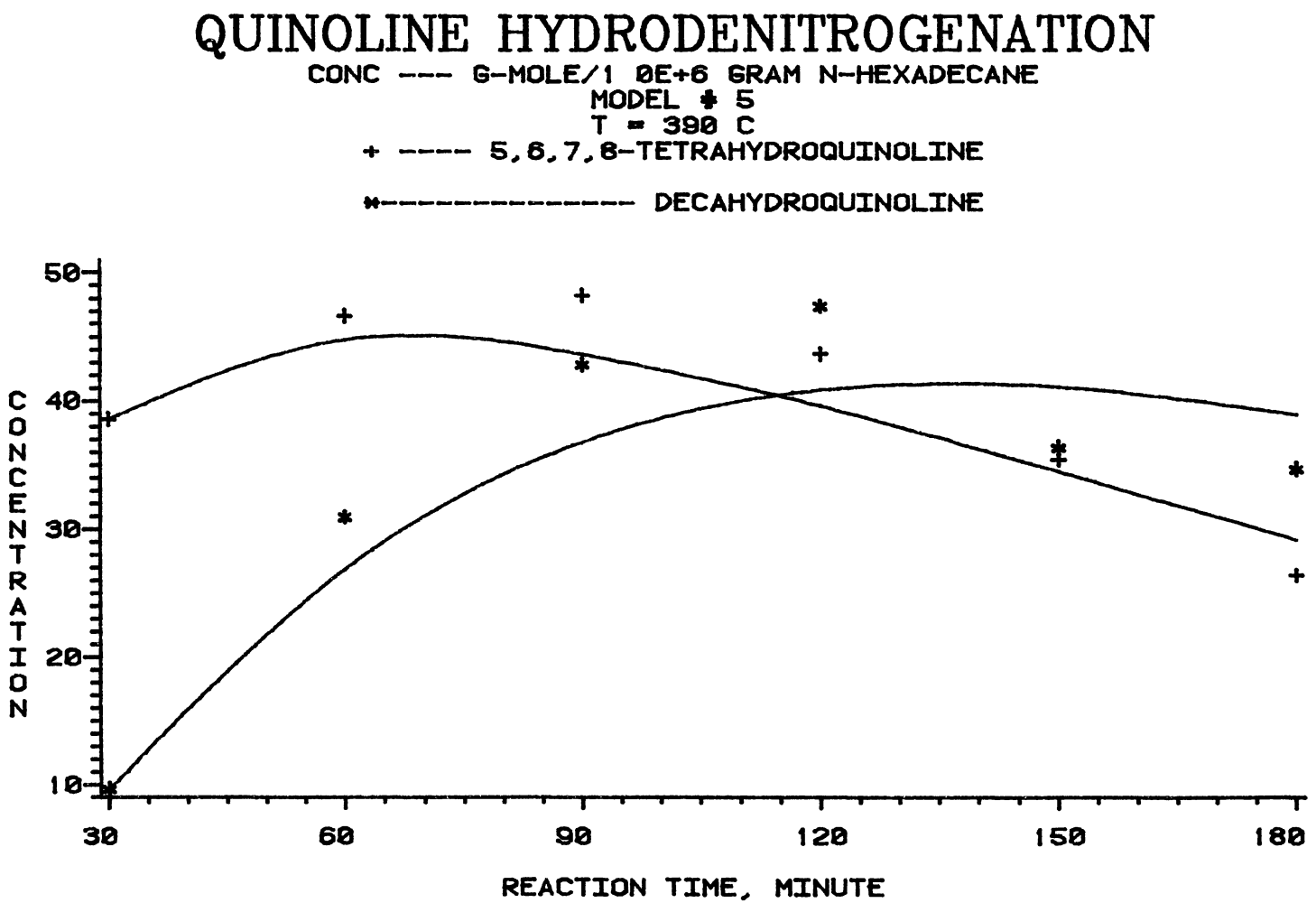

Figure 108. Quinoline HDN Products at 390°C - Model #5

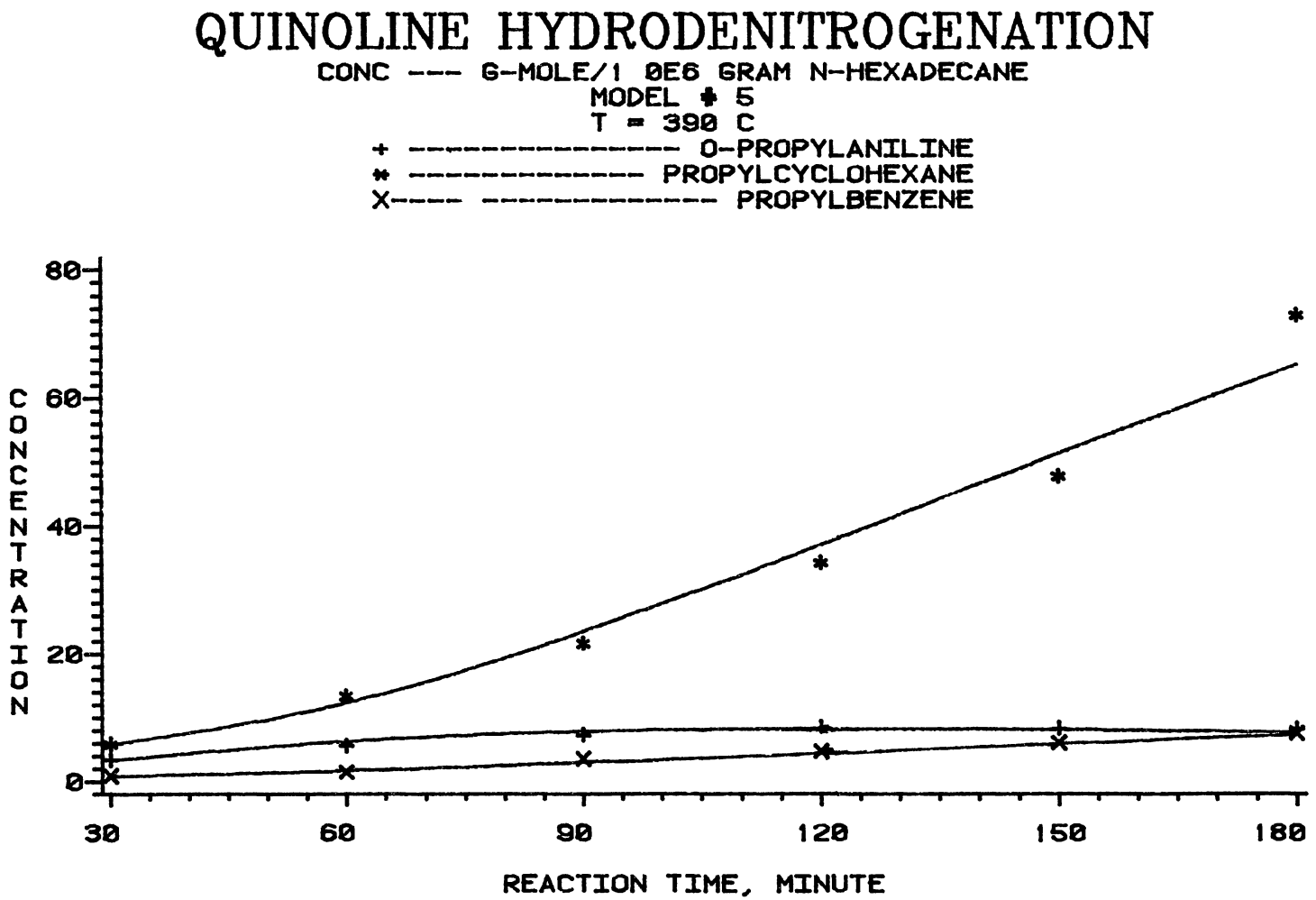

Figure 109 Quinoline HDN Products at 390°C - Model #5

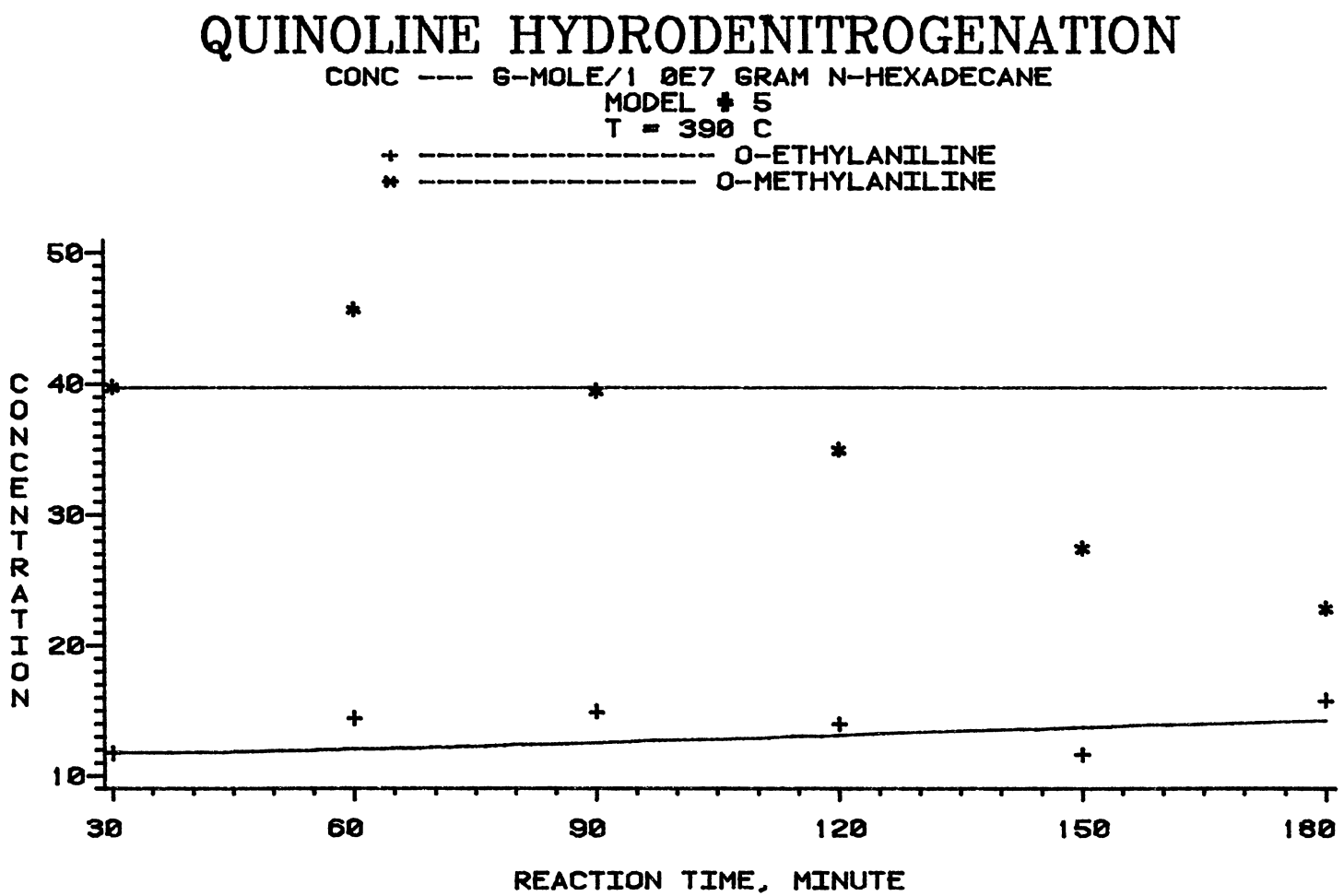

Figure 110. Quinoline HDN Products at 390°C - Model #5

are listed in Table XXXIV. It can be seen from these results that the PRE is less than 10% for 91 2% of the points at 357°C and 370°C, whereas it is less than 16.2% for 88.9% of the points at 390°C. In fact, this is a reasonable fit

Model # 6

The results of acridine HDN were fitted with this model. The estimated kinetic parameters are listed in Table XXXV, whereas both model predicted concentrations and practical concentrations are plotted in Figures 111-116. At 357°C, the PRE is less than 10 0 for 83.3% of the data points. The PRE varies between -14 9 and 14.6 At 370°C, the PRE is less than 10.0 for 80.6% of the data points. The PRE varies between -38.7 and 45.0 In fact, this large PRE is not unexpected since we are dealing with very low concentrations. At 390°C, the PRE is less than 12.0 for 88.9% of the data points The PRE varies between -15 1 and 17.7 From Table XXXV it can be seen that increasing reaction temperature enhances THA formation, whereas decreasing it enhances ASOHA formation. Finally, considering these results, it can be concluded that all the reactions in the reaction network, except the reaction 5 --> 6, are reversible ones.

Model # 7

The quinoline-acridine mixture HDN data were fitted with this model Both Marquardt's method and Runge-Kutta

TABLE XXXIV

PARAMETERS OF MODEL # 5 FOR QUINOLINE HDN

Temperature	357°C	370°C	390°C
a_{12}	0.541 E-1	0.403 E-1	0 632 E-1
a_{13}	0.133 E-2	0.217 E-2	0.185 E-1
a_{21}	0.155 E-2	0.436 E-2	0.526 E-1
a_{24}	0.119 E-2	0.304 E-2	0.272 E-2
a_{25}	0.119 E-3	0.239 E-3	0.897 E-3
a_{34}	0.292 E-2	0.525 E-3	0.934 E-2
a_{46}	0.710 E-3	0.235 E-2	0.115 E-1
a_{57}	0.135 E-2	0.159 E-2	0.597 E-2
a_{58}	0.466 E-3	0.520 E-3	0.240 E-3
a_{59}	0.111 E-2	0.100 E-8	0.100 E-10
a_{510}	0.100 E-10	-----	-----
K_{12}	0.145 E+2	0.904 E+1	0.484 E+1
K_{13}	0.593 E-1	0.153 E+0	0.228 E+0

TABLE XXXV

PARAMETERS OF MODEL # 6 FOR ACRIDINE HDN

Parameter	357°C	370°C	390°C
a_{12}	0.3603 E-1	0.4191 E-1	0.4400 E-1
a_{13}	0.2036 E-1	0.5804 E-2	0.2562 E-2
a_{24}	0.9875 E-1	0.5932 E-1	0.4107 E-1
a_{35}	0.3300 E-1	0.7848 E-2	0.5875 E-2
a_{45}	0.2561 E-2	0.6555 E-2	0.2629 E-2
a_{56}	0.3182 E-2	0.2162 E-1	0.2415 E-1
K_{12}	0.2533 E+3	0.1000 E+9	0.1830 E+2
K_{13}	0.4746 E+1	0.3208 E+1	0.1386 E+2
K_{24}	0.2085 E+2	0.1279 E+2	0.5969 E+1
K_{35}	0.6555 E+1	0.5621 E+2	0.1078 E+8
K_{45}	0.2009 E+1	0.8359 E+0	0.9032 E+0

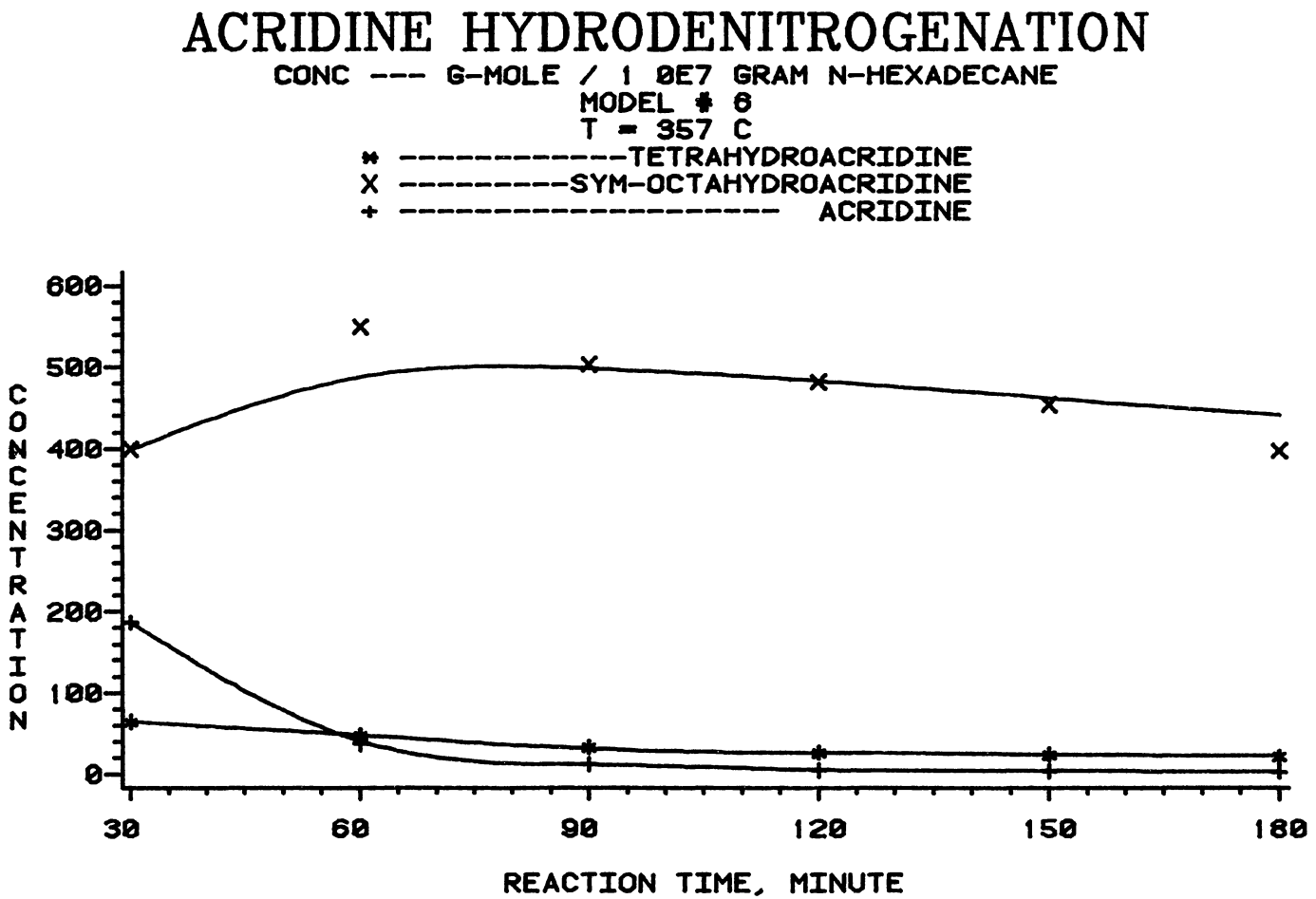

Figure 111. Acridine HDN Products at 357°C - Model #6

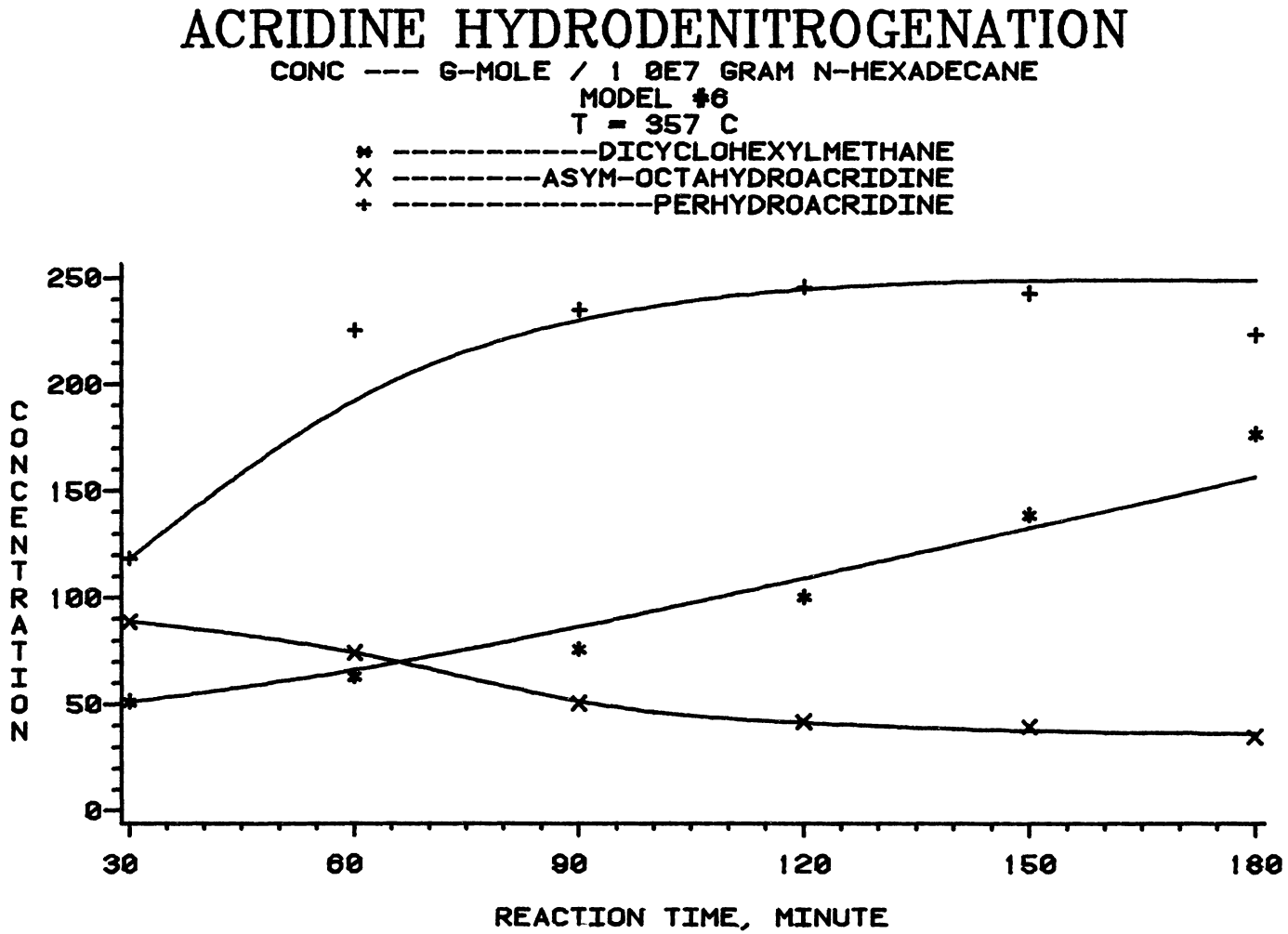

Figure 112. Acridine HDN Products at 357°C - Model #6

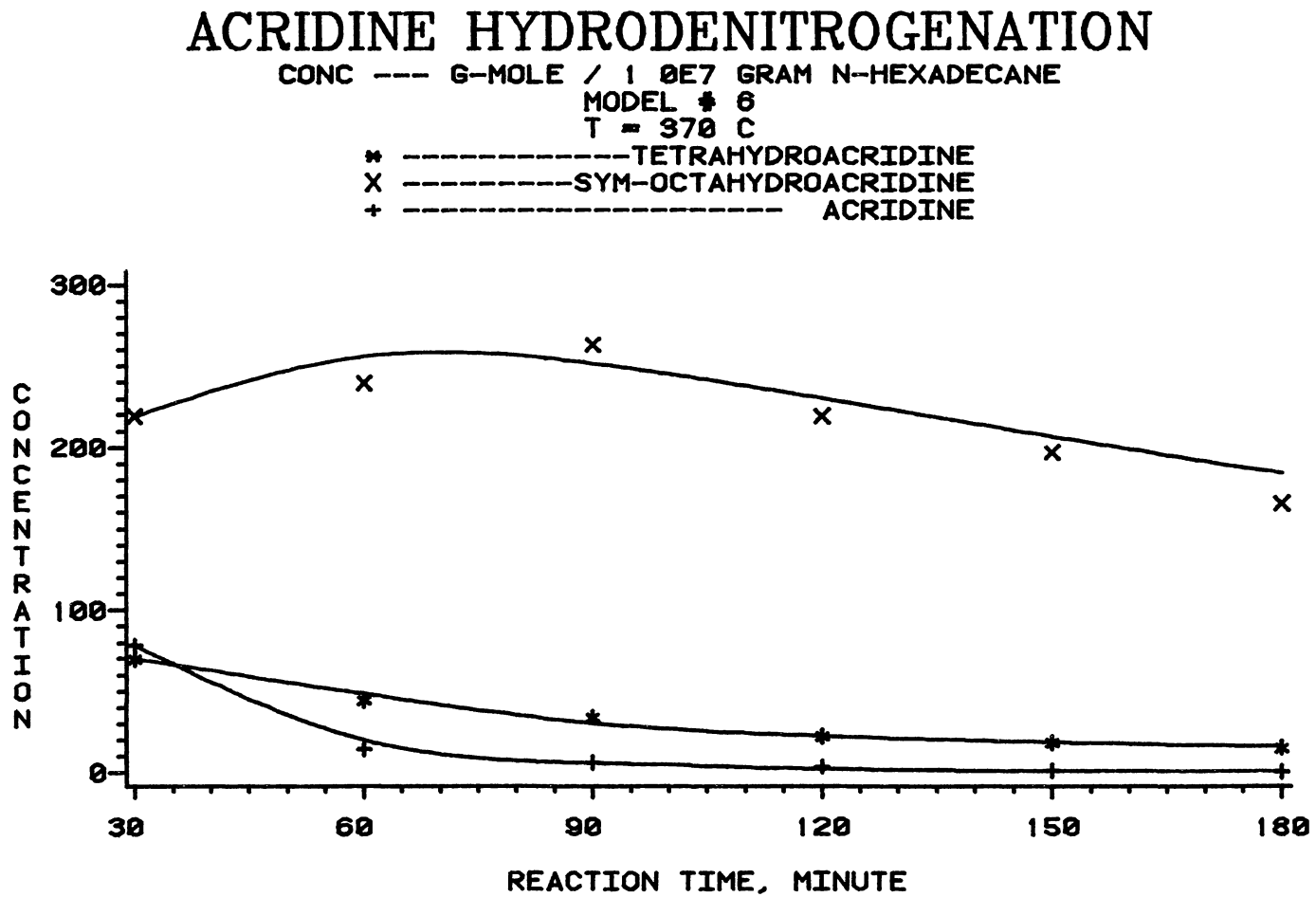

Figure 113 Acridine HDN Products at 370°C - Model #6

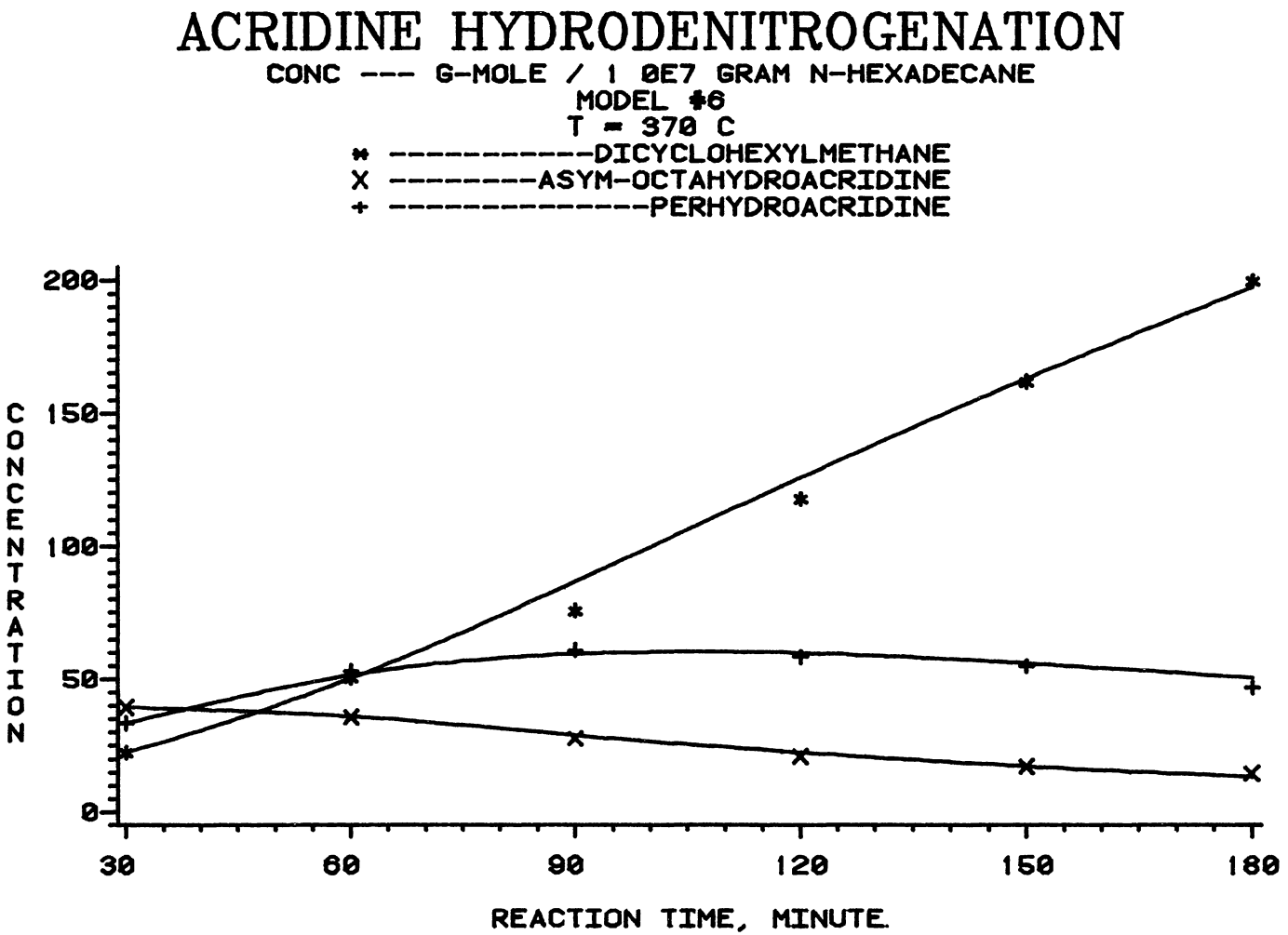

Figure 114 Acridine HDN Products at 370°C - Model #6

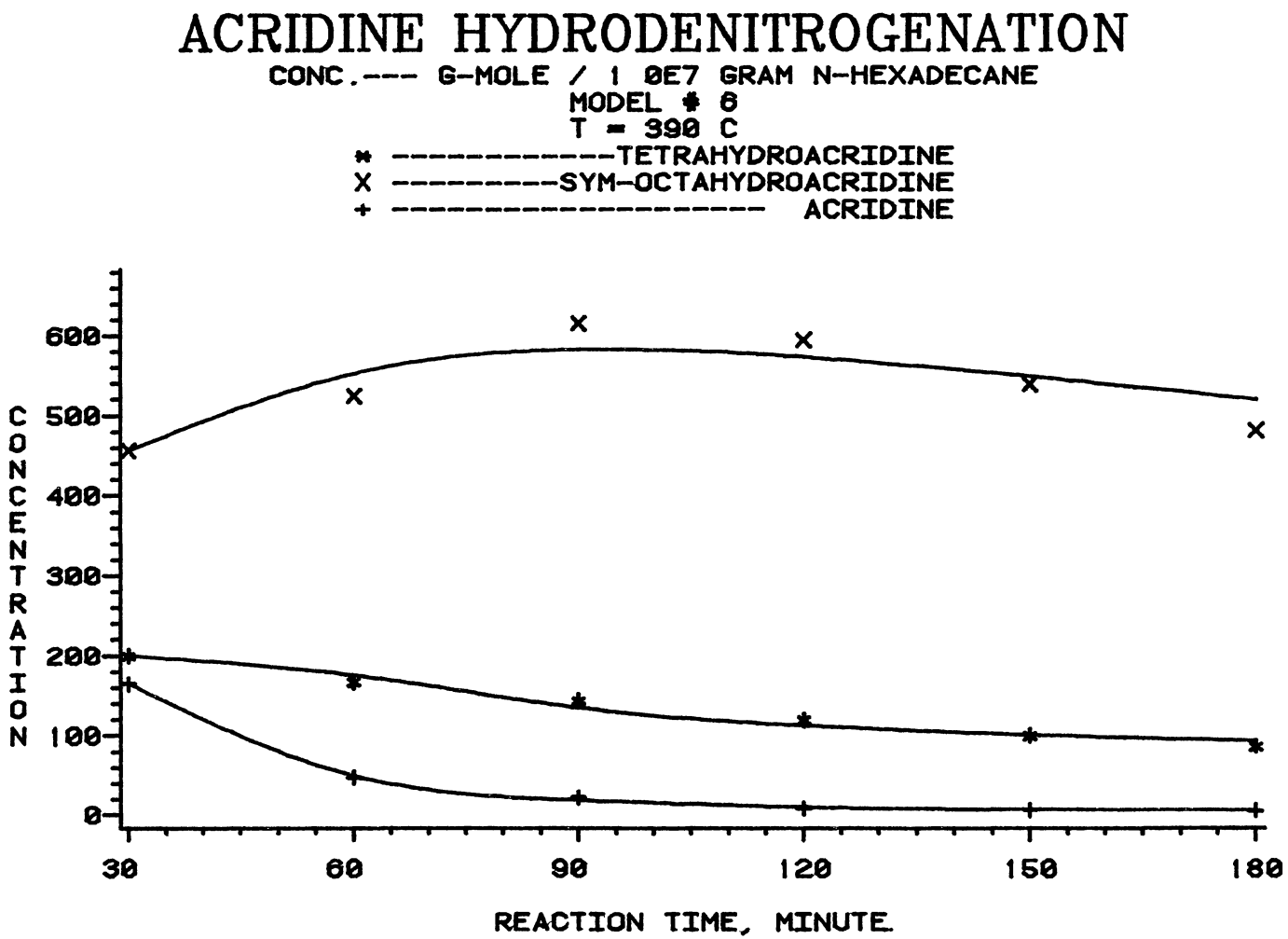

Figure 115. Acridine HDN Products at 390°C - Model #6

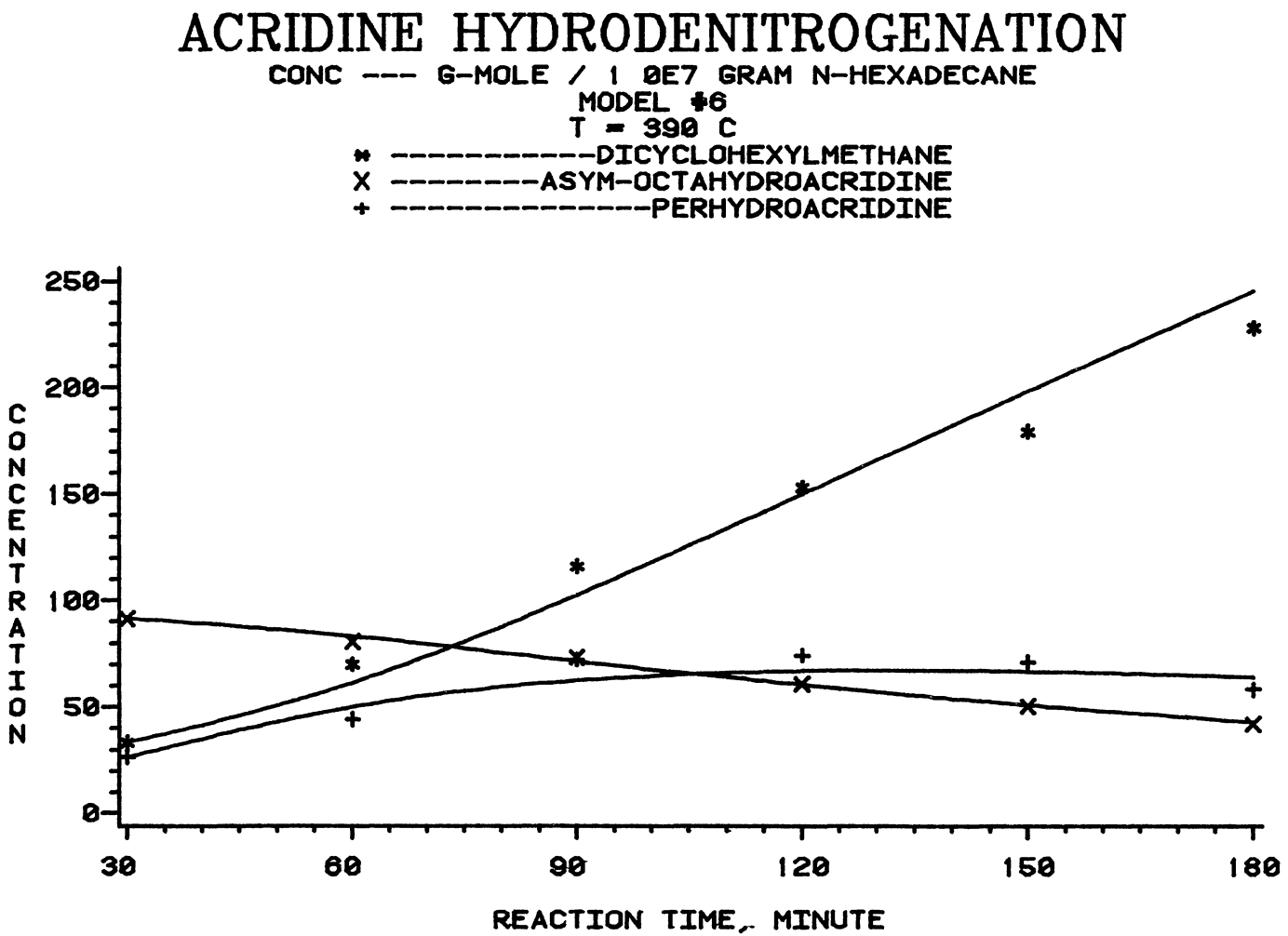

Figure 116 Acridine HDN Products at 390°C - Model #6

technique were used in the solution of this model The estimated parameters for quinoline reactions and acridine reactions are presented in Tables XXXVI and XXXVII. Both the models predicted and measured concentrations are plotted in Figures 117-134 OMA, OEA, and DCHM predicted concentrations are far from the actual values as can be seen in Figures 120,122,126, and 132 In fact, these large deviations are due to the model assumption that these three compounds are final products.

At 357°C, the PRE is less than 11 0% for 77 8% of the data obtained for the major quinoline HDN products, compounds 1 --> 6 Higher errors were observed for the other products, which appeared in a concentration of about 1 g-mole/1 0E6 g n-hexadecane. On the other hand the PRE is less than 11 0% for 70% of the data obtained for nitrogen compounds resulting in acridine HDN However, DCHM showed higher PRE

At 370°C, the PRE is less than 11 0% for 86% of the data obtained for the major quinoline HDN products. Higher PRE was observed for the other products which appeared at a low concentration. On the other hand, the PRE is less than 8% for 66.7% of the data obtained for nitrogen compounds resulting in acridine HDN However, DCHM showed also higher PRE.

At 390°C, the PRE is less than 10% for 91 7% of the data obtained for the major quinoline HDN products, compounds 1 ---> 6 However, the PRE is smaller than 15%

TABLE XXXVI

PARAMETERS OF MODEL # 7 FOR QUINOLINE HDN

Parameter	357°C	370°C	390°C
a_{12}	0.2033 E-1	0.3519 E-2	0.1588 E-1
a_{13}	0.1605 E-1	0.2292 E-1	0 4776 E-1
a_{21}	0.1943 E-4	0 5676 E-4	0.9669 E-4
a_{24}	0.6300 E-2	0.2370 E-1	0.623 E-1
a_{25}	0.7620 E-0	0.1744 E-2	0.9448 E-3
a_{31}	0 1130 E-6	0.4382 E-3	0.1172 E-4
a_{34}	0.1000 E-18	0.4737 E-2	0 2416 E-2
a_{42}	0.5660 E-8	0 1019 E-2	0.8160 E-8
a_{43}	0.1000 E-17	0.1000 E-17	0.1000 E-17
a_{46}	0.1320 E-2	0.3169 E-2	0.4887 E-2
a_{57}	0 100 E-15	0 1742 E-2	0.1000 E-13
a_{58}	0 5472 E-3	0.1862 E-3	0.6406 E-5
a_{59}	0.8346 E-3	0 4393 E-4	0.1000 E-9
a_{510}	0.1000 E-15	0.912 E-16	0.1000 E-15
K_{12}	0.100 E+19	0.1000 E+19	0.1000 E+19
K_{13}	0.1512 E+1	0.2344 E+2	0 2070 E+1
K_{21}	0.7796 E-3	0.7474 E-3	0 3192 E-3
K_{24}	0 1000 E+15	0.1000 E+15	0.1000 E+15
K_{31}	0 5000 E-4	0.3094 E-1	0.4070 E-2
K_{34}	0 6110 E+12	0.1000 E+12	0.100 E+12
K_{42}	0.1200 E-5	0.1129 E+0	0.2047 E-5
K_{43}	0.1460 E-3	0.1460 E-3	0.1460 E-3

TABLE XXXVII

PARAMETERS OF MODEL # 7 FOR ACRIDINE HDN

Parameter	357°C	370°C	390°C
a_{12}	0 1678 E-1	0.2160 E-1	0 1980 E-1
a_{13}	0.4131 E-2	0.2272 E-2	0 3256 E-2
a_{24}	0 1228 E-1	0 3789 E-1	0 1475 E-1
a_{35}	0 2580 E+1	0.1000 E-10	0 2133 E+1
a_{45}	0 5398 E-2	0 1000 E-10	0 1000 E-9
a_{56}	0 1180 E-1	0 1000 E-11	0 7725 E-3
K_{12}	0 2818 E+1	0.3900 E+15	0.198 E+14
K_{13}	0 1000 E+16	0.4300 E+10	0 542 E+12
K_{24}	0 3700 E+11	0.9992 E+1	0 7330 E+1
K_{35}	0 1300 E+02	0 6530 E+9	0 3296 E+1
K_{45}	0 1000 E+13	0.1370 E+9	0 8862 E+0

for all the compounds resulting from quinoline HDN On the other hand, the PRE is 11 0% for 58 3% of the data obtained for the compounds resulting in acridine HDN

Interactions In Quinoline-Acridine Mixture HDN

1 Effects of Acridine on Quinoline HDN

The presence of acridine affects the quinoline HDN reactions to varying degrees Table XXXVIII compares the

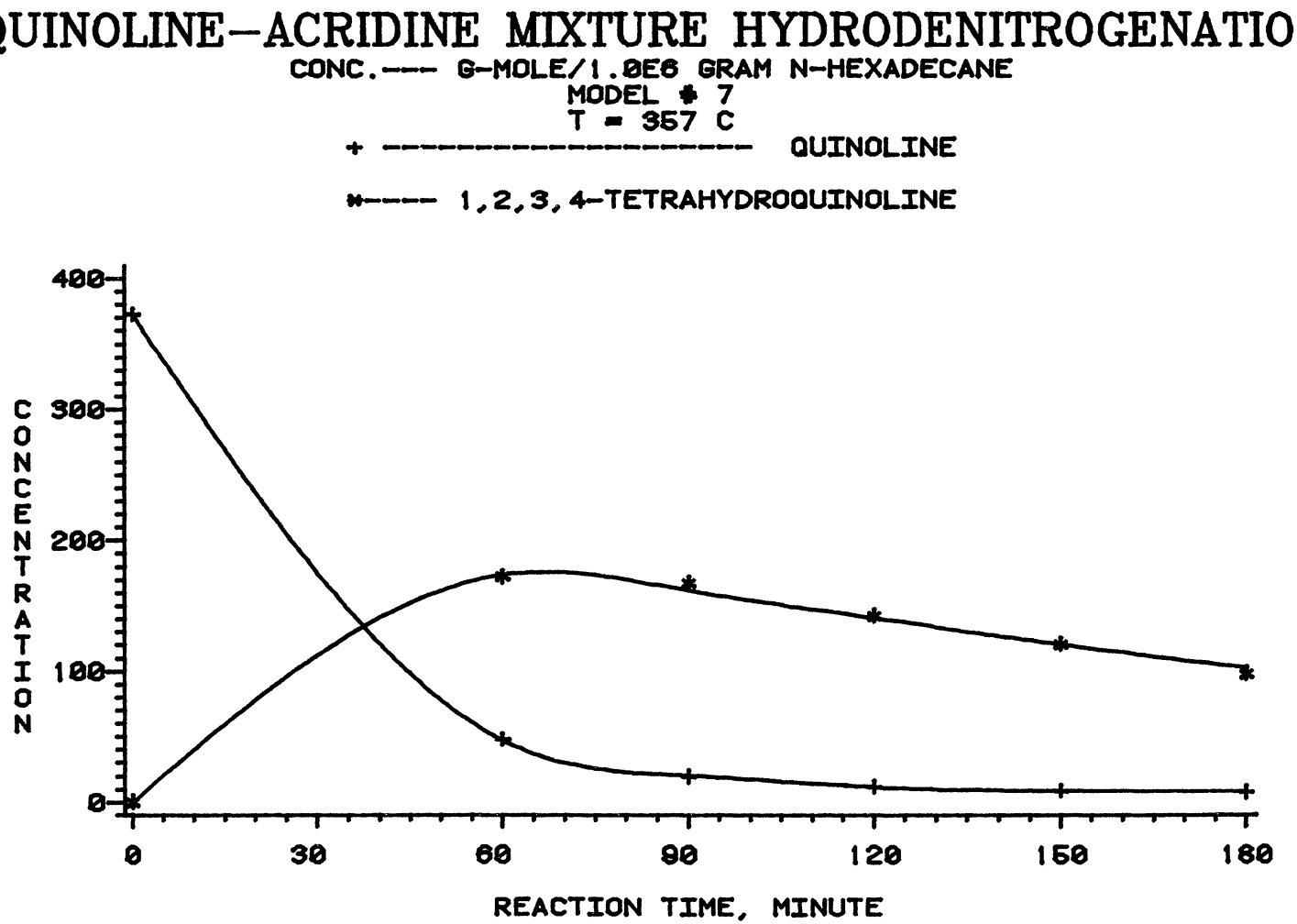

Figure 117. Quinoline-Acridine Mixture HDN Products at 357°C - Model #7

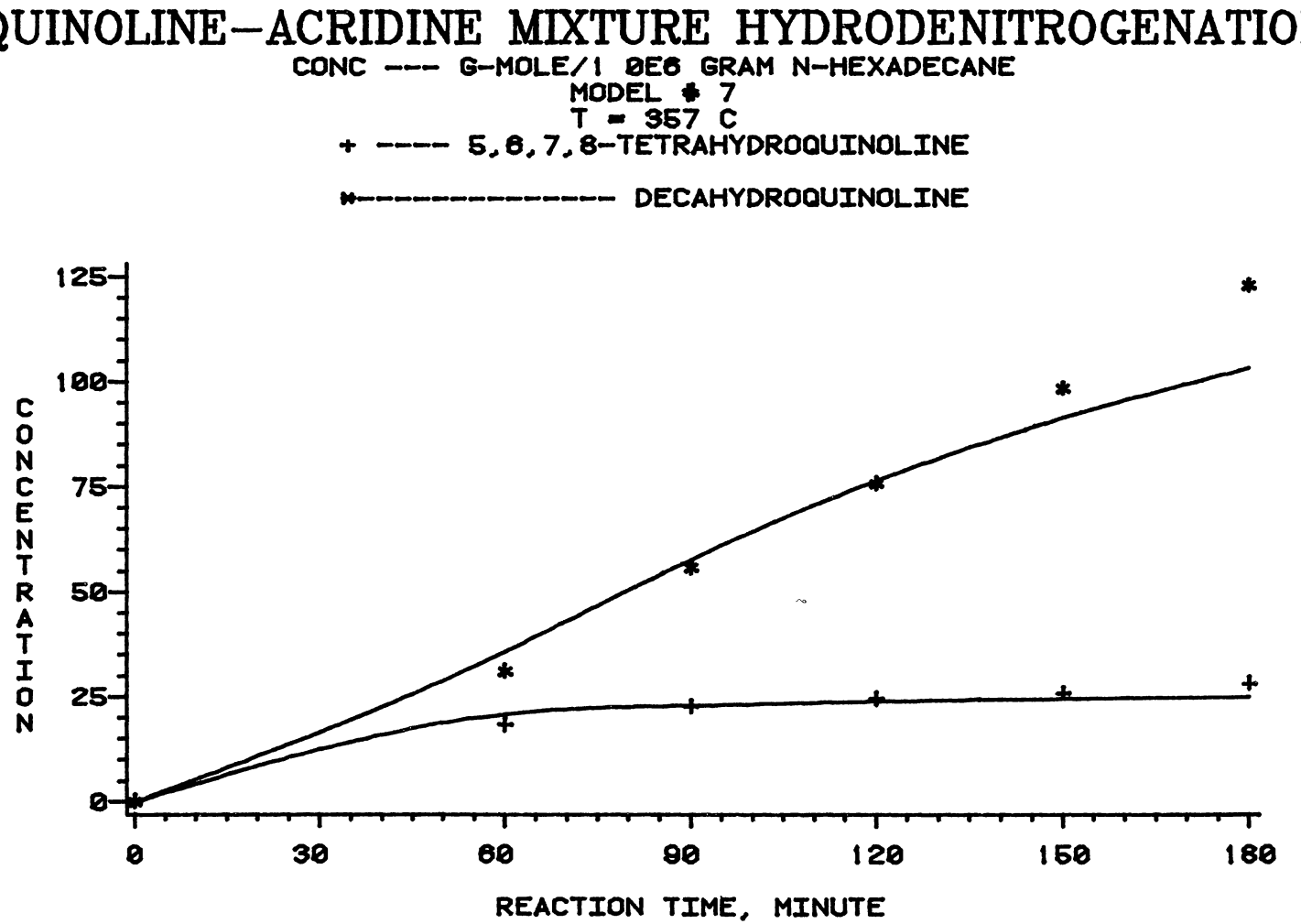

Figure 118. Quinoline-Acridine Mixture HDN Products at 357°C - Model #7

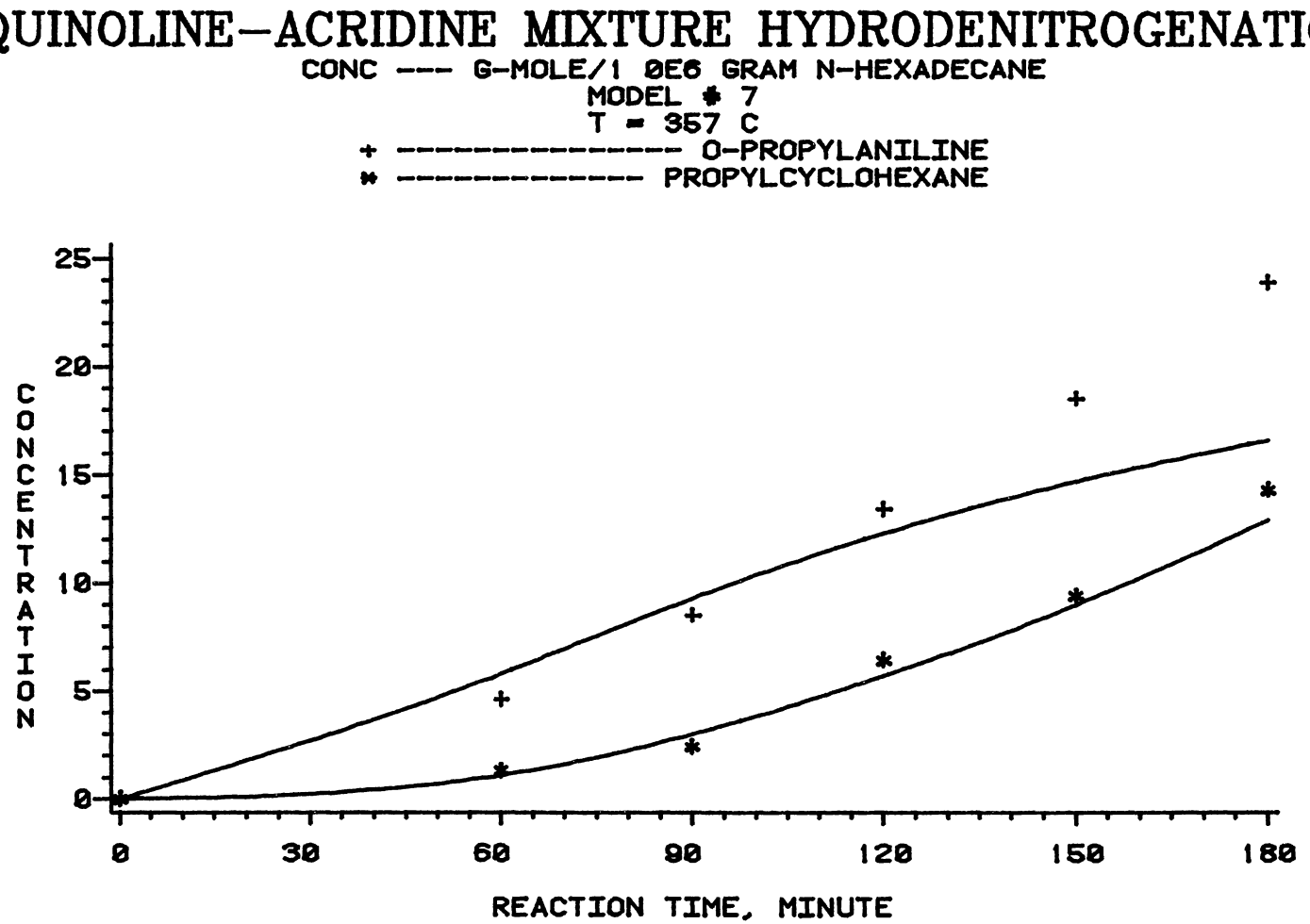

Figure 119 Quinoline-Acridine Mixture HDN Products at 357°C - Model #7

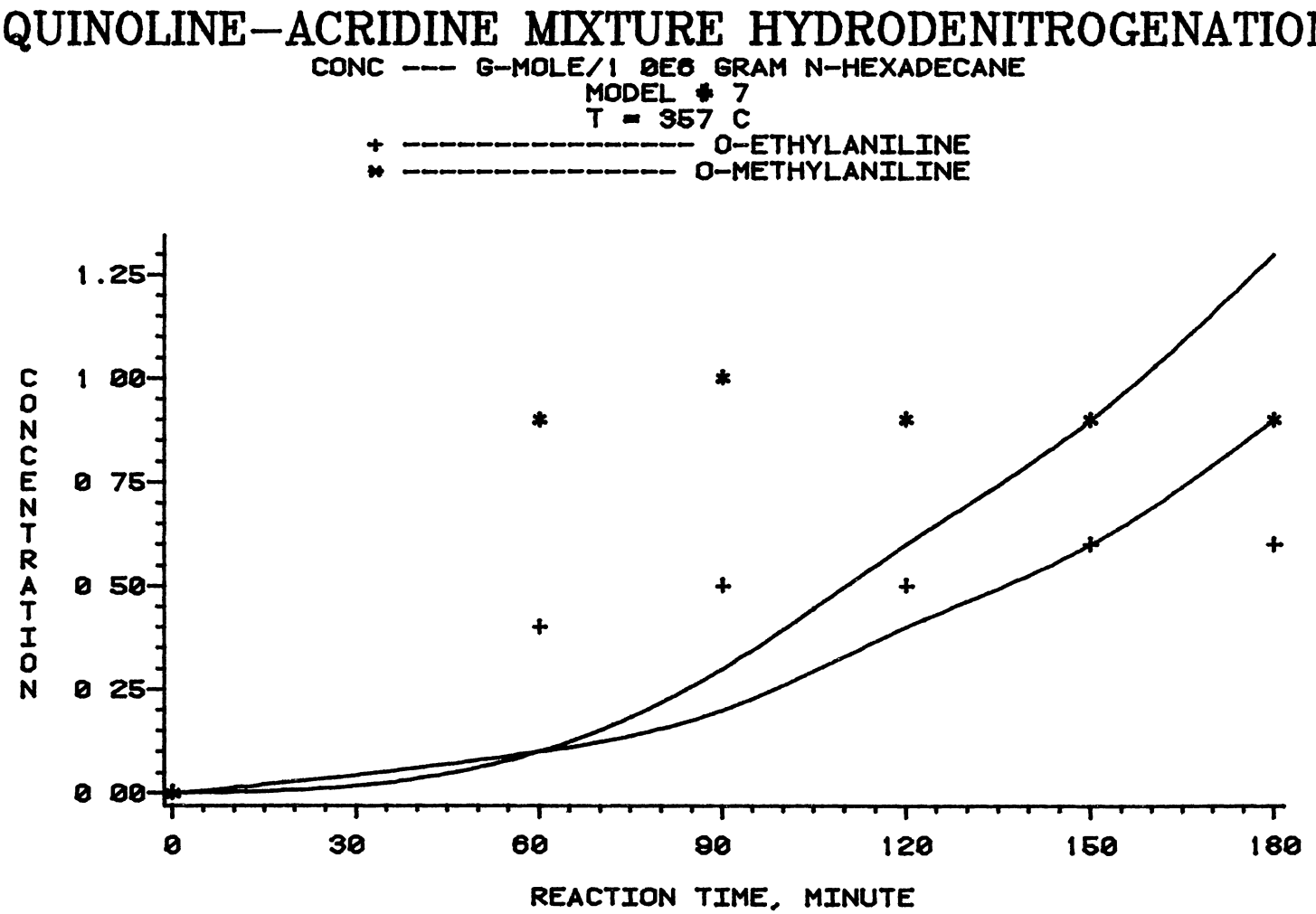

Figure 120 Quinoline-Acridine Mixture HDN Products at 357°C - Model #7

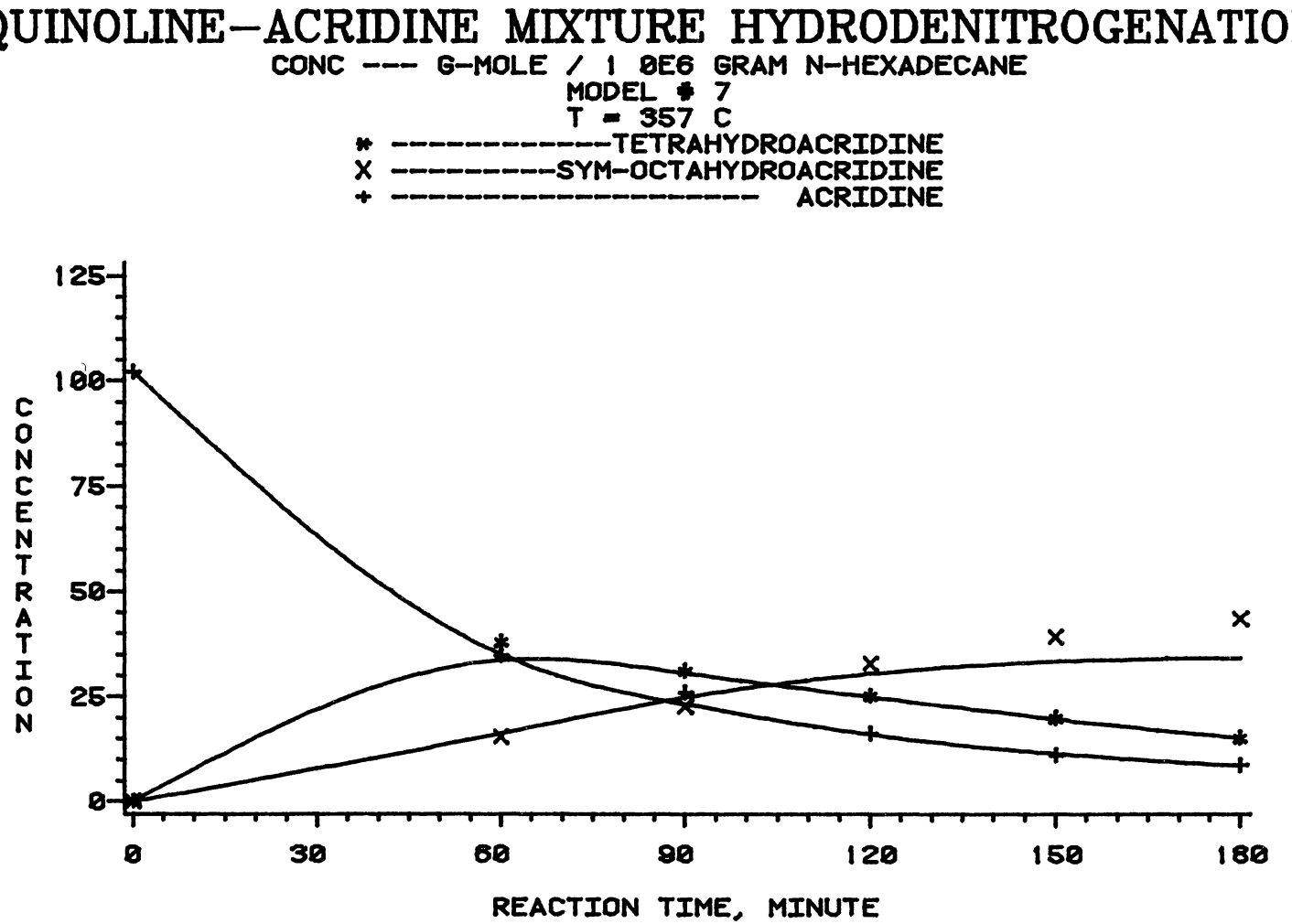

Figure 121. Quinoline-Acridine Mixture HDN Products at 357°C - Model #7

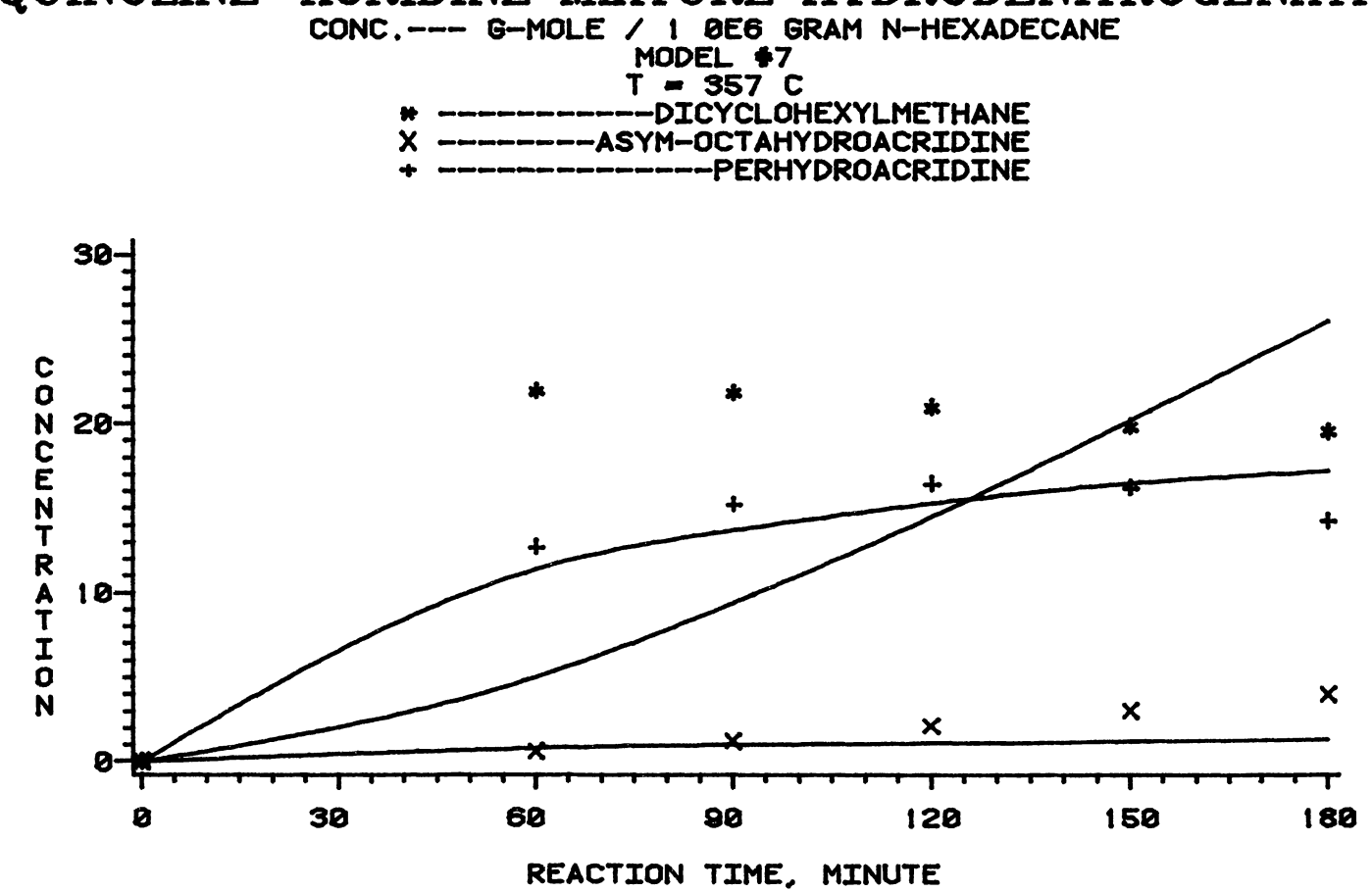

Figure 122. Quinoline-Acridine Mixture HDN Products at 357°C - Model #7

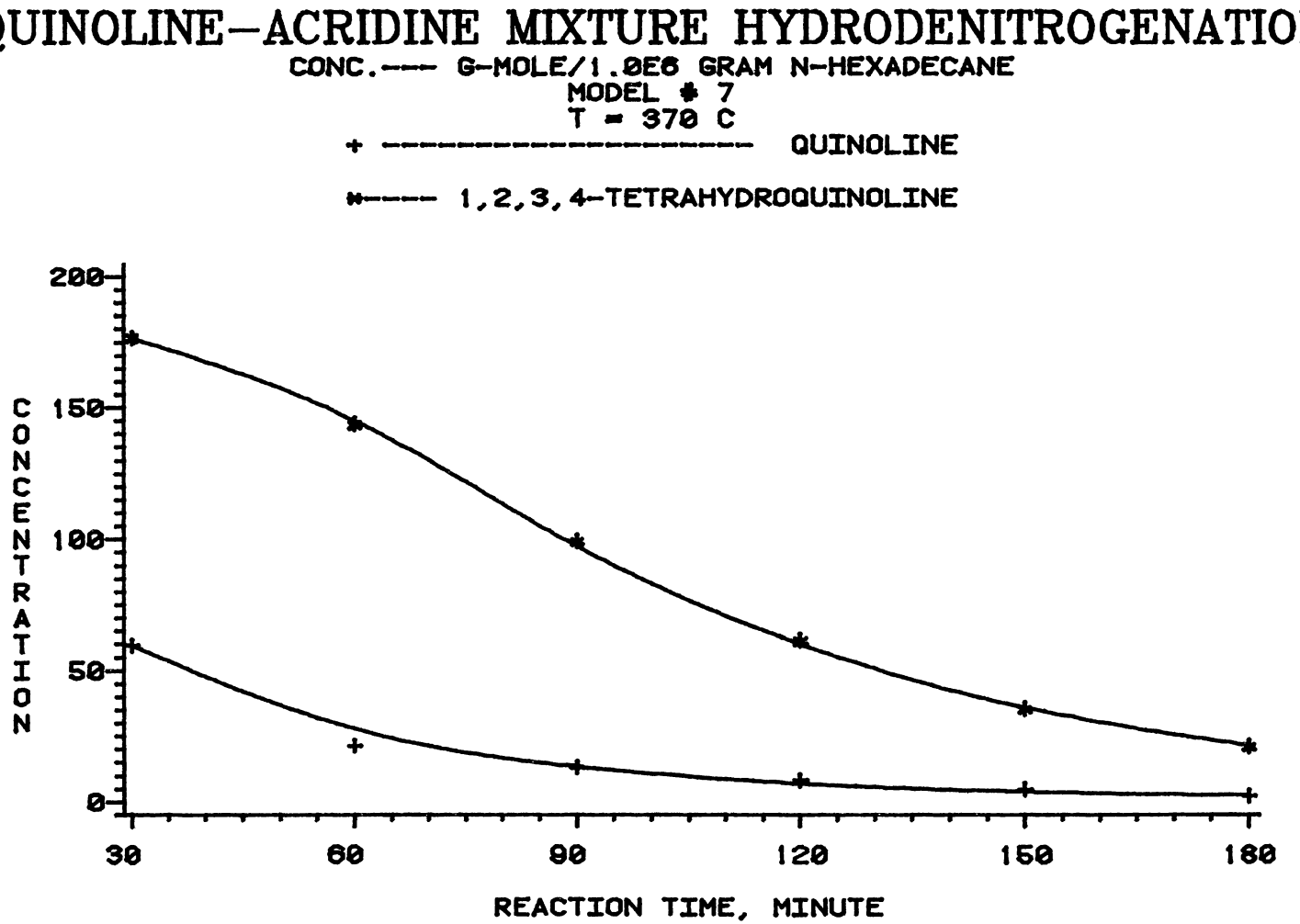

Figure 123. Quinoline-Acridine Mixture HDN Products at 370°C - Model #7

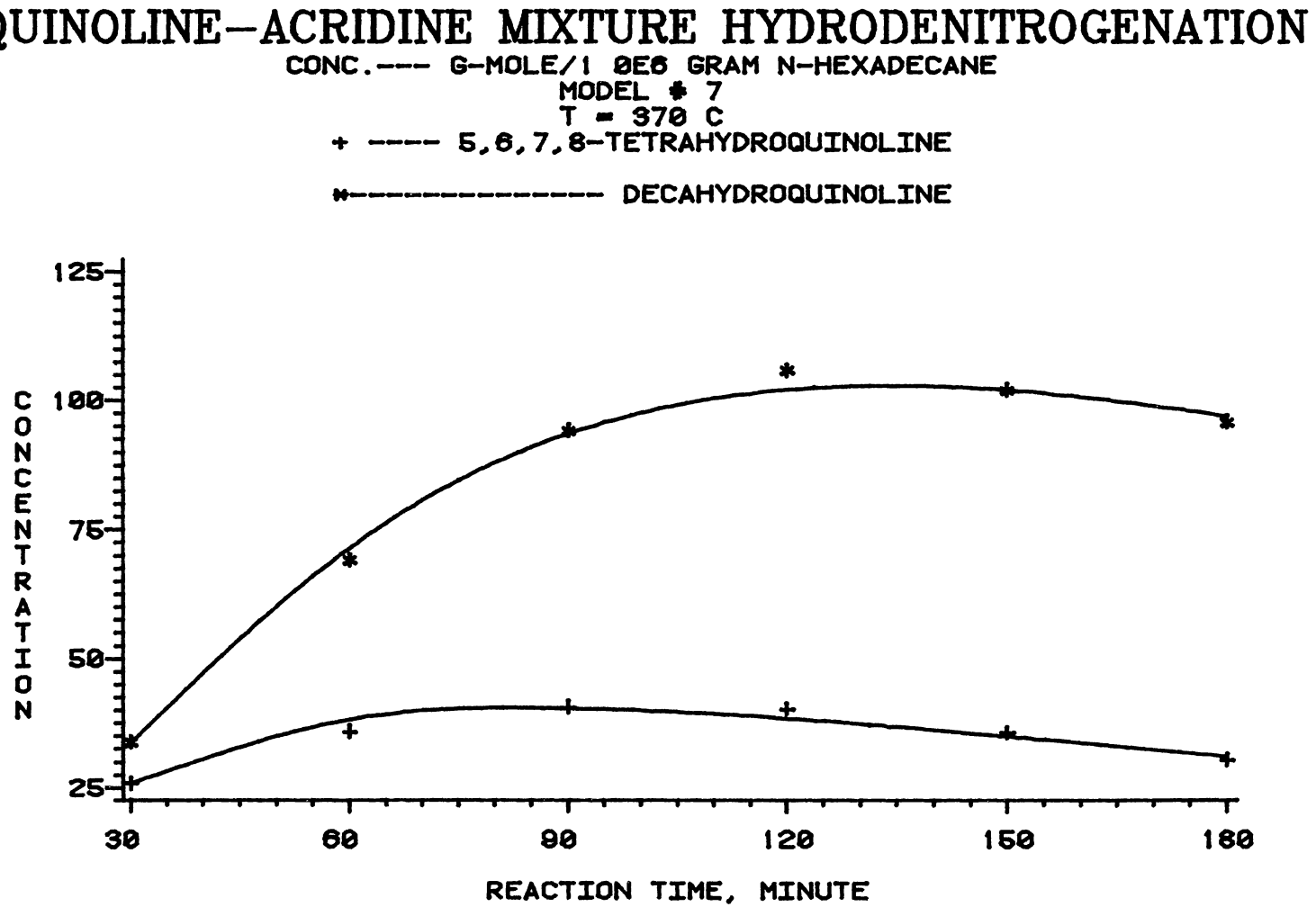

Figure 124. Quinoline-Acridine Mixture HDN Products at 370°C - Model #7

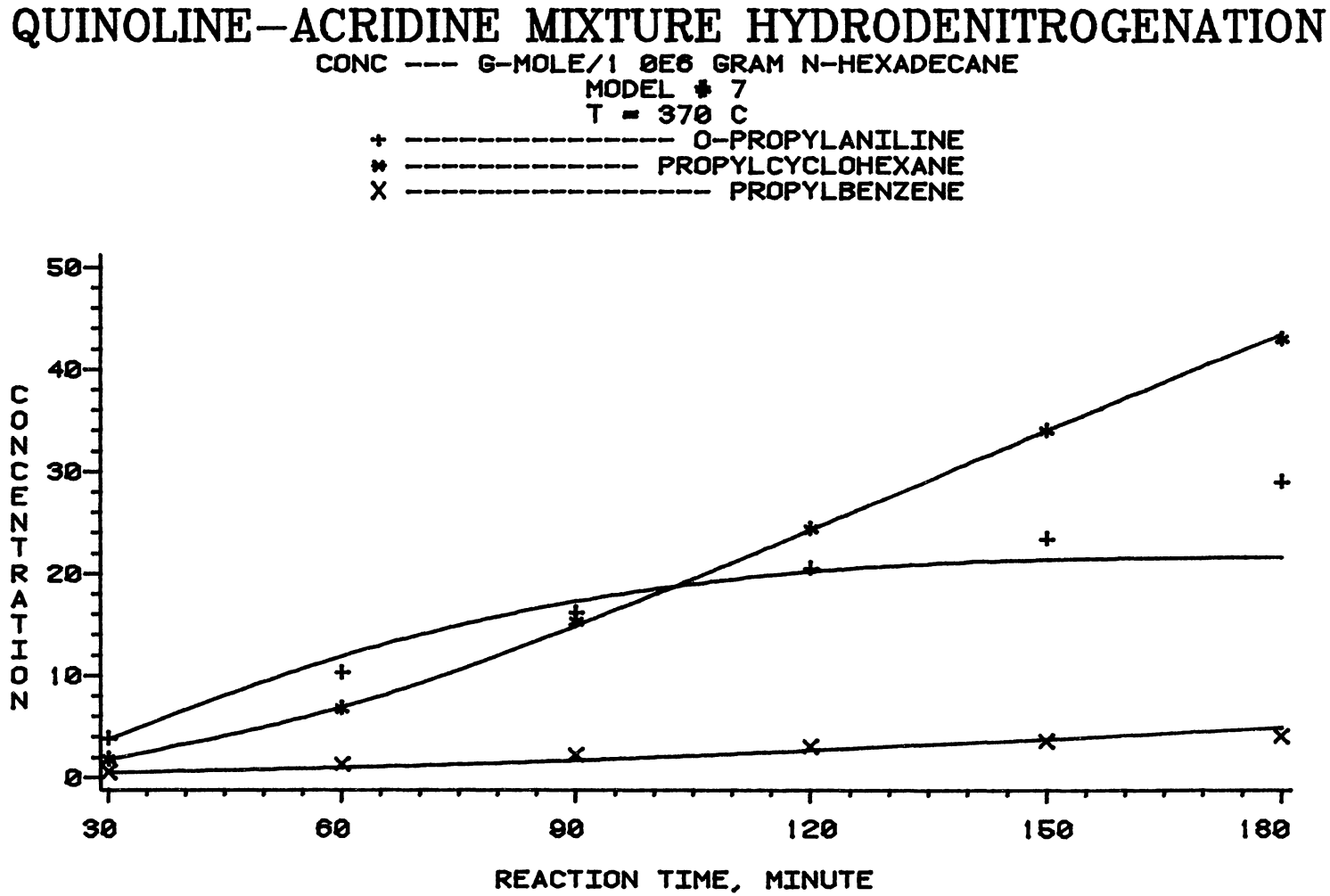

Figure 125 Quinoline-Acridine Mixture HDN Products at 370°C - Model #7

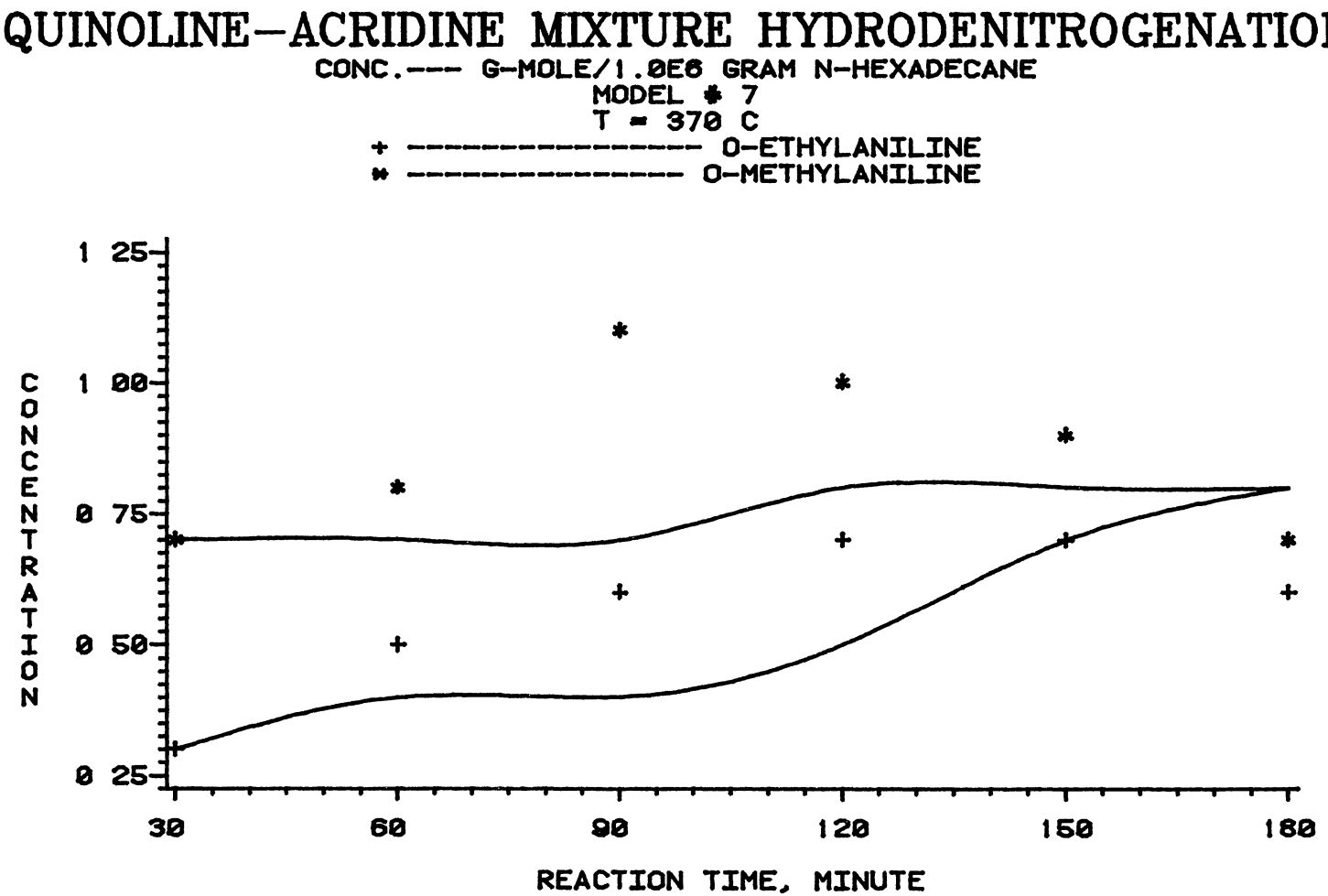

Figure 126. Quinoline-Acridine Mixture HDN Products at 370°C - Model #7

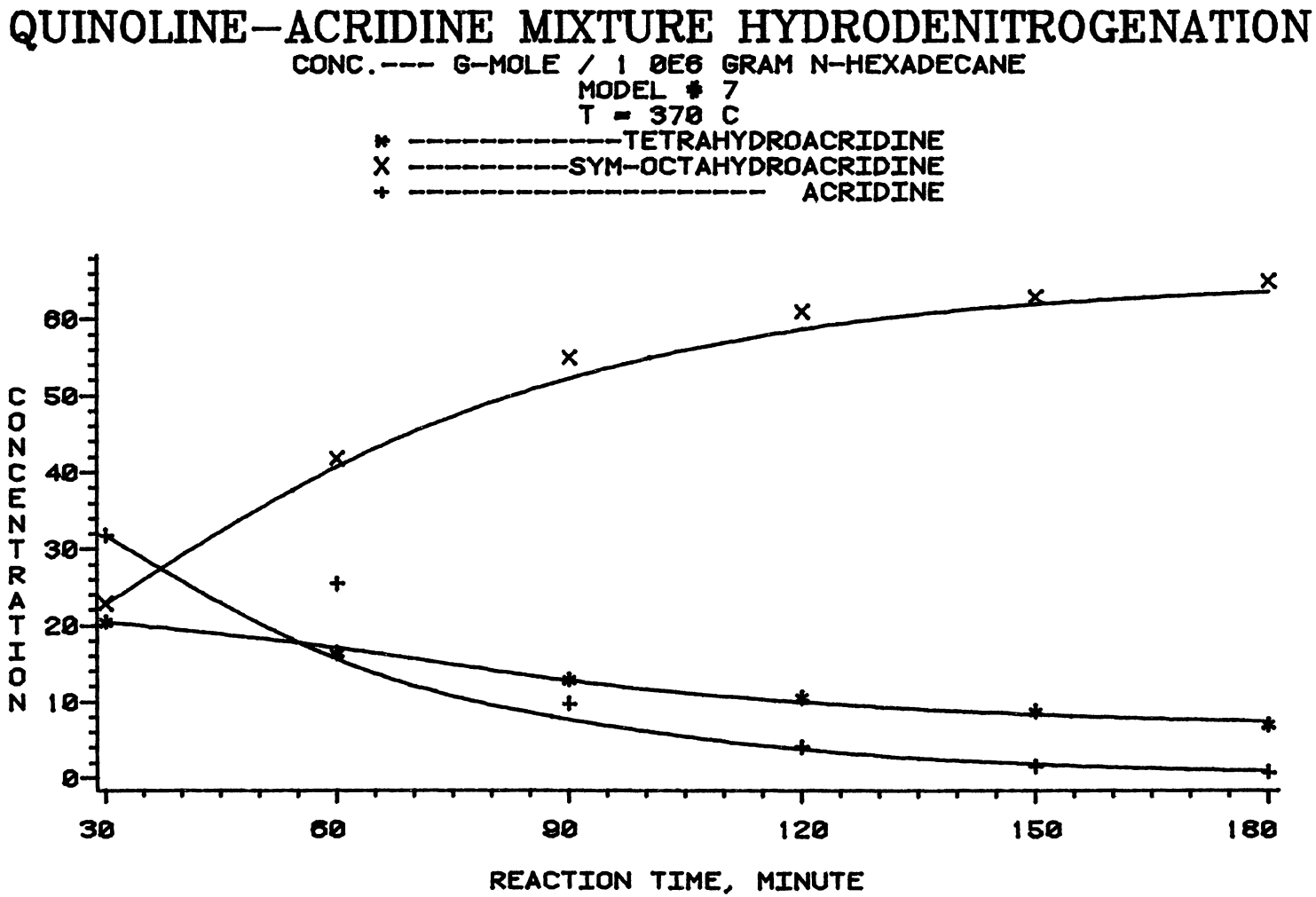

Figure 127. Quinoline-Acridine Mixture HDN Products at 370°C - Model #7

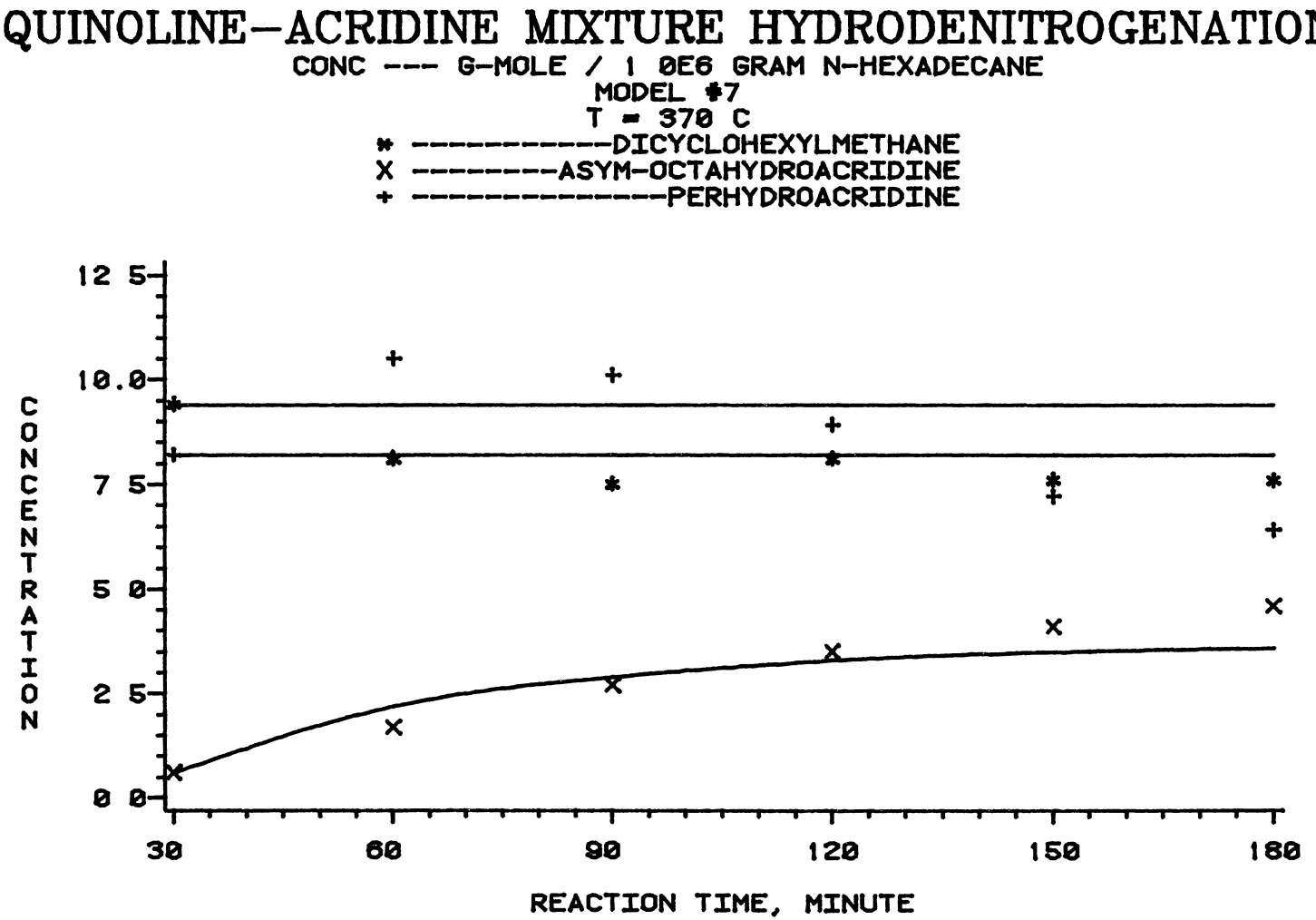

Figure 128 Quinoline-Acridine Mixture HDN Products at 370°C - Model #7

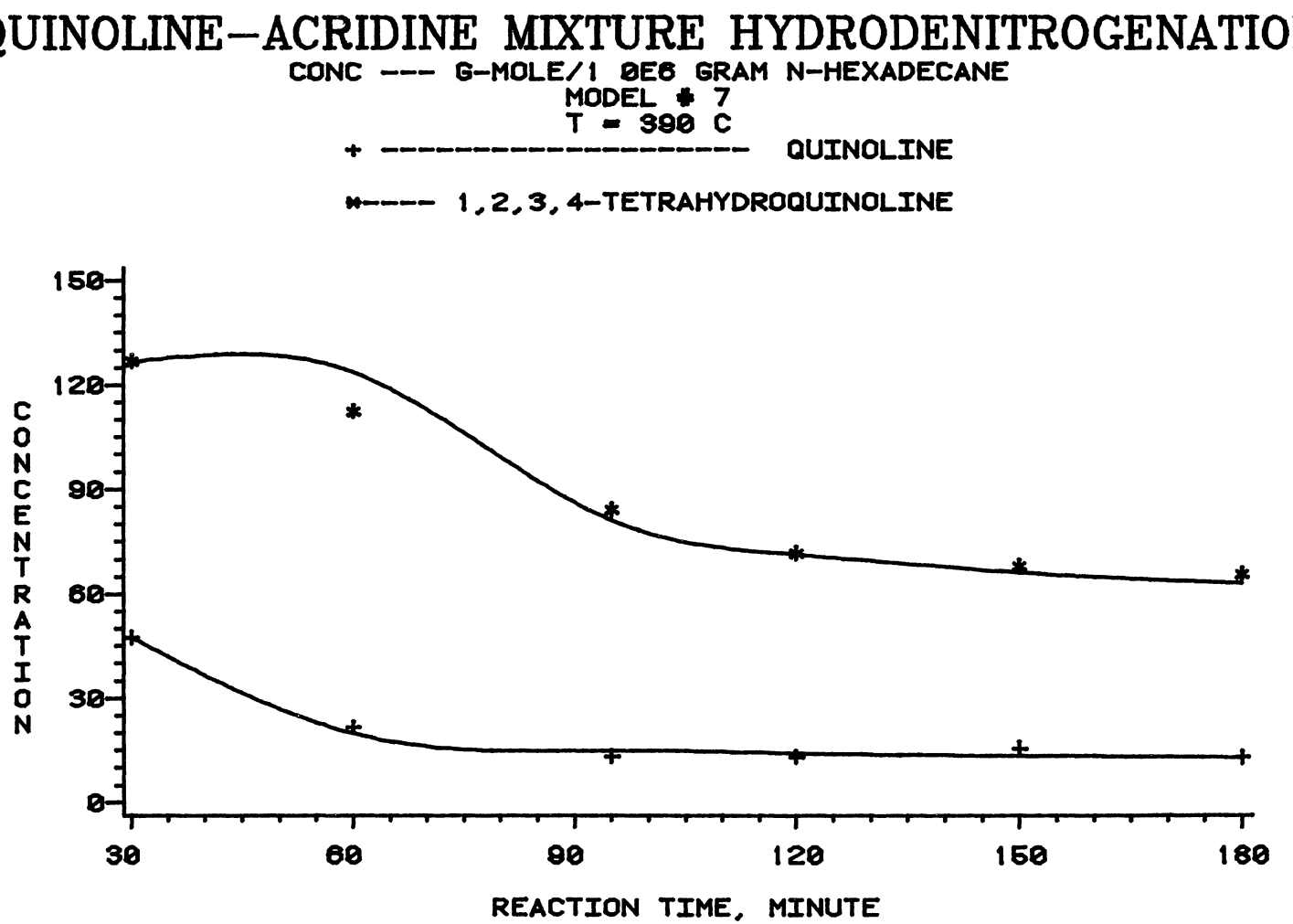

Figure 129. Quinoline-Acridine Mixture HDN Products at 390°C - Model #7

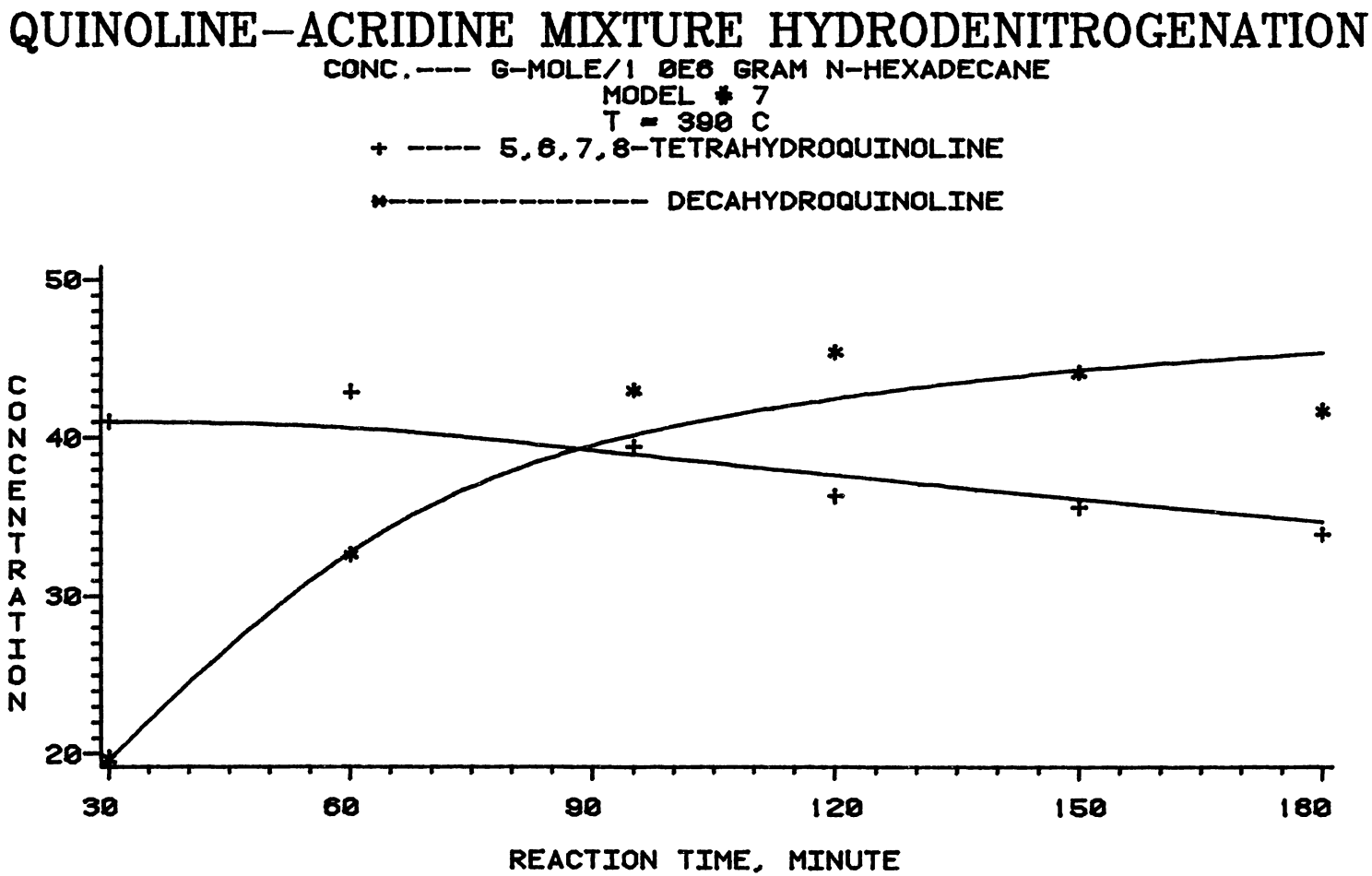

Figure 130. Quinoline-Acridine Mixture HDN Products at 390°C - Model #7

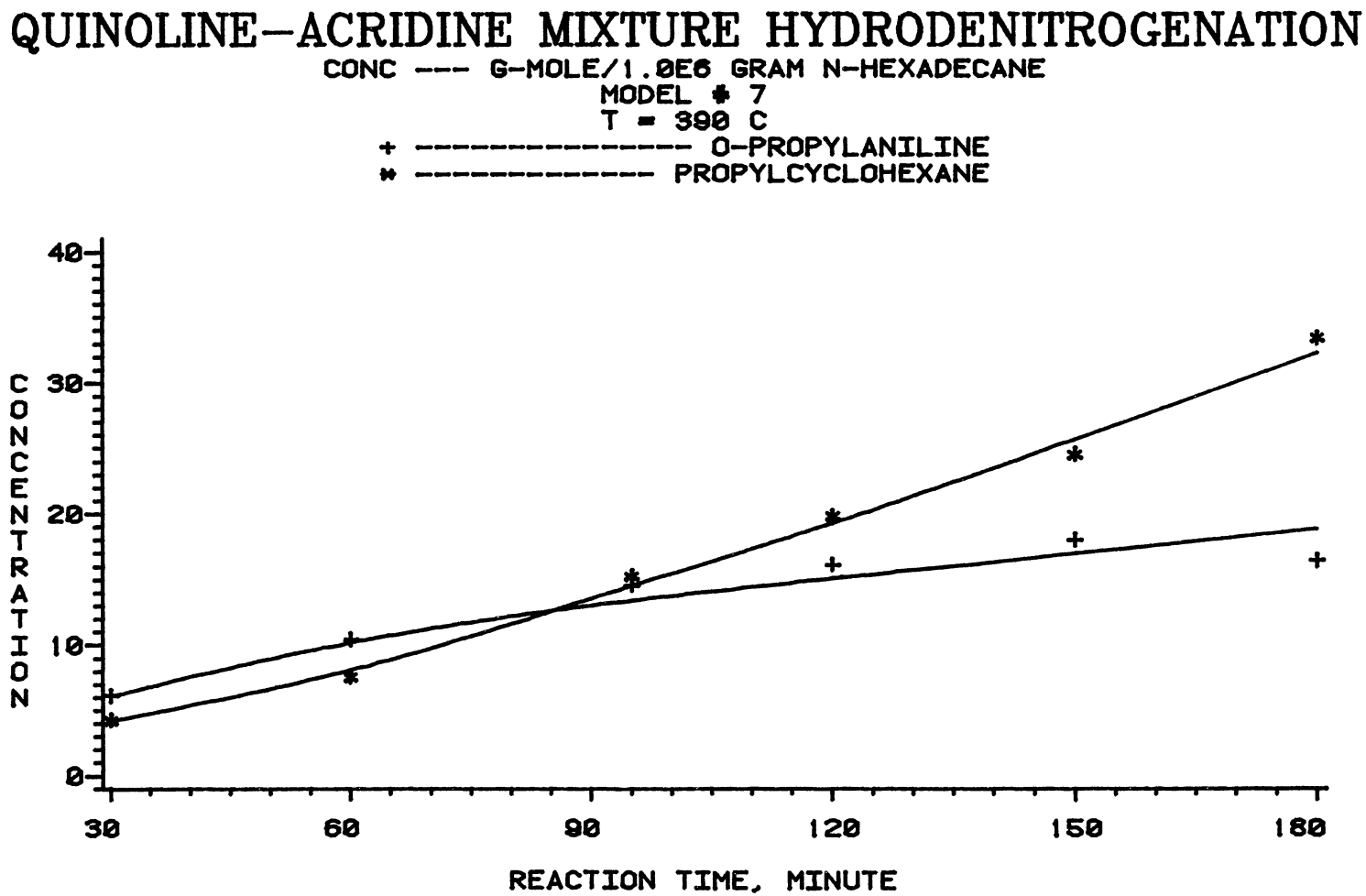

Figure 131. Quinoline-Acridine Mixture HDN Products at 390°C - Model #7

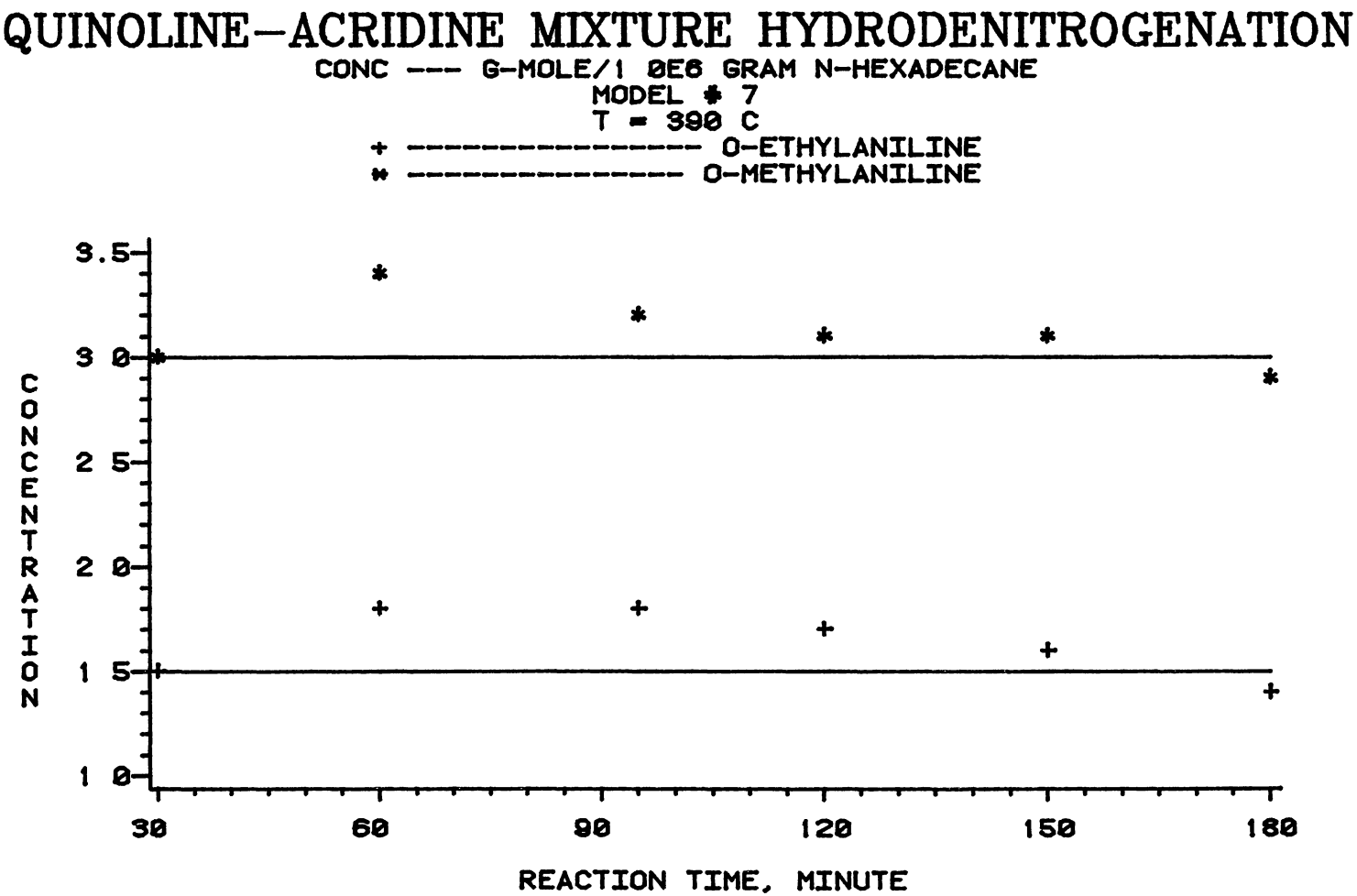

Figure 132. Quinoline-Acridine Mixture HDN Products at 390°C - Model #7

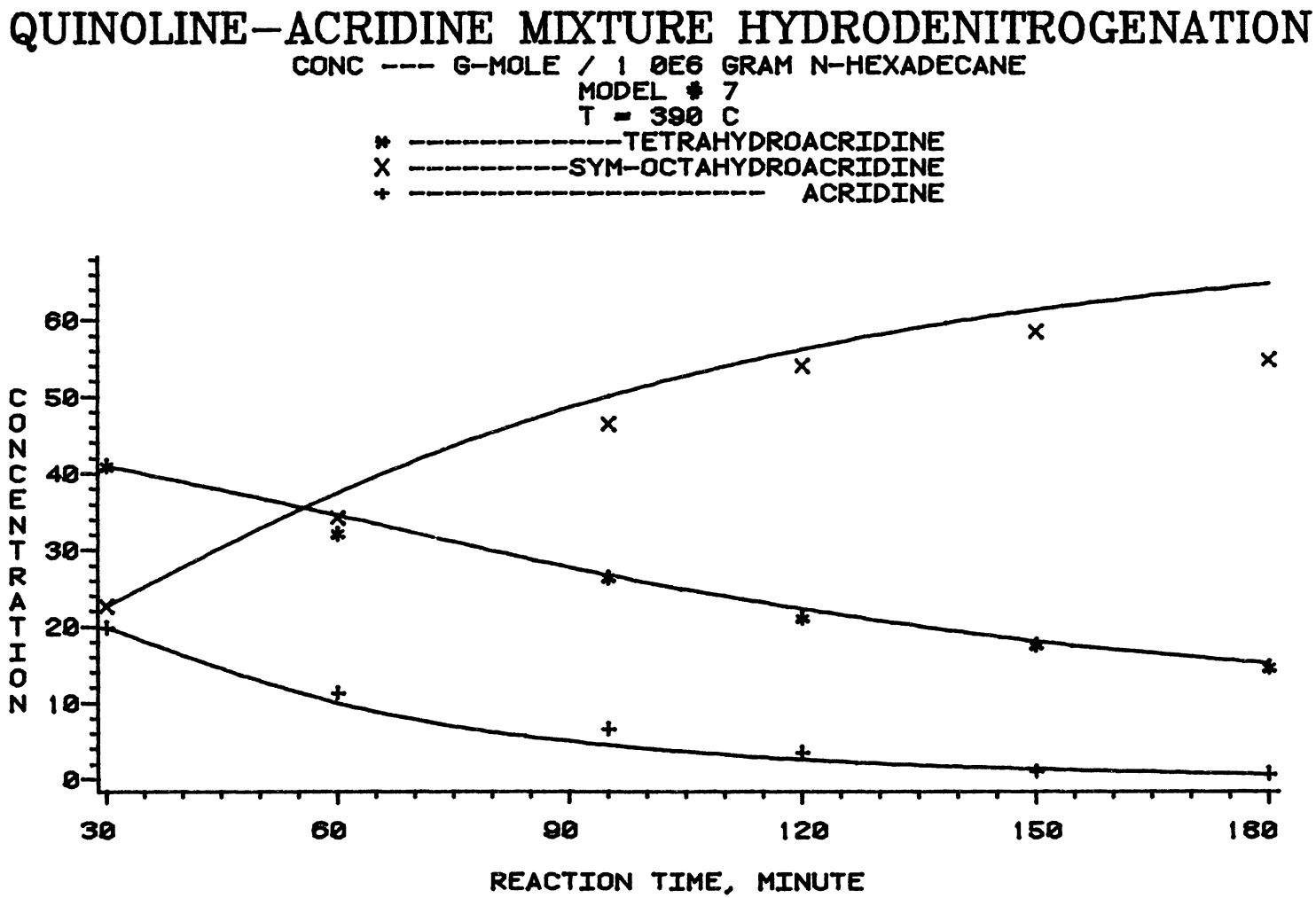

Figure 133. Quinoline-Acridine Mixture HDN Products at 390°C - Model #7

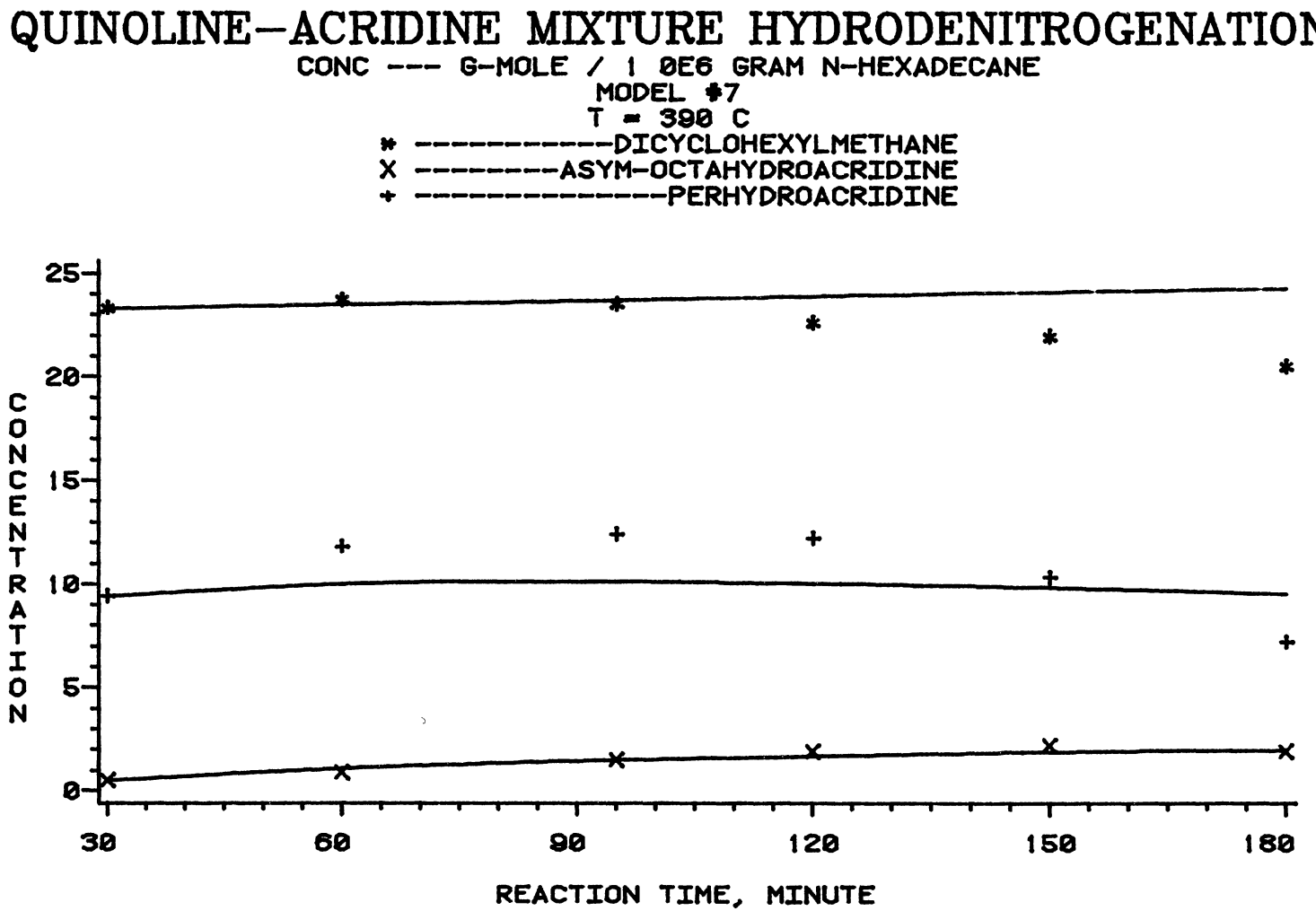

Figure 134 Quinoline-Acridine Mixture HDN Products at 390°C - Model #7

relative concentrations of quinoline, in pure quinoline and quinoline-acridine mixture HDN These results are plotted in Figure 135-137 Quinoline conversion is not affected by the presence of acridine as shown in these Figures Table XXXIX compares the relative concentrations of nitrogen of quinoline and its hydrogenation products, in pure quinoline and quinoline-acridine mixture HDN These results, presented in Figures 138-140, show that the effect of acridine on the nitrogen removal from quinoline and its derivatives is also insignificant.

From a mechanistic point of view, these effects can be observed clearly, when Table XXXIII is compared with Table XXXVI. The rate of conversion of quinoline to Py-THQ is decreased and the reaction can be considered irreversible On the other hand, the rate of conversion to Bz-THQ is increased. Also, the rate of conversion of Py-THQ to DHQ is increased This reaction path is practically irreversible Similarly, the rate of conversion of Py-THQ to OPA is increased The other reaction paths are slightly affected by the presence of acridine and its HDN products In summary, we can conclude that both the formation and the conversion of the major products of quinoline are influenced by the presence of acridine HDN products, but the overall effect of acridine on nitrogen removal from quinoline compounds is insignificant

Acridine is slightly more basic than quinoline (53) Acridine hydrogenation also produces stronger bases than

TABLE XXXVIII

RELATIVE QUINOLINE CONCENTRATIONS

Time	357°C		370°C		390°C	
	Mixture	Pure	Mixture	Pure	Mixture	Pure
0	1 00	1 00	1 00	1 00	1.00	1 00
30	----	0 367	0 157	0.203	0 127	0 131
60	0 128	0 098	0 056	0.087	0.058	0.061
90	0 052	0 051	0 034	0 056	0 035*	0 040
120	0.030	0 039	0 021	0 042	0 035	0.031
150	0 023	0 037	0 012	0 036	0 042	0.022
180	0 020	0 035	0 006	0 031	0 035	0 020

* Time = 95 minutes

itself Thus, hydrogenation products of acridine are more strongly adsorbed on the catalyst than quinoline and its HDN products. Therefore, it is expected that the presence of acridine and its products reduces the total nitrogen removal from quinoline due to competitative adsorption. However, the molecules of acridine and its HDN products are, in general, larger in size than quinoline and its HDN products This results in a steric hindrance towards the intraparticle diffusion of the reactants and hence compensates the effects of stronger basisity of acridine HDN

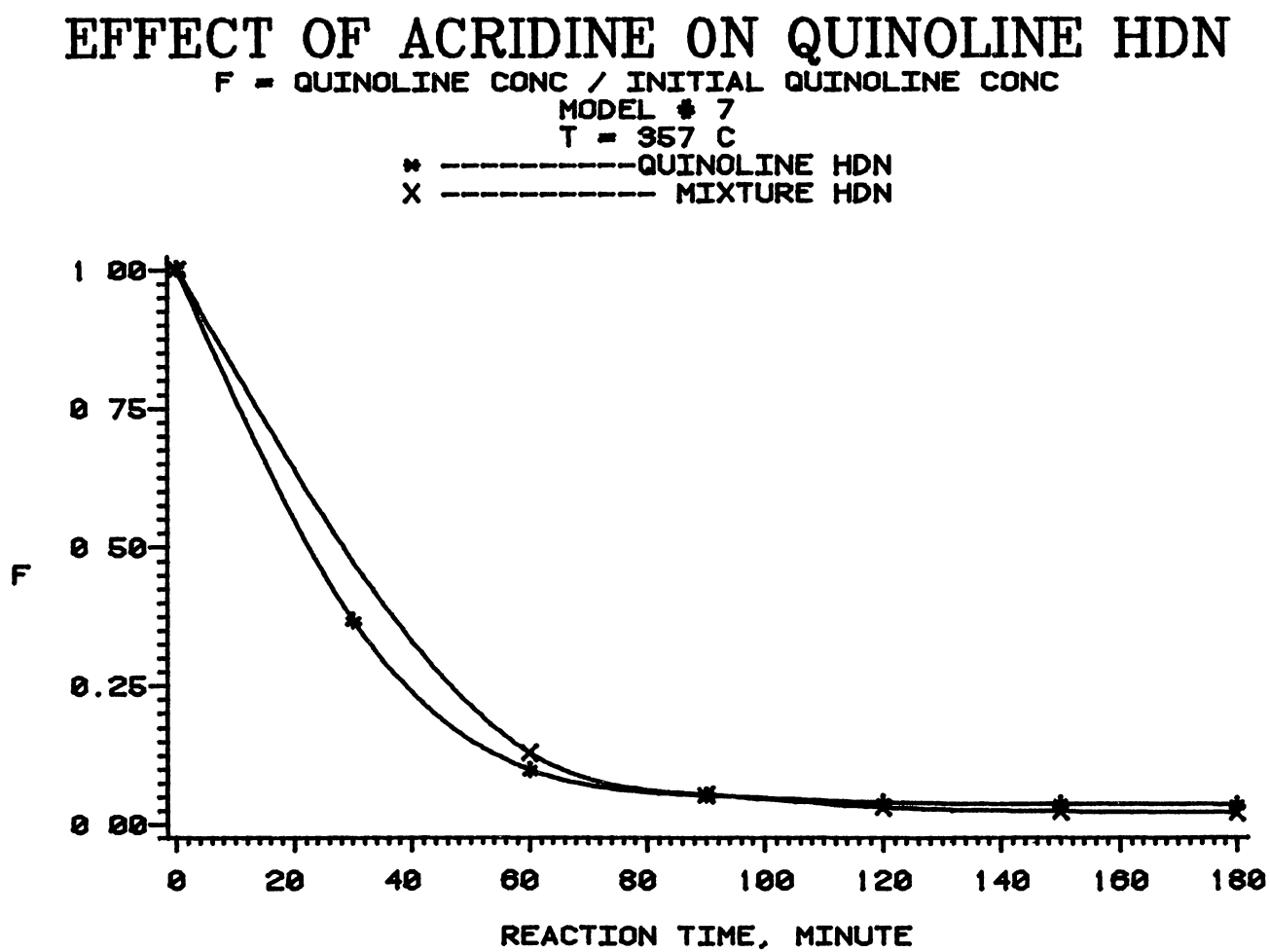

Figure 135. Effect of Acridine on Quinoline Conversion at 357°C

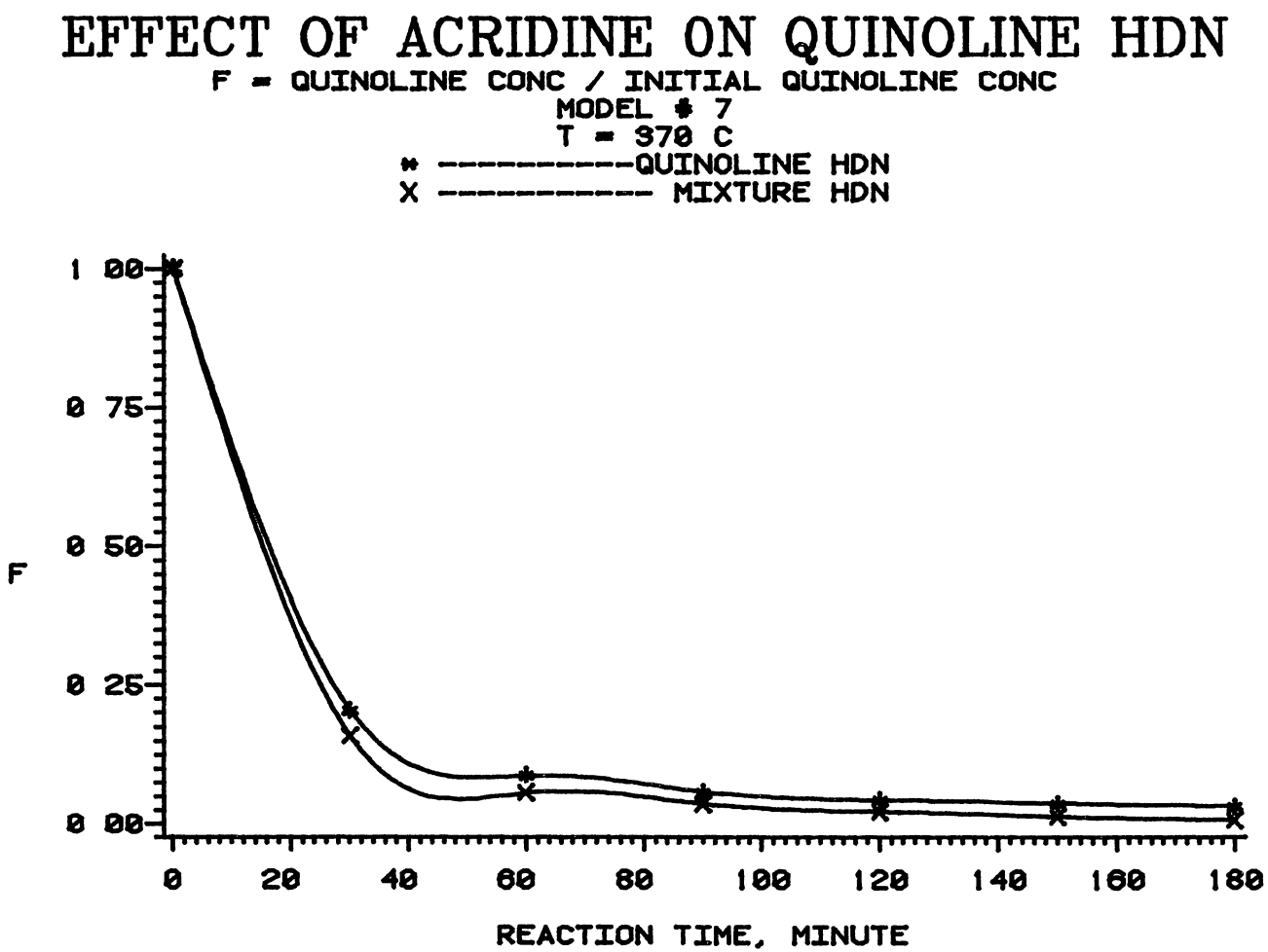

Figure 136. Effect of Acridine on Quinoline Conversion at 370°C

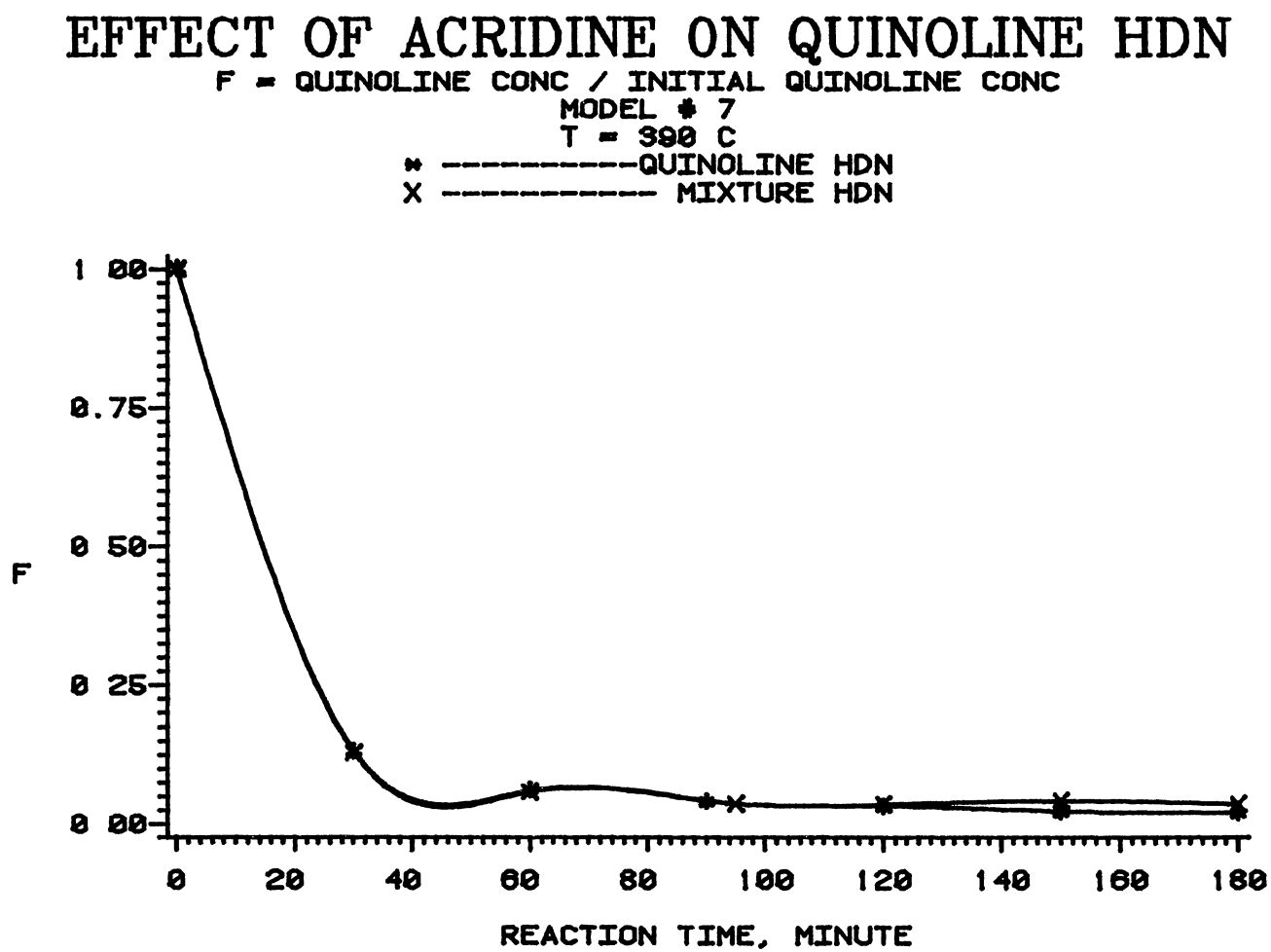

Figure 137. Effect of Acridine on Quinoline Conversion at 390°C

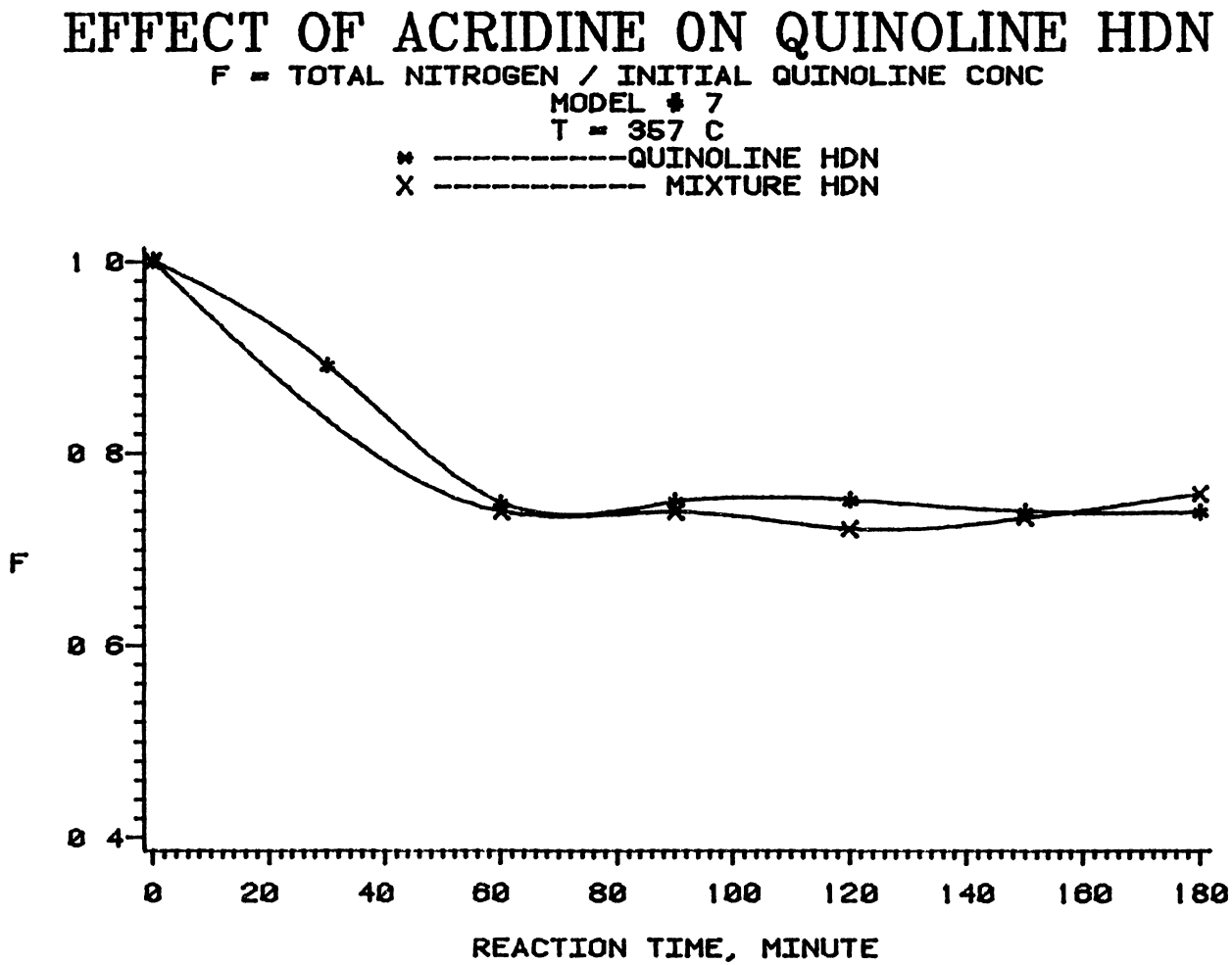

Figure 138 Effect of Acridine on Quinoline -Nitrogen Removal at 357°C

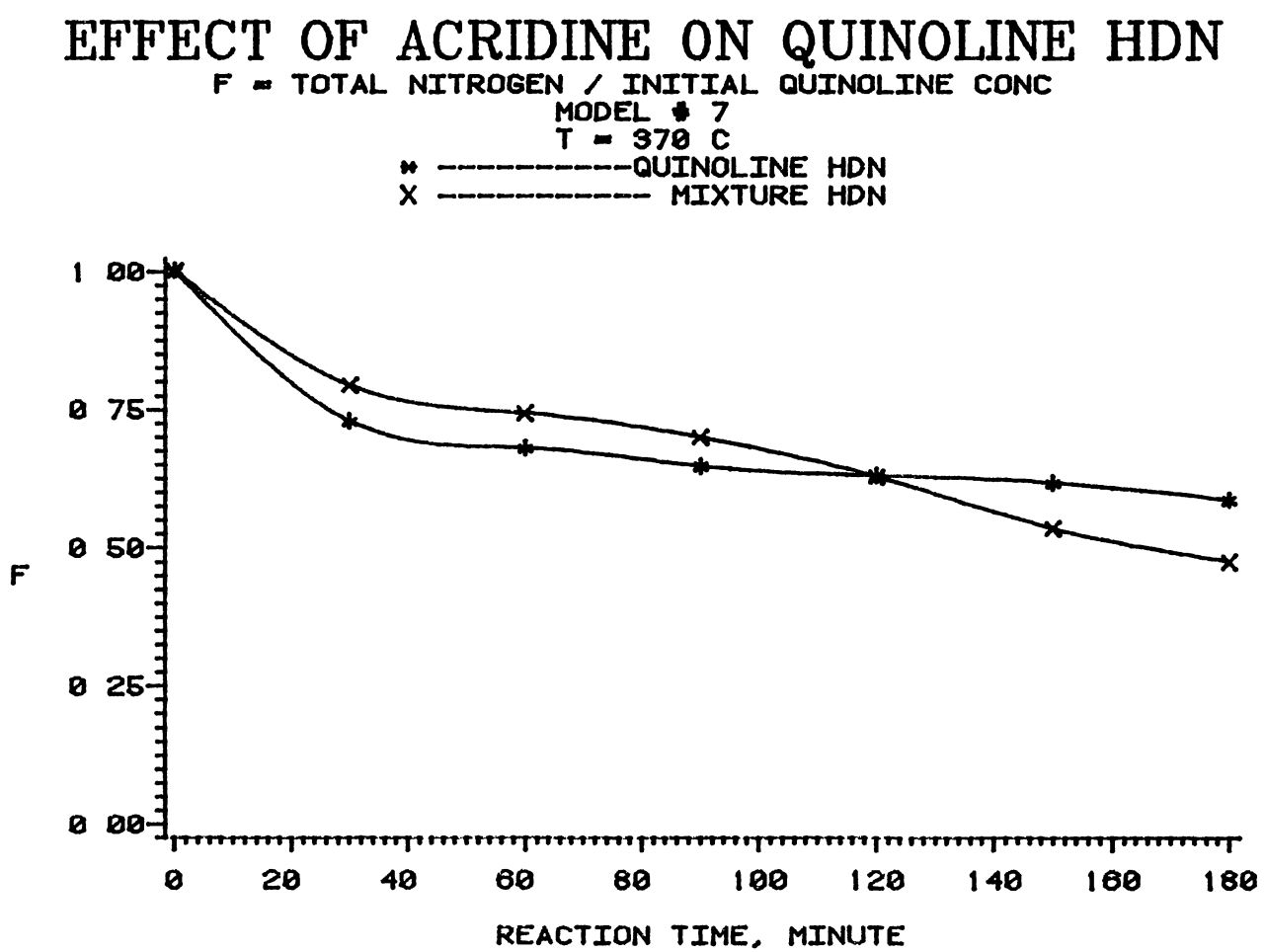

Figure 139 Effect of Acridine on Quinoline -Nitrogen Removal at 370°C

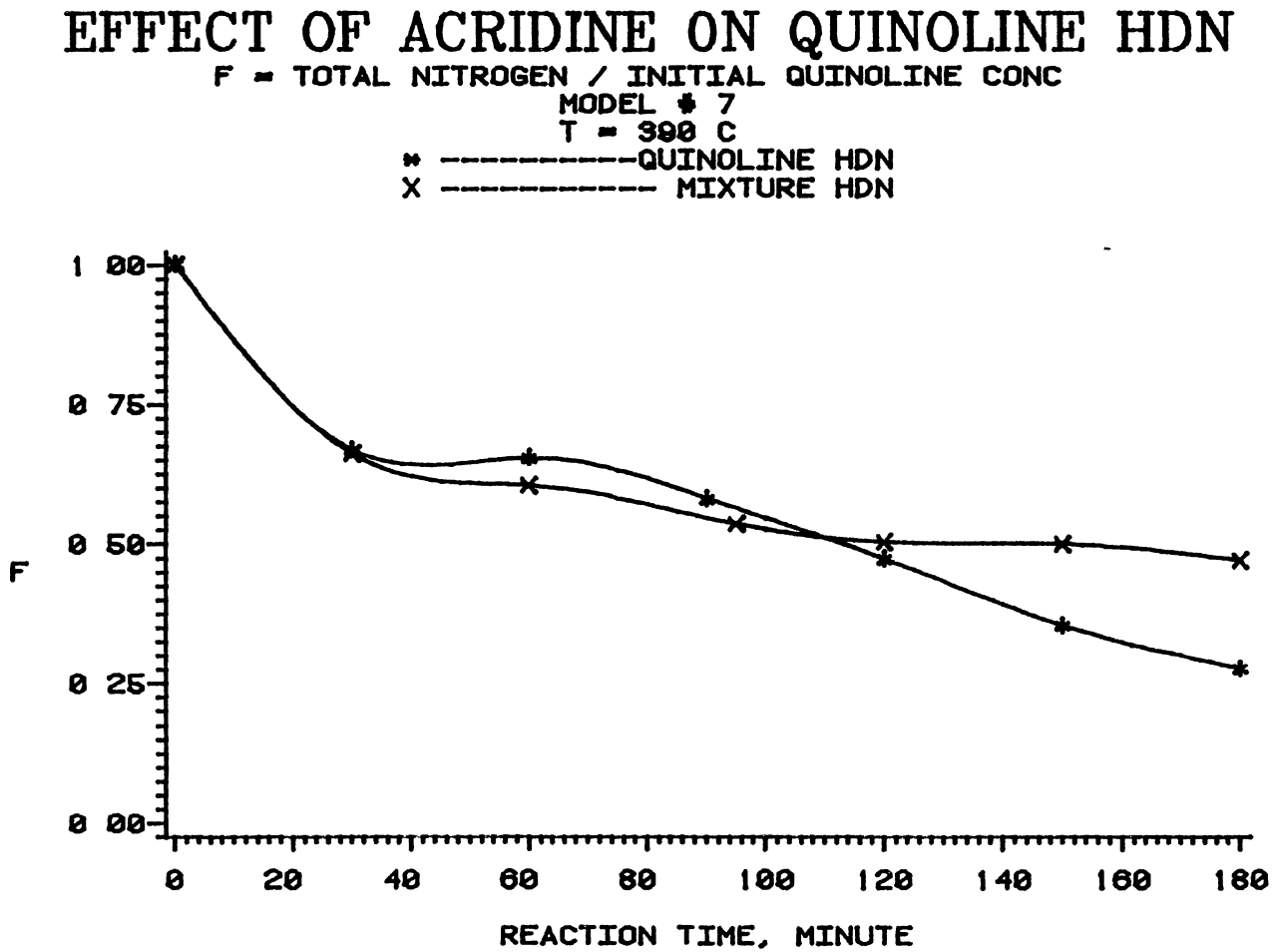

Figure 140 Effect of Acridine on Quinoline -Nitrogen Removal at 390°C

TABLE XL

RELATIVE ACRIDINE CONCENTRATIONS

Time	357°C		370°C		390°C	
	Mixture	Pure	Mixture	Pure	Mixture	Pure
0	1.00	1.00	1 00	1.00	1.00	1 00
30	----	0.184	0.307	0.152	0.194	0 152
60	0 338	0.036	0.246	0.028	0.109	0 043
90	0 253	0 012	0 094	0.012	0.064*	0 020
120	0.158	0 005	0.039	0 007	0.033	0.007
150	0.108	0.003	0.015	0.002	0.010	0 006
180	0.084	0.003	0.008	0 001	0 007	0 006

* Time = 95 minutes

143. Acridine conversion is generally decreased in the presence of quinoline. This decrease is especially significant at 357°C However, the influence of quinoline decreases with temperature as shown in Figures 141-143 From mechanistic point of view, these effects can be observed by comparing the values of kinetic parameters estimated for HDN of pure acridine (Table XXXV) and for HDN of acridine in the presence of quinoline (Table XXXVII). In the presence of quinoline, both the rate of conversion of acridine to THA, and the rate of conversion of THA to SOHA are decreased Similarly, the rate of conversion of acridine to ASOHA is decreased at 357°C, and 370°C, but is slightly increased at 390°C This reaction may be considered irreversible. In summary, all reaction paths are affected by the presence of quinoline to some extents However, the acridine conversion is significantly reduced in the presence of quinoline, due to steric hindrance discussed above

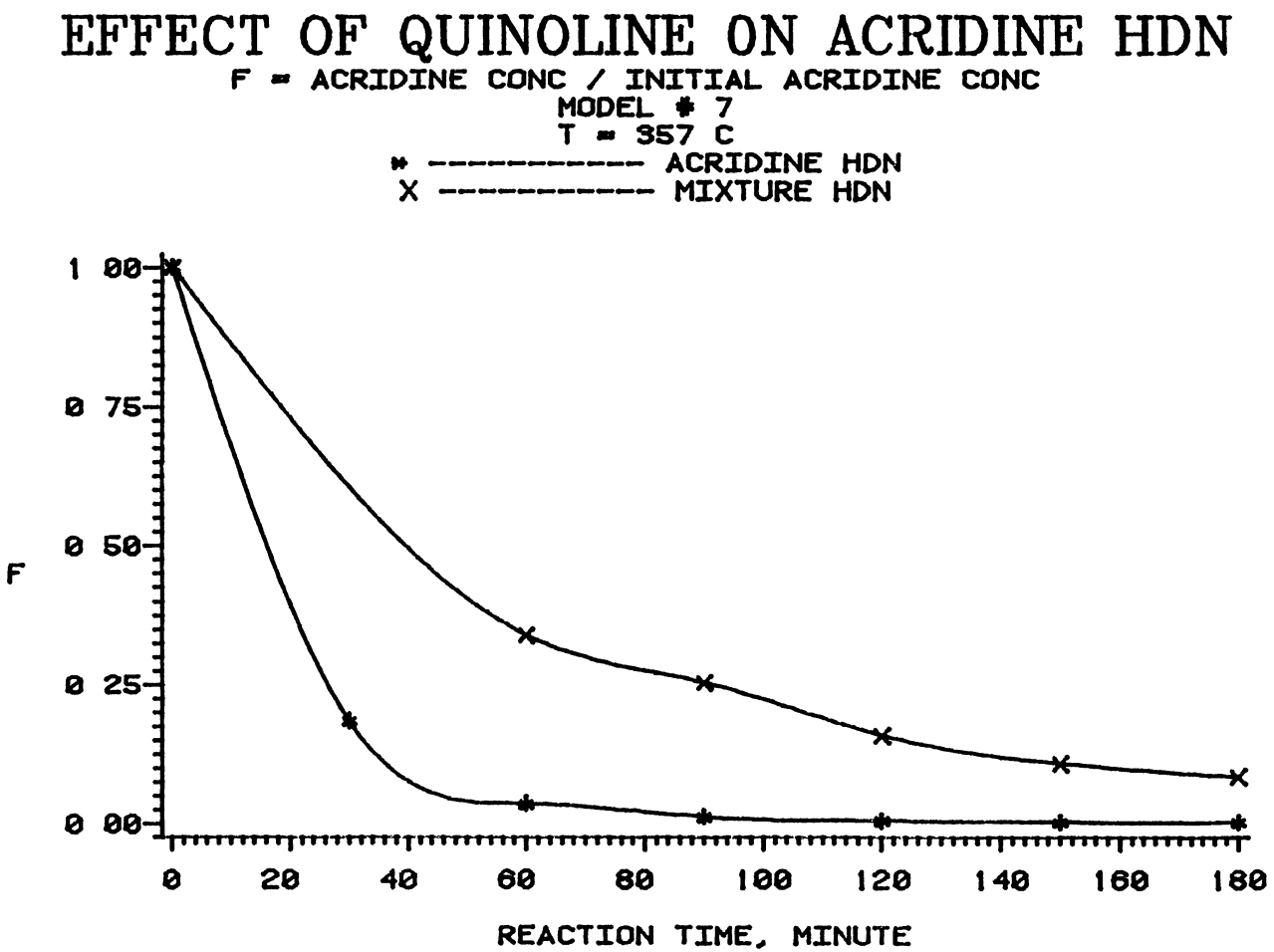

Figure 141 Effect of Quinoline on Acridine Conversion at 357°C

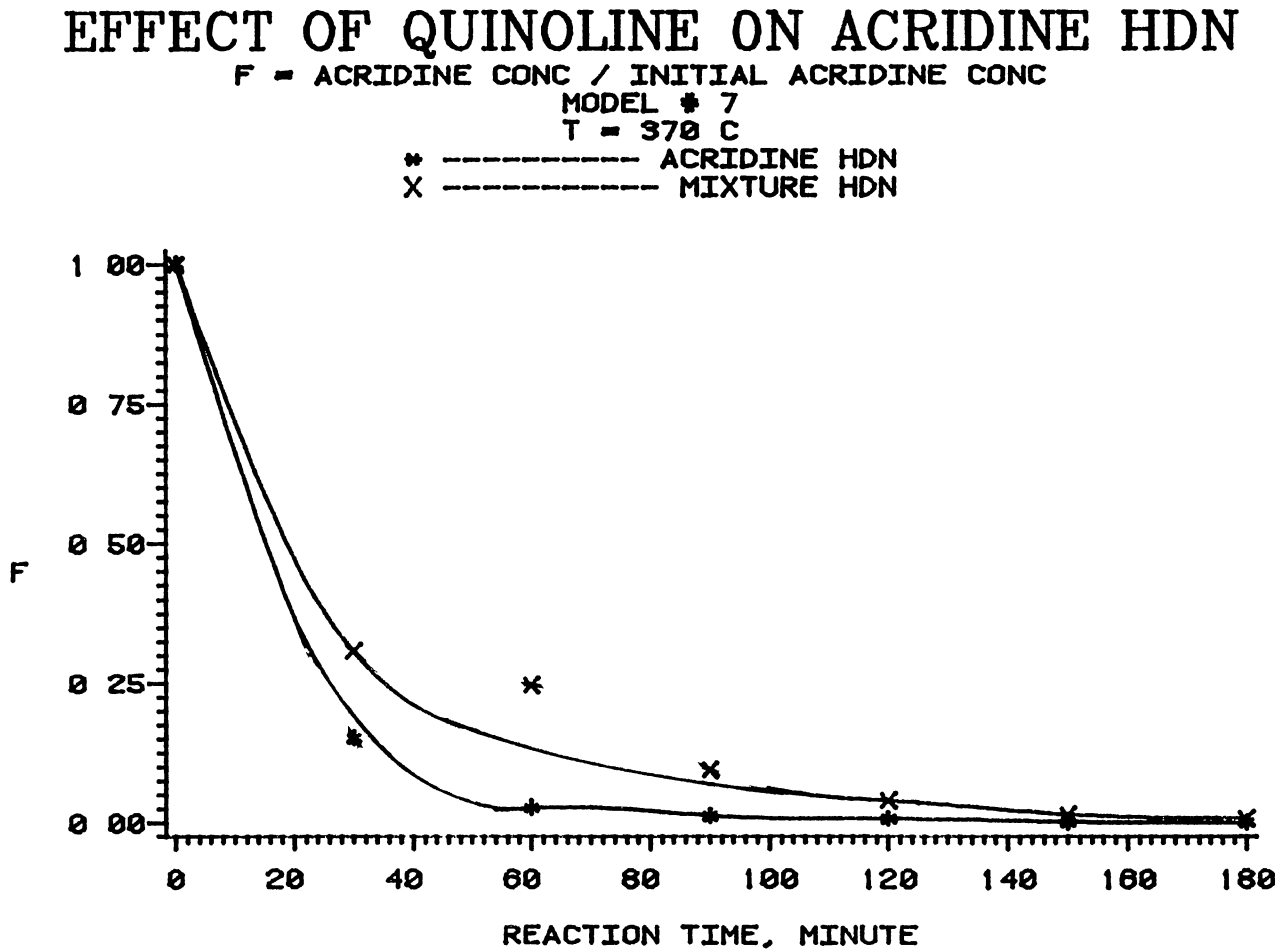

Figure 142 Effect of Quinoline on Acridine Conversion at 370°C

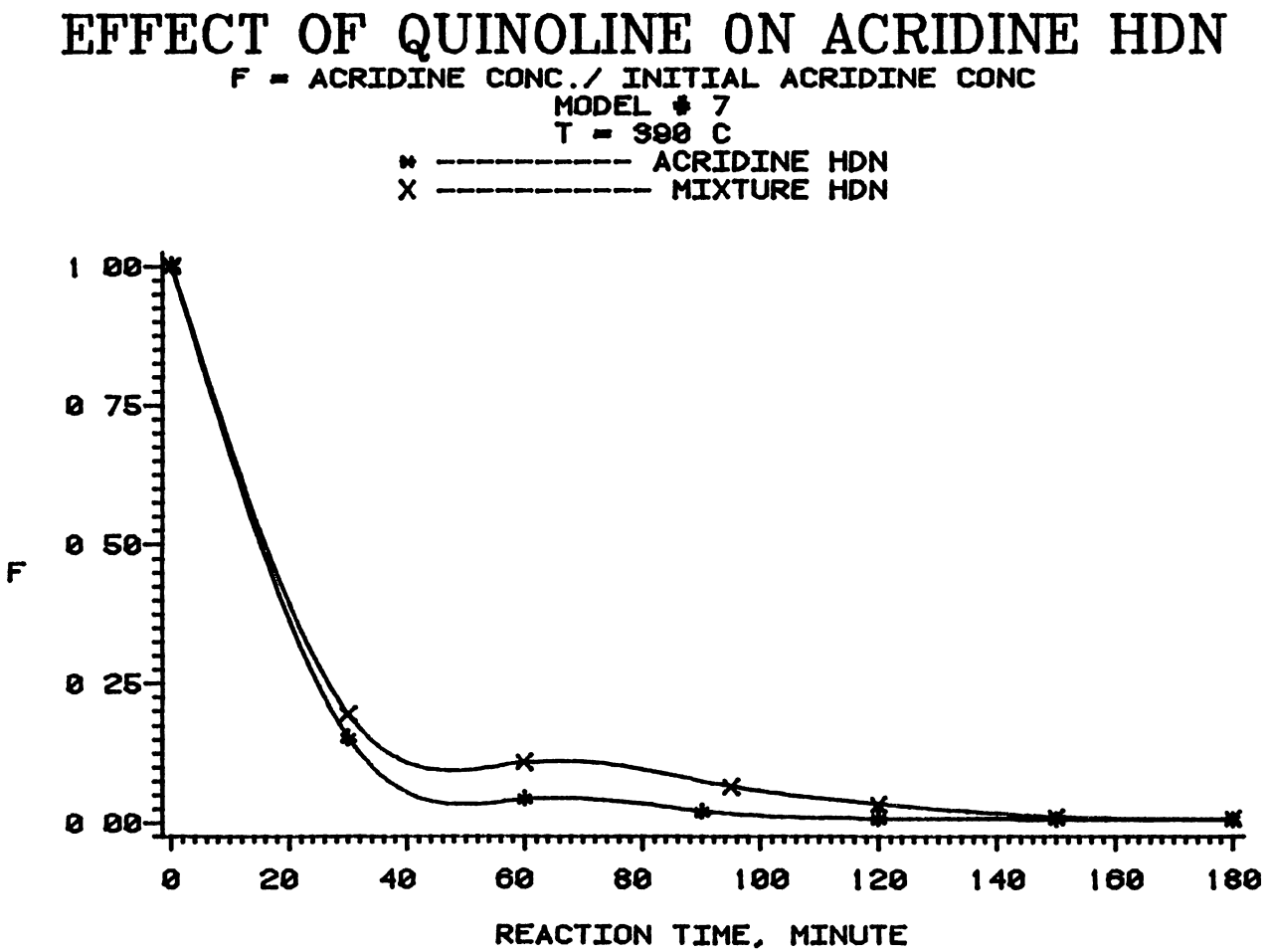

Figure 143. Effect of Quinoline on Acridine Conversion at 390°C

CHAPTER VII

CONCLUSIONS AND RECOMMENDATIONS

In this study, the HDN of quinoline, acridine, and quinoline-acridine mixture was investigated. Reaction networks were developed for both quinoline and acridine. Several models were examined to fit the data, and kinetic parameters were estimated for various models. From this work, the following conclusions were drawn.

1. The pseudo-first order model does not fit well for the rate of total nitrogen removal probably due to thermodynamic equilibrium limitations in quinoline HDN. However, a better fit is obtained in acridine HDN. Poor data fit is observed for total nitrogen removal in the quinoline-acridine mixture HDN. This poor fit may be due to one or more of the following factors: thermodynamic equilibrium, the possible few unidentified nitrogen compounds and the approximations in the response factors used for some acridine products. Model # 2 which considers the adsorption of hydrogen and nitrogen compounds on two different sites, shows the best fit for the rate of total nitrogen removal for quinoline, acridine and quinoline-acridine mixture HDN. This model assumes that the reaction occurs between the adsorbed hydrogen and nitrogen compounds to produce the

final products Model # 3, a model which resembles model #2 except that the reaction of adsorbed hydrogen with adsorbed nitrogen compounds results in an intermediate adsorbed compound does not show reasonable fit for the total nitrogen removal in quinoline HDN.

2 Model # 4 and model # 5 are used for predicting different reaction products in quinoline and HDN and for estimating kinetic parameters for these reactions. Model # 4 gives an excellent fit. This confirms the reaction network developed for quinoline HDN. Model # 5, although results in a reasonable fit, its PRE is higher than model # 4 Model # 6 shows a good fit for acridine HDN which confirms the reaction network developed for acridine HDN. Model # 7 shows an acceptable fit for quinoline-acridine mixture HDN, but some of the parameters do not show a consistent behavior with temperature.

3 Quinoline HDN mechanism is influenced by the presence of acridine and its HDN products Both the formation and the conversion of the major quinoline HDN products are affected The rate of quinoline hydrogenation to Py-THQ is decreased and the reaction becomes practically irreversible. On the other hand, the rate of quinoline hydrogenation to Bz-THQ is increased. Similarly, the rates of hydrogenation of Py-THQ to DHQ and OPA are increased. However, the overall effect of acridine on nitrogen removal from quinoline compounds is insignificant.

4 The rate of conversion of acridine is decreased appreciably at low temperatures due to the presence of quinoline and its HDN products. This decrease in the rate is lower at high temperatures. All reaction paths are affected, but to varying extents.

5. The HDN reaction temperature change in the range of 357-390°C has no significant effect on the percentage of coke deposited, whereas this percentage increases with nitrogen compound concentration.

6. The ampoule technique developed in this work is efficient in defining the zero point of the reaction and eliminating technical problems.

The following reactions are recommended for further investigations.

1 HDN of Bz-THQ to check the possibility of formation of 2-butylpyridine as an intermediate product.

2 HDN of OPA to confirm the formation of aniline, OMA and OEA

3. HDN of 9,10-dihydroacridine to identify its reaction products and thus confirm acridine HDN reaction network.

4. HDN of 1,2,3,4-THA to check the possibility of formation of quinoline as an intermediate product.

5. HDN of both SOHA and ASOHA to check the possibility of forming Bz-THQ and Py-THQ as reaction intermediates.

6 HDN of PHA to check the possibility of forming DHQ

as an ıntermedıate product.

7 HDN of mıxtures of acrıdıne and each of the nıtrogen compounds resultıng from quınolıne HDN to ıdentıfy the nıtrogen compounds whıch ınfluence the rate of conversıon of acrıdıne

Furthermore, followıng consıderatıons are also recommended

8. If possıble, GC/MS and MS/MS should be used to ıdentıfy the reactıon products

9. Develop a more precıse method for makıng the ampoules wıth unıform shapes and unıform breakıng pressure.

REFERENCES

1. Katzer, J R , Sıvasubramanıan, R. Catal Rev. Scı. Eng. 1979, 20(2), 155-208.

2. Hendrıckson, T.A "Synthetıc Fuels Data Handbook", Cameron Engıneers: Denver, Colorado, 1975.

3 Callen, R.B , Bendovıtıs, J.G., Sımpson, C A., Voltz, S.E. Ind. Eng. Chem. Prod. Res. Dev. 1976, 15, 222.

4. Oblad, A G., Mıllıken, T.H., Jr., Mılls, G A. "Advances ın Catalysıs", Acad. Press, Inc. New York, 1951, Vol. III, p 199

5. Voge, H.H., Good, G.M., Greensfelder, B S. 3 World Petroleum Congress, Hange, 1951, Sect IV, p 131

6. Sall, J W , Dart, J C Petroleum Refıner 1952, 31, 101

7 Jewell, D M., Hartung, G.K. J. Chem. Data 1964, 9(2), 297

8. Larson, O.A. Preprınts, Dıv. Petr. Chem., ACS 1967, 12(4), 3-123

9 Nıxon, A C , Cole, C.A. Mınor, H.B. J. Chem. Eng. Data 1959,4,187.

10. Word, C.C.· Schwartz, F.G. Proc. Am. Petrol. Inst 1962, 42, Sect VIII, 129.

11 Oswald, A.A., Noel, F J. Chem. Eng. Data 1961, 6(2), 294.

12. Kartzmark, R., Gılbert, J.B., Hydr. Process. and Petr Refın. 1967, 46(9), 143.

13. Snyder, L.R Preprınts, Dıv. Pet. Chem., ACS, 1970, 4 (2), C43.

14. Nıxon, A.C., Thorpe, R.E. J. Chem. Eng Data 1962, 7, 429.

15. Jewell, D.M., Hartung, G.K. J. Chem. Eng Data 1957, 2, 95.

16 Scheppele, S.E., Greenwood, G J., Benson, P.A. Anal. Chem. 1977, 49, 1847.

17 Aczel, T , Lumpkın, H.E Preprınts, Dıv Pet. Chem., ACS 1977, 22(3), 911

18 Schultz, J L., Frıedel, R A , Sharkey, A G. Jr , "Mass Spectrometrıc Analysıs of Coal Tar Dıstıllates and Resıdues", U.S., Bur. Mınes, Rep. Invest., 7000 (1967).

19. Seapan, M., Crynes, B.L. DOE/BC/10306-11

20. Shah, Y T., Stıgel, G.J., Krıshnamurthy, S Amerıcan Institute of Physıcs 1981, 256.

21 Schıller, J.E Hydrocarbon Processıng 1977, 57(1), 147.

22. Krıshnamurthy, S., Shah, Y. T. , Stıegel, G.J. Fuel (ın press).

23. Akhtar, S., Sharkey, A.G., Shultz, J.L., Yavorsky, P.M. Preprınts, Dıv. of Fuel Chem, ACS 1974, 19(1), 207.

24. Rollmann, L.D. J Catal. 1977,46,243

25 Satterfıeld, C.N., Modell, M., Mayer, J F AIChE J 1975, 21, 1100.

26. Sonnemans, J., Mars, P. J.Catal. 1974, 34, 215.

27 Goudrıaan, F., Gıerman, H., Vlugter, J C. J Inst. Petrol. (London) 1973, 59, 40.

28. Shıh, S.S., Katzer, J R. Kwart, H., Stıles, A B Preprınts, Dıv. Pet. Chem. ACS 1977, 22(3), 919

29 Aboul-Gheıt, A.K., Abdou, I.K. J. Inst. Perol. (London) 1973, 59, 188.

30. Aboul-Gheıt, A.K. Can. J. Chem. 1975, 53, 2575.

31 Sonnemans, J., Vandeberg, G.H., Mars, P.J. Catal. 1973, 31, 220.

32. Satterfıeld, C.N., Cochetto, J.F. AICHE J. 1975, 21, 1107.

33 Sonnemans, J., Neyens, W.J , Mars, P.J.Catal. 1974, 34, 230.

34. Nelson, N., Levy, R B. J. Catal. 1979, 58, 485

35. Cox, K.E Ph.D. Thesıs, Montana State College, Bozeman, Montana, 1961.

36. McIlvrıed,H.G. Ind. Eng. Chem., Proc Des. Dev. 1971, 10, 1, 125.

37 Flınn, R.A., Larson, O.A., Beuther, H. Hydrocarbon Process Petrol Refıner 1963, 42, 129.

38. Doelman, J., Vlugter, J.C. Proc. World Petrol Congr , 6th, Frankfurt, Germany, Sect. III, 1963

39. Nıxon, A C , Thrope, R.E. Preprınts, Dıv. Pet. Chem., ACS 1956,1(3), 265.

40. Anabtawı, J.A., Mann, R.S., Khulbe, K.C. J Catal. 1980, 63, 456.

41. Satterfıeld, C N.; Model, M., Wllkens, J.A. Ind. Eng. Chem., Proc. Des. Dev. 1980, 19, 154

42. Kobe, K.A., McKetta, J.J.Jr. Advan. Petol Chem. Reınıng 1960,3, Chap. V.

43. Satterfıeld, C.N , Model, M , Hıtes, R.A., Declerck, C J Ind. Eng. Chem. Proc Des. Dev 1978, 17(2), 141.

44. Bhınde, M.V. Ph D. Thesıs, Unıversıty of Delaware, Delaware, 1979

45. Cocchetto, J.F , Satterfıeld, C.N. Ind. Eng. Chem., Proc. Des. Dev. 1981, 20, 49.

46. Satterfıeld, C.N., Cocchetto, J F. Ind. Eng Chem., Proc. Des. Dev. 1981,20,53.

47. Satterfıeld, C.N.; Gültekln, S. Ind. Eng. Chem , Proc. Des. Dev. 1965, 4, 177.

48. Satterfıeld, C.N., Carter, D.L. Ind. Eng. Chem., Proc. Des. Dev. 1981, 20, 538.

49. Satterfıeld, C.N., Yang, S.H. Ind. Eng. Chem., Proc. Des. Dev. 1984, 23, 11

50. Yang, S.H., Satterfıeld, C.N. Ind. Eng. Chem., Proc Des Dev. 1984, 23, 20.

51 Satterfıeld, C.N., Smıth, C.M. Quarterly Report, DOE/PC60798-4.

52. Miller, J.T., Hineman, M.F. J Catal. 1984, 85, 117

53. Gates, B. C., Katzer, J.R , Oslon, J H., Kwart, H., Stiles, A.B. Quarterly Report, Fe-2028-12, 1978.

54. Nagai, M., Sawahiraki, K., Kabe, T. Nippon Kagaku Kaishi 1979, 10, 1350.

55 Qader, S.A., Wiser, W.H., Hill, G R. Ind. Eng Chem., Proc. Des. Dev. 1968, 7, 3, 390.

56. Ryffel, J R. Ph.D Dissertation, Montana State College, Bozeman, Montana, 1961.

57. Rosenheimer, M.O., Kiovsky, J R. Preprints, Div. Pet Chem , ACS 1967, 12,(4), B-147.

58. Cox, K.E., Berg, L. Chem Eng. Prog. 1962, 58(12), 54.

59. Aboul-Gheit, A.K. Rev. Inst. Mex. Pet. 1979, 11(3),72.

60. Stern, E.W. J Catal. 1979, 57, 390.

61. Gates, B.C., Katzer, J.R., Oslon, J.H., Kwart, H., Stiles, A.B Quarterly Report, FE-2028-17, 1979.

62. Thakkar, V.P., Baldwin, R.M., Bain, R.L Fuel Processing Technology 1981, 4, 235.

63. Nagai, M., Sawahiraki, K., Kabe, T. Nippon Kagaku Kaishi 1980, 1, 69.

64. Qader, S.A., Hill, G.R. Ind. Eng. Chem., Proc. Des. Dev. 1969, 8(4), 457.

65. Qader, S.A., Wiser, W.H., Hill, G.R. Fuel 1972, 54, 51

66. Schneider, A., Hollstein, E.J., Janoski, E.J., Janoski, E.J., Scheibel E.G. Quarterly Technical Progress Report FE-2306-35, 1979.

67. White, P.G., Jones, J.F , Eddinger, R T. Hydrocarbon Processing 1968, 97(12), 47.

68. Jacobs, H.E.; Jones, J.E., Eddinger, R T Ind. Eng. Chem. Proc. Des. Dev. 1971, 10(4), 558.

69. Ahmed, M.M. Ph.D. Dissertation, Oklahoma State University, Stillwater, Oklahoma, 1979.

70. Sivsubramanian, R. Ph.D. Dissertation, Oklahoma State University, Stillwater, Ok. 1977.

71. Satchell, D.P Ph D Dissertation, Oklahoma State University, Stillwater, Ok. 1974.

72. Heck, R H., Stein, T R. Preprints, Div Pet. Chem., ACS 1977, 22(3), 948

73 Stein, T R et al. Annual Report EPRI-AF-873, 1978.

74 Soni, D S , Crynes, B L Symp Series, ACS 1981, 156, 207

75. Gary, J.H., Golden, J O , Bain, R.L., Dickerhoof, D.W Department of Energy Report FE-2047-10, 1978.

76. Flinn, R.A , Larson, O.A., Beuther, H. Hydrocarbon Processing 1968, 97(12), 47.

77. Shih, S S , Angevine, P.J , Heck, R.H , Sawruk, S Preprints, Div. of Fuel Chem. 1980, 25(1), 152.

78. Kang, C C Adv Chem. Ser. 1979, 179, 193.

79. Furimsky, E. Ind. Eng. Chem., Prod. Res Dev. 1979, 18(3), 206.

80 Nagai, M., Kabe, T Nippon Kagaku Kaishi 1983, 11,1634.

81. Olalde, A , Perot, G Applied Catalysis 1985,13, 373, Elsevier Science Publishers B.V., Amsterdam

82 Adkins, H , Connradt, H.L J. Org. Chem. 1941, 63, 63,1563

83. Ponomarev, A.A , Chegolya, A.S Dyukareva, V.N Khim. Geterotisikl. Soedin, Akad Nauk. Latv. SSR 1966,00,239.

84. Graebe, C. Chem. Ber. 1883,16,2828.

85. Birch, A.J., Mantsch, H H , Aust J Chem. 1969, 22,1103.

86 Masamune, T., Wakamatsu, S. J. Fac Sci. Hokkaido Univ. 1957,5,47,Ser.III, Chem Abstr. 1958, 52, 11850.

87. Masamune, T., Homma, G. J. Fac. Sci Hokkaido Univ. 1957,5,64, Ser.III, Chem. Abstr. 1958,52,14581

88. Graebe, C , Caro, H. Justus Liebigs Ann Chem. 1871,158,265.

89 Perkin, W.H., Sedgwick, W G. J Chem Soc. 1924, 2437.

90 Perkın, W G., Plant, S G P J Chem Soc. 1928, 2583

91 Ermolaeva, V G., Yashunskıı, V G., Polzhaeva, A. I., Mashkovkıı, M D. Khım-Farm Zh 1968,2,20.

92 Hayashı, E., Nagao, T Yakugaku Zasshı 1964,84, 198, Chem. Abstr. 1964,61,3071.

93 Klımov, G a , Tılıchenko, M N., Karaulov, E S Khım Geterotsıkl Soedın 1969,2,297

94 Tılıchenko, M N , Vysotskıı, V.I Dokl Akad Nauk SSSR 1958,119,1162.

95 Kamınskıı, V A , Tılıchenko, M N Khım. Geterotsıkl. Soedın 1967,4,708

96 Kamınskıı, V A , Vysotskıı, V I , Tılıchenko, M.N Khım Geterotsıkl Soedın. 1969,2,273

97 Klımov, G.A., Tılıchenko, M N Khım. Geterotsıkl. Soedın 1967,1,306.

98. Freımıller, L R , Nemec, J.W U S Patent 3,326, 917, Chem. Abstr 1968,68,49469c.

99. Stonık, V A., Klımov, G A., Vystotskıı, V I , Tılıchenko, M.N Khım. Geterotsıkl Soedın. 1969,5, 953

100 Masamune, T., Ohno, M., Takenura,K , Ohuchı, S Bull Chem Soc Japan 1968,41,2458.

101 Hartung, G.K., Jewell, D.M. Analytıca Chımıca Acta 1962, 26, 514.

102. Hartung, G.K , Jewell, D M. Analytıca Chımıca Acta 1962, 27, 219

103 Ternan, M , Furımsky, E., Parsons, B I Fuel Processıng Technology, Elsevıer Scıentıfıc Publıshıng Company, Amsterdam 1979, 2, 45.

104 Wentrcek, P R , Wood, B J , Wıse, H J Catal 1976, 43, 363

105. Blakely, D.W., Somorjaı, G.A J Catal 1976, 42, 181

106 Mıloudı, A , Duprez, D , Bastıck, J C R Acad Scı , Ser C 1976, 282, 183

107 Jackson, L.W. M S. Thesıs, Oklahoma State Unıversıty, Stıllwater, Ok., 1978.

108. Albert, D.K. Analytıcal Chemıstry 1978, Nov, 50, 1822.

109 Clayton, G D., Clayton, F E. "Palty's Industrıal Hygıene and Toxıcology", John Wıley and Sons New York, 1981

110. Sax, N.I. "Handbook of Dangerous Materıals", Reınhold Publıshıng Co New York, 1951.

111. Froment, G F , Bıschoff, K.B. "Chemıcal Reactor Analysıs and Desıgn", John Wıley and Sons. New York, 1979.

112. Reıd, R C , Prausnıtz, J.M , Sherwood, T K. "The Properties of Gases and Lıquıds"; McGraw Hıll Book Co New York, 1977.

APPENDIX A

SPECIFICATIONS OF MAIN VALVES AND ACCESSORIES

TABLE XLI

MAIN VALVES

Valve Type	Company	Valve #	Part #	Notes
Shut off valve	AE	2,16,19, 24,26,27, 30,34	6V71U4-TG*	2-way straight
	AE	13,15	6V72U4-TG	2-way angle
Shut off and Regulating	PH	22	316R202B	
	Whitey	35,36,37	IRM4-S4	
	AE	1,3,6,7	6V81U4-TG	2-way straight
	AE	31	6V82U4-TG	2-way angle
	Parker	32	4Z-V4LR-SS	
	Parker	21,23,38	2Z-V4LR-SS	
Vee Stem	AE	11,18	30VM-4072 HT-46672 P-755	High temperature Packing
	HEX	9,10,12,14	2OUV41V-GR**	

TABLE XLI (continued)

Valve Type	Company	Valve #	Part #	Notes
Micrometering valve	AE	17,20	30VRMM-4812 -TG	2-way, angle
	AE	8	30VRMM-4872 -HT-TG	High Temperature extended stuffing box.
O-Ring check valve	AE	5,29,33	UKO 4400	
Inline safety relief valve	Circle Seal	25,28	5132T-2MP -2000	303-SS, 13.8 MPa cracking pressure

* Teflon glass packing

** Grafoil packing

TABLE XLII

ACCESSORIES

Accessory	Comparing	Notes
Pressure gauge	Solferunt	4.5 in. dial, 0.25 in. NPT, 316-SS Bourdon tube, 0.5% accuracy, 3500 psig maximum pressure.

TABLE XLII (continued)

Accessory	Comparing	Notes
Pressure regulator	Grove Valve and Regulator	Mity-Mite, model 94, 0.25 in. NPT, internally loaded, 34.5 MPa inlet pressure, 20 5 MPa outlet pressure.
Feeding Tank	Hoke	1-liter, ss-sampling cylinder, (1/2 in. female NPT), specially designed to hold 13.8 MPa at 427°C in the presence of H_2 and H_2S gases.
Sampling Cylinder	Hoke	30 ml ss-sampling cylinder 1/4 in. female (NPT), specially designed to to hold the above.
Traps	Hoke	500 ml ss-sampling cylinders, 34.5 MPa working pressure.
In-line filters		100 mesh, ss.
Band heaters	Waltow	Mica, 3.5 in. i d., 2.5 in. width, one piece with post terminals and clamping strips
Thermocouples	Omega	Quick disconnect thermocouple assembly (E-type)
Extension wire	Omega	Chromel-constantan, extension grade wire
Digital Readout indicator	Omega	Model 402 A-E-C, 1°C resolution, 5 point selector switch.
Temperature Controller	Omega	Digital Set Point indicating, model 165 for use with E-thermo-couple, range-190° to +1000°C
Temperature recorder	Leeds and Northrup	Speadomax X1 recorder, model 621-61-000-3089-6-59.

APPENDIX B

ANALYTICAL PROCEDURES

The major analytical tool to measure the concentrations of the reaction products was a model 3700 Varian Gas Chromatograph (GC), equipped with a Thermionic Specific Detector (TSD), and an HP 3390A Reporting Integrator. The system was used for the analysis of quinoline/n-hexadecane, acridine/n-hexadecane, and quinoline/acridine/n-hexadecane hydrogenation products In order to optimize the measurement procedure, different columns with different temperatures were used, which are described here. In this Appendix the column selection, quantitative analysis, and precision and accuracy of measurement for each case will be discussed

Quinoline Hydrogenation Products Analysis

Column Selection

The main compounds which result from the HDN of quinoline in n-hexadecane, the manufacturer, and the purity are listed in Table XLIII. Samples of most of these compounds were obtained and used to identify and calibrate their chromatographic peaks, except for propylcyclohexylamine which was not available. In search of a suitable GC column a 5% OV 101 CHROM G H P 100/120, 50 cm x 1/8 in., stain-

TABLE XLIII

HDN PRODUCTS OF QUINOLINE IN N-HEXADECANE

Compound	Manufacturer	Molecular Weight	Boiling Point, °C	Purity
PCH	(P&B)	126 24	155	97%
PB	(P&B)	120.2	159	98%
propylcyclohexylamine		141.2	*	
aniline	(Aldrich)	93 13	184	99 5%
OMA	(Aldrich)	107 16	199-200	99%
OEA	(P&B)	121 18	210	98%
Bz-THQ	(Alfa)	133 19	218	
3-phenyl-1-propylamine	(Aldrich)	135 21	221	98%
OPA	(Aldrich)	135 21	222-224	97%
Quinoline	(Alfa)	129 16	237	99 9%
Py-THQ	(K&K)	133 19	249	98%
decahydroquinoline	(Alfa)	139 19	99 99/20mm.	
n-hexadecane	(Alfa)	226.45	287	99%

*not available

less steel column was tried first. Both isothermal and temperature programmed conditions were tested However, the separation was inadequate and either a capillary or a polar column was required.

Following Albert's (108) work, we used a column of 6'x0.25" o d., 2mm i.d , glass tubing packed with 10% Carbowax 20 M on 80-100 mesh Gas Chrom Q, for the separation of a blend of several compounds representing pyridines, quinolines, indoles and carbazoles A similar column, 10'x1/8 in. o d., o.1 in. i d., stainless steel, 10% Carbowax 20 M on 80-100 mesh CHROM W-HP, was constructed and tried for the analysis of quinoline HDN products.

Using the Carbowax various operating conditions were tried for the major compounds listed in Table XLIII. The best conditions to separate these compounds were identified as

Injector temperature	220°C	
Detector temperature	220°C	
Column temperature	200°C	
Range	10^{-11}	amp/mv
Bead current	4 8	amp
Hydrogen pressure	30	psig
Volume injected	0 1	ml

Retention times for these compounds are listed in Table XLIV. A standard solution of a mixture of these compounds in n-hexadecane was prepared to test the precision. The composition of this standard solution was predicted by comparing its chromatogram with those obtained from single component standard solutions These results were used to develop a comprehensive understanding about the errors of analysis. These results are presented in Table XLIV

TABLE XLIV

PRECISION AND ACCURACY OF ANALYSIS

Compound	RT	$\bar{A}$	PRS	Cpr	Ca	PRE
PCH	1.06	5,895	4 17	423.3	427 2	-0 92
PB	1.36	7,350	3.35	463.3	467 8	-0 97
n-hexadecane	2.50	7,798,200	3.16	976,283	998,836	-2 26
Bz-THQ	4.17	42,672	2.49	56.8	60 3	-6 16
OPA	5 83	27,932	3 00	54.2	59 8	-9 42
Q	6.74	48,566	3.15	63 3	65 9	-4 11
1,2,3,4-THQ	9 33	77,776	8.74	81 9	82 9	-0 73
DHQ	2 28**	*	*	*	*	*
Anıline	3.75**	*	*	*	*	*
O-toluıdıne	4.36**	*	*	*	*	*
3-phenyl-1-propylamıne	5.71**	*	*	*	*	*

*Not measured

** The solvent was acetone

where RT is the retentıon tıme ın mınute,

$\bar{A}$ is the average area of at least three ınjectıons,

PRS is the percentage relatıve standard devıatıon,

Cpr is the predıcted concentratıon, ppm,

Ca is the actual concentratıon, ppm,

and PRE is the percentage relatıve error

Table XLIV shows that, for the seven compounds studied, most of the results have relative standard deviations lower than 5%, which means an acceptable and adequate precision. Also, most of the predicted results have relative errors lower than 7% which indicates a high degree of accuracy. These results indicate that the technique is a potentially suitable one.

However, similar studies on the other hydrogenation products of quinoline, as shown in Table XLIV, were unsuccessful because some of these compounds are sparingly soluble in n-hexadecane. This led to the use of acetone as an alternative solvent. Also, some of those compounds have retention times very close to each other. Furthermore, DHQ peak was found to overlap the n-hexadecane peak. The retention times of the compounds that are insoluble in n-hexadecane were determined in acetone and are presented in Table XLIV. The problem was resolved by lowering the column temperature and using a temperature program. Finally, a suitable temperature program was found, which is given here along with its operating conditions.

Injector temperature	220°C
Detector temperature	220°C
Initial column temperature	150°C
Initial time	8 minutes
Program rate	10°C/minute
Final column temperature	200°C
Final time	10 minutes

Hydrogen pressure	30 psig
Bead current	4.8 amp
Range	10^{-11} amp/mv

Quantitiative Analysis

The retention times for different compounds under these conditions are listed in Table XLV. As shown in Table XLV, several of the reference compounds contained impurities which appeared as impurity peaks. This complicated the calibration and the analysis process. It was necessary to prepare several standard solutions from mixtures of these compounds for calibration purposes. Initially two standard solutions were prepared from a mixture of each major compound in n-hexadecane as solvent. Standard solution #1 was relatively concentrated, whereas standard solution #2 was dilute. Relative Response Factors (RRF=weight/peak area) were determined for each compound in both standards. It was found that RRF varied with concentration. A third standard solution was prepared from the rest of the expected compounds (the minor ones) in acetone. However, it was difficult to analyze with standard solutions which had different components, since the retention times of some compounds were close. Therefore, a solution of a mixture of all these compounds in n-hexadecane was tried. Thus, standard solution # 4 was prepared. However, it was found that 3-phenl-1-propylamine did not dissolve in

TABLE XLV

RETENTION TIMES* OF QUINOLINE HDN PRODUCTS

Compound	Main peak	Other Peaks**
Acetone	1.25	
Benzene	1.41	18.98,14.92,13.39, 1.08
N-propylcyclohexane	1.54	
Propylbenzene	2.44	
Decahydroquinoline	5.82	
N-hexadecane	7.65	19.50,6.55,10.06, 10.60
Aniline	11.63	1.46
5,6,7,8-tetrahydro-quinoline	11.87	15.41
O-methylaniline	12 62	8.09,19.76
O-ethylaniline	13.64	19 86,9.49,15.35, 11.69,11.18
3-phenyl-1-propylamine	14 46	2.05,17.22,4.79
O-propylaniline	14.59	
Quinoline	15.37	
1,2,3,4-tetrahydro-quinoline	18.34	

*Retention time in minutes

**Peaks arranged in a decreasing order

the solution. In fact standard solution #4 was not sufficient for the analysis since the concentration of some compounds varied widely Quinoline concentration, for example, varies from about 45,000 ppm to lower than 5000 ppm. Similarly, RRF varies with concentration. Hence, two other standard solutions were prepared

1 Standard solution #5 which was a highly concentrated solution of Quinoline in h-hexadecane.

2. Standard solution #6 which was a highly concentrated solution of a mixture of the major compounds in n-hexadecane.

In fact, the standard solutions 4 thru 6 were used in the analysis of each run The compositions of these solutions are presented in Table XLVI. However, other compounds compounds which were expected to occur in the HDN of quinoline were analyzed and their retention times are listed in Table XLVII together with the retention time of n-hexadecane for comparison.

The analysis is performed in three steps:

1. Determining the RRF for each compound by calibrating with a standard solution.

2. Determining the area for each compound from the chromatogram

3. Multiplying the area of each compound in a sample by its RRF to obtain its concentration.

Initially, it was intended to perform analysis on diluted

TABLE XLVI

COMPOSITION OF STANDARD SOLUTION, PPM.

Compound	Solution #4	Solution #5	Solution #6
N-hexadecane	958,329	954,427	917,132
Bz-THQ	3,278	----	15,758
OPA	3,304	----	16,530
Quinoline	4,766	43,843	33,122
Py-THQ	4,472	----	16,257
Isoquinoline	----	1,730	1,201
PCH	4,960	----	----
PB	5,856	----	----
DHQ	3,193	----	----
Aniline	1,615	----	----
OMA	2,525	----	----
OEA	4,017	----	----
3-phenyl-1-propylamine	3,685	----	----

TABLE XLVII

RETENTION TIMES FOR OTHER EXPECTED COMPOUNDS

Compound	RT, minute
n-octane	1 20
cyclohexane	1.22
n-decane	1 50
n-undecane	1.78
ethylbenzene	1 87
o-xylene	2 17
pyridine	2.29
n-dodecane	2.36
n-tridecane	3.03
n-tetradecane	4.18
isoquinoline	16.05
Indole	33.88

samples, but it was found later that such dilution could lead to the loss of some minor compounds which would not show up in the chromatogram. Therefore, analysis was done for each sample without dilution. However, it was needed to make some interpolation to determine the suitable RRF for a certain concentration

Analysis of Acridine Hydrogenation Products

Column Selection

It was reported in Chapter III that acridine hydrogenation results in a mixture of compounds which, theoretically, varies between one and seventeen reduced acridines, and DCHM. Only three of these compounds were available during this project. So they were used to identify their corresponding peaks and calibrate the GC. For the rest of the compounds we were obliged to use the available physical property data to guess their peaks, in chromatograms and to estimate their response factors for calibration. These predicting and estimating methods are dicussed later.

In seaching for a suitable GC column for analysis of acridine HDN products, a 5% OV 101 CHROM G.H.P. 100/20, 2.0 m. x 1/8 in., SS column was used. After many trails, the following operating conditions were found suitable for separating the HDN products.

Injector temperature	300°C
Detector temperature	300°C
Initial column temperature	165°C
Initial time	12 minutes
Program rate	1°C/minute
Final temperature	180°C
Final time	3 minutes
Range	10^{-11} amp/mv

Hydrogen pressure	33 psig
Bead current	5.4 amp

Quantitative Analysis

Several qualitative injections were performed, using this column under the stated conditions to determine the retention times for the various compounds which are expected to be present during the quantitative analysis. Retention times of the other expected reaction products, which are not available for use, are estimated form the analysis of the actual HDN samples, using their melting points. It is assumed that the compounds elute from a non-polar column in an order similar to the volatility order. Thus, the lower the boiling point of a compound, the earlier is its elution. Also, it is assumed that the lower the melting point of a compound, the lower is its boiling point. The retention times of all the compounds are presented in Table XLVIII.

Several standard solutions with varying concentrations were prepared for calibration. The compositions of these solutions are presented in Table XLIX. The relative response factor (RRF) for each of the available compounds is measured directly. For compounds which are not available, the RRF is assumed to be proportional to the extent of hydrogenation of the compound. Therefore, the RRFs are estimated as follows

TABLE XLVIII

RETENTION TIMES FOR ACRIDINE HDN PRODUCTS

Compound	Retention Time, minutes
DCHM	5.57
1,2,3,4-THA	10 73
n-hexadecane	14.04
SOHA	18.38
ASOHA	19 64
PHA	20 96
Acridine	22 64
9,10-DHA	26 80

1 The RRF of ASOHA is assumed to be equal to that of SOHA

2 The RRF of 1,2,3,4-THA is considered equal to the average value of the RRF of acridine and that of OHA

3 The RRF of PHA is expected to be lower than that of SOHA Therefore it is estimated by extra-polation. Quantitative analysis is performed in the same way as described for quinoline.

TABLE XLIX

COMPOSITION OF STANDARD SOLUTIONS, PPM.

Compound	Standard Solution #				
	10	13	14	15	16
Toluene	985,140				
N-hexadecane		979,169	981,108	969,150	993,604
DCHM		5,317	4,148		
SOHA		5,601	5,147	12,500	2,990
Acridine	14,860	9,913	9,597	18,350	3,406

Precision and Accuracy

The average percentage relative standard deviation is less than 5%. This means an adequately high precision For accuracy calculations, two methods were used

1 Predicting feed concentration by using standard solution #10. For this purpose, several injections were made of both the feed to run NA1 and the standard solution #10 The following data were obtained

N-hexadecane density	0 773 g/ml.
Toluene density	0.867 g/ml
Injection volume	0 3 µl

Average area for acridine in standard solution #10 9,508,533

Average area for acridine in NA1 feed 5,458,500

Mass of acridine in 0 3 µl of standard sol. #10

$= (1\ 486/100) \times 0\ 3 \times 10^{-3} \times 0\ 867$

$= 3\ 865 \times 10^{-6}$ g

RRF for standard sol #10 $= (3.865 \times 10^{-6}/9,508,533)$

$= 4.065 \times 10^{-13}$ g/unit area

Predicted acridine in 0 3 µl feed $= 4.065 \times 10^{-13} \times 5,458,500$

$= 2.2189 \times 10^{-6}$ g

Actual mass of acridine in 0.3 µl feed

$= (0\ 916/100) \times 0.3 \times 10^{-3} \times 0\ 773$

$= 2\ 125 \times 10^{-6}$ g

Percentage relative error

$= [(2.2189 - 2\ 125)/2,125 \times 10^{-6}] \times 10^{-6} \times 100\%$

$= 4.4\%$

2 Comparing RRF obtained from standard solution #10 with that from #13

Average area from 0.3 µl standard solution #13 = 5,508,800

Mass corresponding to this area $= (0\ 9913/10^{2})(0.3/10^{3})(0.773)$

$= 2.2988 \times 10^{-6}$ g

RRF $= 2\ 2988 \times 10^{-6}/5,508,800$

$= 4\ 173 \times 10^{-13}$ g/unit area

Error in RRF = $[(4.173 - 4\ 065) \times 10^{-13}/4.173 \times 10^{-13}] \times 100\%$

= 2.59%

Hence, high degree of accuracy is attained in our analysis.

Mixture Hydrogenation Products Analysis

Column Selection

Several investigations were performed to select a suitable column for quinoline-acridine mixture products analysis. These led to the selection of a column, 10'X1/8 in. i.d., stainless steel, 10% Carbowax 20M on 80-100 mesh CHROM W-HP. The following operating conditions were found suitable for separating the HDN products:

Injector temperature	230°C
Detector temperature	230°C
Initial column temeperature	150°C
Inital time	8 minutes
Program rate	5°C/minute
Final temperature	225°C
Final time	30 minutes
Range	10^{-11} amp/mv
Hydrogen Pressure	33 psig
Bead current	4.8 amp

Quantitative Analysis

Several qualitative analyses were performed,using these

operating conditions, to determine the retention times for the various compounds which were expected in the product solution Retention times of the other expected unavailable products, were estimated from the analysis of the actual HDN samples The retention times for all these compounds are presented in Table L

Two standard solutions were prepared for calibration. The compositions of these solutions are presented in Table LI The RRF for each of the available compounds was measured directly, whereas it was estimated for the other compounds, as described in acridine products analysis. Also, quantitative analysis was performed in the same way as described for quinoline A typical chromatogram is presented in Figure 144

Precision and Accuracy

The average percentage relative standard deviation is less than 5% which means a high precision. Accuracy is checked by the same way described in acridine products analysis under method #1. Feed concentration of NQA1 is measured directly. It resulted in PRE's of -3.74 , -2 29 for quinoline and acridine concentrations respectively This, in fact, is a high degree of accuracy.

Safety of The Chemicals

Safety hazards of both quinoline and acridine were considered Quinoline is moderately toxic by most routes of exxposure In one experiment, inhalation of its satu-

TABLE L

RETENTION TIMES FOR QUINOLINE-ACRIDINE MIXTURE HDN PRODUCTS

Compound	Retention Time, minute
PCH	1 21
PB	1 99
DHQ	4 39
DCHM	5 90
N-hecadecane	6 95
Aniline	10 87
Bz-THQ	11.15
OMA	12 31
OEA	13.90
ASOHA	14 76
OPA	15 57
THA	15 72
Quinoline	16 19
Py-THQ	19 24
SOHA	25.61
PHA	30.50
Acridine	43 11

rated vapor (17ppm) for 8 hours caused no death (109) Acridine is a strong irritant to skin, eye and mucous membranes of the body It causes Lachrymation and irritation

TABLE LI

COMPOSITION OF STANDARD SOLUTIONS
USED IN MIXTURE ANALYSIS

Compound	Solution #17	Solution #18
PCH	-----	1,590
PB	-----	1,521
DHQ	-----	9,024
DCHM	-----	2,450
n-hexadecane	896,820	938,571
Anıline	3,550	6,658
Bz-THQ	-----	9,745
OMA	-----	1,958
OEA	-----	1,889
OPA	-----	4,692
Quınolıne	49,006	5,070
Iso-quınolıne	1,777	183
Py-THQ	23,211	9,331
SOHA	10,673	5,337
Acrıdıne	14,963	1,981

of the conjuntıve (110) No health hazard ınformatıon on other chemıcals, were avaılable ın the lıterature To avoıd any adverse effects, skın contact or ınhalatıon of these chemıcals should be avoıded

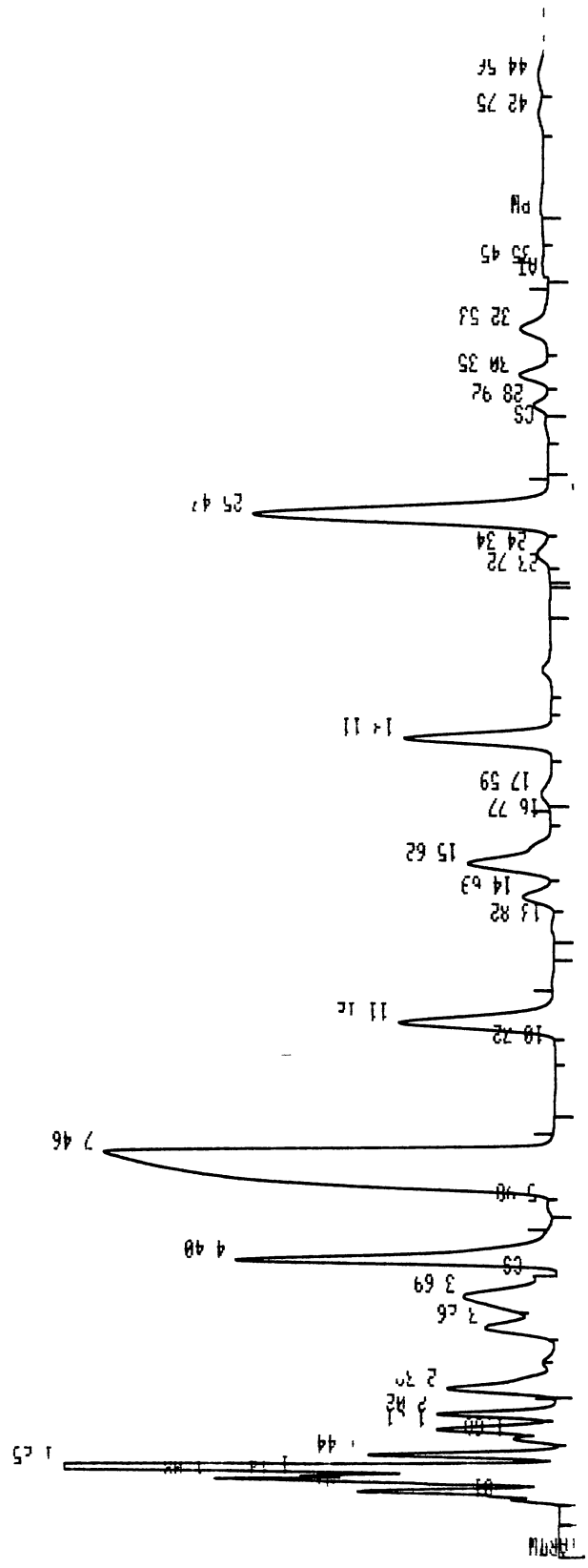

Figure 144. A Typical Chromatogram for Quinoline-Acridine Mixture HDN Products

APPENDIX C

REACTOR OPERATING PROCUDURE

The sealed ampoule containing the presulfided catalyst is hanged inside the autoclave, where the reactants are placed The autoclave is heated to the required temperature. Then hydrogen pressure inside the autoclave is raised to the required level which breaks the ampoule and the reaction starts. This procedure includes several steps: purging and leakage checking, reaction, sampling and shut down.

Purging and Leakage Checking

1. The liquid reactants are poured in the glass liner which is placed in the autoclave.

2. The catalyst ampoule is attached to the autoclave cover (between the cooling coil and the stirrer).

3. The autoclave is carefully covered and tightened and all the valves are closed

4. Nitrogen is slowly introduced into the autoclave until the pressure reaches 200 psig. The system is tested for any leaks. A pressure drop of less than 10 psi in two hours is considered acceptable.

5. The pressure inside the system is released

slowly. Then hydrogen is slowly admitted to the system allowing the pressure to rise up to 100 psig. Hydrogen is then slowly released to the atmosphere. This step is repeated.

Reaction

1. Now hydrogen is allowed to build up slowly in the system to attain 200 psig pressure. All valves are closed.

2. The set point of the temperature controller is raised to the required level. Then heating of the autoclave is started.

3. Temperature is monitored by a digital indicator and plotted by a chart recorder.

4. During the heating process the pressure inside the system is also recorded.

5. When the desired reaction temperature is attained, the stirrer is started at a low speed. Hydrogen is slowly admitted into the system until the pressure builds up to the required level. During this step the ampoule fractures under the high pressure and the zero time of the reaction is recorded as a jump of about 3°C on the chart recorder.

6. The stirrer speed is raised to 750 rpm.

7. The valve 18 is gently opened. Then the valve 19 is opened. A very small stream of gas is allowed to vent to the atmosphere by opening the valve 21 and adjusting both the valves 8 and 20. The valve 24 is also opened.

Sampling

When sampling time approaches, nitrogen is introduced through the valve 31 to the sampling cylinder to a pressure of about 600 psig. Then the valve 31 is closed. The valve 12 is opened and quickly closed. The valve 13 is opened slowly to rlease the pressure. Then the valve 14 is opened slowly to receive sample. Finally, the valve 14 is closed and the pressure inside the sampling system is released through the valves 19 and 20.

Shut Down

1. The electric power for autoclave heater is turned off.

2. Hydrogen supply is cut by closing the valves 3,6, 7,8,10,11 and 18.

3. The rate of the stirrer is decreased to 150 rpm.

4 A stream of nitrogen is passed through the cooling coil inside the autoclave to quench the reaction.

5. When the temperature is about 300°C the stream of cooling nitrogen is cut off and the stirrer is turned off.

6. The current to the temperature measuring, recording and controlling instruments is turned off.

APPENDIX D

EFFECTIVENESS FACTOR

The quinoline effectiveness factor, η, was calculated using the following equations suggested by Froment and Bishcoff (111) for heavy petroleum feedstocks.

$$\eta = (3/H^2)\ [H \coth(H) - 1]$$

$$H = R_c\ (k_{obs}/D_{eff})^{1/2}$$

$$D_{eff} = (\epsilon D/\tau)\ [1 - (R_m/R_p)]^4$$

The free liquid diffusivity, D, was calculated using Scheibel's correlation (112).

$$D = (KT/\mu)/V_R^{1/3}$$

where $K = Z\ [1 + (3V_L/V_R)^{2/3}]$

and $Z = 8.2 \times 10^{-8}$

The solvent viscosity, μ, was calculated using Letsou and Steil's correlation for high temperature liquids (112)

$$\mu\epsilon = [(\mu\epsilon)' + w\ (\mu\epsilon)'']$$

$$(\mu\epsilon)' = 0.015174 - 0.02135\ T_r + 0.0075\ T_r^2$$

$$(\mu\epsilon)'' = 0.042552 - 0.07674\ T_r + 0.0340\ T_r^2$$

$$\epsilon = T_c^{1/6}/(MW_L\ P_c)^{1/2}$$

$$R_c = 3V_p/S_x$$

The values of the parameters used in these equations are listed in Table LII.

By substitution

$(\mu\epsilon)' = 0.0021$

$(\mu\epsilon)' = 0.0011$

$\mu\epsilon = 0\ 0029$

$\epsilon = (717)^{1/6}/(226 \times 14)^{0.5} = 0.0532$

$\mu = 0\ 0029/0\ 0532 = 0.055$ cP

$K = 8.2\ X10^{-8}\ [1 + (3 \times 350/140.9)^{2/3}]$

$= 39.48 \times 10^{-8}$

$D = 39\ 48\ X\ 10^{-8} \times 643/0\ 055/(140.9)^{1/3}$

$= 0.0009$ $cm^2/sec.$

$D_{eff} = (0\ 5)\ (0\ 0009)\ [1-(3.8/50)]^4/2.5$

$= 1\ 3 \times 10^{-4}$ $cm^2/sec.$

$Rc = 3 \times 0.18 \times 0.061/4/[0.061/2 + 0.18]$

$= 0\ 039" = 0.1$ cm

k_{obs} = (k) (volume of solvent/vol of catalyst)

$= (6.3\ E\text{-}5 \times 350)/(5.4 \times 0\ 016/48) = 3\ 14 \times 10^{-3}$

$H = 0.1\ [3\ 14 \times 10^{-3}/(1.3 \times 10^{-4})]^{1/2} = 0\ 492$

$\eta = 3[0\ 492 \coth (0.492)-1]/(0\ 492)^2 = 0.98$

TABLE LII

PARAMETERS USED IN EFFECTIVENESS FACTOR CALCULATIONS

MW_L - n-hexadecane molecular weight (226 g/mole)

Pc - N-hexadecane critical pressure (14 0 atm)

Rc - average catalyst particle radius

Rm - quinoline molecule size (3 8°A)

Rp - average pore radius (50°A)

Tc - n-hexadecane critical temerature (717°K)

V_L - n-hexadecane molar volume at mornal boilig point (350 ml /g-mole)

V_R - quinoline molar volume at normal boiling point (140.9 ml /g-mole)

ϵ - catalyst void fraction (0 5)

τ - catalyst tortuosity factor (2 5)

w - n-hexadecane accentric factor (0 74)

D - free liquid diffusivity (cm^2/sec)

k_{obs} - observed reaction rate constant

S_x - external surface area of a pellet (cm^2)

V_p - volume of a pellet (cm^3)

T - Reaction temperature (643°k)

T_r - Reduced temperature

VITA

Ribhi Fayez El-Bishtawi

Candidate for the Degree of

Doctor of Philosophy

Thesis HYDRODENITROGENATION OF QUINOLINE, ACRIDINE, AND THEIR MIXTURE

Major Field Chemical Engineering

Biographical

Personal Data Born in Nablus, Jordan, November 21, 1938, the son of Fayez El-Bishtawi

Education Graduated from Salahyyeg High School, Nablus, Jordan, in 1955, received the Bachelor in Chemical engineering from Cairo University in July, 1961, recieved Master of Science degree from Cairo University in December 1974, completed requirements for the Doctor of Philosophy degree at Oklahoma State University in May, 1986.

Professional Experience Teaching Assistant, Department of Chemical engineering, University of Bahdad February 1962 to August 1971, lecturer at Amman Polytechnic Institute 1975 to 1978, lecturer at the University of Jordan 1978 to 1980